STUDIA UNIVERSITATIS
BABEŞ-BOLYAI

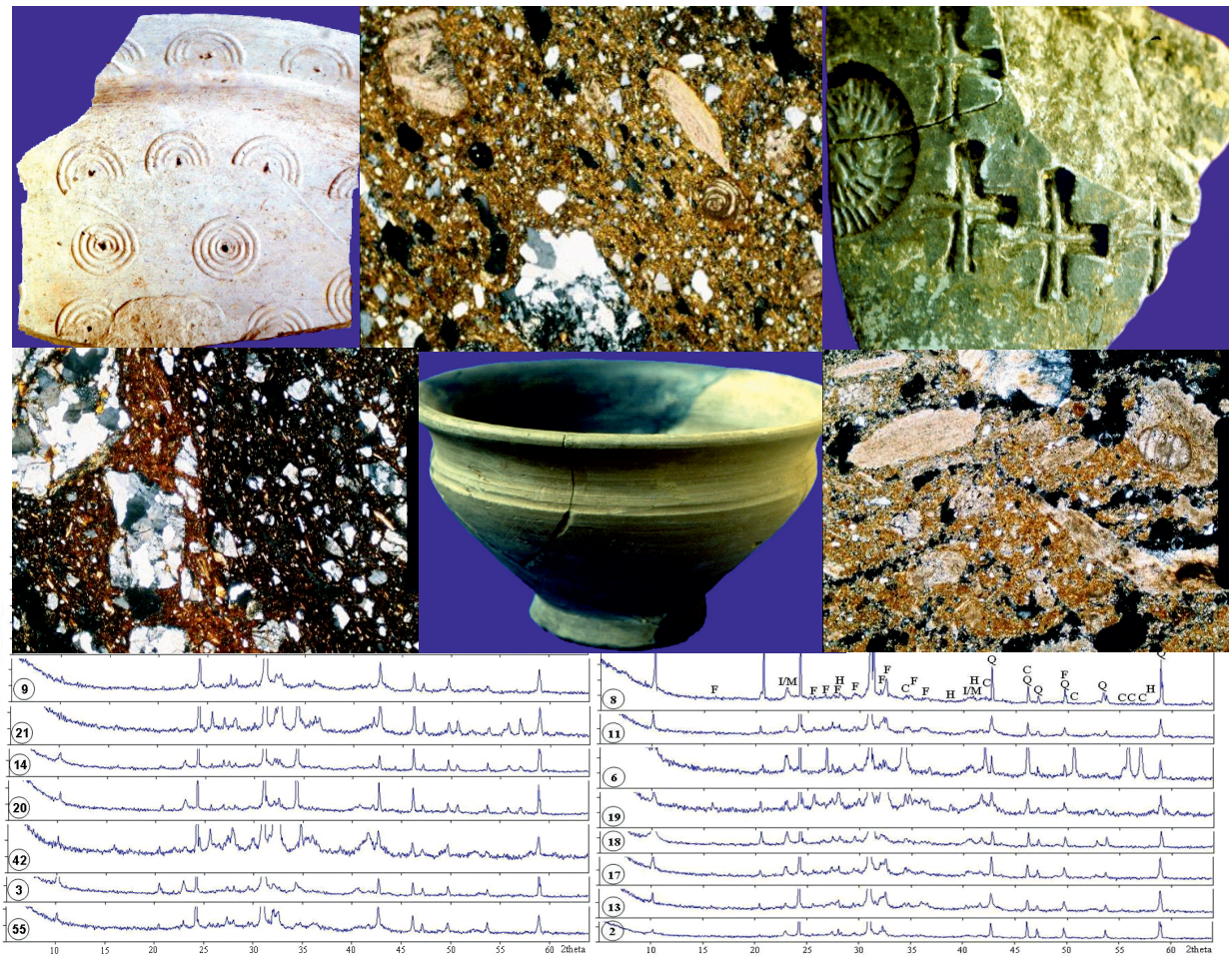

CHEMIA

2/2016

STUDIA
UNIVERSITATIS BABEŞ-BOLYAI

CHEMIA

2/2016

http://chem.ubbcluj.ro/~studiachemia/; studiachemia@chem.ubbcluj.ro
http://www.studia.ubbcluj.ro/serii/chemia/index_en.html

YEAR **Volume 61 (LXI) 2016**
MONTH **JUNE**
ISSUE **2**

S T U D I A
UNIVERSITATIS BABEŞ–BOLYAI
CHEMIA

2

STUDIA UBB EDITORIAL OFFICE: B.P. Hasdeu no. 51, 400371 Cluj-Napoca, Romania, Phone + 40 264 405352

CUPRINS – CONTENT – SOMMAIRE – INHALT

ANDREA VARGA, ALINA FILIP, LÁSZLÓ-CSABA BENCZE, PÉTER SÁTORHELYI, EVELIN BELL, BEÁTA G. VÉRTESSY, LÁSZLÓ POPPE, CSABA PAIZS, Expression and Purification of Recombinant Phenylalanine 2,3-Aminomutase from *Pantoea Agglomerans* 7

NORBERT ARTUR DIMA, ALINA FILIP, LÁSZLÓ CSABA BENCZE, MÁRK OLÁH, PÉTER SÁTORHELYI, BEÁTA G. VÉRTESSY, LÁSZLÓ POPPE, CSABA PAIZS, Expression and Purification of Recombinant Phenylalanine Ammonia-Lyase from *Petroselinum Crispum*..... 21

ANDREA FAZAKAS, ERIKA CSATÓ-KOVÁCS, ZSOLT BODOR, SZABOLCS LÁNYI, BEÁTA ÁBRAHÁM, Production of Chemicals with Genetically Modified *Escherichia Coli* Strains from Renewable Resources 35

GHEORGHE ROMAN, Synthesis of Unsymmetrically Substituted Isoxazoles as Intermediates for Bent-Core Mesogens 47

HOREA POPENECIU, DUMITRU RISTOIU, IOAN BRATU, GHEORGHE BORODI, ATTILA BENDE, LUCIAN BARBU, Inclusion Compounds of β-Cyclodextrin-Pitofenone Hydrochloride. Investigations of Solid Forms..... 61

MARCEL BENEA, VLAD-ANDREI LĂZĂRESCU, MARIA GOREA, Contribution to the Study of Suceag Pottery, Cluj County, Romania 73

IRINA SMICAL, ADRIANA MUNTEAN, ZOLTÁN TÖRÖK, Human Health Risk Associated with the Transfer of Heavy Metals into the Trophic Chain by Cattle Grazing on the Area in the Vicinity of the Tailing Ponds in the East of Baia Mare City, Romania..... 89

ADRIANA PAUCEAN, SIMONA MARIA MAN, SONIA ANCUŢA SOCACI, Wheat Germ Bread Quality and Dough Rheology as Influenced by Added Enzymes and Ascorbic Acid 103

ORLÉANS NGOMO, JEAN BAPTISTE BIKE MBAH, RICHARD KAMGA, RODICA DINICA, Adsorption of Palm Oil Carotenes on Natural and Acid Activated Montmorillonite Clays 119

MIOMIR ŠOŠKIĆ, DRAGICA BOJOVIĆ, VANJA TADIĆ, Comparative Chemical Analysis of Essential Oils from Lavender of Different Geographic Origins 127

MONICA DAN, MARIA MIHET, MIHAELA DIANA LAZAR, LIANA MARIA MURESAN, Promoted Alumina Supported Ni Catalyst for Ethanol Steam Reforming..... 137

SIMION DRĂGAN, IVETTE KULIC, A Macrokinetic Study of the Oxidation of Methanol to Formaldehyde on Fe_2O_3 – MoO_3 Oxide Catalyst.....155

MANUELA MINCEA, COSMIN IONASCU, KATALIN KIS, VASILE OSTAFE, Detection of Ochratoxin A in Instant Coffee by UPLC-MS/MS 167

CONEAC ANDREI, ORĂSAN MEDA SANDRA, CRIŞAN MARIA, MARE CODRUŢA, DECEA NICOLETA, MIHU CARMEN MIHAELA, MUREŞAN ADRIANA, LAZAR LEORDEAN VIORICA, FILIP MIUŢA, HPLC Monitoring of Curcumin in Preventive and Therapeutic Treatment of Rats to Diminish Acute Inflammation and Oxidative Stress 177

MOCAN-HOGNOGI RADU FLORIN, COSTIN NICOLAE, CONSTANTIN CRACIUN, MALUTAN ANDREI, TRIF IOANA, CIORTEA RAZVAN, MIHU DAN, Reactivity of Ovariectomised Female Rats after Administration of Injectable Oestrogens by TEM Microscopy..... 195

ALEXANDRU-VICTOR BURDE, STANCA CUC, ADRIAN RADU, MIRCEA AURELIAN RUSU, COSMIN SORIN COSMA, RADU SEPTIMIU CÂMPIAN, DAN LEORDEAN, Microstructural Analysis of the Interface between Some Superalloys and Composite/Ceramic Materials..... 205

IOANA ROXANA BORDEA, PATRICIA ONDINE LUCACIU, BOGDAN CRIŞAN, CAMELIA-MANUELA MÎRZA, DANIELA POPA, ANCA ŞTEFANIA MESAROŞ, STAVROS PELEKANOS, RADU SEPTIMIU CÂMPIAN, The Influence of Chromophore Presence in an Experimental Bleaching Gel on Laser Assisted Tooth Whitening Efficiency 215

ELENA CICAL, CRISTINA MIHALI, MIRCEA MECEA, ANCA DUMUŢA, THOMAS DIPPONG, Considerations on the Relative Efficacy of Aluminum Sulphate Versus Polyaluminum Chloride for Improving Drinking Water Quality 225

DANIELA CORNEA, LAURA SILAGHI-DUMITRESCU, ROBERT BALAZSI, RADU OPREAN, DIANA DUDEA, MĂRIOARA MOLDOVAN, The Study of Pit and Fissure Sealants Concerning Water Sorption and Solubility 239

MĂDĂLINA-ANCA LAZAR, HORAŢIU ROTARU, DOINA PRODAN, GABRIEL ARMENCEA, PAUL BERE, CĂLIN RAREŞ ROMAN, RADU SEPTIMIU CÂMPIAN, Evaluation of the Morphology and Structure of E Glass Fiber-Reinforced Composites for Cranio-Facial Bone Reconstruction 249

DANIELA POPA, MARIANA CONSTANTINIUC, RADU-SEPTIMIU CÂMPIAN, Fixing Systems for Dental CAD/CAM Prosthetic Restorations: a Systematic Review 261

Studia Universitatis Babes-Bolyai Chemia has been selected for coverage in Thomson Reuters products and custom information services. Beginning with V. 53 (1) 2008, this publication is indexed and abstracted in the following:

- Science Citation Index Expanded (also known as SciSearch®)
- Chemistry Citation Index®
- Journal Citation Reports/Science Edition

STUDIA UBB CHEMIA, LXI, 2, 2016 (p. 7-19)
(RECOMMENDED CITATION)

EXPRESSION AND PURIFICATION OF RECOMBINANT PHENYLALANINE 2,3-AMINOMUTASE FROM *PANTOEA AGGLOMERANS*

ANDREA VARGA[a], ALINA FILIP[a], LÁSZLÓ-CSABA BENCZE[a], PÉTER SÁTORHELYI[b], EVELIN BELL[c], BEÁTA G. VÉRTESSY[d,e], LÁSZLÓ POPPE[f,c,*], CSABA PAIZS[a,*]

ABSTRACT. In the present study, the gene of phenylalanine 2,3-aminomutase from *Pantoea agglomerans* (*Pa*PAM) was cloned into pET-19b vector and used for its expression in competent *Escherichia coli* cells. The recombinant plasmid, *Pa*PAM-pET-19b, was transformed into competent *E. coli* strain BL21(DE3)pLysS cells. Overnight culture of the transformed bacteria was induced by the addition of isopropylthio-*β*-D-galactoside (IPTG) to the final concentrations of 0.1, 0.5 and 1 mM. Also, the effects of different temperatures (18, 25 and 30°C) and the incubation time of *Pa*PAM were examined. The fermentation process was scaled up to 10 L fermentor. Affinity purification conditions were analyzed by SDS-PAGE. The T_m and the activity of the purified enzyme was also investigated.

Keywords: *phenylalanine 2,3-aminomutase, Pantoea agglomerans, optimization, protein expression*

INTRODUCTION

Over the past decades, the preparation of optically pure *α*-amino and *β*-amino acids has received increasing attention because they have

[a] *Babeş-Bolyai University, Faculty of Chemistry and Chemical Engineering, Arany János str. 11, RO-400028, Cluj-Napoca, Romania*
[b] *Fermentia Ltd, Berlini u. 47-49., H-1045 Budapest, Hungary*
[c] *Department of Organic Chemistry and Technology Budapest University of Technology and Economics Műegyetem rkp. 3, H-1111 Budapest, Hungary*
[d] *Department of Biotechnology and Food Sciences Budapest University of Technology and Economics Szt. Gellért tér 4, H-1111 Budapest, Hungary*
[e] *Institute of Enzymology Research Centre for Natural Sciences of Hungarian Academy of Sciences Magyar tudósok körútja 2, H-1117 Budapest, Hungary*
[f] *SynBiocat Ltd Lázár deák u 4/1, H-1173 Budapest, Hungary*
[*] *Corresponding authors: poppe@mail.bme.hu; paizs@chem.ubbcluj.ro*

many applications in their free form and as fundamental building blocks of bioactive natural products[1].

An attractive alternative enzymatic route to obtain enantiomerically pure *α*- and *β*-amino acids involves the use of phenylalanine ammonia-lyases (PALs) and phenylalanine 2,3-aminomutases (PAMs) [2].

Phenylalanine ammonia-lyases and 2,3-aminomutases are emerging as important enzymatic systems, not only in green synthetic routes to chiral amines, but also as potential target for treating diseases such as phenylketonuria and cancer [2].

PAL catalyzes the nonoxidative elimination of ammonia from L-phenylalanine to give *trans*-cinnamic acid, whereas PAM catalyzes the isomerization of *α*- into *β*-phenylalanine [3].

PAMs and PALs are members of the class I lyase-like family that includes tyrosine 2,3-aminomutases (TAMs) [4], tyrosine ammonia-lyases (TALs)[5], and histidine ammonia-lyases (HALs) [6]. All these enzymes rely on a protein-derived cofactor, 4-methylideneimidazol-5-one (MIO), which is generated autocatalytically from three active site residues, Ala-Ser-Gly (Thr-Ser-Gly in *Pa*PAM), forming a MIO signature motif [7,8].

The reactions catalyzed by these enzymes have considerable potential for biotechnological applications. They are used as biocatalysts for the synthesis of (*S*)-*α*-amino acids from arylacrylates (PALs), in kinetic resolution processes for obtaining (*R*)-*α*-amino acids starting from their racemates (PALs), or for the synthesis of (*R*)- or (*S*)-*β*-amino acids (*Tc*PAM and *Pa*PAM respectively) [9,10, 11,12,13].

Further, although *Tc*PAM and *Pa*PAM are both aryl amino acid 2,3-aminomutases and share the same cofactor dependency and similarity (26.7% identity and 42% similarity)[14], they catalyze the *α*-*β*-isomerization with different stereochemistry. *Tc*PAM catalyzes the isomerization of (*S*)-*α*-amino acids to (*R*)-*β*-amino acids, whereas *Pa*PAM converts (*S*)-*α*-amino acids to (*S*)-*β*-amino acids. In this way, both (*R*) and (*S*) enantiomers can be obtained in enantiomerically pure form.

*Tc*PAM has been widely used as biocatalyst for synthetic procedures related to *β*-amino acids but the use of *Pa*PAM as biocatalyst is not so frequently reported. In the consciousness of this fact, the aim of this work is to develop methods for recombinant production of phenylalanine 2,3-aminomutase from *Pantoea agglomerans* (*Pa*PAM) by optimization and scaling up the expression process for high level protein expression, in order to obtain *Pa*PAM efficient biocatalyst for the preparation of enantiomerically pure (*S*)-*β*-amino acids.

RESULTS AND DISCUSSION

Optimization of *Pa*PAM overexpression in *E. coli*

E. coli is still the preferred host for recombinant protein expression because it is easy to genetically manipulate, it is inexpensive to culture, and expression occurs fast [15]. pET system also has many advantages that determine us to use it for the expression of our gene. pET is one of the most powerful systems developed for the expression of recombinant proteins in *E. coli* [16]. *E. coli* strain BL21(DE3)pLysS is also the most widely used host for recombinant gene expression.[17] Therefore, *E. coli* was selected as host for expression of *Pa*PAM. The aim of this investigation was to examine the effect of different experimental conditions on the expression of *Pa*PAM in order to obtain high purity and yields for the enzyme which can be used as biocatalyst.

Inducer concentration optimization

Varying the concentration of IPTG, expression of proteins can be regulated at different levels, lower level expression can increase the solubility and activity of the target proteins [18]. With some proteins, it is important to induce the transcription of the expression plasmid with lower IPTG concentrations, while others tend to aggregate at high concentrations of IPTG [18].

For the optimization of *Pa*PAM expression, the effect of different concentrations of inducer (0.1, 0.5 and 1 mM IPTG) was tested on the growing culture of BL21(DE3)pLysS containing the pET-19b-*Pa*PAM recombinant plasmid. The SDS-PAGE bands are similar for 0.5 and 1 mM IPTG concentrations (**Figure 1**, Lane C and D), indicating the same level of expression of the 72 kDa *Pa*PAM, despite the increasing inducer concentration. Only a slight difference can be observed at 0.1 mM IPTG. (**Figure 1**, Lane B), showing the most intensive signal at the 72 kDa band of the recombinant *Pa*PAM. Based on these results, the final concentration of IPTG was set up to 0.1 mM.

Effect of incubation temperature and time on the overexpression of PaPAM

The recombinant plasmid pET-19b-*Pa*PAM was overexpressed to produce the target protein with an *N*-terminal His_{10} tag in *E. coli* BL21(DE3)pLysS. Generally, the optimum temperature for the recombinant protein production in *E.coli* is 37°C and several studies reported 37°C as the best temperature for maximum protein production [19]. On the other hand, studies showed that the rate of expression and culture temperature can affect the proper folding of recombinant proteins and formation inclusion bodies.[20] Lowering the expression temperature usually leads to slower growth of bacteria, slower rate of protein production and lower aggregation of target protein and also most proteases are less active at lower temperatures [21,22].

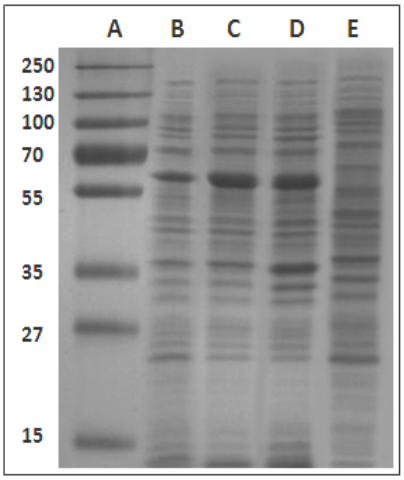

Figure 1. Induction of the expression of *Pa*PAM by different concentrations of IPTG in *E.coli* BL21(DE3)pLysS cells, after 4h. Lane **A**: protein ladder, Lane **B**: induction with 0.1 mM IPTG, Lane **C**: induction with 0.5 mM IPTG, Lane **D**: induction with 1 mM IPTG, Lane **E**: control (0 mM IPTG). The samples were prepared as described in experimental section.

To evaluate the effect of growth temperature on the expression of *Pa*PAM after induction, the cultures were incubated at different temperatures (18, 25, and 37°C). Initially the cell cultures were incubated at 37°C. After the density of cells reached OD_{600} ~0.6 (approx. 4 h) the temperature was reduced (to 18 or 25°C) and the cultures were induced with 0.1 mM IPTG. The density of the cells was monitored in time (**Graphic 1.**).

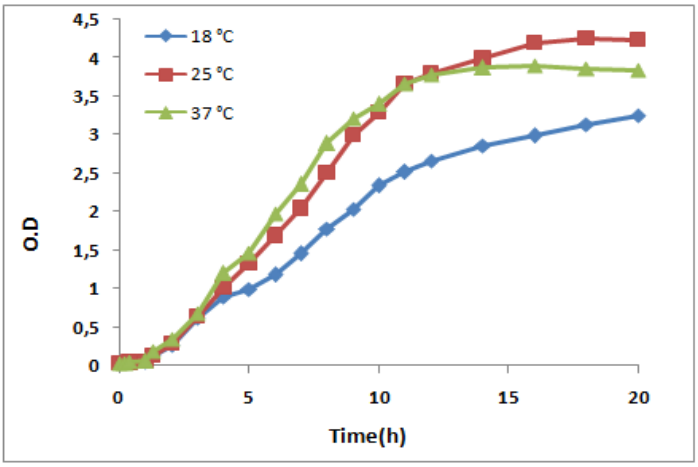

Graphic 1. Effect of growth temperature on the expression of *Pa*PAM

Due to the reduced incubation temperature the protein synthesis rate is slower at 18°C than at 25 or 37°C, longer induction times are necessary for cells growing. At higher incubation temperature (25 or 37°C), the protein synthesis is faster and the stationary phase is reached sooner than at lower temperatures. After 20 h the cells were harvested by centrifugation, followed by sonication and the protein was purified by metal affinity chromatography on Ni-NTA resin. The maximum yield of enzyme was obtained in case of 25°C incubation temperature. The optimal post-induction time on the expression of *Pa*PAM was 15-16 hours. The determined optimal conditions were also been used for the large-scale fermentation of *E. coli* BL21(DE3)pLysS.

Purification using Ni-NTA chromatography

Ni–NTA chromatography system is a rapid and easy purification technique. Proteins fused with His-tag at either ends (*N*- or *C*-terminus) bind tightly with high affinity on immobilized nickel ions. The strong binding between His-tag and matrix allows easy washing and efficient elution of bounded His-tagged protein by competition with imidazole [23].

In the pET-19b vector a His_{10}-tag at the *N*-terminus is included which is longer than the usual His_6-tag. Lengthening the His-tag increases the affinity of the enzyme to the Ni-NTA resin. Consequently, higher imidazole concentrations are required to elute all the bounded enzyme from the resin (from 250 mM up to 500 mM) [24]. Accordingly, as the SDS-PAGE gel analysis revealed, only small amount of protein remained in the flow through (**Figure 2**, Lane D) and in the washing buffer solutions (**Figure 2**, Lane E-G).

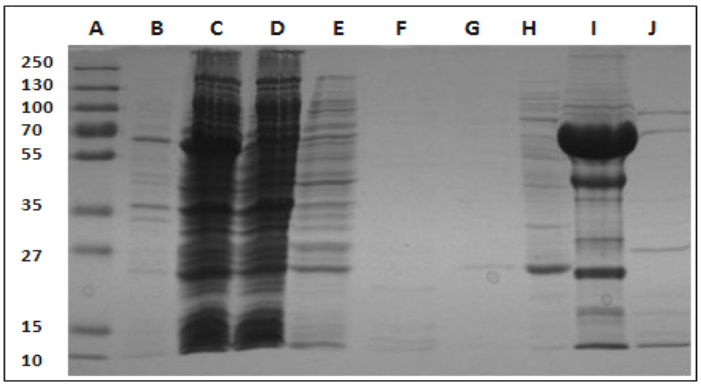

Figure 2. Purification of *Pa*PAM with Ni-NTA, in absence of protease inhibitor cocktail. Lane **A**: protein ladder, Lane **B**: supernatant, Lane **C**:pellet, Lane **D**: flow through Lane **E**: LS1, Lane **F**: HS, Lane **G**:LS2, Lane **H**: 20 mM Imidazole, Lane **I**: 500 mM Imidazole, Lane **J**: 1 mM Imidazole. The samples were prepared as described in experimental section.

It has been observed that *Pa*PAM activity descreased after elution from the Ni-NTA column probably due to prolonged exposure to very high imidazole concentration and we also observed that the obtained enzyme has some unspecific bands on the SDS-PAGE gel (**Figure 2**, Lane I) due to the protease activity for the enzyme. In order to eliminate these facts we added protease inhibitor cocktail to the lysis buffer and we reduced de imidazole concentration, testing 250, 350, 450, 500 mM imidazole solutions for protein elution. The best result was obtained by elution with 350 mM imidazole, resulting in protein solution appearing as single band on the SDS-PAGE (**Figure 3**, Lane I), indicating a highly purified enzyme.

Thermal stability

Thermal shift (ThermoFluor) assays offer a rapid and simple technique for assessing the thermal stability of proteins and to investigate factors affecting this stability. An environmentally sensitive fluorescent dye is used to monitor protein unfolding with respect to temperature [25]. In the ideal case, no fluorescence is observed at low temperature because the protein is completely and correctly folded and no hydrophobic areas are exposed. Upon an increase in temperature the protein starts to unfold and hydrophobic areas become exposed and the fluorescent dye can bind to these areas and fluorescence occurs.

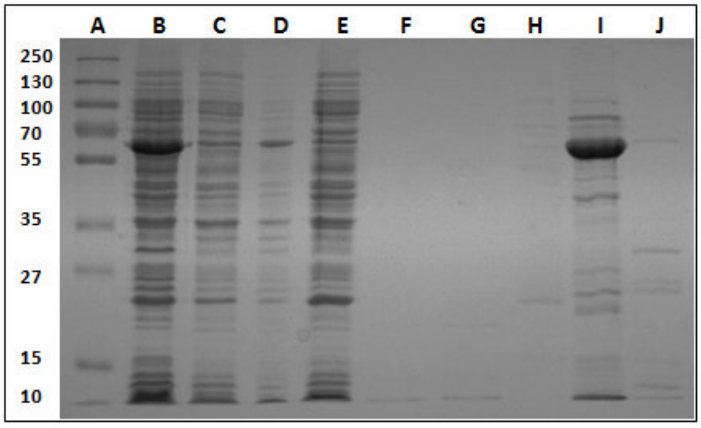

Figure 3. Purification of *Pa*PAM with Ni-NTA, in presence of protease inhibitor cocktail. Lane **A**: protein ladder, Lane **B**: supernatant, Lane **C**: flow through, Lane **D**: pellet, Lane **E**: LS1, Lane **F**: HS, Lane **G**:LS2, Lane **H**: 20 mM Imidazole, Lane **I**: 350 mM Imidazole, Lane **J**: 1 mM Imidazole. The samples were prepared as described in experimental section.

The *Pa*PAM enzyme presents a good thermal stability, it can be observed in **Figure 4** that its maximum melting temperature is approximately 73°C.

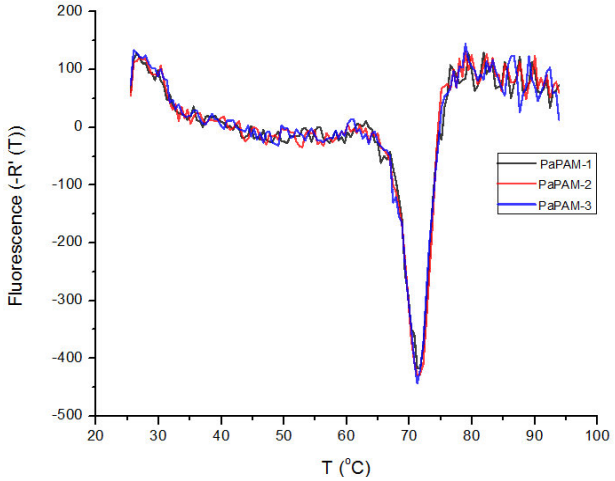

Figure 4. The first derivative of the melt curves.

We also investigated if the substrate of the enzyme has a stabilizing effect. Therefore following measurements were performed in TRIS buffer solution, pH 8.5 in the presence of L-phenylalanine.

The melting temperature was read from the negative curve of the first derivative of the experimental curve. By comparing the results of the measurements obtained in presence and in absence of the substrate, it can be observed that the modification of melting temperature in presence of L-phenylalanine is minor (from 73°C to 74°C), suggesting no stability increase of the enzyme upon substrate binding.

Activity assay

In nature, phenylalanine 2,3-aminonutase from *Pantoea agglomerans* is an (*S*)-selective enzyme, transforming the (*S*)-*α*-phenylalanine in (*S*)-*β*-phenylalanine [8].

The activity and the selectivity of *Pa*PAM was tested using *rac*-*α*-phenylalanine as substrate (**Scheme 1**). HPLC analysis of the reaction supports the formations of the (S)-β-phenylalanine (**Figure 5B**) with maximum selectivity (compared to the racemic mixture, **Figure 5A**).

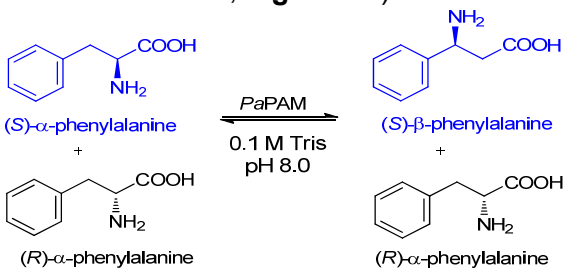

Scheme 1. Transformation of the *rac*-*α*-phenylalanine by *Pa*PAM.

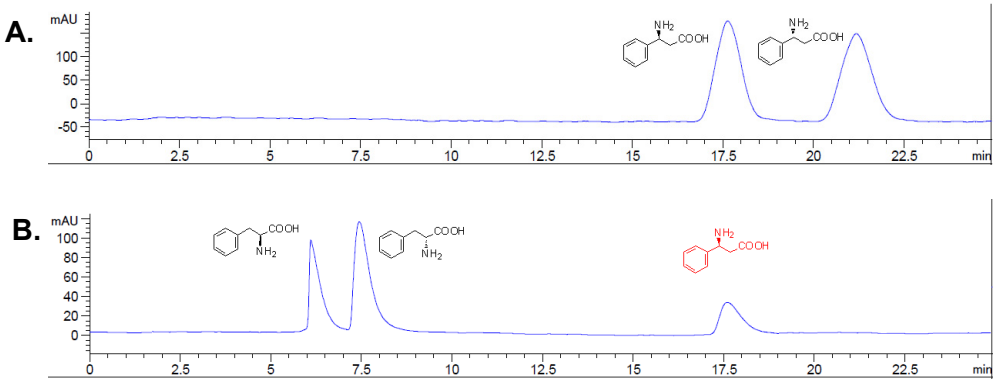

Figure 5. HPLC chromatograms for: **A.** *rac*-*β*-phenylalanine as control. **B.** Transformation of *rac*-*α*-phenylalanine by *Pa*PAM.

CONCLUSIONS

We examined different experimental conditions regarding the expression and purification of *Pa*PAM in order to obtain high purity and yield for the enzyme. IPTG concentrations, various post-induction temperatures on the expression, the imidazole concentration in the purification steps, the thermal stability and the activity of the enzyme were also examined.

The results showed that induction with 0.1 M IPTG was sufficient to induce the expression of *Pa*PAM, which is 10 times less than normally used IPTG concentration. Moreover, 15 hour post-induction incubation at 25°C was found to be optimal for producing a higher level of *Pa*PAM. Reducing the imidazole concentration to 350 mM and adding protease inhibitor cocktail improved the stability of the yielding enzyme. Furthermore, electrophoretically pure recombinant *Pa*PAM enzyme preparation was obtained using Ni affinity chromatography.

The detemined optimized parameters were also successfully applied for large scale fermentation of *Pa*PAM, obtaining high levels of protein.

EXPERIMENTAL SECTION

PaPAM gene synthesis and cloning

The gene of the *Pantoea agglomerans* PAM (Uniprot code: Q84FL5, PBD code: 3UNV, encoding 623 AA – **Figure 6**) was optimized to the codone usage of *E. coli*. The 1639 bps long synthetic gene was produced by *Life*

Tehnologies. The gene was cloned into pET-19b host vector using *XhoI* and *Bpu1102I* cloning site (**Figure 7**). The pET-19b vector in which the *Pa*PAM gene was cloned contains a His_{10}-tag *N*-terminal sequence, an enterokinase cleavage site, a gene resistant to ampicillin and the T7*lac* promoter sequence. In the supplementation of the growth medium ampicillin was replaced by carbenicillin, due to the highest stability of later.

w*t-Pa*PAM

MSIVNESGSQPVVSRDETLSQIERTSFHISSGKDISLEEIARAARDHQPV
TLHDEVVNRVTRSRSILESMVSDERVIYGVNTSMGGFVNYIVPIAKASEL
QNNLINAVATNVGKYFDDTTVRATMLARIVSLSRGNSAISIVNFKKLIEI
YNQGIVPCIPEKGSLGTSGDLGPLAAIALVCTGQWKARYQGEQMSGAMAL
EKAGISPMELSFKEGLALINGTSAMVGLGVLLYDEVKRLFDTYLTVTSLS
IEGLHGKTKPFEPAVHRMKPHQGQLEVATTIWETLADSSLAVNEHEVEKL
IAEEMDGLVKASNHQIEDAYSIRCTPQILGPVADTLKNIKQTLTNELNSS
NDNPLIDQTTEEVFHNGHFHGQYVSMAMDHLNIALVTMMNLANRRIDRFM
DKSNSNGLPPFLCAENAGLRLGLMGGQFMTASITAESRASCMPMSIQSLS
TTGDFQDIVSFGLVAARRVREQLKNLKYVFSFELLCACQAVDIRGTAGLS
KRTRALYDKTRTLVPYLEEDKTISDYIESIAQTVLTKNSDI

Figure 6. Amino acids sequence of recombinant *wt-Pa*PAM.

Figure 7. pET-19b-*Pa*PAM vector map.
The vector map was generated using Snapgene.

Transformation in E.coli host cells

Transformation of plasmid DNA into *E.coli* XL1-Blue (for plasmid amplification) and BL21(DE3)pLysS (for expression) was performed using the heat shock method, inserting the foreign plasmid into bacteria. After 20 min

incubation on ice, the mixture of 100 µL chemically competent bacterial cells and 2 µL of plasmid DNA was incubated at 42°C for 45 seconds (heat shock) and then placed back on ice for 25 min. 200 µL SOC media was added and the transformed cells were incubated at 37°C for 1 h. In case of XL1-Blue transformation, the transformed bacteria were plated on LB agar-plates containing tetracycline (30 µg/mL) and carbenicilin (50 µg/mL). In case of BL21(DE3)pLysS transformation, 50 µg/mL carbenicillin and 30 µg/mL chloramphenicol were used. Both cultures were then incubated overnight at 37°C, forming single colonies of bacteria bearing the plasmid encoding the recombinant protein.

Expression and production of the recombinant PaPAM

The recombinant *Pa*PAM carrying *N*-terminal $(His)_{10}$-tag was overexpressed in *E.coli* host cells (BL21(DE3)pLysS. For the expression step, a colony of the transformed plasmid was grown overnight at 37°C in 5 mL of Luria-Bertani (LB) medium containing carbenicillin (50 µg/mL) and chloramphenicol (30 µg/mL). A 0.5 L of LB medium was inoculated with 1% (v/v) of the overnight culture in an Erlenmeyer flask and grown until the measured optical density at 600 nm (OD_{600}) reached 0.6-0.7 at 37°C (optimal temperature for *E. coli* growth) and only at the induction phase the temperature was reduced to 18, 25, 37°C and the cells were induced by the addition of (0.1, 0.5, 1 mM) IPTG. The culture was shaken at 200 rpm for 16 h.

Large scale fermentation of the recombinant PaPAM

Ten litres of Luria-Bertani (LB) medium were sterilized at 121°C, 1.2 bar for 25 min. After sterilization, the media was cooled down to 37°C and ampicillin sodium salt was added to the fermentation broth for a final concentration of 100 µg/mL. The fermentation media was inoculated with 100 mL of the overnight seed culture of the *E. coli* producer strain. The following fermentation parameters were set up: temperature at 37°C, agitation 300 rpm, overpressure 0.2 bar and bottom air inlet 5 L/min. The pH value of the fermentation broth was controlled at pH 7.1±0.1. The dissolved oxygen (DO) value was set to a minimum of 30% and was controlled by the stirring speed. When the OD_{600} of the culture reached 0.7±0.1, the temperature was set to 25°C and the culture was induced with IPTG (0.1 mM final concentration), The fermentation broth was harvested after 16 h when the culture reached the stationary growth phase.

Purification of the recombinant PaPAM

The cells were harvested by centrifugation (25 min, 5000×g) and resuspended in 50 mL lysis buffer (150 mM NaCl, 50 mM TRIS pH 7.5,)

supplemented with DNAse, RNAse, Lysosyme, 2 mM PMSF and EDTA-free protease-inhibitor cocktail. Further, the cells were lysed by sonication and cell debris was removed by centrifugation (10000 × g, 30 min).

The proteins were further purified using a Ni-NTA-agarose column and washed with different buffer solutions.

The column was washed: LS (low salt) buffer, pH 7.5 (4-5V; V=resin volume), HS (high salt) buffer, pH 7.5 (2V), LS (2-4V), LS with 20 mM imidazole, LS with (250, 350, 450, 500 mM) imidazole (protein elution), LS with 1 M imidazole (4V), ddH_2O (7V) and 20% ethanol (1-2V), the resin was stored in 20% ethanol at 4°C.

The resulting eluate was dialyzed in 50 mM PBS, 4-5h at 4°C. The purity of the resulting fractions was verified by SDS-PAGE analysis. The samples were boiled for 5 min in Laemmli buffer and were loaded on a 12% SDS-PAGE. After dialysis the fractions containing purified protein were concentrated by centrifugal ultrafiltration. The concentration of the purified protein was determined by Bradford method.

Optimization parameters

To determine the *optimal IPTG concentration* on the recombinant protein production, the recombinant clone culture was grown to OD_{600} of about 0.6-0.7, and induced by adding IPTG to final concentrations of 0.1, 0.5 and 1 mM. After 4 hours of induction, 1 mL samples were colected, centrifuged and the pellet resuspended in 0.5 mL dH_2O. The samples were lysed by boiled for 5 min in Laemmli buffer, and were loaded on a 12% SDS-PAGE.

To examine the *effect of temperature*, recombinant protein expression was induced by addition of 0.1 mM IPTG at different temperatures (18, 25 and 37°C). The OD_{600} was monitored by time, after 20 hours of induction, cells were harvested by centrifugation, followed by sonication and the protein was purified by Ni-NTA.

Thermostability assay

The thermal stability of the enzyme was determined by thermofluor measurements using real-time PCR as described earlier [26].

The assay was performed using a 96-well iCycler iQ Real Time PCR plate. The total reaction volume was 25 µL and the plate was set up on ice. 20 µL of 0.1M TRIS buffer solution was pipetted into the wells of the plate. A 5000 × SYPRO Orange stock solution in DMSO was diluted 1:100 in water and 1 µL was added to the 20 µL well solution which contained 1.5 mg/mL *Pa*PAM protein. The plates were sealed with Optical Quality Sealing Tape and centrifuged at 2000 rpm for 1 min. The plate was heated from 20 to 90°C in 1°C increments in of iCycler iQ Real Time PCR Detection System.

Activity assay

*Pa*PAM activity was determined by the conversion of (*S*)-*α*-Phe to (*S*)-*β*-Phe. Into the solution of *rac*-*α*-phenylalanine (2 mg) in TRIS buffer (100 mM, pH 8.0, 2 mL), wt-*Pa*PAM (0.8 mg) was added and the reaction mixtures was stirred at room temperature. A 100 µL sample was taken and the reaction was stopped by heating for 10 min at 90°C in the presence of a small amount of activated charcoal. After filtration, the sample was analyzed with high performance liquid chromatography (HPLC), using a Chiralpak ZWIX(+) column, and MeOH (50 mM formic acid and 100 mM diethyl amine): ACN:H_2O 49:49:2 (v/v/v) as eluent, respectively.

ACKNOWLEDGMENTS

AV thanks for the financial support of the Sectorial Operational Programme for Human Resources Development 2007-2013, co-financed by the European Social Fund, under the project POSDRU/159/1.5/S/137750 - “Doctoral and postdoctoral programs - support for increasing research competitiveness in the field of exact Sciences”. CP thanks for financial support from the Romanian National Authority for Scientific Research, CNCS – UEFISCDI (PN-II-IDPCE-2011-3-0799). This work was also supported by the Hungarian OTKA Foundation (Project NN-103242), by the New Hungary Development Plan (Project TÁMOP-4.2.2.B-10/1–2010–0009), by the Hungarian Research and Technology Innovation Fund (KMR 12-1-2012-0140) and by the EU COST (Action CM1303 “SysBiocat”).

REFERENCES

[1] K. Faber, Biotransformations in Organic Chemistry. A Textbook, 6th Edition, **2011**.
[2] B. Wu, W. Szymanski, C.G. Crismaru, B.L. Feringa, D.B. Janssen, in "*Enzyme Catalysis in Organic Synthesis"*. Eds. K. Drauz, H. Gröger, O. May, Wiley-VCH Verlag GmbH & Co. KGaA, **2012**, Vol. 2.
[3] B. Wu, W. Szymanski, S. de Wildeman, G.J. Poelarends, B.L. Feringa, D.B. Janssen, *Advanced Synthesis and Catalysis,* **2010**, *352,* 1409.
[4] M.J. MacDonald, G.B.D. Cunha, *Biochemistry and Cell Biol*ogy, **2007***, 85,* 273.
[5] J.A. Kyndt, T.E. Meyer, M.A. Cusanovich, J.J. Van Beeumen, *FEBS Letters*, **2002**, *512, 240.*
[6] M. Baedeker, G.E. Schulz, *European Journal of Biochem*istry, **2002**, *269,* 1790.
[7] H.A. Cooke, S.D. Bruner, *Biopolymers,* **2010**, *93,* 802.
[8] S. Strom, U. Wanninayake, N.D. Ratnayake, K.D. Walker and J.H. Geiger, *Angewandte Chemie,* **2012**, *124*, 2952.

[9] C. Paizs, A. Katona, J. Rétey, *Chemistry - A European Journal,* **2006**, *12*, 2739.
[10] C. Paizs, M.I. Toșa, L.C. Bencze, J. Brem, F.D. Irimie, J. Rétey, *Heterocycles,* **2010**, *82*, 1217
[11] A. Gloge, J. Zon, A. Kővári, L. Poppe, J. Rétey, *Chemistry A European Journal,* **2000**, *6*, 3386.
[12] K. Klettke, S. Sanyal, W. Mutatu , K.D. Walker, *Journal of the American Chemical Society*, **2007**, *129,* 6988.
[13] B. Wu, W. Szymanski, P. Wietzes, S. Wildeman, G.J. Poelarends, B.L. Feringa, D.B. Janssen, *ChemBioChem*, **2009**, *10*, 338.
[14] http://www.rcsb.org/pdb/workbench/showPrecalcAlignment.do?action= pw_fatcat_flexible&name1=3UNV.A&name2=3NZ4.A
[15] F. Baneyx, *Current Opinion in Biotechnology*, **1999**, *10*, 411.
[16] R.C. Mierendorf, B.B. Morris, B. Hammer, R.E. Novy, *Methods in Molecular Medicine,* **1998**, *13,* 257.
[17] http://www.yrbio.com/bioresource/sites/yrbio.com.bioresource/files/ document/vector/226410/c183-001.pdf
[18] J. Sambrook, D.W. Russell, Molecular Cloning a Laboratory Manual. 3rd Edition, New York: Cold Spring Harbor Laboratory Press, **2001**.
[19] H.M. Sadeghi, M. Rabbani, E. Rismani, F. Moazen, F. Khodabakhsh, K. Dormiani Y. Khazaei, *Research in the Pharmaceutical Science,* **2011**, *6*, 87.
[20] R.Y. Li, C.Y. Cheng. *Journal Bioscience and Bioengineering,* **2009**, *107,* 512.
[21] A. Vera, N. Gonzalez-Montalban, A. Aris, A. Villaverde, *Biotechnology and Bioengineering,* **2007**, *96,* 1101.
[22] J.A. Vasina, F. Baneyx, *Protein Expression and Purif*ication **1997**, *9,* 211.
[23] J. Crowe, H. Dobeli, R. Gentz, E. Hochuli, D. Stiber, K. Hence, *Methods in Molecular Biol*ogy, **1994**, 31, 371.
[24] T. Tanaka, M. Kubota, K. Samizo, Y. Nakajima, M. Hoshino, T. Kohno, E. Wakamatsu, *Protein Expression and Purif*ication, **1999**, *1,* 207.
[25] M.W. Pantoliano, E.C. Petrella, J.D. Kwasnoski, V.S. Lobanov, J. Myslik, E. Graf, T. Carver, E. Asel, B.A. Springer, P. Lane, F.R. Salemme, *Journal of Biomolecular Scree*ning **2001**, *6*, 429–440.
[26] J.E. Nettleship, J. Brown, M.R. Groves, A. Geerlof, *Methods in Molecular Biology*, **2008**, *426,* 299.

STUDIA UBB CHEMIA, LXI, 2, 2016 (p. 21-34)
(RECOMMENDED CITATION)

EXPRESSION AND PURIFICATION OF RECOMBINANT PHENYLALANINE AMMONIA-LYASE FROM *PETROSELINUM CRISPUM*

NORBERT ARTUR DIMA[a], ALINA FILIP[a], LÁSZLÓ CSABA BENCZE[a], MÁRK OLÁH[b], PÉTER SÁTORHELYI[c], BEÁTA G. VÉRTESSY[d,e], LÁSZLÓ POPPE[b,f*], CSABA PAIZS[a*]

ABSTRACT. In the present study the molecular cloning, expression and purification of recombinant *Pc*PAL, with a cleavable *N*-terminal His-tag is described. The *Pc*PAL gene was cloned into pET-19b vector and transformed to different *E.coli* host cells. The optimization of expression and purification processes provided recombinant protein with high purity in its native, tetrameric fold with a yield of 7-8 mg protein / 1 L culture. The activity of the recombinant protein was tested towards its natural substrate L-Phe, the K_M, and k_{cat} values suggesting excellent catalytic properties of the recombinant enzyme.

Keywords: *phenylalanine ammonia-lyase, Petroselinum crispum, molecular cloning, expression and expression optimization*

INTRODUCTION

In higher plants, phenylalanine ammonia-lyase catalyses the conversion of L-phenylalanine to *trans*-cinnamic acid, the first step of the phenylpropanoid pathway. This process produces many secondary metabolites that fulfill many essential functions for plants growth and development, such as mechanical

[a] *Babeş-Bolyai University, Faculty of Chemistry and Chemical Engineering, Arany János str. 11, RO-400028, Cluj-Napoca, Romania*
[b] *Department of Organic Chemistry and Technology Budapest University of Technology and Economics Műegyetem rkp. 3, H-1111 Budapest, Hungary*
[c] *Fermentia Ltd, Berlini u. 47-49., H-1045 Budapest, Hungary*
[d] *Department of Biotechnology and Food Sciences Budapest University of Technology and Economics Szt. Gellért tér 4, H-1111 Budapest, Hungary*
[e] *Institute of Enzymology Research Centre for Natural Sciences of Hungarian Academy of Sciences Magyar tudósok körútja 2, H-1117 Budapest, Hungary*
[f] *SynBiocat Ltd Lázár deák u 4/1, H-1173 Budapest, Hungary*
[*] *Corresponding authors: poppe@mail.bme.hu; paizs@chem.ubbcluj.ro*

support, pigment and flavonoid production [1,2]. PAL, the first enzyme involved in the metabolism of phenylpropanoid derivatives, has been extensively studied for its crucial function as a branch point between primary and secondary metabolism [3,4].

The currently known aromatic ammonia-lyases use an auto-catalytically formed 5-methylene-3,5-dihydro-imidazole-4-one (MIO) electrophilic prosthetic group, and show high structural and sequence similarities [5].

The recent advances in improving the functional properties of these enzymes increased both their biocatalytic and therapeutic applications. Sufficiently stable phenyalanine ammonia-lyases (PALs) are used in enzyme replacement therapy [6] of phenylketonuria (PKU) [7], or as a potential therapeutic enzyme in cancer treatment [8]. DSM company incorporated a recombinant PAL into the chemoenzymatic synthesis of (*S*)-2-indolinecarboxylic acid [9], a key intermediate for hypertension pharmaceuticals; while BASF (Germany) recently patented [10] hydroamination reactions catalyzed by recombinant PALs originating from *Petroselinum crispum* (*Pc*PAL) and *Rhodoturula glutinis* (*Rg*PAL). In the academic area the substrate scope of *Pc*PAL was expanded to several aryl-, heteroaryl alanines [11,12,13] and even to the non-aromatic propargylglycine [14]. Furthermore the immobilization of *Pc*PAL on single-walled carbon nanotubes [15] and magnetic nanoparticles [14,16] provided their successful employment for the synthesis of non-natural amino acid in continuous-flow microreactors. Therefore the importance of the large-scale production of recombinant *Pc*PAL gained increased attention. Herein we describe the molecular cloning, expression, purification and large scale production of *Pc*PAL. The purity, oligomerization state and the activity of the isolated enzyme suggest its correct, native-like tetrameric folding [17].

RESULTS AND DISCUSSION

Molecular cloning of recombinant *Pc*PAL

Based on the sequence of *Pc*PAL (PDB code: 1W27) we designed a codon optimized gene sequence for expression in *E.coli* and for directional cloning into the pET-19b vector, using *XhoI* and *BpuI1102I* cloning sites.

The designed gene sequence was obtained through gene synthesis services, and was cloned successfully into the expression vector, obtaining the novel recombinant plasmid encoding *Pc*PAL (**Figure 1a**) with an *N*-terminal His_{10}-tag and an enterokinase cleavage site, serving for the His-tag removal ulterior to protein purification. The recombinant plasmid was transformed through

heat-shock into different *E.coli* competent cells in order to optimize the expression yields. The successful outcome of the cloning and transformation step was determined by agarose gel electrophoresis (**Figure 2**).

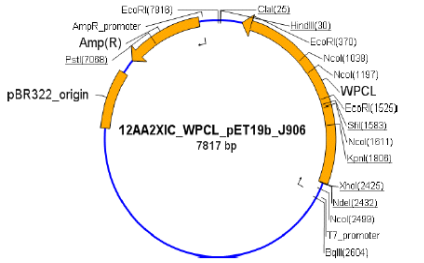

MGHHHHHHHHHHSSGHIDDDDKHMLEMENGNGATTNGHVNGNGMDFCMKT
EDPLYWGIAAEAMTGSHLDEVKKMVAEYRKPVVKLGGETLTISQVAAISA
RDGSGVTVELSEAARAGVKASSDWVMDSMNKGTDSYGVTTGFGATSHRRT
KQGGALQKELIRFLNAGIFGNGSDNTLPHSATRAAMLVRINTLLQGYSGI
RFEILEAITKFLNQNITPCLPLRGTITASGDLVPLSYIAGLLTGRPNSKA
VGPTGVILSPEEAFKLAGVEGGFFELQPKEGLALVNGTAVGSGMASMVLF
EANILAVLAEVMSAIFAEVMQGKPEFTDHLTHKLKHHPGQIEAAAIMEHI
LDGSAYVKAAQKLHEMDPLQKPKQDRYALRTSPQWLGPQIEVIRSSTKMI
EREINSVNDNPLIDVSRNKAIHGGNFQGTPIGVSMDNTRLAIAAIGKLMF
AQFSELVNDFYNNGLPSNLSGGRNPSLDYGFKGAEIAMASYCSELQFLAN
PVTNHVQSAEQHNQDVNSLGLISSRKTSEAVEILKLMSTTFLVGLCQAID
LRHLEENLKSTVKNTVSSVAKRVLTMGVNGELHPSRFCEKDLLRVVDREY
IFAYIDDPCSATYPLMQKLRQTLVEHALKNGDNERNLSTSIFQKIATFED
ELKALLPKEVESARAALESGNPAIPNRIEECRSYPLYKFVRKELGTEYLT
GEKVTSPGEEFEKVFIAMSKGEIIDPLLESLESWNGAPLPIS

Figure 1. The genetic map of the created recombinant plasmid containing the gene encoding *Pc*PAL and the amino acid sequence of the designed recombinant *Pc*PAL.

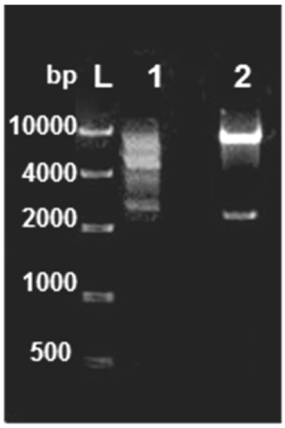

Figure 2. Agarose gel electrophoresis. L: DNA Ladder, 1. circular plasmid DNA, extracted from colonies obatined after transformation in Rosetta (DE3) pLysS cells, 2. Plasmid DNA from 1, digested with restriction enzymes *XhoI* and *Bpu1102I*.

Optimization of *Pc*PAL overexpression in *E.coli*

Further we performed the optimization of overexpression in *E.coli*, studying the influence of the nature of host cells (*E.coli* Rossetta, BL21, C41 all with (DE3), pLysS modifications), of the inducer (IPTG) concentration and of the temperature upon the expression levels of the *Pc*PAL. Varying the concentration of IPTG, expression of proteins can be regulated at different levels, lower level expression can increase the solubility and activity of the target proteins [18] For the optimization of *Pc*PAL expression, the effect of different concentrations of inducer (0.1, 0.5 and 1 mM IPTG) was tested on the growing culture of BL21(DE3)pLysS containing the pET-19b-*Pc*PAL recombinant plasmid and the cells before and after induction were analyzed by SDS-PAGE. No significant difference was observed in the *Pc*PAL protein expression levels of the differently induced cells, therefore the lowest 0.1 mM IPTG concentration was used in further experiments.

The effect of the nature of host *E.coli* cells proved to be crucial, in BL21 and C41 the yields of the isolated protein were low, while in Rosetta 20-30 mg *Pc*PAL / liter ferment was obtained. This might be due to the fact that Rosetta encodes for a larger number of rare-codons than BL21 and C41 [19], providing successful translation of the recombinant gene.

To evaluate the effect of growth temperature on the expression of *Pc*PAL after induction, the cultures were incubated at different temperatures (18, 25, and 37°C). Initially the cell cultures were incubated at 37°C. After the density of cells reached OD_{600} ~0.6 (approx. 4 h) the temperature was reduced (to 18 or 25°C) and the cultures were induced with 0.1 mM IPTG. The density of the cells was monitored in time (**Figure 3**), the maximum yield of enzyme being obtained in case of 25°C incubation temperature, with an optimal post-induction time of 12-14 h, where the cell growth reaches the stationary phase.

Therefore the optimal overexpression conditions *E.coli* Rosetta (DE3)pLysS as host strain, 0.1 mM IPTG and 25°C fermentation temperature were further used for the large scale (10 L) production of the enzyme.

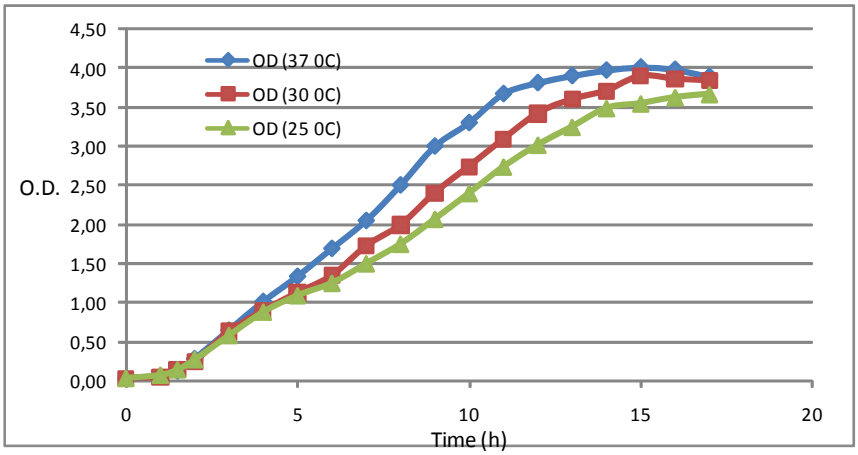

Figure 3. Effect of growth temperature on the expression of *Pc*PAL.

Production, purification and characterization of recombinant *Pc*PAL

After overexpression optimization, the production and purification of the recombinant *Pc*PAL protein was performed. The *N*-terminal $(His)_{10}$-tag of the protein allows affinity purification with Ni-NTA resin. Ni–NTA affinity chromatography is a rapid and easy purification technique for proteins fused with His-tag at either ends (*N*- or *C*-terminus). The strong binding between

His-tag and the immobilized nickel ions allows easy washing and efficient elution of bounded His-tagged protein by competition with imidazole [20].

Performing the Ni-NTA purification, the protein fraction eluted with 250 mM imidazole, besides the *Pc*PAL protein (81 kDa), contains additional proteins with lower molecular weight (**Figure 4**, lane 6). Despite our optimization efforts (varying the imidazole concentration of the elution buffer, introducing intermediate washing steps with high and low salt concentration buffers, according to the manufacturer description [21]) the protein purity, determined by SDS-PAGE remained below 80%.

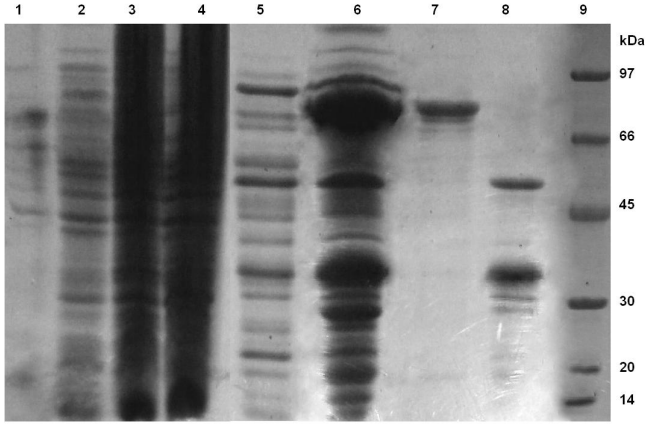

Figure 4. SDS-PAGE gel containing samples from the purification steps of *Pc*PAL: 1: before induction; 2: after induction; 3: supernatant after centrifugation of the lysate; 4: flow through after application; 8: low salt; 5: 25mM fraction of imidazole; 6: 400mM fraction of imidazole; 7: fraction eluted at 10-12 mL from the column; 8: fraction eluted at 14-16 mL from the column; 9: marker. Samples were prepared as described in the experimental section.

In order to increase the purity of the isolated *Pc*PAL we introduced additional chromatographic purification steps. Due to the large difference in the molecular weights of the target protein and of the other, unwanted protein impurities we opted for size-exclusion chromatography, using a Superdex 200 10/300 GL. This chromatography step also allows the determination of the oligomerization state of the protein, and thus the homogeneity of the isolated protein [22]. This is crucial since different oligomerization states of the same protein (including aggregated forms of the protein) on SDS-PAGE cannot be distinguished, they migrate at the same molecular weight corresponding to the monomer however their enzyme activity can significantly differ. Thus, besides the separation of the protein impurities, the SEC method will provide additional results related to the correct, native-like oligomerization state of the isolated protein.

Performing the SEC purification of the fraction eluted with 250 mM imidazole from the Ni-NTA column, several protein peaks were eluted (**Figure 5**). The identity of the protein peaks eluted was determined by SDS-PAGE (**Figure 4**, lane 7-8). These results show that the protein fractions eluted at 8.4 and 11.2 mL retention volumes are pure *Pc*PAL proteins, presumably having different oligomerization states. In order to determine the molecular weight determination by SEC the comparison of an elution volume parameter, such as K_{av} of the protein of interest, with the values obtained for several known calibration standards (**Table 1**) should be done [23].

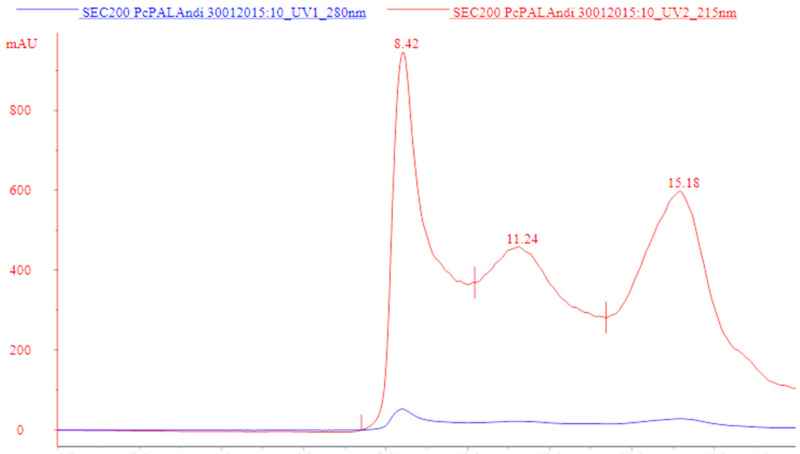

SEC200 PcPALAndi 30012015:10_UV2_215nm@02,PEAK1

No	Ret ml	Area mAU*ml	Height mAU
1	-2.02	0.0928	10.989
2	-1.86	37.0035	38.647
3	8.42	1152.3995	946.250
4	11.24	1191.1324	459.374
5	15.18	1512.1388	598.230
6	18.45	87.8232	148.133

Figure 5. Purification of *Pc*PAL on Superdex 200 10/300 GL size-exclusion column.

Thus the molecular weight of an unknown protein can be determined from the calibration curve (**Figure 6**, plot of K_{av} versus the logarithm of molecular weight) once its K_{av} value is calculated from its measured elution volume [23].

Accordingly the molecular weight of the *Pc*PAL protein fractions eluted were estimated to be 355 kDa for the peak eluted at 11,2 mL and > 600 kDa for the fraction eluted at 8,4 mL, corresponding to the presumed native tetrameric and higher oligomerization states (octameric or even higher aggregated forms) of the protein, respectively.

Table 1. Elution volume parameters K_{av} of standard globular proteins used for the calibration curve set-up

Protein standard	Mol. weight (Da)	Volume of elution (V_e) (mL)	K_{av}*	Log_{MW}
Thyroglobulin	669000	8,26	0,074	5,83
Ferritin	440000	10,56	0,209	5,64
Aldolase	158000	12,38	0,316	5,20
BSA	67000	13,9	0,406	4,83
Ovalbumin	45000	15,08	0,475	4,65
Chimotrypsinogen A	25000	17,21	0,601	4,40

- **$K_{av} = (V_e-V_o)/(V_c-V_o)$; V_c = 24 mL (column volume); V_o = 8.1 mL (column void volume)**

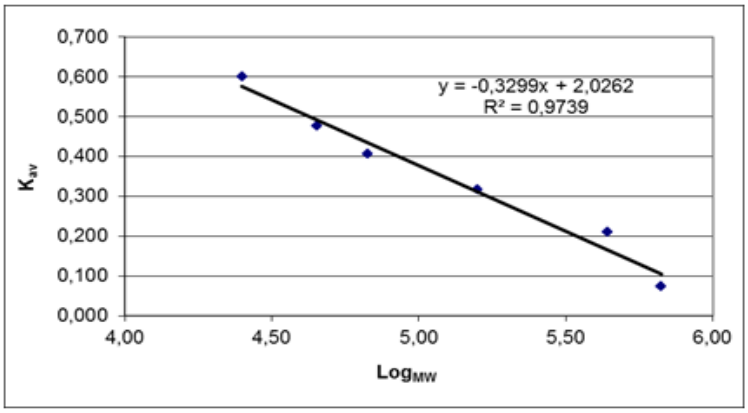

Figure 6. Calibration curve for Superdex 200 10/300 GL column. Resolution range of the column is 10-600 kDa.

Furthermore we compared the enzyme activities of the presumed largely aggregated and tetrameric forms of *Pc*PAL, separated by size-exclusion chromatography, towards the natural substrate L-Phe. Performing the experiment at 1 mM substrate concentration, we observed three times higher activity for the presumed native, tetrameric form of the protein.

$$\frac{v_{tetramer}}{v_{aggregate}} = \frac{3{,}409 * 10^{-2}[\frac{\mu M}{s}]}{1{,}149 * 10^{-2}[\frac{\mu M}{s}]} \cong 3$$

These results directed us to optimize the isolation and purification procedure in order to achieve high yields for the production of the *Pc*PAL tetramer. The presence of higher oligomerization states of the protein might be the results of aggregation processes, caused by the presence of free thiol

groups, able to form intermolecular disulphide bridges, or hydrophobic aggregation processes, caused by high protein or salt concentration in the solution [24]. Furthermore the removal of the 35 kDa protein impurity during isolation steps is also preferable for yield and purity increasements. This protein band coelutes with *Pc*PAL at the Ni-affinity purification step, furthermore during longer incubation times (>4 hours) its amount increases in the protein sample (checked by SDS-PAGE), suggesting that it is *Pc*PAL fragment, containing the *N*-terminal His_{10}-tag, obtained by proteolytic degradation.

Therefore in order to alleviate these problems several modification were introduced in the isolation and purification protocol: *i*) the imidazole concentration used for the elution at the Ni-affinity chromatography was decreased, *ii*) the concentration steps of the solutions with high imidazole content were avoided, performing the protein concentration step after the removal of the imidazole with SEC chromatography or dialysis, *iii*) the use of protease inhibitor cocktail (mini-tablets from Roche) during all isolation and purification steps. These modifications provided an optimal isolation and purification procedure for the recombinant *Pc*PAL, resulting in protein with high purity (> 95% on SDS-PAGE, **Figure 8**) and presumable in its native, tetrameric fold (**Figure 7**).

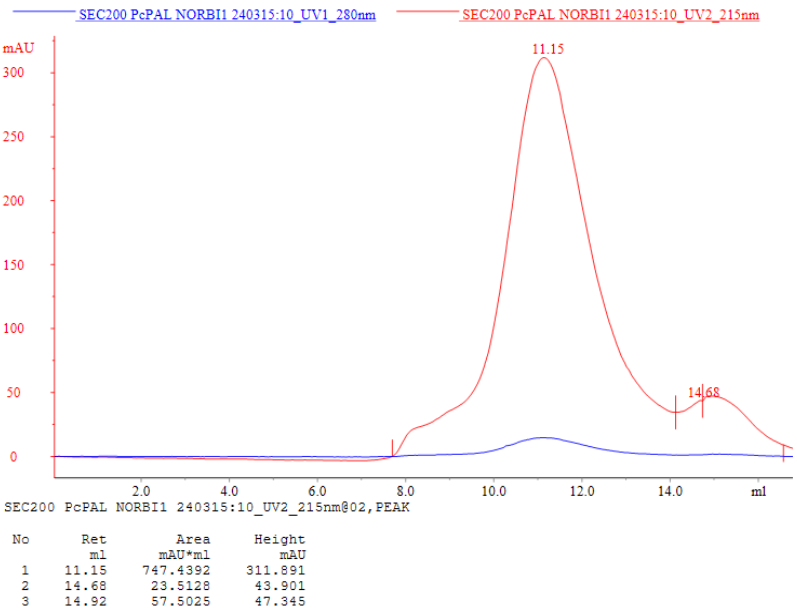

Figure 7. FPLC chromatogram of the pure tetramer obtained with the optimized procedure.

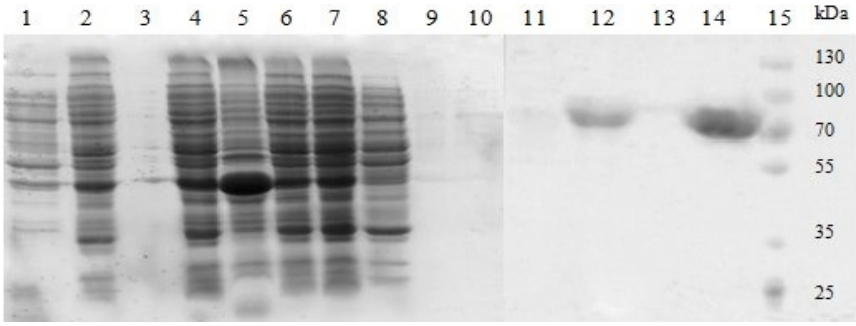

Figure 8. SDS-PAGE gel containing samples from the purification steps of *Pc*PAL: 1: before induction; 2: after induction; 3: supernatant of cells; 4: cell lysate 5: pellet of the cell lysate; 6: supernatant after centrifugation of the lysate; 7: flow through after application; 8: low salt; 9: high salt; 10: low salt; 11: 25mM fraction of imidazole; 12: 400mM fraction of imidazole (pure elute); 13: 1M fraction of imidazole; 14: fraction eluted at 10-12 mL from the column and 15: marker. Samples were prepared as described in the experimental section.

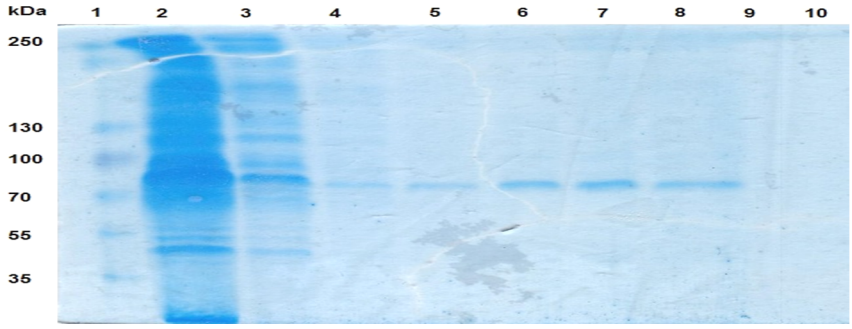

Figure 9. SDS-PAGE gel containing samples from the purification steps of *Pc*PAL with the support Dv1000-EDTA-La: 1: marker; 2: flow through after application; 3: low salt; 4: high salt; 5: low salt; 6: 5 mM fraction of EDTA 7: 25 mM fraction of EDTA; 8: 50 mM fraction of EDTA; 9: 100 mM fraction of EDTA; 10: empty. Samples were prepared as described in the experimental section.

Besides the commercially available Qiagen Ni-NTA affinity chromatography resin another silica based support was investigated with the optimized purification procedure of $(His)_{10}$-tagged *Pc*PAL. This product allows purification of recombinant proteins through its high surface area (>100 m^2/g) and mesoporous structure (100 nm) in addition strong binding capability between the His-tag and EDTA-immobilized lanthanum ions. The purification method was performed in batch mode by shaken the suspension of support (Dv1000-EDTA-La) and supernatant of the centrifuged cell lysate. Thereafter the nonspecific proteins were desorbed by buffers (**Figure 9**,

lane 3-4) and the target protein, *Pc*PAL was eluted by gradient elution with different concentration of EDTA solutions and given in high purity (> 95% on SDS-PAGE, **Figure 9**, lane 6-8). The purity and yields of the isolated protein were in similar range as those obtained from the Ni-NTA affinity purification (7-8 mg protein / 1 L culture).

Further we determined the activity of the recombinant *Pc*PAL towards its natural substrate L-Phe and compared the values with those obtained in the literature [6,7,8,14].

The activity measurements were performed by UV-monitoring the production of acrylic acid at 290 nm. The obtained K_M value of 116 ± 4 and k_{cat} value of 1±0.05 were highly reproducible and suggested better catalytic properties of the enzyme than those described in the literature [11,12,25]. The Michaelis-Menten plot of the measurement using the purified enzyme is shown at **Figure 10**. The K_M, v_{max} and k_{cat} values were determined using the Lineweaver-Burk plot (**Figure 11**).

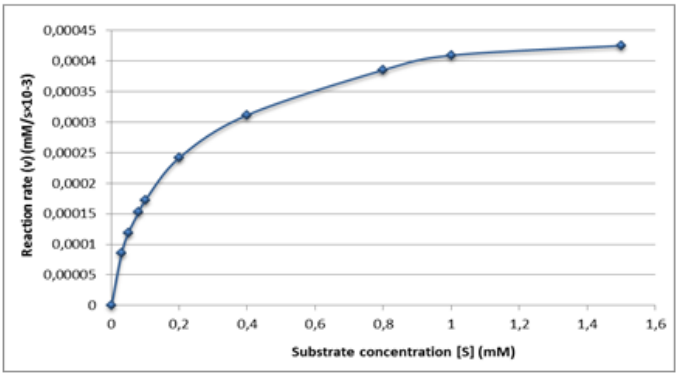

Figure 10. Michaelis-Menten curve on different concentrations of L-Phe.

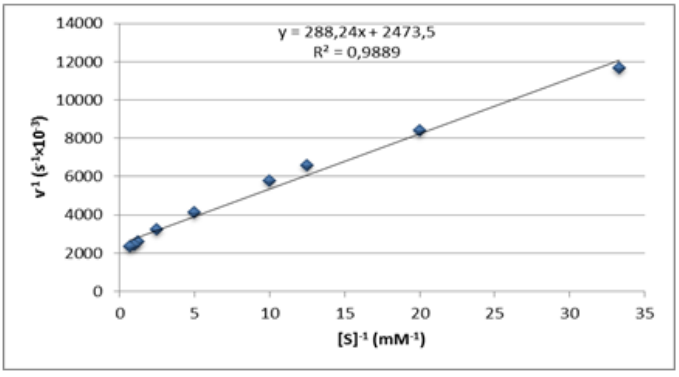

Figure 11. Lineweaver-Burk plot of the kinetic measurement.

CONCLUSIONS

During this study we report the successful cloning, expression and isolation of recombinant *Pc*PAL with a removable *N*-terminal His_{10}-tag. The oligomerization state of the expressed protein was determined with size-exclusion chromatography and suggested that the tetrameric *Pc*PAL is the most active oligomerization form. Optimization of the isolation and purification protocol provided pure, homogeneous *Pc*PAL tetramer, with excellent and reproducible catalytic activities.

EXPERIMENTAL SECTION

Materials and methods

IPTG, tetracycline, chloramphenicol, carbenicillin, imidazole, Tris,HCl, phenylalanine, LB medium, tryptone, yeast extract, NaCl, KCl, NaH_2PO_4, Na_2HPO_4, EDTA, SDS, TEMED, glycerol, β-mercaptoethanol, Coomassie Brilliant Blue, FastRuler™ High Range DNA Ladder, Lysozyme, DNAse, RNAse are reagents used in experiments and were purchased from companies Sigma, Aldrich, Carl Roth GmbH, Poch, Liofilchem or ThermoFischer. The gel filtration calibration protein kit were purchased from GE Healthcare, while the Complete Protease Inhibitor Cocktail Tablets from Roche. *E. coli* host strains, XL1-Blue, BL21(DE3)pLysS, Rosetta (DE3)pLysS and C41(DE3)pLysS were purchased from Novagen.

The kinetic measurements were performed on a Varian Cary 50 and on an Agilent 8453 UV-Vis Spectrophotometer. The gel filtration purifications were made on a Äkta purifier fast protein liquid chromatograph with autofractioner.

Molecular cloning and expression optimization

The gene encoding phenyalanine ammonia-lyase from *Petroselinum crispum* has been codon optimized for bacterial expression in *E. coli*. (**Figure 2**). The synthetic gene produced by Life Technologies was introduced into the pET-19b vector using the *XhoI* and *Bpu1102I* cloning sites, for expression with an *N*-terminal $(His)_{10}$-tag and an enterokinase cleavage site, for His-tag removal.

The obtained plasmid was transformed in *E.coli* XL1-Blue competent cells by heat shock as well as in different *E.coli* host strains (Rosetta (DE3)pLysS, BL21(DE3)pLysS, C41(DE3)pLysS) in order to optimize the expression yields.

Different concentrations of IPTG (0.1 mM, 0.5 mM and 1 mM) and different fermentation temperatures (25°C, 30°C and 37°C) were tested during the expression optimization.

Expression and production of the recombinant *Pc*PAL – optimized procedure

The recombinant plasmids which contains a *N*-terminal $(His)_{10}$-tag were produced in *E. coli* Rosetta(DE3)pLysS cells using LB media supplemented with the carbenicillin and chloramphenicol.

Batch mode fermentation: First a preculture was prepared by the inoculation of 100 mL of sterile LB medium, containing carbenicillin (50 µg/mL) and chloramphenicol (30 µg/mL) with the bacterial cells from the agar plate, followed by overnight incubation at 37°C and shaking at 200 rpm. 8 × 0.5 L of LB medium (in 2 L flasks) was inoculated with 2% (v/v) of the preculture and grown at 37°C, 200 rpm until OD_{600} reached 0.7-0.8. Protein expression was induced *via* the addition of 0.1 mM IPTG, and the cell growth was maintained at 25°C for another 12 h, reaching an OD_{600} value of 3.4-3.6

Large scale fermentation of the recombinant PcPAL: ten litres of Terrific broth (TB) medium were sterilized at 121°C, 1.2 bar for 25 min. After sterilization, the media was cooled down to 37°C and ampicillin was added to the fermentation broth for a final concentration of 100 µg/mL. The fermentation media was inoculated with 100 mL of the overnight seed culture of the *E. coli* producer strain. The following fermentation parameters were set up: temperature at 37°C, agitation 300 rpm, overpressure 0.2-0.5 bar and bottom air inlet 5 L/min. The pH value of the fermentation broth was controlled at pH 7.1±0.1. The dissolved oxygen (DO) value was set to a minimum of 30% and was controlled by the stirring speed. When the OD_{600} of the culture reached 0.8±0.1, the temperature was set to 25°C and the culture was induced with IPTG (0.1 mM final concentration). The fermentation broth was harvested after 21 h, when the culture reached the stationary growth phase.

*Purification of the recombinant Pc*PAL – optimized procedure

Cells were harvested by centrifugation (30 min, 2000 × g, 4500 rpm); followed by their resuspension (with vortex and pipetting) in 100 mL lysis buffer (50 mM Tris.HCl, 300 mM NaCl, 0.5 mM EDTA; pH 8) supplemented with RNAse (3 mg), Lysozyme (10 mg), PMSF (20 mg/ 1 mL EtOH) and one tablet from the protease inhibitor cocktaile of Roche. The cells were lysed by sonication (2 sec pulse, 40% intensity, 30 min, T < 20 ^{0}C) and the cell debris, respectively membrane fractions were removed by centrifugation (24000 × g, 15000 rpm, 35 min). The supernatant was loaded on Ni-NTA affinity chromatography, using appoximately 2 mL of Ni-NTA superflow resin from Qiagen and using the protocol described by the manufacturer. The *Pc*PAL protein with the *N*-terminal His-tag eluted with the 400 mM imidazole fraction. The protein was 4 × fold concentrated through amicons with 10 kDa cut-off, followed by their further purification with size-exclusion chromatography, using Superdex 200 10/300 GL column and 20 mM Tris,150 mM NaCl, pH 7.5 buffer as eluent. The

homotetrameric protein eluted at 10.5-12 mL retention volumes. The protein was stored until further use at -20 ^{0}C, with 10% glycerol.

***Purification with Dv1000-EDTA-La support* – alternative procedure**

The Dv1000-EDTA-La [26] support (100 mg) was dispersed in 1 mL lysis buffer (50 mM Tris.HCl, 300 mM NaCl, 0.5 mM EDTA, pH 8.0) and the suspension was shaken (10 min, 350 rpm). Thereafter 1 mL of centrifuged supernatant of cell lysate was added and shaken further (30 min, 350 rpm). This suspension was centrifuged (3 min, 3500 rpm) and the supernatant was removed. Then the support was shaken (10 min, 350 rpm) with the following solutions and between two fractions the supernatant was removed after centrifugation: low salt buffer (50 mM HEPES, 30 mM KCl, pH 7.5), high salt buffer (50 mM HEPES, 300 mM KCl, pH 7.5), low salt buffer and four different concentration ethylenediaminetetraacetic acid disodium dihydrate solutions (5, 25, 50, 100 mM of disodium salt of EDTA and 50 mM HEPES, 30 mM KCl, pH 8.0). The fractions were investigated by SDS-PAGE.

SDS-PAGE electrophoresis was performed according to the Laemmli-protocol [27] using acrylamide gels.

Samples were taken for every step of the expression and purification stage and prepared by denaturation at 95°C for 5-10 min with addition of reducing 3x sample buffer.

Enzyme activity measurements: Activity of *Pc*PAL was determined spectrophotometrically by monitoring the production of *trans*-cinnamic acid at 290 nm for 10 min, using Quartz cuvettes of 1.4 mL. The measurements were performed at 37°C for 10 min, in presence of 30 µg of enzyme, varying the substrate concentration between 0.03-1.5 mM. Kinetic constants (K_M and v_{max}) were obtained by determining the initial rate of reactions at different substrate concentrations. The extinction coefficient (ε) was determined in 0.1 M Tris-buffer (pH 8.8) at 290 nm: ε_{290}=8.8 $mM^{-1}\times s^{-1}$.

ACKNOWLEDGMENTS

This work was possible due to the financial support of the Sectorial Operational Program for Human Resources Development 2007-2013, co-financed by the European Social Fund, under the project number POSDRU/159/1.5/S/ 132400 with the title „Young successful researchers – professional development in an international and interdisciplinary environment”. This work was also supported by the Romanian National Authority for Scientific Research and Innovation, CNCS-UEFISCDI, project number PN-II-RU-TE-2014-4-1668, by the Hungarian OTKA Foundation (Project NN-103242), by the New Hungary Development Plan (Project TÁMOP-4.2.2.B-10/1–2010–0009), by the Hungarian Research and Technology Innovation Fund (KMR 12-1-2012-0140) and by the EU COST (Action CM1303 “SysBiocat”).

REFERENCES

[1] M. WenLi, W. Min, R. ZhuMei, Z. Yang, *Plant Cell Reports*, **2013**, *32*, 1179.
[2] G. Jihai, et al., *Molecular Biology Reports*, **2012**, *39*, 3443.
[3] T. Vogt, *Molecular Plant*, **2010**, *3*, 2.
[4] C.M. Fraser, C. Chapple, *The Arabidopsis Book*, **2011**, e0152.
[5] L. Poppe, J. Rétey, *Current Organic Chemistry*, **2003**, *7*, 1297.
[6] C. W. Abell, D. S. Hodgins, W. J. Stith, *Cancer Research*, **1973**, *33*, 2529.
[7] A. Belanger-Quintana, A. Burlina, C.O. Harding, A.C. Muntau, *Molecular Genetics and Metabolism,* **2011**, *104*(Suppl), S19.
[8] O.O. Babich, V.S. Pokrovsky, N.Y. Anisimova, N.N. Sokolov, A.Y. Prosekov, *Biotechnology and Applied Biochemistry*, **2013**, *60*, 316.
[9] B. de Lange, D.J. Hyett, P.J.D. Maas, D. Mink, F.B.J. van Assema, et al., *ChemCatChem,* **2011**, *3*, 289.
[10] B. Hauer, N. Schneider, D. Drew, K. Ditrich, N. Turner, B.M. Nestl, *US patent*, **2012**, US2012/0123155A1.
[11] A. Gloge, J. Zon, A. Kővári, L. Poppe, J. Rétey, *Chemistry - A European Journal,* **2000**, *6*, 3386.
[12] C. Paizs, A. Katona, J. Rétey, *Chemistry - A European Journal,* **2006**, *12*, 2739.
[13] C. Paizs, A. Katona, J. Rétey, *European Journal of Organic Chemistry,* **2006**, 1113.
[14] D. Weiser, L.C. Bencze, G. Bánóczi, F. Ender, R. Kiss, E. Kókai, A. Szilágyi, B.G. Vértessy, O. Farkas, C. Paizs, L. Poppe, *ChemBioChem*, **2015**, *16*, 2257.
[15] J.H. Bartha-Vári, M.I. Toşa, F.D. Irimie, D. Weiser, Z. Boros, B.G. Vértessy, C. Paizs, L. Poppe, *ChemCatChem*, **2015**, *7*, 1122.
[16] F. Ender, D. Weiser, B. Nagy, L.C. Bencze, C. Paizs, P. Pálovics, L. Poppe, *Journal of Flow Chemistry*, **2016**, *6(1)*, 43–52.
[17] H. Ritter, G.E. Schultz, *Plant Cell*, **2004**, *16*, 3426.
[18] J. Sambrook, D.W. Russell, Molecular Cloning a Laboratory Manual. 3rd Edition, New York: Cold Spring Harbor Laboratory Press, **2001**.
[19] Novagen, User Protocol TB009 Rev. F 0104, 1.
[20] J. Crowe, H. Dobeli, R. Gentz, E. Hochuli, D. Stiber, and K. Hence, *Methods in Molecular Biol*ogy, **1994**, *31*, 371.
[21] Ni-NTA Agarose Purification of 6xHis-tagged Proteins from *E. coli* under Native Conditions, Quick-Start Protocol, Qiagen, **2011.**
[22] E.R.S. Kunji, M. Harding, P.J.G. Butler, P. Akamine, *Methods*, **2008,** *46*, 62.
[23] GE Healthcare - *Gel Filtration Calibration Kits*, Product booklet.
[24] M. Lebendiker, T. Danieli, *FEBS Letters,* **2014**, *588*, 236.
[25] a) D. Röther, L. Poppe, G. Morlock, S. Viergutz, J. Rétey, *European Journal of Biochemistry*, **2002**, *269*, 3065; b) L. Poppe, J. Rétey, *Angewandte Chemie International Edition*, **2005**, *44*, 3668; c) S. Bartsch, U.T. Bornscheuer, *Protein Engineering, Design & Selection*, **2010**, 1; d) M.I. Toşa, J. Brem, A. Mantu, F.D. Irimie, C. Paizs, J. Rétey, *ChemCatChem*, **2013**, *5*, 779; e) S.L. Lovelock, N.J. Turner, *Bioorganic & Medicinal Chemistry*, **2014**, *22*, 5555.
[26] L. Poppe, Z. Boros, B.G. Vértessy, K. Kovács, A. Tóth, G. Hornyánszky, J. Nagy, B. Erdélyi, V.E. Bódai, P. Sátorhelyi., *WO* 179072 A1, **2013**.
[27] U.K. Laemmli, *Nature*, **1970**, *227*, 680.

STUDIA UBB CHEMIA, LXI, 2, 2016 (p. 35-46)
(RECOMMENDED CITATION)

PRODUCTION OF CHEMICALS WITH GENETICALLY MODIFIED *ESCHERICHIA COLI* STRAINS FROM RENEWABLE RESOURCES

ANDREA FAZAKAS[a], ERIKA CSATÓ-KOVÁCS[a], ZSOLT BODOR[a], SZABOLCS LÁNYI[a,b*], BEÁTA ÁBRAHÁM[a]

ABSTRACT. The main aim of this study was to create mutant strains with lambda Red recombination system from an *Escherichia coli* strain which was isolated from animal faeces. *E. coli* Ter8/1 strain was genetically modified using lambda Red recombination system and two mutant strains were obtained, TerP01, in which the gene of pyruvate formate lyase was inactivated, and TerPL02, in which the genes of pyruvate formate lyase and lactate dehydrogenase were inactivated. The analysis of product formation in dual-phase fermentation and in minimal salts medium with three carbon sources was performed. The first mutant, TerP01, produced a large amount of lactic acid with small amount of byproduct formation. In the case of the second mutant, TerPL02, lactic acid production has been finished and succinic acid production increased significantly.

Keywords: *Escherichia coli, lambda Red recombination system, fermentation, glycerin, glucose, xylose*

INTRODUCTION

A large part of chemicals are derived from crude oil. Depletion of the earth's fossil energy resources, increasing prices and the adverse environmental effects of oil-based industries have given reasons to develop the production of bio-based chemicals from renewable feedstocks [1, 2]. In many cases, biosynthesis of chemicals is uneconomical, because the product yield and productivity are very low. Metabolic engineering provides a solution to these problems [3].

[a] *Sapientia Hungarian University of Transylvania, Faculty of Science, Department of Bioengineering, Piața Libertății Nr. 1, Miercurea Ciuc, RO-530104, Romania, andrea_iuhasz@yahoo.com*
[b] *Politehnica University of Bucharest, Faculty of Applied Chemistry and Material Science, Splaiul Independenţei Nr. 313, sector 6, RO-060042, Romania*
[*] *Coresponding author: lanyiszabolcs@sapientia.siculorum.ro*

An effective and commonly used tool of metabolic engineering is the lambda Red recombination system. This system, developed by Datsenko and Wanner, is an efficient method for preparing insertions, deletions and point mutations in the bacterial chromosomes [4]. The lambda Red system consists of three genes: Gam, Exo and Bet. This three genes encoding the major proteins, which are involved in the process [4, 5]. The first protein is Gam protein which inhibits the RecBCD and SbcCD nuclease activities, protecting linear DNA fragments from degradation [6-8]. The second protein is Exo which has a 5' to 3' double-stranded DNA (dsDNA) exonuclease activity and degrades dsDNA in the 5' to 3' direction generating 3'-ended overhangs [7, 9, 10]. The third protein is Beta which binds stably to the single-stranded DNA (ssDNA) and promotes annealing of two complementary DNA molecules and thereby promotes recombination [6-8]. Ellis et al. [10] demonstrated that Beta is the only protein which is required for recombination with ssDNA.

The recombineering method developed by Datsenko and Wanner has four main steps: (1) creating of a selectable antibiotic resistance gene by polymerase chain reaction (PCR) using primers, which are homologous to the target chromosomal gene, (2) transformation of the strain with a helper plasmid which contains the lambda Red genes, (3) electroporation of the PCR product into the host cell, where the recombination occurs between the target gene and the antibiotic resistance cassette and (4) elimination of the antibiotic resistance cassette [4].

Many researchers have also used this recombination method in order to develop a bacterial strain, which is able to produce chemicals in high yields, mostly in *E. coli* strains [11-13], but has also been used in other microorganisms, such as *Pseudomonas* [14] or in *Salmonella* strains [9].

In this paper, we have been developed a genetically engineered *E. coli* Ter8/1 strain, which was previously isolated from animal faeces by our team [15]. We was successfully used the lambda Red recombination system resulting two mutant strains, *E. coli* TerP01 and TerPL02, in which the pyruvate formate lyase (*pfl*) and pyruvate formate lyase together with lactate dehydrogenase (*ldh*) were knocked out and the fermentation of different carbon sources with these mutant strains have been examined.

RESULTS AND DISCUSSION

The wild-type *E. coli* strain Ter8/1 produced a mixture of acids during the fermentation from different carbon sources (Table 1). As we can see in Table 1, the main product was formic acid for all carbon sources used. In the case of glycerol, no lactate was detected, a small amount of acetate and

succinate were produced. With xylose and glucose, in addition to the acetate and succinate, a small amount of lactate was produced. Therefore, in order to alter the metabolic pathway to another useful product, the *pflB* gene was knocked out at first, thus preventing the production of formic acid (Figure 1). The elimination of *pflB* gene from the chromosomes of *E. coli* Ter8/1 strain was previously published [16]. This *E. coli* Ter8/1 *pflB* mutant is designated TerP01.

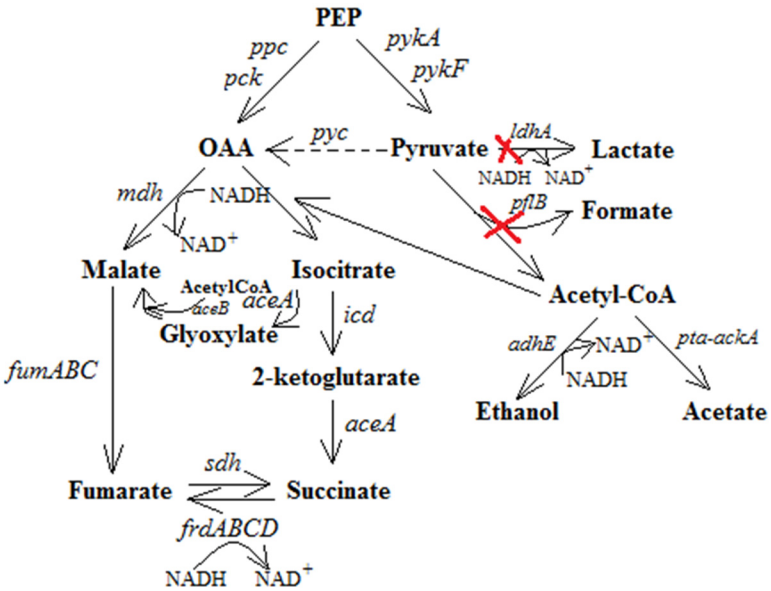

Figure 1. A simplified illustration of metabolic pathways from phosphoenolpyruvate (PEP) to fermentation products in *E. coli*. The genes inactivated in this study are illustrated by red cross bars (pyruvate formate lyase, lactate dehydrogenase). OAA, oxaloacetate; *ppc*, phosphoenolpyruvate carboxylase; *pck*, phosphoenolpyruvate carboxykinase; *pykA* and *pykF*, pyruvate kinases; *pyc*, pyruvate carboxylase; *ldhA*, lactate dehydrogenase; *mdh*, malate dehydrogenase; *pflB*, pyruvate formate lyase; *aceA*, isocitrate lyase; *aceB*, malate synthase; *fumABC*, fumarase isoenzymes; *icd*, isocitrate dehydrogenase; *adhE*, aldehyde-alcohol dehydrogenase; *pta*, phosphate acetyltransferase; *ackA*, acetate kinase; *sdh*, succinate dehydrogenase; *frdABCD*, fumarate reductase; NAD^+, nicotinamide adenine dinucleotide; NADH, reduced nicotinamide adenine dinucleotide

The fermentation products produced in dual-phase fermentation from different carbon sources by *E. coli* TerP01 strain were examined. The substrate utilization and the cell growth decreased with a large reduction in the production of formic acid in all three carbon sources. During glycerol fermentation, TerP01 strain grew slower, than during xylose or glucose

fermentation. The cell yield decreased with 45%, 29% and 6% in glycerol, xylose and glucose fermentation, respectively (Table 1). Production of acetic acid was also declined, succinic acid reduced in the case of glycerol fermentation, but increased slightly in xylose and glucose fermentation. However, the lactic acid formation increased significantly. Lactic acid is a widely used special chemical in the food, pharmaceutical, textile and chemical industries, and it is used as a monomer in the production of polylactate, which is a biodegradable plastic [17, 18]. Several studies deal with lactic acid production with various bacteria and fungi [19-23]. Based on the published studies, the *E. coli* strains correspond well for the purpose of lactic acid production. Good results have been achieved with glucose fermentation, Dien et al. [24] designed an *E. coli* B mutant (FBR11) which produced lactic acid in anaerobic conditions with concentration of 93% of the theoretical maximum. Afterwards, Grabar et al. [25] and Zhu et al. [26] better results have been achieved with the *E. coli* mutants, TG114 and ALS974, respectively.

Table 1. Product synthesis of *E. coli* Ter8/1 and mutant strains after 96 h fermentation in M9 minimal medium with different carbon sources

Strain	Genetic modification	Sub-strate	Cell mass (g/l)	Sub-strate used (mM)	Fermentation product conc (mM)[b]					
					Lac	Lac yield[a]	Suc	Suc yield[a]	For	Ac
Ter8/1	Wild-type	gly	0.4	33	ND	-	14	0.42	62	13
		xyl	0.58	33	7	0.21	10	0.3	52	11
		gluc	0.53	25	13	0.52	4	0.16	57	15
TerP01	Δ*pflB*	gly	0.22	30	29	0.97	6	0.2	ND	4
		xyl	0.41	30	49	1.63	13	0.43	ND	7
		gluc	0.5	27	48	1.77	7	0.26	2	ND
TerPL02	Δ*pflB* Δ*ldhA*	gly	0.21	30	ND	-	27	0.9	ND	5
		xyl	0.4	29	ND	-	35	1.2	ND	2
		gluc	0.42	22	ND	-	28	1.27	ND	ND

ND not detected

[a] Calculated as mol of lactate/succinate produced in the anaerobic phase divided by the mol of substrate metabolized in the anaerobic phase.

[b] Fermentations were carried out in M9 minimal medium supplemented with the appropriate carbon source in concentration of 5 g/l (37°C, 150 rpm).

Abbreviations: gly, glycerol; xyl, xylose; gluc, glucose; Lac, lactic acid; Suc, succinic acid; For, formic acid; conc, concentration. Data represent an average of three experiments.

TG114 mutant produced 98% lactic acid in mineral salts medium and with ALS974 mutant 99% of the theoretical yield in dual-phase fed-batch fermentation was achieved. Zhou et al. [27] and Zhao et al. [28] produced lactic acid with engineered *E. coli* strains from xylose. In complex media, a mutant of *E. coli* B produced 62 g/l lactic acid from xylose, which was 97% of the theoretical maximum [28]. With the *E. coli* W3110 mutant (SZ85) in minimal salts medium, Zhou et. al achieved a yield of 93% [27]. There are some studies which were directed to the production of lactic acid from glycerol [29-31]. A mutant strain of *E. coli* K-12 MG1655 (LA02Δ*dld*) designed by Mazumdar et al. [29] produced lactic acid in minimal medium with a yield of 85%. Tian et al. [30] and Chen et al. [31] published a yield of 78 g lactic acid/100 g glycerol and 75.4 g lactic acid/100 g glycerol with engineered strains of *E. coli*, CICIM B0013-070(pUC-*ldhA*) and B0013-070-pTHldhA, respectively. Our engineered strain, *E. coli* TerP01, produced lactic acid in concentration of 29 mM from glycerol with a molar yield of 0.97 mol/mol (Table 1, Figure 2), which is 97% of the theoretical maximum. From xylose, the mutant strain produced a concentration of 49 mM of lactic acid with a yield of 1.63 mol/mol (Table 1, Figure 2), which is 98% of the theoretical maximum. In the case of glucose, lactic acid concentration was 48 mM and the molar yield was 1.77 mol/mol (Table 1, Figure 2), which is 89% of the theoretical maximum.

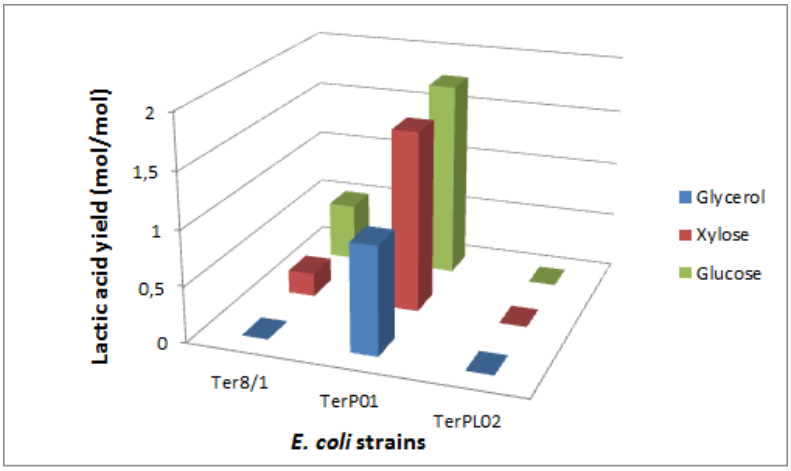

Figure 2. Effect of the genetic modification and substrates on the lactic acid yield

In order to divert the carbon flux to succinic acid, the *ldhA* gene was knocked out (Figure 1). The steps of gene deletion are shown in Figure 3A. The *ldhA*1-FRT-camR-FRT-*ldhA*2 antibiotic resistance gene was first amplified by PCR from pKD3 plasmid using *ldhA*1 and *ldhA*2 primers (Table 3). *E. coli*

TerP01 was second transformed with pKD46 plasmid, which contains the genes required for the recombination [4]. These enzymes catalyzed the recombination between the *ldhA*1-FRT-camR-FRT-*ldhA*2 cassette and the *ldhA* locus in the chromosome. The correct transformants were selected on plates containing chloramphenicol and the pKD46 plasmid have lost by growing at high temperature. For elimination of the antibiotic resistance, the pCP20 plasmid was used. This plasmid encodes the enzyme flippase, which is recognized the FRT sites and removed the section between them, leaving behind a short nucleotide sequence with one FRT site [32]. The correct replacement of the *ldhA* and the later removal of antibiotic resistance were confirmed by PCR analysis (Figure 3B) using *ldhA*3 and *ldhA*4 primers (Table 3). This *E. coli* Ter8/1 *pflB* and *ldhA* double mutant is designated TerPL02.

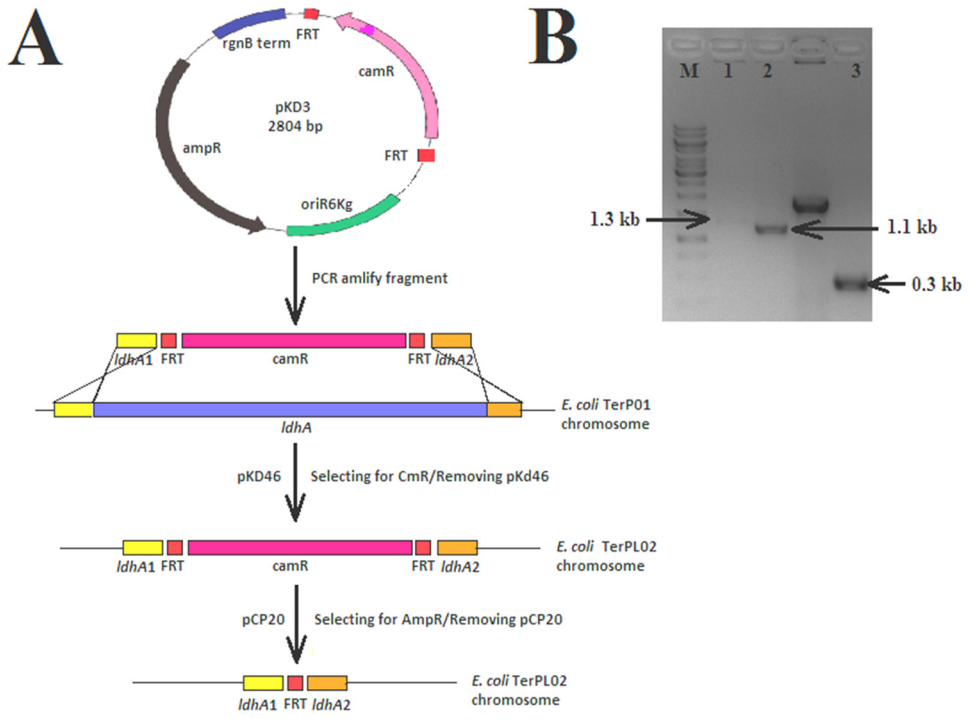

Figure 3. Elimination of *ldhA* gene from the chromosomes of *E. coli* TerP01. **A**. The *ldhA* gene was replaced with the antibiotic resistance gene amplified by PCR using pKD46 plasmid and then, the chloramphenicol resistance was eliminated with the help of pCP20 plasmid. **B**. Verification of deletions by PCR analysis (M: 1 kb DNA molecular weight marker, Fermentas, 1: *ldhA* gene from the chromosomes of *E. coli* TerP01, 2: antibiotic resistance gene from *E. coli* TerPL02, 3: remaining part *of ldhA* gene in chromosomes of *E. coli* TerPL02

During dual-phase fermentation, the cell yield of *E. coli* TerPL02 double mutant strain was a little less, than the cell yield of strain TerP01. Production of acetic acid and formic acid decreased or remained unchanged. After deletion of the second gene, *ldhA*, lactic acid formation stopped and the production of succinic acid increased significantly. Succinic acid is an important chemical in the agricultural, pharmaceutical and food industries. It has a wide range of application and it is a raw material for many special chemicals such as biodegradable polymers and solvents, and fuel additives [3, 33]. There are several studies aimed at the production of succinic acid with genetically modified *E. coli* strains [33-36]. In the production of succinic acid from glucose, researchers have achieved good results, such as Wang et al. [37] obtained a yield of 0.84 g succinic acid/g glucose with an *E. coli* mutant, TUQ19(pQZ26), in dual-phase fermentation. Vemuri et al. [38] achieved a yield of 1.1 g succinic acid/g glucose with *E. coli* strain AFP111(pTrc99A-*pyc*) using complex medium. Andersson et al. [33] produced succinic acid from xylose by *E. coli* strain AFP184 in dual-phase fermentation with a yield of 0.5 g/g. Glycerol was also used as carbon source for the production of succinic acid. Blankschien et al. [36] and Zhang et al. [39] produced succinic acid from glycerol in anaerobic conditions, achieved a yield of 0.69 g succinic acid/g glycerol and 0.49 g succinic acid/g glycerol, respectively. Our results for succinic acid production from glycerol was 0.9 mol/mol (1.15 g/g), which was higher 2.1-fold compared to the wild-type strain and it was 90% of the theoretical maximum (Table 1, Figure 4). The succinic acid yield in xylose was 1.2 mol/mol (0.94 g/g), which was higher 4-fold compared to the Ter8/1 strain and it was 85% of the theoretical maximum (Table 1, Figure 4). In the case of glucose as carbon source, we obtained a yield of 1.27 mol/mol (0.83 g/g), which was higher 7.9-fold compared to the wild-type strain and it was 74% of the theoretical maximum (Table 1, Figure 4).

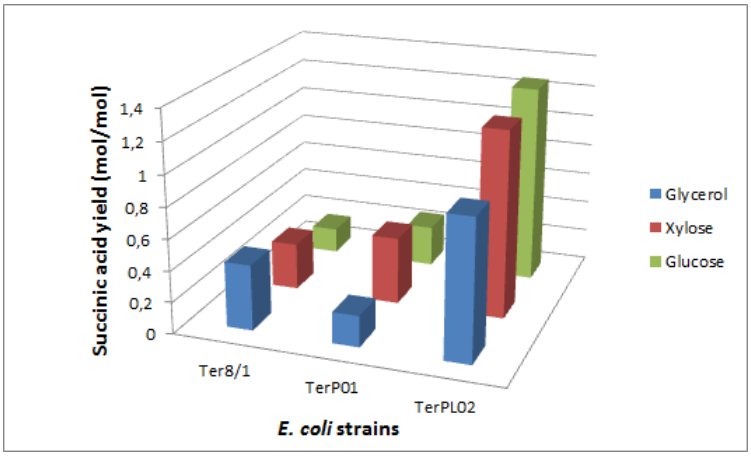

Figure 4. Effect of the genetic modification and substrates on the succinic acid yield

CONCLUSIONS

In this study, an *E. coli* strain Ter8/1, which was isolated from animal faeces, was engineered to produce organic acids by blocking the formic acid and lactic acid formation pathways. The first mutant, TerP01, in which the pyruvate formate lyase was inactivated, was able to convert glucose, xylose and glycerol to lactic acid effectively. Lactate fermentation can theoretically be achieved in *E. coli* with a lactate yield of 2 mol/mol glucose and we obtained a lactic acid yield of 1.77 mol/mol glucose under dual-phase fermentation in minimal medium. From xylose, lactic acid formation can theoretically be reached a lactate yield of 1.67 mol/mol xylose and we achieved a lactic acid yield of 1.63 mol/mol xylose. During the fermentation of glycerol in minimal salts medium with dual-phase fermentation, we obtained a molar yield of 0.97 mol lactic acid/mol glycerol, which was 97% of the theoretical yield. In the case of the second mutant, TerPL02, in which the pyruvate formate lyase and lactate dehydrogenase were inactivated, the succinic acid production increased significantly. The yields obtained from different carbon sources were 0.9 mol/mol glycerol, 1.2 mol/mol xylose and 1.27 mol/mol glucose, which were 90%, 85% and 74% of the theoretical maximum, respectively. Our results confirmed that an isolated strain can be genetically modified and the genetic engineering to reduce the reductive by-product is important in point of view product formation. All these results further suggested that the engineered TerP01 and TerPL02 strains are a promising alternative in the bioconversion of different carbon sources to lactic acid and succinic acid.

In the future, fermentation process will be optimized for lactic acid and succinic acid production in order to improve the productivity and the mutant strains obtained will be further engineered to reduce all of the remaining byproducts.

EXPERIMENTAL SECTION

Bacterial strains and plasmids

The bacterial strains and plasmids used in this study are listed in Table 2. The *E. coli* strains were cultured in Luria Bertani (LB) broth at 37°C.

To the construction of *E. coli* TerPL02 strain, the lambda Red recombination system was used [4]. The lactate dehydrogenase (*ldhA*) gene was knocked out from the chromosomes of *E. coli* TerP01 (Figure 3). The gene-specific antibiotic resistance cassette was amplified from pKD3 plasmid by PCR using primers *ldhA*1 and *ldhA*2 (Table 3). The PCR program was as follows: 94°C for 5 min,

followed by 34 cycles at 94°C for 15 s, 60°C for 30 s, 68°C for 2 min, plus an additional 7 min at 68°C and a subsequent incubation at 4°C. The PCR product obtained was purified with AccuPrep PCR Purification Kit (Bioneer, South Korea) according to the manufacturer's protocol. The purified PCR product was treated with 1U *Dpn*I in a total volume of 50 µl at 37°C for 2 hours, followed by ethanol precipitation and resuspension in 10 µl dH_2O.

Table 2. Bacterial strains and plasmids used in this study

Strains/Plasmids	Relevant characteristics	Source or reference
Strains		
E. coli Ter8/1	Wild-type *E. coli* isolated from animal faeces	[15]
E. coli TerP01	Ter8/1 Δ*pflB*: FRT, sequential deletion of *pflB* in Ter8/1	[16]
E. coli TerPL02	Ter8/1 Δ*pflB*: FRT, Δ*ldhA*: FRT, sequential deletion of *pflB* and *ldhA* in Ter8/1	This study
Plasmids		
pKD46	araBp-gam-bet-exo, bla(ApR), oriR101, repA101(ts)	CGSC Yale University
pKD3	oriR6Kgamma, bla(ApR), rgnB(Ter), FRT-cat-FRT	CGSC Yale University
pCP20	ts-rep, cI857(lambda)(ts), bla(ApR), cat, FLP	CGSC Yale University

Table 3. Primers used in PCR analysis

Primer name	Sequence	Description
*ldhA*1	5'-GAATAGAGGATGAAAGGTCATTGGGGATTAT CTGAATCGGCTGTAGGCTGGAGCTGCTTCG-3'	Used for camR cassette amplification
*ldhA*2	5'-TGTGATTCAACATCACTGGAGAAAGTCTTAT GAAACTCGCATGGGAATTAGCCATGGTCC-3'	
*ldhA*3	5'-GCACAAAGCGATGATGCTGTAG-3'	Used to confirm camR presence in *ldhA* gene and/or *ldhA* disruption
*ldhA*4	5'-CCGTTCAGTTGAAGGTTGCG-3'	

Underlined Nucleotides are homologous to *ldhA* regions

Then, the prepared cassette was electroporated into *E. coli* TerP01 strain, in which the pKD46 plasmid previously has been introduced by electroporation. With the help of L-ara-induced helper plasmid, the recombination takes place between the *ldhA* gene and antibiotic resistance cassette. The transformants were selected on LB agar containing 10 µg/ml chloramphenicol at 37°C. To the

elimination of antibiotic resistance, the pCP20 plasmid was introduced into the mutant cells by electroporation. The cells were selected on LB agar containing 100 µg/ml ampicillin and incubated at 30°C. The successful insertion and deletion of the resistance cassette was confirmed by colony-PCR using *ldhA*3 and *ldhA*4 primers (Table 3). The removal of pKD46 and pCP20 was done by incubation at 42°C for two days. The resulting PCR products were checked on a 1% agarose gel stained with ethidium bromide and visualized using a BioRad transilluminator.

Fermentation condition

Two-phase fermentation was used for analyzing the product formation by mutant *E. coli* strains. In the first step, the cells were grown aerobically in 5 ml LB broth at 37°C and 150 rpm overnight. Cells were harvested by centrifugation at 4500 rpm for 5 min and resuspended in fermentation broth. Fermentation was carried out in M9 minimal medium containing (per liter): 12.8 g $Na_2HPO_4 \cdot 7H_2O$, 3 g KH_2PO_4, 0.5 g NaCl, 1 g NH_4Cl, micronutrients final concentration: 1 mM $MgSO_4$, 100 µM $CaCl_2$, $3 \cdot 10^{-9}$ M $(NH_4)_6Mo_7O_{24} \cdot 4H_2O$, $4 \cdot 10^{-7}$ M H_3BO_3, $3 \cdot 10^{-8}$ M $CoCl_2 \cdot 6H_2O$, $1 \cdot 10^{-8}$ M $CuSO_4 \cdot 5H_2O$, $8 \cdot 10^{-8}$ M $MnSO_4$, $1 \cdot 10^{-8}$ M $ZnCl_2$, $1 \cdot 10^{-6}$ M $FeSO_4 \cdot 7H_2O$. Concentration of the carbon sources, glucose, xylose and glycerol were used in 5 g/l. Cells were placed into a 100 ml flask containing 20 ml fermentation broth and were cultivated aerobically at 37°C and 200 rpm for 16 hours. After 16 hours, cells were harvested by centrifugation at 4500 rpm for 10 min and transferred in sealed 150 ml bottles containing 75 ml fermentation broth with appropriate carbon source and the air above the liquid layer was changed with oxygen free CO_2 gas. The anaerobic production phase was carried out at 37°C for 96 hours.

Analysis

Cell dry-weight was determined by measuring the optical density at 550 nm using a Carry 50 UV-Visible spectrophotometer. We used the 1 OD_{550}=0.34 g dry weight/l simple assumption to estimate the cell mass.

In order to determine the concentration of fermentation end-products, 1 ml of culture sample was centrifuged at 14000 rpm for 10 min and the supernatant was filtered through 0.2 µm pore-size syringe filter. The resulting sample was used for high-performance liquid chromatography (HPLC) analysis. The HPLC system was equipped with UV detector, refractive index detector, and an ion-exchange column (7.8 mm x 300, ICSep Coregel 87H3, Transgenomic). The mobile phase was 0.008 N H_2SO_4 and the flow rate 0.6 ml/min during elution. The column temperature was 50°C. Acids were measured by UV detector at 210 nm and sugars were measured by the RI detector.

ACKNOWLEDGMENTS

The work has been funded by the "Sectoral Operational Programme Human Resources Development 2007-2013 of the Romanian Ministry of Labour, Family and Social Protection through the Financial Agreement POSDRU/6/1.5/S/16" and by "BIOBUILD-Synthesis of some C4, C5 carboxilic acid building block chemicals from renewable biomass resources" PN-II-PCCA-2011-3.2-1367.

REFERENCES

[1]. Th. Willke, K.-D. Vorlop, *Applied Microbiology and Biotechnology*, **2004**, *66*, 131.
[2]. C. Yu, Y.Cao, H. Zou, M. Xian, *Applied Microbiology and Biotechnology*, **2011**, *89*, 573.
[3]. Ch. Thakker, I. Martínez, K.-Y. San, G.N. Benett, *Biotechnology Journal*, **2012**, *7*, 213.
[4]. K.A. Datsenko, B.L.Wanner, *PNAS*, **2000**, *97*(12), 6640.
[5]. A. Jaeger, P. Sims, R. Sidsworth, N. Tint, *Journal of Experimental Microbiology and Immunology*, **2004**, *5*, 65.
[6]. J.A. Mosberg, M.J. Lajoie, G.M. Church, *Genetics*, **2010**, *186*, 791.
[7]. M. Madyagol, H. Al-Alami, Z. Levarski, H. Drahovská, J. Turňa, S. Stuchlík, *Folia Microbiologica*, **2011**, *56*, 253.
[8]. J.A. Sawitzke, L.C. Thomason, N. Costantino, M. Bubunenko, S. Datta, D.L. Court, *Methods in Enzymology*, **2007**, *421*, 171.
[9]. A.R. Poteete, *Microbiology Letters*, **2001**, *201*, 9.
[10]. H.M. Ellis, D. Yu, T. DiTizio, D.L. Court, *PNAS*, **2001**, *98*(12), 6742.
[11]. L. Beamish, R. Greenwood, K. Petty, E. Preston, *Journal of Experimental Microbiology and Immunology*, **2004**, *12,* 94.
[12]. J. Zhu, K.Shimizu, *Applied Microbiology and Biotechnology*, **2004**, *64*, 367.
[13]. Z. Zheng, T. Chen, M. Zhao, Z. Wang, X. Zhao, *Microbial Cell Factories*, **2012**, *11*, 37.
[14]. B. Lesic, L.G. Rahme, *BMC Molecular Biology*, **2008**, *9*, 20.
[15]. A. Fazakas, Zs. Bodor, E. Kovács, É. Laslo, Sz. Lányi, B. Ábrahám, *Studia UBB Chemia*, **2014**, *59*(1), 177.
[16]. A. Fazakas, Zs. Bodor, E. Kovács, Sz. Lányi, B. Ábrahám, *Műszaki Szemle*, **2014**, *63*, 10.
[17]. Y.-J. Wee, J.-N. Kim, H.-W. Ryu, *Food Technology and Biotechnology*, **2006**, *44*(2), 163.
[18]. J. Doran-Peterson, D.M. Cook, S.K. Brandon, *The Plant Journal*, **2008**, *54*, 582.
[19]. B.S. Dien, N.N. Nichols, R.J. Bothast, *Journal of Industrial Microbiology and Biotechnology*, **2002**, *29*, 221.

[20]. S. Zhou, T.B. Causey, A. Hasona, K.T. Shanmugam, L.O. Ingram, *Applied and Environmental Microbiology*, **2003**, *69*(1), 399.
[21]. K. Kyla-Nikkila, M. Hujanen, M. Leisola, A. Palva, *Applied and Environmental Microbiology*, **2000**, *66*(9), 3835.
[22]. M. Ilmen, K. Koivuranta, L. Ruohonen, P. Suominen, M. Penttila, *Applied and Environmental Microbiology*, **2007**, *73*, 117.
[23]. S. Saitoh, N. Ishida, T. Onishi, K. Tokuhiro, E. Nagamori, K. Kitamoto, H. Takahashi, *Applied and Environmental Microbiology*, **2005**, *71*(5), 2789.
[24]. B.S. Dien, N.N. Nichols, R.J. Bothast, *Journal of Industrial Microbiology and Biotechnology*, **2001**, *27*(4), 259.
[25]. T.B. Grabar, S. Zhou, K.T. Shanmugam, L.P. Yomano, L.O. Ingram, *Biotechnology Letters*, **2006**, *28*(19), 1527.
[26]. Y. Zhu, M.A. Eiteman, K. DeWitt, E. Altman, *Applied and Environmental Microbiology*, **2007**, *73*(2), 456.
[27]. S. Zhou, K.T. Shanmugam, L.O. Ingram, A*pplied and Environmental Microbiology*, **2003**, *69*(4), 2237.
[28]. J. Zhao, L. Xu, Y. Wang, X. Zhao, J. Wang, E. Garza, R. Manow, S. Zhou, *Microbial Cell Factories*, **2013**, *12*, 57.
[29]. S. Mazumdar, J.M. Clomburg, R. Gonzalez, *Applied and Environmental Microbiology*, **2010**, *76*(13), 4327.
[30]. K. Tian, X. Chen, W. Shen, B.A. Prior, G. Shi, S. Shing, Z. Wang, *African Journal of Biotechnology*, **2012**, *11*(21), 4860.
[31]. X.-Z. Chen, K.-M. Tian, D.-D. Niu, W. Shen, G. Algasan, S. Singh, Z.-X. Wang, *Green Chemistry*, **2014**, *16*, 342.
[32]. P.P. Cherepanov, W. Wackernagel, *Gene*, **1995**, *158*(1), 9.
[33]. C. Andersson, D. Hodge, K.A. Berglund, U. Rova, B*iotechnology Progress*, **2007**, *23*, 381.
[34]. H. Lin, G.N. Bennett, K. San, *Metabolic Engineering*, **2005**, *7*(5-6), 337.
[35]. J. Wang, J. Zhu, G.N. Bennett, K. San, *Metabolic Engineering*, **2011**, *13*, 328.
[36]. M.D. Blankschien, J.M. Clomburg, R. Gonzalez, *Metabolic Engineering*, **2010**, *12*, 409.
[37]. Q. Wang, X. Chen, Y. Yang, X. Zhao, *Applied Microbiology and Biotechnology*, **2006,** *73*, 887.
[38]. G.N. Vemuri, M.A. Eiteman, E. Altman, *Journal of Industrial Microbiology and Biotechnology*, **2002**, *28*, 325.
[39]. X. Zhang, K.T. Shanmugam, L.O. Ingram, *Applied and Environmental Microbiology*, **2010**, *76*(8), 2397.

STUDIA UBB CHEMIA, LXI, 2, 2016 (p. 47-60)
(RECOMMENDED CITATION)

SYNTHESIS OF UNSYMMETRICALLY SUBSTITUTED ISOXAZOLES AS INTERMEDIATES FOR BENT-CORE MESOGENS

GHEORGHE ROMAN[a*]

ABSTRACT. 3,5-Disubstituted isoxazoles have been designed and synthesized to be used as central units for bent-core mesogens. The substituents at position 3 of the isoxazole ring are either hydroxymethyl or carboxyl, while alkenyl-terminated substituents have been inserted at position 5. A multi-step reaction sequence comprising the *O*-alkylation of 4-hydroxyacetophenone with the suitable alkenyl halide, the Claisen-type condensation with diethyl oxalate and the cyclization to isoxazole led to the isoxazole esters as key intermediates, which were subsequently reduced and hydrolyzed to the corresponding isoxazol-3-ylmethanols and isoxazole-3-carboxilic acids, respectively.

Keywords: *liquid crystals, bent-core, ring closure, isoxazole*

INTRODUCTION

The design of liquid crystals (LCs) having molecular architectures that differ from those of classical calamitic- or discotic-shaped molecules is of great interest. As representatives of unusually shaped molecules with LC properties, bent-core mesogens are a rather recent addition to the LC family [1], and a class of atypical LCs whose unconventional behavior never ceases to amaze [2]. The great majority of bent-core mesogens have a 1,3-phenylene moiety as central unit, but LCs derived from other carbocyclic cores such as 3,4′-disubstituted biphenyls [3,4], 2,7-disubstituted naphthalenes [5,6] or 1,7-disubstituted naphthalenes [7,8] are also well represented. In addition, recent reports that describe the LC properties of bent-core mesogens based on various heterocyclic systems are also available. Whereas examples of bent-core mesogens derived from six-membered heterocycles such as 2,6-disubstituted

[a] *Petru Poni Institute of Macromolecular Chemistry, Department of Inorganic Polymers, 41A Aleea Gr. Ghica Vodă, Iaşi 700487, Romania*
[*] *Corresponding author: gheorghe.roman@icmpp.ro*

pyridines [9], 2,6-disubstituted pyrimidines [10] or 1,3,5-triazines [11] are so far scarce, bent-core mesogens incorporating various five-membered heterocycles as central structural units (*e.g.*, 1,2,4-oxadiazole [12,13],1,3,4-oxadiazole [14,15],1,3,4-thiadiazole [16,17], 1,2,3-triazole [18,19] or thiophene [20,21])

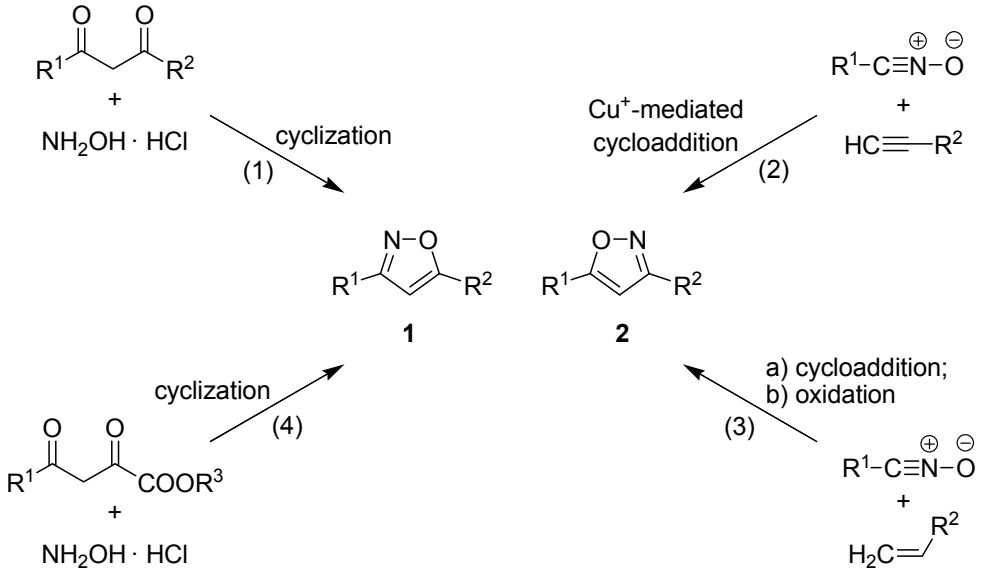

Scheme 1

are abundant. In addition, 3,5-diarylisoxazoles are nowadays well-established mesogens, but structure–property relationships for isoxazole-based LCs still remain fairly uncharted. The difficulty in obtaining only one of the two possible unsymmetrically substituted regioisomers **1** and **2** has initially been a setback in the investigation of the aforementioned relationship. In the early 1990s, the favored approach towards the synthesis of isoxazole-based mesogens was the cyclization of 1,3-diarylpropane-1,3-diones with hydroxylamine (path (1) in Scheme 1), which is an excellent synthetic methodology leading to pure isoxazoles only in the case of identical aryl substituents R^1 and R^2 [22,23], but has been shown to yield mixtures of regioisomeric isoxazoles **1** and **2** when these aryl substituents are different [24,25]. Fortunately, the advent of Cu(I)-catalyzed [3+2]-cycloaddition of nitrile oxides to acetylenes (path (2) in Scheme 1) [26] provided a novel synthetic tool for the regioselective preparation of mesogens having unsymmetrically substituted 3,5-diarylisoxazoles of type **1** as central structural unit [27,28]. A two-step sequential synthetic strategy combining the

cycloaddition of nitrile oxides to alkenes with the oxidation of the resulting isoxazoline (path (3) in Scheme 1) also appears to have been successfully employed for the regioselective preparation of LCs containing unsymmetrically 3,5-disubstituted isoxazoles **1** in their structure [29,30]. Finally, a series of isoxazole-based mesogens of type **2** (R^2 = $COOR^3$) have been generated regioselectively through the ring closure of 4-aryl-2,4-dioxobutanoates using hydroxylamine, followed by the transformation of the ester function at position 3 of the isoxazole ring (path (4) in Scheme 1) [31,32]. Based on the latter synthetic approach, the present paper reports the design, synthesis and structural characterization of novel isoxazoles useful as intermediates in the preparation of LCs.

An initial literature survey has showed that the field of LCs having isoxazole-3-carboxylic acids as central unit is currently underexplored in terms of relationships between the structure and LC properties of these mesogens. Apparently, only a small number of derivatives of type **3** [31,32] and of type **4** [31] (with R^1 and R^2 as long alkyl chains) has been synthesized so far (Fig. 1).

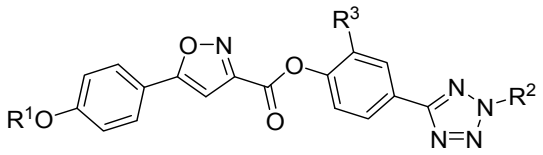

3

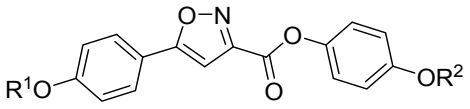

4

Figure 1. Examples of bent-core LCs having isoxazole-3-carboxilic acids as central unit.

Prompted by this observation, we have based our design for novel LCs on isoxazole-3-carboxylic acids whose carboxylic group could be converted into an ester function featuring various mesogen moieties such as alkoxyarylethynylaryl [33], alkoxyaryloxycarbonylaryl [4] or alkoxyarylazoaryl [34]. In addition, isoxazol-3-ylmethanols can be easily prepared through the reduction of the corresponding esters. Recently, simple 5-(alkoxyphenyl)isoxazol-3-ylmethanols have been shown to possess mesomorphic properties [35], while their partially hydrogenated counterparts, namely 5-alkoxyphenyl-4,5-dihydroisoxazol-3-ylmethanols, have been successfully employed as platforms for liquid-crystalline

materials [36]. In light of these facts, isoxazol-3-ylmethanols have also been considered as central units in the design of novel bent-core LCs. Finally, the introduction of oligosiloxane or carbosilane units has been shown to have a significant impact on the properties of the mesophases of bent-core molecules [37,38]. To the best of our knowledge, no LCs containing both the isoxazole bent-core central unit and terminal silicon-containing mesogenic moieties have been reported yet. With a view to gain insight on the properties of LCs combining these two features in their structure, the aforementioned isoxazole-3-carboxylic acids and isoxazol-3-ylmethanols have been designed to incorporate terminal alkenyl groups as well. These alkenyl groups have been deemed suitable for the subsequent introduction of silicon-containing units via hydrosilylation.

RESULTS AND DISCUSSION

The multi-step synthesis of the designed isoxazole-derived intermediates for bent-core LCs features in its first stage the introduction of the alkenyl groups through the *O*-alkylation of 4-hydroxyacetophenone **5** either with allyl bromide or with 4-vinylbenzyl chloride in ethanol in the presence of KOH as base (Scheme 2). 4-Allyloxyacetophenone **6** has been previously obtained from the same reagents, but in the presence of K_2CO_3 as base and under various different reaction conditions [39–43]. 4-(4-Vinylbenzyloxy)acetophenone **7** has been previously reported [44], but its complete characterization is presented herein for the first time.

Claisen-type condensation of the resulting acetophenones **6** and **7** with diethyl oxalate in the presence of sodium ethoxide in absolute ethanol afforded 2,4-dioxobutanoates **8** and **9** (Scheme 2). The proton spectra of compounds **8** and **9**, taken in $CDCl_3$, revealed that they exist in solution as one diastereomeric enol form (presumably *Z*). Thus, the presence of a broad singlet in the off-set of the ^{1}H NMR spectra of these compounds has been attributed to the proton of the enolic hydroxyl, while the sharp singlet at approximately 7 ppm is indicative for a proton at an olefinic carbon atom. In addition, no signal associated with the protons in the methylene group between the two carbonyl functions in the diketone tautomer has been noticed in the proton spectrum of compounds **8** and **9**. The preferred existence of compounds **8** and **9** as enol tautomers has been explained through the possibility for the depicted *Z*-diastereomers to form H-chelates through intramolecular hydrogen bonding [45]. In contrast, NMR analysis of structurally similar 1,3-diarylpropane-1,3-diones proved that these compounds exist as mixtures of corresponding tautomeric diketone and enol-ketone in $CDCl_3$ [46].

Ring closure to isoxazoles **10** and **11** was achieved through a [3+2]-cyclization of 2,4-dioxobutanoates **8** and **9**, respectively, with hydroxylamine hydrochloride (Scheme 2). Despite the presence of two potential oximation sites in their structure, aroylpyruvic esters similar to **8** or **9** have been long known to preferentially lead to esters of 5-aryl-isoxazole-3-carboxylic acids [47], presumably owing to their aforementioned preferred enolic form that is stabilized through an intramolecular hydrogen bonding. Treatment of esters **8** and **9** with hydroxylamine hydrochloride in refluxing ethanol at low pH for a short time, followed by neutralization with a mild base such as alkaline carbonates or bicarbonates, afforded the desired isoxazoles **10** and **11** in good yields [48]. Recrystallization from ethanol gave the pure samples of these key intermediates, which were fully characterized and subsequently used in the preparation of the target compounds, the isoxazolylmethanols **12** and **13** and the isoxazole acids **14** and **15** (Scheme 2).

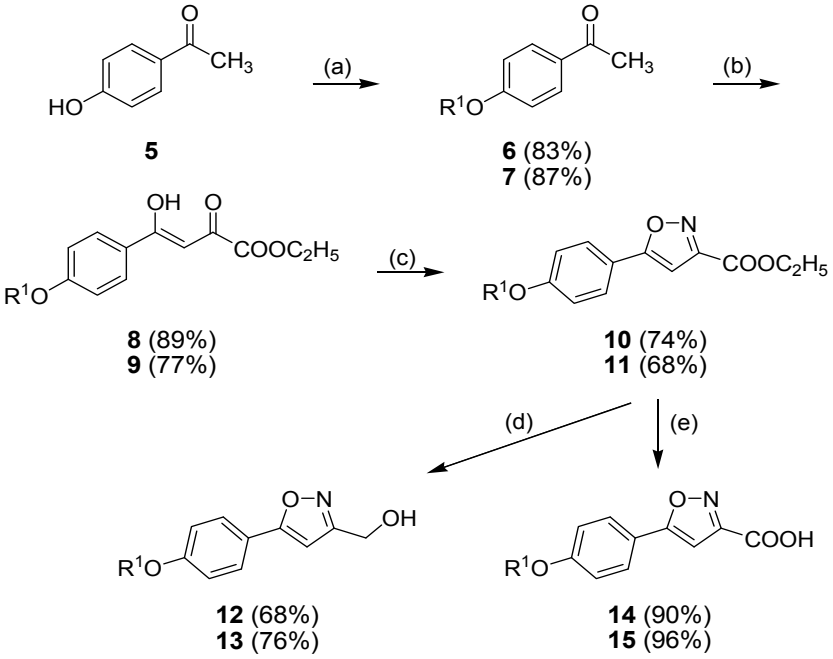

6, 8, 10, 12, 14: R^1 = allyl;
7, 9, 11, 13, 15: R^1 = 4-vinylbenzyl

(a): allyl bromide, EtONa, EtOH, reflux, 2 h (for **6**), or 4-vinylbenzyl chloride, KOH, EtOH, reflux, 2 h (for **7**);
(b) diethyl oxalate, EtONa, EtOH, reflux, 2 h;
(c) hydroxylamine hydrochloride, EtOH, reflux, 2 h;
(d) $NaBH_4$, EtOH, rt, overnight;
(e) $LiOH \cdot H_2O$, THF:MeOH:water, rt, overnight.

Scheme 2

Transformation of esters of isoxazole-3-carboxylic acids into corresponding methanols has been reported to proceed through the general, well-established approach that uses $LiAlH_4$ in THF [49] or diethyl ether [50], and although most of these processes have been conducted at low temperature, examples of similar reactions at room temperature are also available [35]. However, even a weaker reducing agent such as $NaBH_4$ was found to be effective in this particular transformation [48], and $NaBH_4$ appears to be the favorite reducing agent for isoxazole esters [51–53], presumably because of its well-known advantages over $LiAlH_4$ (increased stability, easy handling, use of non-anhydrous solvents). Esters **10** and **11** have been completely reduced to methanols **12** and **13**, respectively, by treatment with an excess of $NaBH_4$ in ethanol at room temperature for 24 h. Because of its better solubility in ethanol, the volume of solvent employed in the reduction of ester **10** under these conditions was smaller than that required in the case of ester **11**. An attempt at reducing ester **11** in the same volume of ethanol used for ester **10** led to an incomplete reaction. Nonetheless, either the extension of the reduction time for ester **11** up to 48 h when a smaller volume of ethanol was used, or the use of larger volumes of ethanol when the reaction time was 24 h drives the reaction to completion. As the reduction started, ester **10** was gradually consumed, and the initial suspension soon turned into a clear solution before the salt of the alcohol began to separate. In the case of ester **11**, no clear solution was obtained during the reduction, even when a large volume of ethanol was used. Crude methanols **12** and **13** were isolated in quantitative yield and practically pure by diluting the reaction mixture with water and slowly lowering the pH with dilute HCl under efficient stirring. Alcohol **12** was very soluble in common organic solvents, and the analytical sample was obtained by recrystallization from a mixture of 2-propanol and hexanes, albeit with a significant loss; on the other hand, alcohol **13** could be recrystallized from 2-propanol alone prior to analysis. The structure of methanol **12** was confirmed by its NMR spectra, which were recorded in $CDCl_3$. The proton spectrum presented a sharp singlet integrating for two protons at 4.78 ppm (protons in the methylene group adjacent to hydroxyl) and a somewhat broad singlet integrating for one proton at 2.72 ppm (proton in the hydroxyl), whereas the ^{13}C NMR spectrum had a peak at 57 ppm assigned to the carbon atom of the carbinol moiety. No peak for the hydroxyl proton of alcohol **13** could be evidenced in its proton spectrum recorded in DMSO-d_6, but the protons and the carbon atom in the methylene group of the carbinol function were assigned the signals at 5.17 ppm and 55 ppm, respectively.

Hydrolysis of esters of isoxazole-3-carboxylic acids has been often performed in lower alcohols in the presence of hydroxides of alkaline metals [54–56]. Because of the limited solubility of ester **11** in lower alcohols at room

temperature, we adopted a different procedure, one that employs as solvent a mixture in which tetrahydrofuran is the major component along with methanol and water as minor components, and a twofold excess of LiOH as base [57]. Under these conditions, ester **10** dissolved readily, while ester **11** formed a suspension from which the solid disappeared soon after LiOH had been added. Although the hydrolysis has been reported to proceed swiftly, the reaction mixture was allowed to react overnight. Isoxazole acids **14** and **15** were isolated in excellent yields after treatment of their lithium salts with dilute HCl, and the NMR analysis of the crude compounds showed that they were essentially pure. No trace of the signals associated with the hydrogen atoms in the ethyl moiety of parent esters could be noticed in the ^{1}H NMR spectra of acids **14** and **15** recorded in DMSO-d_6, while a very broad signal in the off-set of these spectra could be assigned to the hydrogen atom in the carboxyl function. The identity of the known isoxazole acid **14** has been also confirmed by comparing its NMR spectra with the data reported in the literature [42].

CONCLUSIONS

Two novel isoxazol-3-ylmethanols and two isoxazole-3-carboxylic acids (one of them being hitherto unknown) have been designed with the view to afford bent-core LCs after derivatization with suitable mesogen moieties. These four isoxazole-based central units feature at one end an alkenyl moiety that is amenable to subsequent hydrosilylation, and either a carboxyl function or a primary alcohol moiety at the other end, which could be each converted into an ester using a plethora of well-established mesogens. The successful multi-step synthesis of these intermediates was accomplished through a sequence involving *O*-alkylation of 4-hydroxyacetophenone, Claisen-type condensation with diethyl oxalate, ring closure to isoxazole and chemical modification of the ester function. The target compounds were obtained with the purity required for intermediates in the synthesis of LCs without any need for chromatographic separations, and with satisfactory total yields of 35% (for isoxazol-3-ylmethanols) and approximately 45% (for isoxazole-3-carboxylic acids) after four synthetic steps.

EXPERIMENTAL SECTION

Melting points were taken on a Mel-Temp II apparatus and are uncorrected. Elemental analysis was conducted in-house, on a Perkin-Elmer 2400 Series II CHNS/O system. ^{1}H and ^{13}C NMR spectra were recorded on a Bruker Avance 400-MHz spectrometer. The signals owing to residual protons in the deuterated solvents were used as internal standards for the ^{1}H NMR

spectra. The chemical shifts for the carbon atoms are given relative to deuteriochloroform (δ = 77.16 ppm) or dimethyl sulfoxide-d_6 (δ = 39.52 ppm) [58]. The chemical reagents were obtained from Sigma–Aldrich, whereas the solvents were purchased from Chemical Company (Iaşi, Romania), and they were used without purification.

1-[4-(Allyloxy)phenyl]ethanone (6). Sodium (230 mg, 10 mmol) was added to abs. ethanol (15 mL), and the mixture was stirred with cooling in a water bath until sodium was consumed entirely. 4-Hydroxyacetophenone **5** (1.36 g, 10 mmol) was then added, followed by allyl bromide (1.82 g, 15 mmol), and the mixture was heated at reflux temperature for 2 h. The solvent was removed under reduced pressure to give a semisolid, which was partitioned between water (80 mL) containing 5% KOH (2 mL) and chloroform (20 mL). The aqueous phase was further extracted with chloroform (10 mL), then the combined organic phase was washed with water (15 mL) and dried over anhyd. Na_2SO_4. Removal of the solvent under reduced pressure afforded a light yellow oil (1.47 g, 83%), which was sufficiently pure to be used in the next stage. ^{1}H- and ^{13}C NMR spectra of a sample were identical to those reported in literature [42].

1-[4-(4-Vinylbenzyloxy)phenyl]ethanone (7). To a solution of KOH (660 mg, 10 mmol, 85% purity) in 96% ethanol (10 mL), 4-hydroxyacetophenone **5** (1.36 g, 10 mmol) was added, and then the mixture was stirred at room temperature for 5 min. 4-Vinylbenzyl chloride (1.7 g, 10 mmol, 90% purity) was then added, and the reaction mixture was heated at reflux temperature for 2 h. Aqueous 5% KOH (2 mL) was gradually added to the hot mixture, followed by water (50 mL), and the mixture was further stirred at room temperature for 30 min. The resulting solid was filtered, air-dried, and recrystallized from ethanol to give colorless crystals (2.19 g, 87%), mp 108–109 °C; ^{1}H NMR ($CDCl_3$, 400 MHz): δ 2.55 (s, 3H), 5.12 (s, 2H), 5.28 (d, *J* = 10.8 Hz, 1H), 5.77 (d, *J* = 17.6 Hz, 1H), 6.72 (dd, *J* = 10.8 and 17.6 Hz, 1H), 7.00 (d, *J* = 8.8 Hz, 2H), 7.39 (d, *J* = 8.0 Hz, 2H), 7.44 (d, *J* = 8.0 Hz, 2H), 7.93 (d, *J* = 8.8 Hz, 2H); ^{13}C NMR ($CDCl_3$, 100 MHz): δ 26.5, 70.0, 114.5, 114.7, 126.6, 127.8, 130.7, 130.8, 135.8, 136.4, 137.7, 162.7, 196.9. *Anal.* Calcd. for $C_{17}H_{16}O_2$: C, 80.93; H, 6.39. Found: C, 80.75; H, 6.52.

Ethyl 4-[4-(allyloxy)phenyl]-4-hydroxy-2-oxobut-3-enoate (8). A solution of sodium ethoxide obtained from sodium (368 mg, 16 mmol) and abs. ethanol (10 mL) was added dropwise to an efficiently stirred solution of 1-[4-(allyloxy)phenyl]ethanone **6** (1408 mg, 8 mmol) and diethyl oxalate (2336 mg, 16 mmol) in abs. ethanol (10 mL) at room temperature. The mixture was heated at reflux temperature for 2 h, cooled to room temperature, and

gradually added to a vigorously stirred mixture of finely chopped ice (50 g) and water (150 g). The pH of the mixture was brought to 1 with 5% HCl, then the solid was filtered and washed thoroughly with water to give off-white crystals (1965 mg, 89%), mp 42–43 °C; ^{1}H NMR ($CDCl_3$, 400 MHz): δ 1.40 (t, *J* = 7.2 Hz, 3H), 4.39 (q, *J* = 7.2 Hz, 2H), 4.62 (d, *J* = 5.2 Hz, 2H), 5.33 (d, *J* = 10.8 Hz, 1H), 5.43 (dd, *J* = 1.2 and 17.2 Hz, 1H), 5.98–6.11 (m, 1H), 6.97 (s, 1H), 7.01 (d, *J* = 8.8 Hz, 2H), 7.97 (d, *J* = 8.8 Hz, 2H), 15.46 (br s, 1H); ^{13}C NMR ($CDCl_3$,100 MHz): δ 14.2, 62.7, 69.1, 97.9, 115.0, 118.5, 127.9, 130.4, 132.4, 162.6, 163.5, 168.3, 190.4. *Anal.* Calcd. for $C_{15}H_{16}O_5$: C, 65.21; H, 5.84. Found: C, 64.98; H, 5.72.

Ethyl 4-[4-(4-vinylbenzyloxy)phenyl]-4-hydroxy-2-oxobut-3-enoate (9). The mixture of 1-[4-(4-vinylbenzyloxy)phenyl]ethanone **7** (2016 mg, 8 mmol) and diethyl oxalate (2336 mg, 16 mmol) in abs. ethanol (10 mL) was treated at room temperature with an ethanolic solution of sodium ethoxide that has been previously obtained from sodium (368 mg, 16 mmol) and abs. ethanol (10 mL). The mixture was heated at reflux temperature for 2 h, cooled to room temperature, and gradually added to a vigorously stirred mixture of finely chopped ice (50 g) and water (150 g). Treatment with 5% HCl gave a solid that was filtered, washed thoroughly with water and recrystallized from ethanol to give yellow crystals (2.17 g, 77%) mp 79–80 °C; ^{1}H NMR ($CDCl_3$, 400 MHz): δ 1.41 (t, *J* = 7.2 Hz, 3H), 4.39 (q, *J* = 7.2 Hz, 2H), 5.14 (s, 2H), 5.28 (d, *J* = 10.8 Hz, 1H), 5.77 (d, *J* = 17.6 Hz, 1H), 6.73 (dd, *J* = 10.8 and 17.6 Hz, 1H), 7.03 (s, 1H), 7.05 (d, *J* = 8.8 Hz, 2H), 7.39 (d, *J* = 8.4 Hz, 2H), 7.44 (d, *J* = 8.4 Hz, 2H), 7.98 (d, *J* = 8.8 Hz, 2H), 15.46 (br s, 1H); ^{13}C NMR ($CDCl_3$, 100 MHz): δ 14.2, 62.6, 70.2, 97.9, 114.6, 115.2, 126.7, 127.9, 128.0, 130.5, 135.5, 136.4, 137.8, 162.6, 163.5, 168.3, 190.4. *Anal.* Calcd. for $C_{21}H_{20}O_5$: C, 71.58; H, 5.72. Found: C, 71.76; H, 5.59.

Ethyl 5-[4-(allyloxy)phenyl]isoxazole-3-carboxylate (10). Ethyl 4-[4-(allyloxy)phenyl]-4-hydroxy-2-oxobut-3-enoate **8** (1656 mg, 6 mmol) and hydroxylamine hydrochloride (500 mg, 7.2 mmol) were heated at reflux temperature in 96% ethanol (10 mL) for 2 h. The mixture, which solidified when it was cooled to room temperature, was diluted with water (80 mL), treated with a solution of Na_2CO_3 (1.59 g, 15 mmol) in water (15 mL), and further stirred at room temperature for 30 min. The solid was filtered, washed with water, air-dried, and slurried into chloroform (15 mL). Gravitational filtration and subsequent removal of chloroform under reduced pressure yielded a light tan solid, which was recrystallized from ethanol to give off-white leaflets (1210 mg, 74%), mp 80–81 °C; ^{1}H NMR ($CDCl_3$, 400 MHz): δ 1.43 (t, *J* = 7.2 Hz, 3H), 4.46 (q, *J* = 7.2 Hz, 2H), 4.59 (d, *J* = 5.2 Hz, 2H), 5.32 (dd, *J* = 1.2 and

10.4 Hz, 1H), 5.43 (dd, *J* = 1.6 and 17.2 Hz, 1H), 5.98–6.12 (m, 1H), 6.79 (s, 1H), 7.00 (d, *J* = 8.8 Hz, 2H), 7.73 (d, *J* = 8.8 Hz, 2H); ^{13}C NMR ($CDCl_3$,100 MHz): δ 14.3, 62.3, 69.0, 98.7, 115.4, 118.3, 119.9, 127.7, 132.7, 157.0, 160.3, 160.7, 171.8. *Anal.* Calcd. for $C_{15}H_{15}NO_4$: C, 65.92; H, 5.53; N, 5.13. Found: C, 65.69; H, 5.33; N, 5.02.

Ethyl 5-[4-(4-vinylbenzyloxy)phenyl]isoxazole-3-carboxylate (11). Ethyl 4-[4-(4-vinylbenzyloxy)phenyl]-4-hydroxy-2-oxobut-3-enoate **9** (1.76 g 5 mmol) and hydroxylamine hydrochloride (417 mg, 6 mmol) were heated at reflux temperature in 96% ethanol (15 mL) for 2 h. The solvent was removed under reduced pressure, water (70 mL) was added, and the suspension was treated with a solution of Na_2CO_3 (1.27 g, 12 mmol) in water (15 mL). After having been stirred at room temperature for 30 min, the solid was filtered, washed with water and air-dried. The solid was mixed with chloroform (25 mL) and filtered, then the solvent was removed under reduced pressure, and the residue was recrystallized from ethanol to afford colorless leaflets (1190 mg, 68%), mp 119–120 °C; ^{1}H NMR ($CDCl_3$, 400 MHz): δ 1.44 (t, *J* = 7.2 Hz, 3H), 4.46 (q, *J* = 7.2 Hz, 2H), 5.11 (s, 2H), 5.27 (d, *J* = 10.8 Hz, 1H), 5.77 (d, *J* = 17.6 Hz, 1H), 6.73 (dd, *J* = 10.8 and 17.6 Hz, 1H), 6.80 (s, 1H), 7.05 (d, *J* = 8.8 Hz, 2H), 7.39 (d, *J* = 8.4 Hz, 2H), 7.44 (d, *J* = 8.4 Hz, 2H), 7.73 (d, *J* = 8.8 Hz, 2H); ^{13}C NMR ($CDCl_3$, 100 MHz): δ 14.3, 62.3, 70.0, 98.8, 114.5, 115.6, 119.8, 126.6, 127.7, 127.8, 135.9, 136.4, 137.7, 157.0, 160.3, 160.8, 171.8. *Anal.* Calcd. for $C_{21}H_{19}NO_4$: C, 72.19; H, 5.48; N, 4.01. Found: C, 72.37; H, 5.55; N, 3.89.

{5-[4-(Allyloxy)phenyl]isoxazol-3-yl}methanol (12). Sodium borohydride (152 mg, 4 mmol) was gradually added to a suspension of ethyl 5-[4-(allyloxy)phenyl]isoxazole-3-carboxylate **10** (546 mg, 2 mmol) in 96% ethanol (10 mL), and the mixture was stirred at room temperature overnight (20 h). The resulting thick suspension was diluted with water (50 mL) and treated dropwise with 5% HCl until the pH of the mixture reached 1. The residue was filtered, air-dried and recrystallized from a mixture of 2-propanol and *n*-hexane to give colorless crystals (314 mg, 68%), mp 72–73 °C; ^{1}H NMR ($CDCl_3$, 400 MHz): δ 2.72 (s, 1H), 4.57 (d, *J* = 5.2 Hz, 2H), 4.78 (s, 2H), 5.32 (dd, *J* = 1.2 and 10.8 Hz, 1H), 5.43 (dd, *J* = 1.2 and 17.2 Hz, 1H), 5.99–6.12 (m, 1H), 6.44 (s, 1H), 6.95 (d, *J* = 8.8 Hz, 2H), 7.66 (d, *J* = 8.8 Hz, 2H); ^{13}C NMR ($CDCl_3$,100 MHz): δ 57.1, 69.0, 97.1, 115.2, 118.2, 120.3, 127.5, 132.8, 160.3, 164.3, 170.4. *Anal.* Calcd. for $C_{13}H_{13}NO_3$: C, 67.52; H, 5.67; N, 6.06. Found: C, 67.19; H, 5.79; N, 5.88.

{5-[4-(4-Vinylbenzyloxy)phenyl]isoxazol-3-yl}methanol (13). A suspension of ethyl 5-[4-(4-vinylbenzyloxy)phenyl]isoxazole-3-carboxylate **11** (523 mg, 1.5 mmol) in 96% ethanol (25 mL) was gradually treated with $NaBH_4$ (114 mg, 3 mmol), then the mixture was stirred at room temperature overnight. The solvent was removed under reduced pressure, water (50 mL) was added to the residue, and then the pH of the suspension was slowly brought to 1 with 5% HCl. After having been stirred for 30 min, the solid was filtered, air-dried, and recrystallized from 2-propanol to give colorless crystals (350 mg, 76%), mp 145–146 °C; ^{1}H NMR (DMSO-d_6, 400 MHz): δ 4.53 (d, J = 6.0 Hz, 2H), 5.17 (s, 2H), 5.27 (d, J = 11.2 Hz, 1H), 5.52 (t, J = 6.0 Hz, 1H), 5.85 (d, J = 17.6 Hz, 1H), 6.74 (dd, J = 11.2 and 17.6 Hz, 1H), 6.85 (s, 1H), 7.14 (d, J = 8.8 Hz, 2H), 7.44 (d, J = 8.4 Hz, 2H), 7.50 (d, J = 8.4 Hz, 2H), 7.80 (d, J = 8.8 Hz, 2H); ^{13}C NMR (DMSO-d_6, 100 MHz): δ 55.1, 69.1, 98.2, 114.6, 115.5, 119.9, 126.2, 127.2, 128.0, 136.2, 136.3, 136.8, 159.8, 165.2, 168.7. *Anal.* Calcd. for $C_{19}H_{17}NO_3$: C, 74.25; H, 5.58; N, 4.56. Found: C, 73.96; H, 5.77; N, 4.30.

5-[4-(Allyloxy)phenyl]isoxazole-3-carboxylic acid (14). Lithium hydroxide monohydrate (168 mg, 4 mmol) was added to a solution of ethyl 5-[4-(allyloxy)phenyl]isoxazole-3-carboxylate **10** (546 mg, 2 mmol) in a mixture of THF : methanol : water (10 mL, 3 : 1 : 1, v/v/v), and the mixture was stirred at room temperature overnight. The organic solvents were removed under reduced pressure, water (50 mL) was added, and the mixture was gradually treated with 5% HCl until pH reached 1. The solid was filtered, washed thoroughly with water and air-dried to give a colorless powder (440 mg, 90%), mp 176–177 °C; ^{1}H NMR (DMSO-d_6, 400 MHz): δ 4.65 (d, J = 5.2 Hz, 2H), 5.28 (dd, J = 1.2 and 10.4 Hz, 1H), 5.41 (dd, J = 1.2 and 17.2 Hz, 1H), 5.98–6.12 (m, 1H), 7.10 (d, J = 8.8 Hz, 2H), 7.87 (d, J = 8.8 Hz, 2H), 14.02 (br s, 1H, exchangeable with deuterium); ^{13}C NMR (DMSO-d_6,100 MHz): δ 68.4, 99.4, 115.4, 117.8, 127.6, 133.3, 157.8, 160.1, 161.0, 170.8. *Anal.* Calcd. for $C_{13}H_{11}NO_4$: C, 63.67; H, 4.52; N, 5.71. Found: C, 63.33; H, 4.58; N, 5.44.

5-[4-(4-Vinylbenzyloxy)phenyl]isoxazole-3-carboxylic acid (15). Ethyl 5-[4-(4-vinylbenzyloxy)phenyl]isoxazole-3-carboxylate **11** (349 mg, 1 mmol) was suspended in a mixture of THF : methanol : water (10 mL, 3 : 1 : 1, v/v/v), then $LiOH \cdot H_2O$ (84 mg, 2 mmol) was added, and the resulting solution was stirred at room temperature overnight. The organic solvents were removed under reduced pressure to give a colorless residue, which was suspended in water (50 mL) and gradually brought to pH 1 with 5% HCl. After 30 min, the solid was filtered, washed thoroughly with water and air-dried to yield colorless microcrystals (310 mg, 96%), mp 193–195 °C (dec.); ^{1}H NMR (DMSO-d_6, 400 MHz): δ 5.18 (s, 2H), 5.27 (d, J = 10.8 Hz, 1H), 5.84 (d, J =

17.6 Hz, 1H), 6.74 (dd, *J* = 11.2 and 17.6 Hz, 1H), 7.17 (d, *J* = 8.8 Hz, 2H), 7.25 (s, 1H), 7.44 (d, *J* = 8.0 Hz, 2H), 7.50 (d, *J* = 8.0 Hz, 2H), 7.88 (d, *J* = 8.8 Hz, 2H), 14.02 (br s, 1H, exchangeable with deuterium); ^{13}C NMR (DMSO-d_6, 100 MHz): δ 69.2, 99.4, 114.6, 115.6, 119.1, 126.3, 127.6, 128.1, 136.2, 136.3, 136.8, 157.8, 160.2, 161.0, 170.8. *Anal.* Calcd. for $C_{19}H_{15}NO_4$: C, 71.02; H, 4.71; N, 4.36. Found: C, 70.68; H, 4.89; N, 4.03.

REFERENCES

1. H. Takezoe, Y. Takanishi, *Japanese Journal of Applied Physics*, **2006**, *45*, 597.
2. A. Eremin, A. Jákli, *Soft Matter*, **2013**, *9*, 615.
3. M. Martínez-Abadía, B. Robles-Hernández, B. Villacampa, M. Rosario de la Fuente, R. Giménez, M.B. Ros, *Journal of Materials Chemistry C*, **2015**, *3*, 3038.
4. D. Güzeller, H. Ocak, B. Bilgin-Eran, M. Prehm, C. Tschierske, *Journal of Materials Chemistry C*, **2015**, *3*, 4269.
5. S. Aurel, C.-C. Huzum, I. Carlescu, G. Lisa, M. Balan, D. Scutaru, *Journal of the Serbian Chemical Society*, **2015**, *80*, 673.
6. S. Radhika, R.N. Keshava Murthy, B.K. Sadashiva, R. Pratibha, *Liquid Crystals*, **2015**, *42*, 1043.
7. S.K. Lee, Y. Naito, L. Shi, M. Tokita, H. Takezoe, J. Watanabe, *Liquid Crystals*, **2007**, *34*, 935.
8. X. Li, M. Zhan, K. Wang, *New Journal of Chemistry*, **2012**, *36*, 1133.
9. J.M. Marković, N.P. Trišović, T. Tóth-Katona, M.K. Milčić, A.D. Marinković, C. Zhang, A.J. Jákli, K. Fodor-Csorba, *New Journal of Chemistry*, **2014**, *38*, 1751.
10. M.L. Rahman, G. Hegde, M.M. Yusoff, M.N.F.A. Malek, H.T. Srinivasa, S. Kumar, *New Journal of Chemistry*, **2013**, *37*, 2460.
11. E. Beltrán, B. Robles-Hernández, N. Sebastián, J.L. Serrano, R. Giménez, T. Sierra, *RSC Advances*, **2014**, *4*, 23554.
12. G. Shanker, M. Prehm, M. Nagaraj, J.K. Vij, M. Weyland, A. Eremin, C. Tschierske, *ChemPhysChem*, **2014**, *15*, 1323.
13. S.V. Subrahmanyam, P.V. Chalapathi, S. Mahabaleswara, M. Srinivasulu, D.M. Potukuchi, *Liquid Crystals*, **2014**, *41*, 1130.
14. F. Speetjens, J. Lindborg, T. Tauscher, N. Lafemina, J. Nguyen, E.T. Samulski, F. Vita, O Francescangeli, E. Scharrer, *Journal of Materials Chemistry*, **2012**, *22*, 22558.
15. E.-R. Bulai, I. Carlescu, D. Scutaru, *Revista de Chimie (Bucharest)*, **2015**, *66*, 439.
16. J. Seltmann, A. Marini, B. Mennucci, S. Dey, S. Kumar, M. Lehmann, *Chemistry of Materials*, **2011**, *23*, 2630.
17. R.C. Tandel, N.K. Patel, *Liquid Crystals*, **2014**, *41*, 495.
18. G.-Y. Yeap, S. Balamurugan, M.V. Srinivasan, P. Kannan, *New Journal of Chemistry*, **2013**, *37*, 1906.

19. N. Gimeno, R. Martín-Rapún, S. Rodríguez-Conde, J.L. Serrano, C.L. Folcia, M.A. Pericás, M.B. Ros, *Journal of Materials Chemistry*, **2012**, *22*, 16791.
20. S.-B. Yi, H.-F. Gao, Q. Li, Y.-F. Ye, N. Wu, X.-H. Cheng, *Chinese Chemical Letters*, **2015**, *26*, 872.
21. A. Kovářová, M. Kohout, J. Svoboda, V. Novotná, *Liquid Crystals*, **2014**, *41*, 1703.
22. J. Bartulin, R. Martinez, H.J. Müller, Z.X. Fan, W. Haase, *Molecular Crystals and Liquid Crystals*, **1992**, *220*, 67.
23. J. Bartulin, R. Martinez, H. Gallardo, J. Müller, T.R. Taylor, *Molecular Crystals and Liquid Crystals*, **1993**, *225*, 175.
24. J. Barbera, R. Gimenez, J.L. Serrano, R. Alcala, B. Villacampa, J. Villalba, I. Ledoux, J. Zyss, *Liquid Crystals*, **1997**, *22*, 265.
25. D.H. Brown, P. Styring, *Liquid Crystals*, **2003**, *30*, 23.
26. T.V. Hansen, P. Wu, V.V. Fokin, *Journal of Organic Chemistry*, **2005**, *70*, 7761.
27. A.A. Vieira, F.R. Bryk, G. Conte, A.J. Bortoluzzi, H. Gallardo, *Tetrahedron Letters*, **2009**, *50*, 905.
28. M. Tanaka, T. Haino, K. Ideta, K. Kubo, A. Mori, Y. Fukazawa, *Tetrahedron*, **2007**, *63*, 652.
29. R.R. da Rosa, I.S. Brose, G.D. Vilela, A.A. Merlo, *Molecular Crystals and Liquid Crystals*, **2015**, *612*, 158.
30. U.M. Kauhanka, M.M. Kauhanka, *Liquid Crystals*, **2006**, *33*, 121.
31. L. da Silva, H. Gallardo, R.F. Magnago, I.M. Begnini, *Molecular Crystals and Liquid Crystals*, **2005**, *432*, 1.
32. D.R. dos Santos, A.G. Silva de Oliveira, R.L. Coelho, I.M. Begnini, R. Faverzani Magnano, L. da Silva, *ARKIVOC*, **2008**, *(xvii)*, 157.
33. A. Tavares, P.H. Schneider, A.A. Merlo, *European Journal of Organic Chemistry*, **2009**, 889.
34. V. Prasad, S.-W. Kang, X. Qi, S. Kumar, *Journal of Materials Chemistry*, **2004**, *14*, 1495.
35. L.-Y. Lu, H.-M. Kuo, H.-S. Sheu, G.-H. Lee, C.K. Lai, *Tetrahedron*, **2014**, *70*, 5999.
36. A. Tavares, P.R. Livotto, P.F.B. Gonçalves, A.A. Merlo, *Journal of the Brazilian Chemical Society*, **2009**, *20*, 1742.
37. C. Keith, R.A. Reddy, M. Prehm, U. Baumeister, H. Kresse, J.L. Chao, H. Hahn, H. Lang, C. Tschierske, *Chemistry – A European Journal*, **2007**, 2556 and the references cited therein.
38. W.-H. Chen, W.-T. Chuang, U.S. Jeng, H.-S. Sheu, H.-C. Lin, *Journal of the American Chemical Society*, **2011**, *133*, 15674.
39. H. Murakami, T. Minami, F. Ozawa, *Journal of Organic Chemistry,* **2004**, *69,* 4482.
40. E.J. Juárez-Pérez, C. Viñas, F. Teixidor, R. Santillan, N. Farfán, A. Abreu, R. Yépez, R. Núñez, *Macromolecules,* **2010**, *43,* 150.
41. J.A. Rincón, M. Barberis, M. González-Esguevillas, M.D. Johnson, J.K. Niemeier, W.-M. Sun, *Organic Process Research and Development,* **2011**, *15,* 1428.
42. J. Ge, X. Cheng, L.P. Tan, S.Q. Yao, *Chemical Communications,* **2012**, *48,* 4453.
43. N. Sharma, D. Mohanakrishnan, U.K. Sharma, R. Kumar, Richa, A.K. Sinha, D. Sahal, *European Journal of Medicinal Chemistry,* **2014**, *79,* 350.

44. J. Liu, P. Gu, F. Zhou, Q. Xu, J. Lu, H. Li, L. Wang, *Journal of Materials Chemistry C,* **2013**, *1,* 3947.
45. V.V. Zalesov, S.S. Kataev, N.A. Pulina, N.A. Kovylyaeva*, Russian Journal of Organic Chemistry,* **2002**, *38,* 840 and references cited therein.
46. G. Roman, *Research on Chemical Intermediates,* **2014**, *40,* 2039.
47. P. Grünanger, P. Vita-Finzi, "The Chemistry of Heterocyclic Compounds", vol. 49 (Isoxazoles), Part 1, Wiley, New York, **1991**, p. 137**.**
48. P.G. Baraldi, D. Simoni, F. Moroder, S. Manfredini, L. Mucchi, F. Dalla Vecchia, P. Orsolini, *Journal of Heterocyclic Chemistry*, **1982**, *19*, 557.
49. L. Shen, Y. Zhang, A. Wang, E. Sieber-McMaster, X. Chen, P. Pelton, J.Z. Xu, M. Yang, P. Zhu, L. Zhou, M. Reuman, Z. Hu, R. Russell, A.C. Gibbs, H. Ross, K. Demarest, W.V. Murray, G.-H. Kuo, *Bioorganic and Medicinal Chemistry,* **2008,** *16,* 3321.
50. A.K. Roy, S. Batra, *Synthesis,* **2003**, 2325.
51. G. Lopopolo, F. Fiorella, M. De Candia, O. Nicolotti, S. Martel, P.-A. Carrupt, C. Altomare, *European Journal of Pharmaceutical Sciences,* **2011**, *42,* 180.
52. T. Akbarzadeh, A. Rafinejad, J.M. Mollaghasem, M. Safavi, A. Fallah-Tafti, M. Pordeli, S.K. Ardestani, A. Shafiee, A. Foroumadi, *Archiv der Pharmazie (Weinheim),* **2012**, *345,* 386.
53. J.K. Williams, D. Tietze, J. Wang, Y. Wu, W.H. Degrado, M. Hong, *Journal of the American Chemical Society,* **2013**, *135,* 9885.
54. S. Roever, A.M. Cesura, P. Huguenin, R. Kettler, A. Szente, *Journal of Medicinal Chemistry,* **1997**, *40,* 4378.
55. V. Andrzejak, G.G. Muccioli, M. Body-Malapel, J. El Bakali, M. Djouina, N. Renault, P. Chavatte, P. Desreumaux, D.M. Lambert, R. Millet, *Bioorganic and Medicinal Chemistry,* **2011**, *19,* 3777.
56. C. Vergelli, A. Cilibrizzi, L. Crocetti, A. Graziano, V. Dal Piaz, B. Wan, Y. Wang, S. Franzblau, M.P. Giovannoni, *Drug Development Research,* **2013**, *74,* 162.
57. A.P. Kozikowski, S. Tapadar, D.N. Luchini, H.K. Ki, D.D. Billadeau, *Journal of Medicinal Chemistry,* **2008**, *51,* 4370.
58. H.E. Gottlieb, V. Kotlyar, A. Nudelman, *Journal of Organic Chemistry,* **1997**, *62,* 7512.

STUDIA UBB CHEMIA, LXI, 2, 2016 (p. 61-71)
(RECOMMENDED CITATION)

INCLUSION COMPOUNDS OF β-CYCLODEXTRIN-PITOFENONE HYDROCHLORIDE. INVESTIGATIONS OF SOLID FORMS

HOREA POPENECIU[a], DUMITRU RISTOIU[b], IOAN BRATU[a*], GHEORGHE BORODI[a*], ATTILA BENDE[a], LUCIAN BARBU[a]

ABSTRACT. Pitofenone hydrochloride (PF.HCl) is a pharmaceutical substance used as an antispasmodic drug. The inclusion compounds of β-cyclodexdrin (β-CD) with pitofenone hydrochloride (PF.HCl) have been prepared by co precipitation and freeze-drying methods in order to increase the capacity user acceptance to wafer interest in terms of their taste. For physical chemical characterization the inclusion compounds were analyzed by powder X-ray diffraction, FTIR and ss-NMR spectroscopy, DSC, SEM and the structural architecture of the inclusion compound was proposed by molecular modeling techniques. The new product obtained can be used in the pharmaceutical industry because it provides improved smell and taste as compared to the starting substance**.**

Keywords: *pitofenone hydrochloride, β-cyclodextrin, SEM, DSC, magnetic and FTIR spectroscopy, molecular modeling*

INTRODUCTION

Pitofenone hydrochloride (methyl 2-[4-(2-piperidin-1-ylethoxy) benzoyl]benzoate) with molecular formula $C_{22}H_{25}NO_4$ HCl (Fig.1a) and molecular weight 403.9 g/mol is a drug with an antispasmodic activity that is currently available in a combination product with fenpiverinium bromide and metamisol sodium. The combination drug product is called Spasmalgon and is used for release of pain and spasms of smooth muscles despite its availability on the market. The attempts to grow crystals of pitofenone hydrochloride suitable for single crystal analysis were unsuccessful and therefore, we

[a] *National Institute for Research and Development of Isotopic and Molecular Technologies, 67-103 Donat st., 400293 Cluj-Napoca, Romania*
[b] *"Babes-Bolyai" University, Faculty of Environmental Science, 30 Fantanele st., 400294 Cluj-Napoca*
[*] *Corresponding authors: ibratu@itim-cj.ro, borodi@itim-cj.ro*

reported [1-2] the crystal structure as determined from X-ray powder diffraction. Cyclodextrins are formed by the action of the enzyme glucosyltransferase upon starch. Three cyclodextrins are typically formed: α-, β-, and γ-cyclodextrins which contain 6, 7 (Fig. 1b) and 8 α-1,4 linked glucose monomers, respectively. Cyclodextrins are ring or torus-shaped molecules and possess a hydrophobic cavity and a hydrophilic exterior. The hydrophobicity of the cavity allows cyclodextrin to associate with non polar organic molecules or portions of organic molecules to form inclusion complexes [3]. We decided to use β-CD because is very cheap, quite soluble in water and its geometrical dimensions can accommodate guest molecule such as PF.HCl.

Several inclusion compounds of various cyclodextrins with different molecules having practical applications were already reported [3-31].

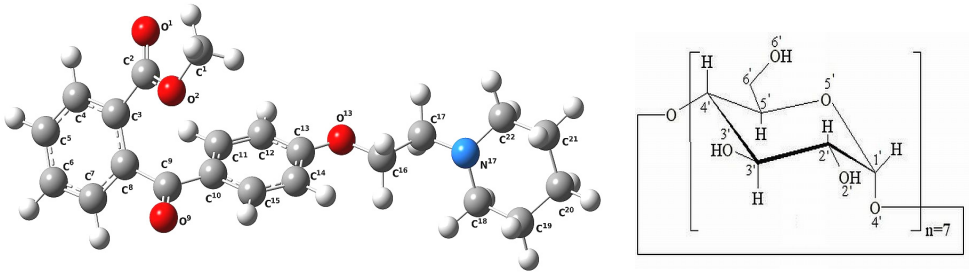

Figure 1. Molecular structure of methyl 2-[4-(2-piperidin-1-ylethoxy) benzoyl] benzoate hydrochloride (pitofenone hydrochloride, PF.HCl) (a), Chemical structure of β–cyclodextrin (b)

The aim of this paper was to prepare inclusion compounds of PF.HCl with β–cyclodextrin by co precipitation and freeze-drying techniques and to characterize them by employing powder–X-ray diffraction, FTIR, ss-NMR spectroscopy, DSC, SEM and molecular modeling DFT techniques.

RESULTS AND DISCUSSION

X-ray diffraction

Powder X-ray diffraction patterns of PTF.HCl, of β–CD and of the inclusion compounds obtained co precipitation and freeze-drying (lyophilization) are presented in Fig. 3. One can observe that X-ray patterns for *co* and *fd* products are different as compared to the patterns of starting compounds, *i.e.* inclusion compounds are obtained. The most important reflections that appear for PF.HCl- β–CD do not belong to β-CD or to PF.HCl. The crystallite

sizes were evaluated using Scherrer relationship [31]. We have obtained for crystallite size D=300Å for PF.HCl-β–CD while crystallite size for β-CD are D=1200Å and for PF.HCl D=1300Å.

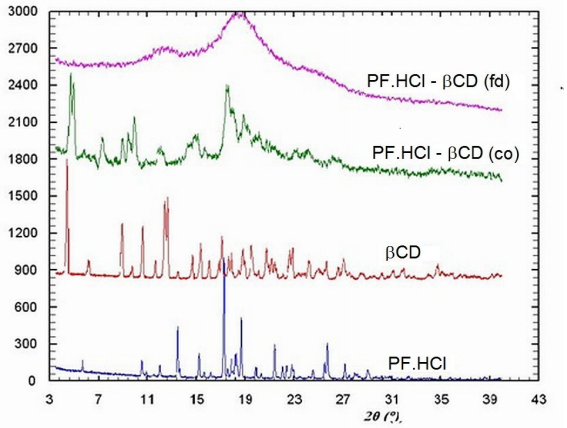

Figure 3. Powder X-ray diffraction patterns of PTF-HCl, of β–CD and of the inclusion compounds obtained co precipitation (*co*) and freeze-drying (*fd*)

The amorphous character of *fd* product and also partially amorphous character for *co* product is confirmed.

DSC

The DSC thermograms of pure PF.HCl, β–CD and PF.HCl-β–CD inclusion compounds, respectively are presented in Fig. 4.

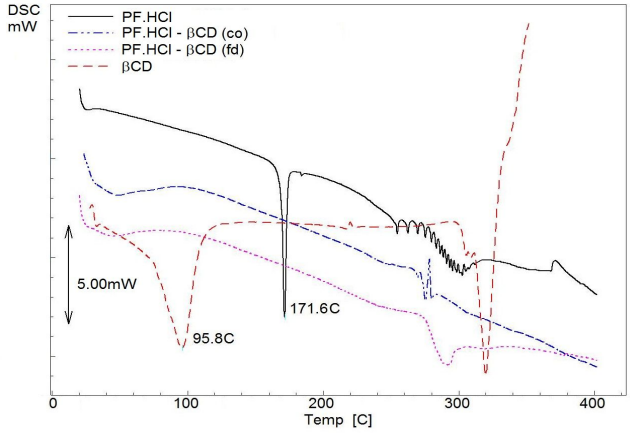

Figure 4. DSC curves of PF.HCl, of β-cyclodextrin and of their inclusion compounds obtained by co precipitation and freeze drying methods

The DSC trace of the β-CD reveals a broad endothermic signal between 74 - 118 ˚C, with ΔH = 190 kJ/mol, that corresponds to the loss of the water molecules existing as residual humidity, as well as those are included in the cavity [27, 28]. From 290 ˚C the melting followed by decomposition of the compound occurs [5, 29]. The DSC curve of the PF.HCl presents a sharp endothermic peak at 171.6 ˚C, with ΔH = 117.7 kJ/mol, corresponding to the melting of the drug, compound shows thermal stability up to 230 ˚C when degradation begin.In the case of the co-precipitated and freeze-dried PF.HCl-β–CD compounds the disappearance of dehydration endothermic peak of β-CD and of melting peak of the PF.HCl were observed. These facts are indications for the occurrence of the inclusion process between PF.HCl and β–CD [30].

ss-NMR Analysis

The solid state ^{13}C CP-MAS NMR spectra of PF.HCl, βCD and those two compounds of PF.HCl-βCD, obtain by co-precipitation (*co*) and freeze-drying (*fd*) techniques are presented in Figure 5.

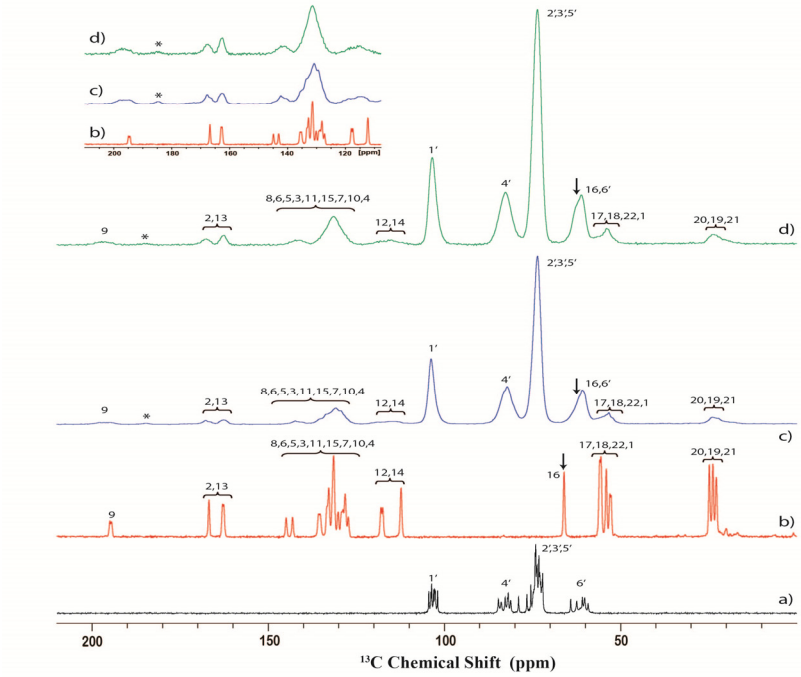

Figure 5. ^{13}C CP-MAS NMR spectra of: a) β-CD, b) PF.HCl, c) PF.HCl- βCD (*co)*, d) PF.HCl- βCD (*fd)*. In the inset figure are the corresponding lines of PF.HCl in the 110 – 200 ppm range. The spinning sidebands are shown by asterisks.

The compound PF.HCl-βCD obtained by co-precipitation (see Fig. 5.c) is a mix of amorphous and crystalline phase whereas that obtained by freeze-drying is an amorphous one (see Fig. 5.d). Despite the amorphous character of the spectra, the most obvious difference observed between free state and complexed state of PF.HCl, is the upfield shift of the line situated at 66.1 ppm in the PF.HCl spectrum, marked with black lines in the NMR spectra (Figs. 5b, 5c, 5d) this indicating a different chemical environment for the corresponding C16 atom of pitofenone and the possibility of inclusion compounds formation.

FTIR spectroscopy

FTIR spectra of PF.HCl, of β–cyclodextrin and of their inclusion compounds obtained by *co* and *fd* are presented in Fig. 6.

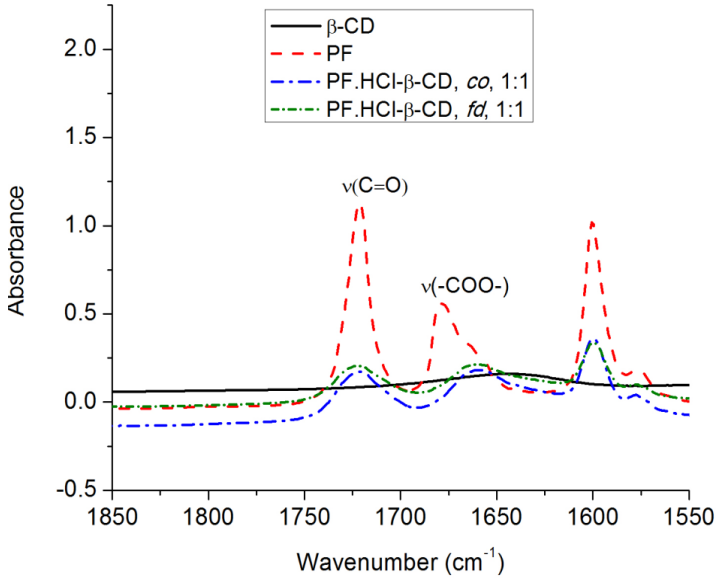

Figure 6. FTIR spectra of pitofenone hydrochloride, β-cyclodextrin, of pitofenone hydrochloride-β-cyclodextrin inclusion compounds obtained by co precipitation (*co*) and by freeze-drying (*fd*) methods, 1850-1550 cm^{-1} spectral domain

One can conclude (see Fig. 6B) that the ν(C=O) vibrational frequency located at ~1721 cm^{-1} is not shifted by complexation, whereas 1679 cm^{-1} the vibrational mode - ν(-COO-) is shifted to 1658 cm^{-1} by complexation with β-CD. It is an indication of the inclusion compound formation both by co precipitation and by freeze-drying processes.

SEM

SEM images of pitofenone hydrochloride, β-cyclodextrin and of pitofenone hydrochloride-β-cyclodextrin inclusion compounds obtained by co precipitation (*co*) and freeze-drying (*fd*) methods are presented in Figs. 7 A-D. On the SEM images of the same size it can be seen that the dimensions of the crystallites are different for pure substances (crystalline substances) and for inclusion compounds.

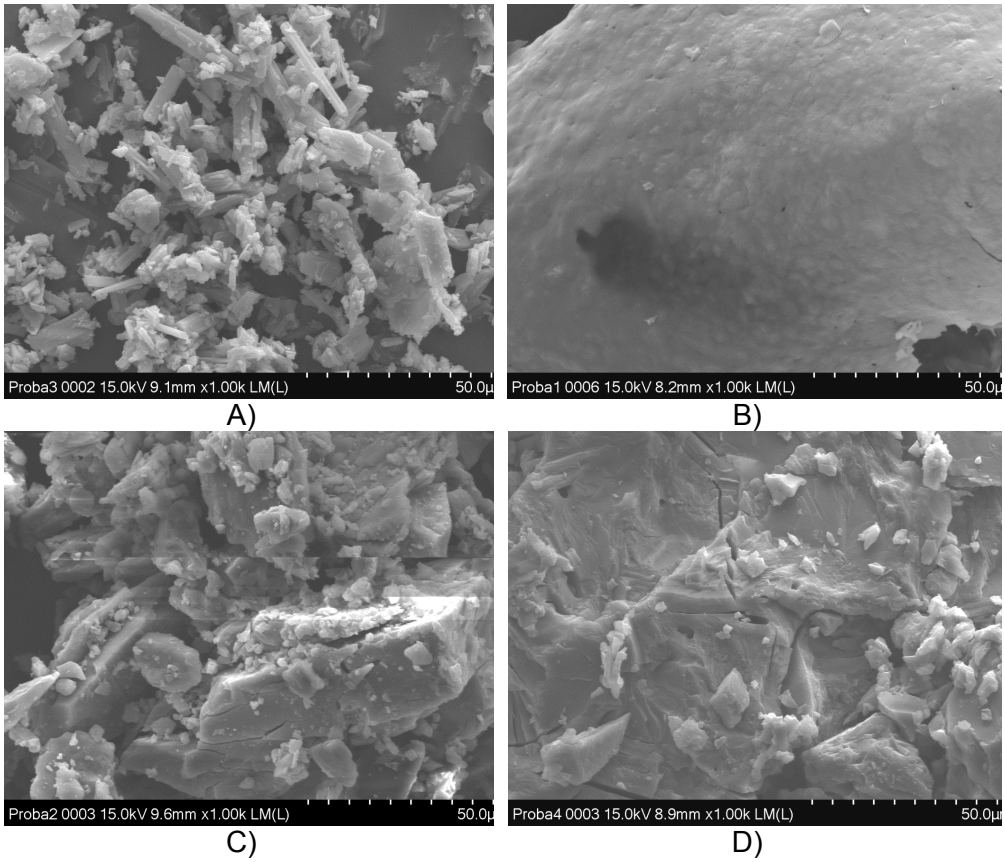

Figure 7. Scanning electron microphotographs: A) β-CD, B) pitofenone HCl, C) PF.HCl- βCD (co) and D) PF.HCl- βCD (fd)

DFT molecular modeling

The equilibrium geometry of the β-CD – pitofenone host-guest supramolecular complex was obtained at DFT level of theory using the M11 [24] exchange-correlation functional considering the def2-TZVP [25] basis

set implemented in the Gaussian09 quantum chemistry program package [26]. The geometry configuration of the pitofenone hydrochloride-β-CD inclusion compound can be seen from two points of views: side view and bottom view, see Figs. 8A and B, respectively. In order to estimate the thermodynamic effects on the inclusion process it was further performed a normal mode analysis to calculate the Gibbs free energy. This calculation was possible to be done only by using the smaller size def2-SVPP [25] basis set. Accordingly, the calculation of intermolecular interaction energy was performed using both the smaller and larger basis sets. The intermolecular interaction energy obtained at M11/def2-SVPP level of theory is -61.41 kcal/mol, while the similar value obtained with the M11/def2-TZVP method is -41.87 kcal/mol. As we can see, with the increasing of the basis set's size the intermolecular interaction energy drastically decrease. In order to take into account the thermodynamic effects, we have computed also the Gibbs free energy considering the M11/def2-SVPP level of theory.

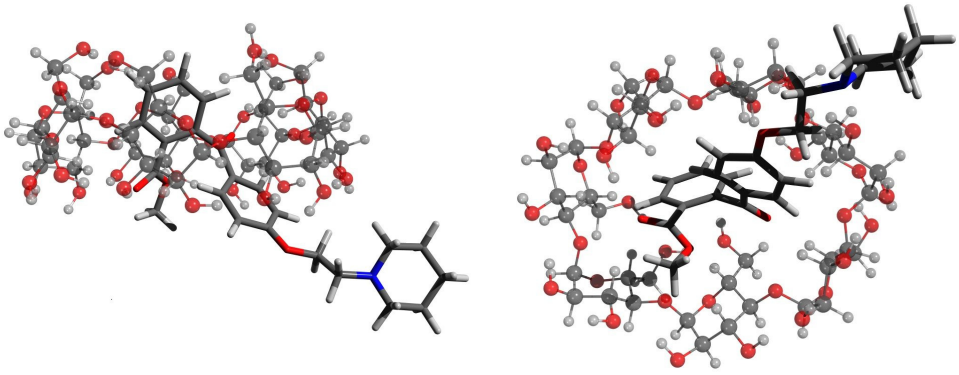

A) B)

Figure 8. A) Side view of the PF.HCl- βCD, B) Bottom view of the PF.HCl- βCD inclusion compound

For this value we have obtained -6.36 kcal/mol showing a spontaneous complexation process, but it should be accepted with some reserve because of the basis size effects. On the other hand it is important to know effects which can hinder the complexation. In this way, we have computed the deformation energy, which is the energy difference between the energy values of the molecular constituents obtained at the equilibrium geometry configuration in isolated and complexed cases. The deformation energy of the β-CD is +29.28 kcal/mol for M11/def2-SVPP case and +19.67 kcal/mol for M11/def2-TZVP, respectively. The similar values for the pitophenone are +6.04 kcal/mol for M11/def2-SVPP case and +2.81 kcal/mol for M11/def2-TZVP,

respectively. It can be observed that the inclusion process also induce a strong deformation of the β-CD cavity, while that of the pitofenone is relatively small. Another interesting feature of the complexation is that the pitofenone molecule makes only two hydrogen bonds with the OH groups of the β-CD, the most part of the interaction is given by the long-range contribution of the dispersion forces. At the same time the line shift in ss-NMR spectra for the C16 carbon atom could be induced by one of the hydrogen bonds made by the O13 atom with an OH group from the bottom part of the β-CD.

CONCLUSIONS

Inclusion compounds of PF.HCl with β-cyclodextrin were prepared by co-precipitation and freeze drying. They were characterized in the solid phase by X-ray diffraction, DSC, FTIR, ss-NMR, SEM and molecular modeling. X-ray diffraction pattern shows a compound in the amorphous state if it is obtained by freeze-drying. By co-precipitation a partially amorphous compound with an important crystalline phase was obtained. DSC curves indicate the formation of different compounds as compared to the starting ones. FTIR spectroscopy indicates the COO^- group's involvement in the complexion process. ss-NMR indicates the formation of an amorphous compound (those obtained by freeze drying) and a partially crystalline compound (those obtained by co-precipitation) with the possibility of inclusion compounds formation (a shifted line of PF.HCl in the ^{13}C CP-MAS spectra of the new compounds as compared to the spectrum of PF.HCl). Based on PXRD and ss-NMR results, the so obtained compounds (by co-precipitation and lyophilization) have partially amorphous and amorphous character, respectively. There are indications that the X-ray diffraction pattern of the obtained inclusion compounds by co precipitation is different as compared to starting one diffractograms. DFT molecular modeling technique gives the spatial architecture of the inclusion compound.

EXPERIMENTAL

Powder X-ray diffraction (PXRD) patterns were collected in the $2\theta=3.5\text{-}40°$ angular domain with a BrukerD8Advance diffractometer, using Cu $K\alpha_1$ radiation (λ = 1.5406 A°) (40 kV; 40 mA). In order to increase the resolution, a Ge 111 monochromator was used to eliminate the $K\alpha_2$ radiation. Data collection was performed with the DIFFRAC plus XRD Commander programs' package at room temperature. The step scan mode was performed with a step

of 0.01° at a rate of 1 step/s. The samples were mildly pre-ground in an agate mortar in order to control crystals size and to minimize the preferred orientation effects.

FTIR spectroscopy. FTIR spectra were recorded in the 4000 to 400 cm^{-1} spectral range with a resolution of 4 cm^{-1} with JASCO 6100 FTIR spectrometer by employing KBr pellet technique; the spectra were processed with Spectral Analysis software.

DSC analysis. DSC thermograms were registered with a DSC60 Shimadzu differential scanning calorimeter by heating about of the 1.5 mg of samples from room temperature up to 400 ˚C, in a crimped aluminium pan, under flowing nitrogen flux, the heating rate being 10 ˚C /min. For data collection the Shimadzu TA-WS60 and TA60 2.1 software were employed.

Solid-State NMR, ss-^{13}C NMR spectra were obtained on a Bruker Avance III 500 MHz wide-bore NMR spectrometer operating at room temperature, using a 4mm CP-MAS probe head. Standard RAMP CP-MAS spectra were acquired at 14 kHz spinning frequency, 2 ms CP contact time, high-power (100 kHz) proton decoupling under TPPM, recycle delay of 5s by averaging 1200 transients for pitofenone hydrochloride and β-cyclodextrin, and 15.500 transients for pitofenone-hydrochloride-β-cyclodextrin. The recorded spectra are calibrated relative to the CH_3 line in TMS (tetramethylsilane), through an indirect procedure which uses α form of L-Glycine as external standard (C – O of Glycine at 176.5 ppm).

SEM was performed on a UHR-SEM HITACHI 8230. The samples were drop casted and evenly distributed on silicon wafers. The measurements advantage: high resolution at low default does not destroy evidence and extract real surface. The samples were analyzed in their natural state without coverage with the conductive layer. The SEM analyzes are performed in high vacuum. The advantages of EDX (EDS) energy dispersive X- ray spectroscopy: xMax were made with 80 mm^2 SDD Oxford instrument type (sylicon drift detector). The SEM parameters: 15kV voltage, more vacuum or equal $\geq 10^{-4}$, Mars and secondary electrons of images were used.

Molecular modeling. Full geometry optimization and frequency calculations for βCD, PF.HCl molecules and their host-guest compound have been carried out in the gas phase at the DFT level of theory considering the M11 [24] exchange-correlation functional together with the def2-SVPP [25] basis set implemented in the Gaussian 09 [26] program package. No negative wavenumbers were obtained for all three cases, proving that true minima of the potential energy surfaces were found in the optimizations.

ACKNOWLEDGMENTS

This work was supported in part by National R&D Institute for Research and Development of Isotopic and Molecular Technologies Cluj Napoca 5, România under the financial support of the PN 09-44 02 05 project, this institute being affiliated with the Faculty of Environmental Science and Engineering of the "*Babes Bolyai"* University.

REFERENCES

[1] M.A. Neumann, X *Journal of Applied Crystallography* **2003**, *36*, 356.
[2] G.E. Engel, S. Wilke, O. Koning, K.D.M. Harris, F.J.J. Leusen, *Journal of Applied Crystallography* **1999**, *32*, 1169.
[3] W.J. Shieh and A.R. Hedges, *Journal of Macromolecular Science, Part A. Pure and Applied Chemistry*, **1996**, *A33(5)*. 673.
[4] Z.-Y. Jin, "Cyclodextrin Chemistry: Preparation and Application", World Scientific Publishing Co. Pte. Ltd., Singapore, **2013**, chapter 7
[5] J. Szejtlij, "Cyclodextrin Technology'', Kluwer Academic Publishers, **1988**.
[6] O. Bradea, I. Kacso, G. Borodi, A. Bende and I. Bratu, *Acta Chimica Slovenica*, **2012**, *59*, 18.
[7] J. Cowins, O. Abimbola, G. Ananaba, X.-Q. Wang, I. Khan, *Journal of Inclusion Phenomena and Macrocyclic Chemistry,* **2015***, 83*, 141.
[8] C.P. Racz, S.S. Maria, T. Cotisel, G. Borodi, I. Kacso, A. Pirnau, I. Bratu, *Journal of Inclusion Phenomena and Macrocyclic Chemistry*, **2013**, *76*, 193.
[9] R. Sbora, Emma A. Budura, G.M. Niţulescu, T. Balaci, D. Lupuleasa*, Farmacia*, **2015**, *63*, 4.
[10] Pravin Nalawade, Anuradha Gajjar, *Journal of Inclusion Phenomena and Macrocyclic Chemistry,* **2015***, 83*, 77.
[11] I. Kacso, G. Borodi, S.I. Farcas, A. Hernanz, I. Bratu*, Journal of Inclusion Phenomena and Macrocyclic Chemistry.,* **2010***, 68*, 175.
[12] S.M. Ali, S. Shamim, *Journal of Inclusion Phenomena and Macrocyclic Chemistry,* **2015***, 83*, 19.
[13] J.A. Ripmeester, *Journal of Inclusion Phenomena Macrocycl Chem*, **1986**, *4*, 129.
[14] A.M. Veselinovi, J.B. Veselinovi, A.A. Toropov, A.P. Toropova, G.M. Nikoli*, International Journal of Pharmaceutics,* **2015***, 495*, 404.
[15] A. Stepniak, S.B. Pacha, S. Rozalska, J. Dlugonski, P. Urbaniak, B. Palecz, *Journal of Molecular Liquids,* **2015***, 211*, 288.
[16] C.X. de Oliveira, N.S. Ferreira, G.V.S. Mota, *Spectrochimica Acta Part A: Molecular and Biomolecular Spectroscopy*, **2016**, *153*, 102.
[17] M. Wulff, M. Alden, and J. Tegenfeldt, *Bioconjugate Chem.*, **2002**, *13,* 240.
[18] T. Sohajdaa, S. Beni, E. Vargab, R. Ivanyi, A. Racza, L. Szente, B. Noszal, *Journal of Pharmaceutical and Biomedical Analysis,* **2009***, 50*, 737.

[19] Y. Hasegawa, Y. Inoue, K. Deguchi, S. Ohki, M. Tansho, T. Shimizu and K. Yazawa, *Journal of Physical Chemistry*, **2012**, *116*, 1758.
[20] A.H. Karoyo, P. Sidhu, L.D. Wilson, and P. Hazendonk, *Journal of Physical Chemistry B*, **2013**, *117*, 8269.
[21] S.S. Braga, I.S. Goncalves, E. Herdtweck and José J.C. Teixeira-Dias*, New Journal of Chemistry*, **2003**, *27*, 597.
[22] L. Chierentin, C. Garnero, A.K. Chattah, P. Delvadia, T. Karnes, M.R. Longhi, and H.R.N. Salgado, *AAPS PharmSciTech*, **2014**,*16(3)*, 683.
[23] M.L. Roldán, A.E. Ledesma, A.B. Raschi, M.V. Castillo, E. Romano, S.A. Brandán, *Journal of Molecular Structure,* **2013**, *1041*, 73.
[24] R. Peverati, D.G. Truhlar, *The Journal of Physical Chemistry Letters,* **2011**, *2(21)*, 2810.
[25] F. Weigend, R. Ahlrichs*, Physical Chemistry Chemical Physics*, **2005**, *7*, 3297.
[26] Gaussian 09, Revision D.01, M.J. Frisch, G.W. Trucks, H.B. Schlegel, G.E. Scuseria, M.A. Robb, J.R. Cheeseman, G. Scalmani, V. Barone, B. Mennucci, G.A. Petersson, H. Nakatsuji, M. Caricato, X. Li, H.P. Hratchian, A.F. Izmaylov, J. Bloino, G. Zheng, J.L. Sonnenberg, M. Hada, M. Ehara, K. Toyota, R. Fukuda, J. Hasegawa, M. Ishida, T. Nakajima, Y. Honda, O. Kitao, H. Nakai, T. Vreven, J.A. Montgomery Jr., J.E. Peralta, F. Ogliaro, M. Bearpark, J.J. Heyd, E. Brothers, K.N. Kudin, V.N. Staroverov, R. Kobayashi, J. Normand, K. Raghavachari, A. Rendell, J.C. Burant, S.S. Iyengar, J. Tomasi, M. Cossi, N. Rega, J.M. Millam, M. Klene, J.E. Knox, J.B. Cross, V. Bakken, C. Adamo, J. Jaramillo, R. Gomperts, R.E. Stratmann, O. Yazyev, A.J. Austin, R. Cammi, C. Pomelli, J.W. Ochterski, R.L. Martin, K. Morokuma, V.G. Zakrzewski, G.A. Voth, P. Salvador, J.J. Dannenberg, S. Dapprich, A.D. Daniels, Ö. Farkas, J.B. Foresman, J.V. Ortiz, J. Cioslowski, D.J. Fox, Gaussian, Inc.: Wallingford CT, **2009**.
[27] J.A. Castro-Hermida, H. Gomez-Couso, M.E. Ares-Mazas, M.M. Gonzales-Bedia, N. Castaneda-Cancio, F.J. Otero-Espinar, J. Blanco-Mendez, *Journal of Pharmaceutical Sciences,* **2004**, *93*, 1197.
[28] M.K. Rotich, M.E. Brown, B.D. Glass, *Journal of Thermal Analysis and Calorimetry*, **2003**, *73*, 671.
[29] F. Trotta, M. Zanetti, G. Camino, *Polymer Degradation and Stability* **2000**, *69*, 373.
[30] R. Agrawal and V. Gupta, Cyclodextrins, *International Journal of Pharmaceutical Frontier Research*, Jan-Mar, **2012**, *2*(1), 95.
[31] H.P. Klug, L.E. Alexander, "X-Ray Diffraction Procedures", John Wiley & Sons Inc., New York ,**1974**, 2nd Ed, 687–703.

STUDIA UBB CHEMIA, LXI, 2, 2016 (p. 73-88)
(RECOMMENDED CITATION)

CONTRIBUTION TO THE STUDY OF SUCEAG POTTERY, CLUJ COUNTY, ROMANIA

MARCEL BENEA[a*], VLAD-ANDREI LĂZĂRESCU[b], MARIA GOREA[c]

ABSTRACT. The site at Suceag, Cluj county, Romania, is composed of three different overlapping settlements, each having its own chronology: the first one is dated during the time of the Roman province of Dacia, the second one dated between the second half of the 4th century and the beginning of the 5th century AD and the last one broadly dated during the 7th-8th century AD. Because of this particular situation, our first attempt was to determine whether some direct connections between them truly existed. The petrographic analysis performed on a series of 56 samples coming from different types of pottery established after analysing all the ceramic material coming from the settlement at Suceag (cca. 4500 pottery fragments) showed that in this case we are only dealing with local products.

The colour of the analysed potsherds vary from grey to black indicating reducing atmosphere (25 samples), from reddish-brown to yellowish-brown (24 samples) suggesting an oxidizing atmosphere during firing and 7 samples have a "sandwich"-type structure probably an incomplete thermal treatment. The matrix is relatively uniform, with clasts of various sizes (up to 3-4 mm). Macroscopically, quartz grains, micas, and ceramoclast could be observed. According to the microscopic grain size, two types of ceramics can be separated: semifine (lutitic-siltic-arenitic), and coarse (lutitic-arenitic-siltic). Based on the ratio between crystalline vs. amorphous phases, microcrystalline, and microcrystalline-amorphous fabrics were identified. As temper, crystalloclasts (quartz, micas, iron oxi-hydroxides, feldspars, amphibole, garnets, epidote, zircon), lithoclasts (quartzite, micaschist, gneiss, limestones), and ceramoclasts were identified. The observed bioclasts are represented by algae, and foraminifera remnants. The porosity consists of both primary, and secondary pores. The pore size vary from 0.5 x 1.5 mm to1.5 x 2.0 mm. Open porosity determined by water absorption capacity vary between 9.09 % - 23.10 %. The X-Ray diffraction analyses

[a] *Babes-Bolyai University, Faculty of Biology and Geology, Department of Geology, Str. M. Kogălniceanu nr.1, 400084 Cluj-Napoca, Romania.*
[*] *Corresponding author: E-mail: marcel.benea@ubbcluj.ro*
[b] *Institute of Archaeology and History of Art Cluj-Napoca, Str. M. Kogălniceanu nr. 12-14, 400084 Cluj-Napoca, România. E-mail: lazarescu_vlad@yahoo.com*
[c] *Babes-Bolyai University, Faculty of Chemistry and Chemical Engineering, Department of Chemical Engineering, Str. Arany Janos nr. 11, 400028 Cluj-Napoca, Romania. E-mail: mgorea@chem.ubbcluj.ro*

confirm the microscopic observations. According to the macroscopic aspects, microscopic features, and physical characteristics the firing temperature of the studied ceramic fragments is estimated to be between 800-900°C.

***Key words**: ancient pottery, mineralogical and physical analysis, Suceag archaeological site, Romania.*

INTRODUCTION

The settlement at Suceag (N46º47', E23º27'), on the Nadăş river valley at about 12 km from the actual city of Cluj-Napoca, was archaeologically researched during the years 1991-2000, in the topographical point known under the name of „Oradba". It was situated on top of a Roman rural habitation, very close to the main Roman road connecting in antiquity the Colonia Aurelia Napocensis to the most important military fort of the Northern frontier, Porolissum (Pl. 1).

The archaeological excavations started in 1989 as rescue excavations for the construction of the Plant Extract facility which partially destroyed the site. During this campaign several archaeological features were identified, but the most important ones refer to the discovery of two pottery kilns which lead to the assumption that the Early Migration Period settlement at Suceag was a pottery production centre. The importance of this site was that beside this new identified settlement, an older Roman *villa rustica* or maybe a *vicus* were formerly known. Scientists thought that maybe by analysing these two settlements, some conclusions regarding the withdrawal of the Roman Dacia and the period immediately after can be drawn [1-2].

The first systematic archaeological excavations started in 1991 and with this occasion several houses were identified alongside numerous storage or waste pits dated during the second half of the 4th century AD. A very interesting discovery was that of a workshop specialized in producing antler combs, a quite rare feature found in Central and Eastern Europe. This made archaeologists believe that we are facing a quite important production centre for the whole Northern Transylvanian region [3-4].

During the 1994 campaign, some new features were identified and documented and for the first time the approximate extent of the site was presumed covering an area of about 4 hectares. The novelty of these excavations consisted apart from the excavating another pottery kiln, the documentation of another settlement overlapping the Roman and the Early Migration Period one, dated during the 7th-8th centuries AD [4-6].

The site at Suceag is composed of three chronologically distinct settlements as follows: the first one is dated during the time of the Roman province of Dacia, the second one dated between the second half of the 4th century and the beginning of the 5th century AD and the last one broadly dated during the 7th-8th century AD. The main aim of the archaeological excavations was that of establishing the topography of each settlement only afterwards some conclusions related to the inhabitancy continuity being possible [7-8]. The analysis needed to focus upon certain aspects of the pottery production such as technological tradition and regional patterns of distribution as well as the habitation of the entire studied area in order to identify possible similar or different models that will clarify the problem of ethnical continuity versus habitation continuity.

As one of the main unknown of the archaeological landscape at Suceag was the extent of the habitation, a comprehensive ground and aerial-based set of physical sensing techniques has been proposed. Within this new approach a large area in the southern part of the settlement was explored in 2012 by the means of geophysical techniques [9] as well as large scale low altitude remote sensing data acquisitions for the entire micro region, which were undertaken in 2014. The site area is highly disturbed by modern human activities and therefore only a total surface of 1.6 hectares, was mapped using geophysical magnetic techniques, while ERT (Electrical Resistivity Tomography) measurements were performed in order to reveal the main stratigraphic sequences only in the areas where the nature of the archaeological features demanded such an approach. Regarding the possible interpretation of the geophysical survey, a series of anomalies can be identified after the processing of the data, having both archaeological significance or being either of recent origin or geologic nature. The results point to the fact that all the investigated area is composed of numerous archaeological features, having a certain tendency of disappears towards the northern part. The soil seems to be abundant in highly remnant magnetized materials, out of which some could be interpreted as pottery kilns (Pl. 2).

As a hypothesis, we can presume, based on the data gathered from the excavations in 2012 that the rectangular structures identified on the magnetic map belong to Roman time while the pottery kilns should be linked to the Early Migration Period settlement. Some fundamental differences observed for the inner structure of the two settlements were documented. The Roman settlement resembles what we all know to be a rural settlement in which at least two large stone structures were determined occupying a very large area inside the site itself while the barbarian settlement is characterized by the agglomeration of archaeological features such as sunken dwellings, pits and pottery kilns clustered in a limited area of the site illustrating the tribal manner of organizing the landscape (such inner structure being typical for the barbarian settlements known from all over Northern Europe). Moreover, these two

settlements do not share the same spatial distribution and landscape arrangement, the Roman site occupying a larger territory. Maybe the best argument in resolving the so called "continuity question" refers to the stratigraphic data that clearly indicates that the two settlements are overlapping one another and thus having no direct chronological or ethnical link. We refer here to a situation observed in 2012 when we managed to identify and date a late 4th century feature overlapping the collapsing layer of one of the Roman stone structures dated with a coin from the 3rd century AD, a fact which implies that the stone structure was already collapsed and therefore not functioning during the 4th century AD.

One of the main problems that the site raised refers to the possibility of identifying certain ceramic imports that might allow us to establish some inter-regional connection patterns. In the same time, following the "chaîne operatoire" concept, our focus was directed upon the technological recurrences rather than on typological aspects while trying to follow and understand problems such as "technological tradition" [10] and in doing so, we tackled these aspects by focusing our attention upon the petrographic and chemical study of a batch of samples that are relevant from this point of view. Such questions have proven to be of great importance while establishing different classifications of the ceramic artefacts [11-12] taking into account not only the shape of the pottery [13] but also other aspects such as the modelling techniques, raw materials and their provenance, forming techniques, firing, decorative aspects, function etc. all of which will contribute to the better understanding of the process of pottery production and distribution [14-16].

The petrographic analysis performed on a series of 56 samples coming from different types of pottery established after analysing all the ceramic material coming from the settlement at Suceag (cca. 4500 pottery fragments) and ranging from the Roman time until the Early Medieval period showed that in this case we are only dealing with local products. This situation, together with the relatively limited number of pottery kilns (3 previously identified during archaeological investigations and other 3 based on the geophysical surveys) suggests that we are facing an autarchic pottery production model which was active only when a certain market demand existed. We are basically talking about closed communities capable of auto-subsistence, as opposed to the big pottery production centres oriented towards the surplus needed in order for the export to different market places that they supply to have place, as for example is the case of the pottery production centre at Medieșul Aurit [17]. As for the history of the economical pottery production we are unable to determine such well established distribution networks which can be only supported by some thorough mineralogical and petrographic analysis of the pottery collected from different contemporaneous settlements situated very close to one another. It is worth to mention several other archaeometry studies on ancient ceramics and the provenience of the raw materials in the nearby regions [18-23].

RESULTS AND DISCUSSION

Macroscopically aspects

The colour of the analysed potsherds vary from grey to black indicating reducing atmosphere (25 samples), from reddish-brown to yellowish-brown (24 samples) suggesting an oxidizing atmosphere during firing and 7 samples have a “sandwich”-type structure due to an incomplete firing or high content of water in raw ceramics. The matrix is relatively uniform, with clasts of various sizes (up to 3 mm) and shapes. Macroscopically, quartz grains, micas, and ceramoclast could be observed.

Porosity is marked by both primary pores, generally elongated from shaping method and irregular to rounded secondary pores resulted by later decomposition of some compounds from raw mixtures or bioclasts combustion. The pore size varies from 0.5 x 1.5 mm to1.5 x 2.0 mm.

Polarized light microscopy

Transmitted light optical microscopy was used for additional information on the mineral components of the matrix and the non-plastic materials, on the thermal treatments, and on the fabric of the potsherds.

According to the microscopic grain size, two types of ceramics can be separated (Table 1 and Plate 3, 4): semifine (lutitic-siltic-arenitic), and coarse (lutitic-arenitic-siltic) [24]. Sample 50 to 56, without inventory number, were described as semifine ceramics.

Table 1. Catalogue of the studied samples based on the microscopic grain size

	Types of ceramic (microscopic grain size)					
	Coarse (lutitic-arenitic-siltic)		Semifine (lutitic-siltic-arenitic)			
	Sample No.	Inv.No.	Sample No.	Inv.No.	Sample No.	Inv.No.
Items	2	3728	1	3745	30	2357
	4	-	3	3749	32	2336
	5	-	6	3708	33	2338
	7	3743	9	3709	35	2882
	8	3727	10	3699	37	2699
	14	3732	11	3665	39	3127
	16	-	12	3735	40	3128
	20	-	13	3733	41	3144
	21	3906	15	3934	42	3147
	25	3992	17	3945	43	3058
	26	3997	18	2716	45	2821
	28	2360	19	3113	46	2838
	31	2353	22	3957	47	2875
	34	2302	23	3966	48	2823
	36	2908	24	3968	49	3027
	38	3154	27	2376		
	44	3069	29	2366		

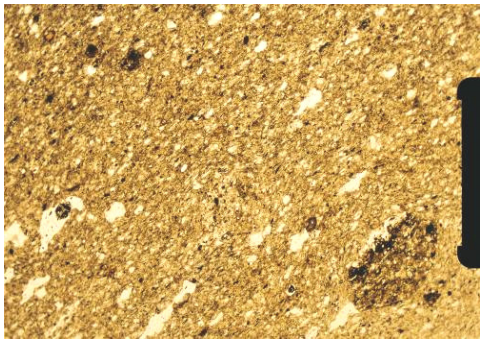

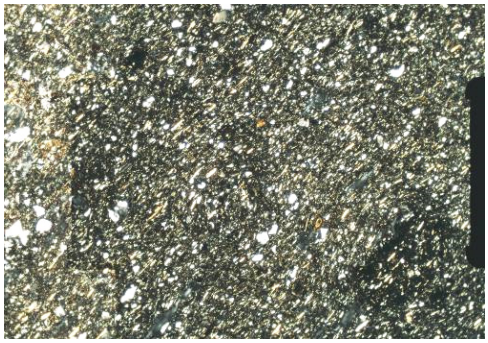

Fig.1 (left) and **Fig.2** (right). Sample 23 – Semifine ceramics with microcrystalline matrix, elongated pores parallel to the micas lamellae, angular quartz crystalloclasts, plagioclase feldspars, quartzite lithoclasts, and ceramoclasts, 1N (left), N+ (right), scale bar = 0.5 mm

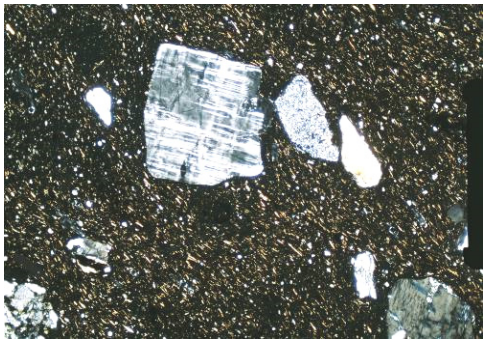

Fig.3. Sample 1 – Semifine ceramics with microcrystalline to microcrystalline - amorphous matrix; angular quartz, feldspars (microcline-perthite), oriented thin mica lamellae, and quartzite lithoclasts; N+, scale bar = 0.5 mm

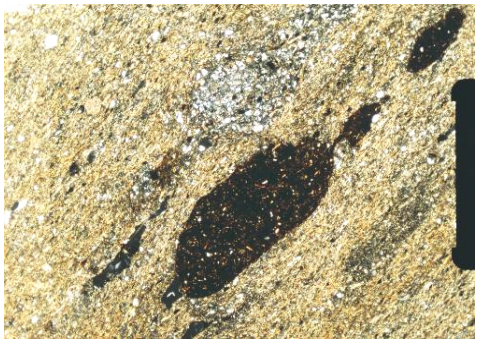

Fig.4. Sample 27 – Semifine ceramics with microcrystalline, with elongated pores and fissures paralel with the thin mica lamellae, angular quartz, quartzite fragments and ceramoclasts; 1N, scale bar = 0.5 mm

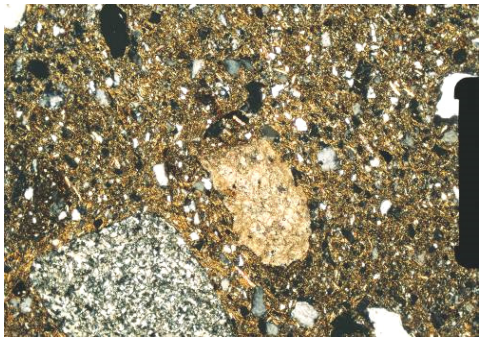

Fig.5. Sample 29 – Semifine to coarse ceramics with microcrystalline matrix; limestone fragments, quartz, plagioclase feldspars, mica lamellae with yellowish birefringence, iron oxi-hydroxide clusters, quartzite, and opaque minerals; N+, scale bar = 0.5 mm

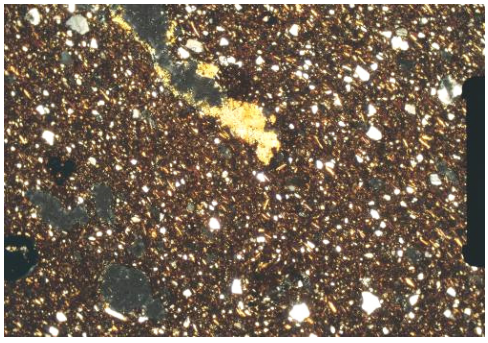

Fig.6. Sample 41 – Semifine to coarse ceramics; microcrystalline reddish matrix with quartz clasts, mica lamellae, plagioclase feldspars, ceramoclasts, and secondary carbonates inside the pores; N+, scale bar = 0.5 mm

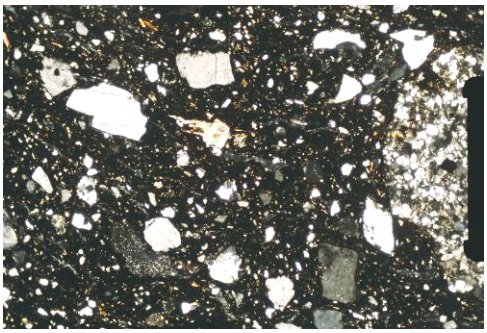

Fig.7. Sample 38 – Coarse ceramics with microcrystalline – amorphous matrix; quartz crystalloclasts, twinned plagioclase feldspars, ceramoclasts, and gneiss, quartzite and limestone lithoclasts; N+, scale bar = 0.5 mm

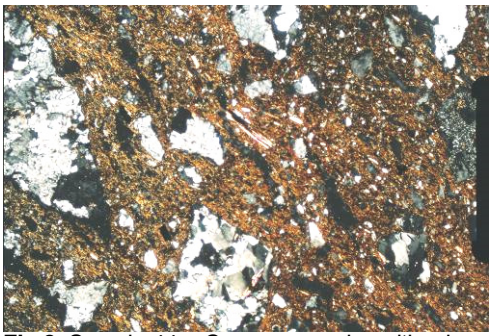

Fig.8. Sample 44 – Coarse ceramics with microcrystalline to microcrystalline - amorphous matrix; quartz, micas, plagioclase feldspars crystalloclasts, and quartzite and gneiss lithoclasts; N+, scale bar = 0.5 mm

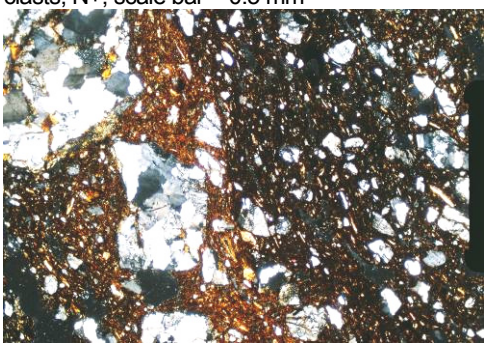

Fig.9. Sample 16 – Contact between inner and outer part of the ceramic body; quartz, micas and feldspars crystalloclasts, iron oxi-hydroxide clusters, quartzite and micaschists lithoclasts; N+, scale bar = 0.5 mm

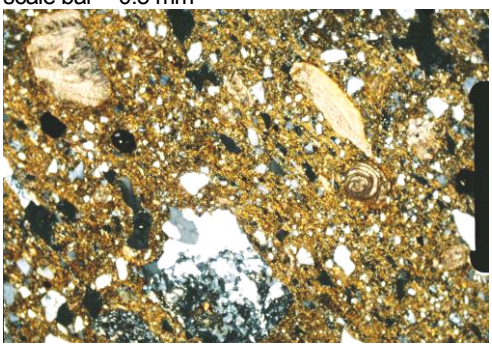

Fig.10. Sample 14 – Semifine ceramics with microcrystalline matrix; ceramoclasts, bioclasts (foraminifera and algae remnants), quartz and micas crystalloclasts, quartzite lithoclasts; N+, scale bar = 0.5 mm

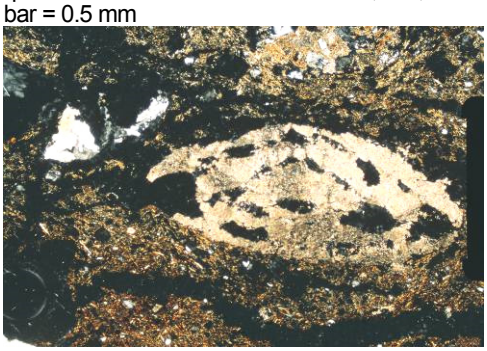

Fig.11. Sample 36 – Semifine to coarse ceramics with microcrystalline - amorphous matrix; quartz, micas, plagioclase felspars, ceramoclasts, bioclasts (foraminifera), and quartzite lithoclasts; N+, scale bar = 0.5 mm

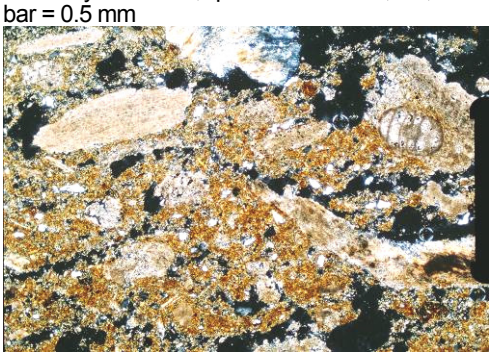

Fig.12. Sample 5 – Semifine to coarse ceramics with microcrystalline matrix; bioclasts (foraminifera, algae), iron oxi-hydroxide clusters, and limestone lithoclasts; N+, scale bar = 0.5 mm

Different types of fabric were described in the ceramic matrix based on the ratio between crystalline *vs.* amorphous phases: microcrystalline, and microcrystalline-amorphous (Fig. 1, 2, 4, 5, 6, 10, 12, respectively 3, 7. 8, 11). As non-plastic materials (temper), crystalloclasts as quartz, micas, feldspars (Fig. 1 to 12) are present in all the samples, while iron oxi-hydroxides (Fig. 5, 9, 12), amphibole, garnets, epidote, zircon were observed in subordinate amounts. Lithoclasts are mainly represented by quartzite (Fig. 1 to 12), and in some samples micaschist (Fig. 9), gneiss (Fig. 7, 8), and limestones (Fig. 5, 6, 7, 12) are to be mentioned. Ceramoclasts (Fig. 1, 2, 4, 6, 7, 10, 11) are present in all the studied potsherds, with participation up to 2 - 3% and sizes between 0.70 x 2.00 mm. The observed bioclasts are represented by algae, and foraminifera remnants (Fig. 10, 11, 12).

X-Ray diffraction

The X-Ray diffraction (XRD) patterns of some selected samples confirm the microscopic observations revealing a relatively simple mineralogical composition (Figs. 13 and 14). All the samples contain quartz, K-feldspars (orthoclase and microcline), Ca-Na feldspars (albite – anorthite) and micas (muscovite/illite) as main minerals. Clay minerals have been thermally affected and they are evidenced only by the lines at 4.5 Å and 2.6 Å. As an exception, in sample 7 and 21, the mica lines are missing. The “accesory” minerals are represented by carbonates (calcite), and iron oxi-hydroxides (hematite – samples 2, 8, 19).

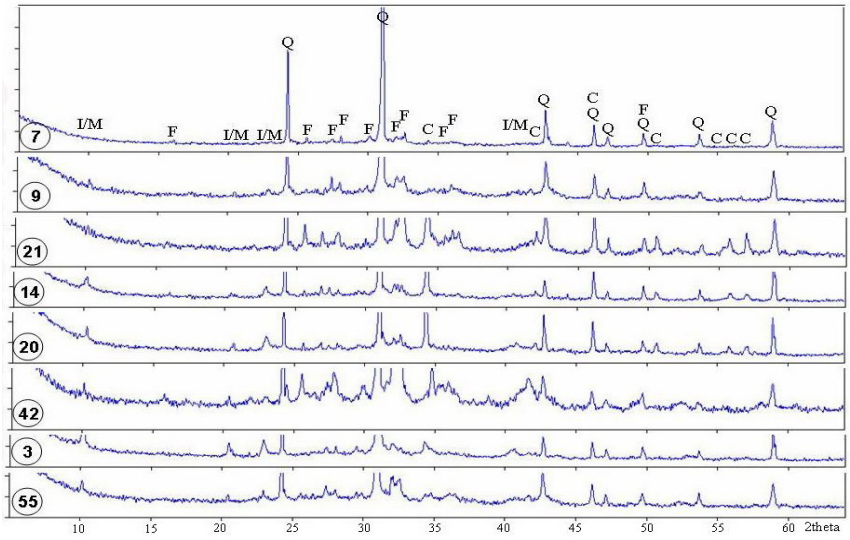

Fig. 13. XRD patterns of the studied ceramic fragments; sample no. is indicated in the lower left corner; Q – quartz, F – feldspars (Ca-Na + K), I/M – illite/muscovite, C – calcite.

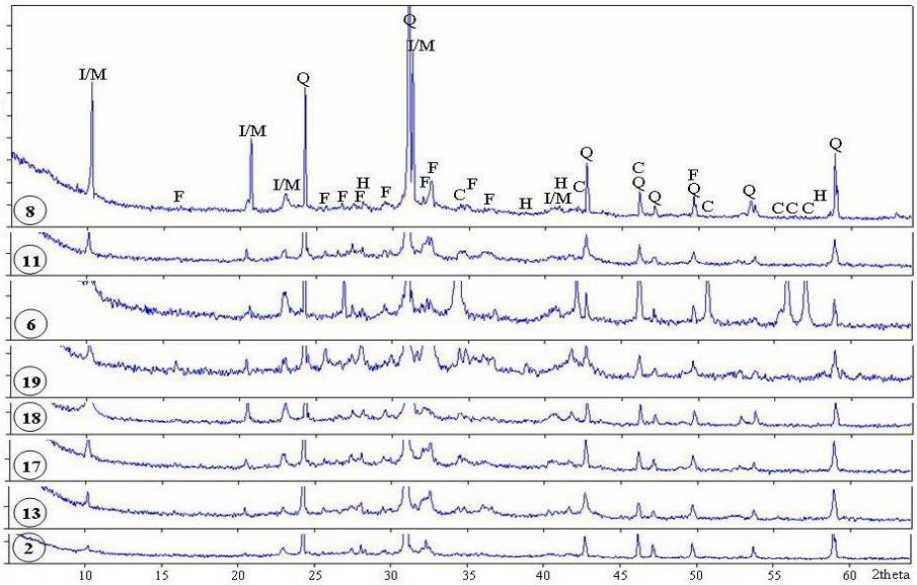

Fig. 14. XRD patterns of the studied ceramic fragments; sample no. is indicated in the lower left corner; Q – quartz, F – feldspars (Ca-Na + K), I/M – illite/muscovite, C – calcite, H – hematite.

Physical characteristics

From every ceramic sample, three fragments were collected for determining of physical characteristics. The fragments were dried in an oven and weighted. Then, they were boiled in water for 2 hours and weighted afterwards again (Archimedes' principle).

The compaction characteristics, *i.e.* water absorption, apparent density and porosity are presented in Table 2. The data for water absorption are showing a broad range of values (9.09 % - 23.10 %) having direct impact upon the functionality of the pottery vessels.

The differences could be explained in correlation with several features: (1) inhomogeneity of the raw materials mixture (clay materials / temper), (2) the thickness of the ceramic body (only 3-4 mm in the case of sample 42), (3) the type (primary, secondary), size, and the abundance of pores and fissures, (4) variable firing temperatures in different parts of the kiln or uncontrolled flames, (5) the „sandwich"-type structure of the shred as a result of a less suitable thermal treatment and the change of the firing condition (oxidizing/reducing atmosphere) or high water content in raw mixture [25-28].

Table 2. Compaction characteristics of some selected ceramic samples

Sample	Apparent density (g/cm^3)	Water absorption (%)	Apparent porosity (%)
13	1.78	16.17	28.89
18	1.82	15.44	28.16
2	1.92	13.79	26.56
7	1.93	14.14	27.28
20	1.98	9.78	19.39
14	1.91	13.67	26.15
55	1.83	15.44	28.24
9	1.83	15.37	28.25
6	1.89	13.31	25.19
17	1.82	15.21	27.73
19	1.70	19.86	33.76
21	1.22	10.48	19.21
42	1.64	23.10	37.94
3	1.86	14.07	26.22
8	1.98	9.09	18.04
11	1.86	14.05	26.13

The apparent porosity for most of studied ceramic samples is in a narrow range (26 – 29 %) fact that demonstrates the similar conditions of firing. Except the sample 42 – 2nd-3rd century AD (Roman period) being fired in an oxidizing firing atmosphere (red colour of the ceramic) that has a high apparent porosity. Sample 8 – 7th-8th century AD (Early Middle Age) fired in reducing firing atmosphere is a dense ceramic due to the presence of Fe^{2+} compounds witch has a lower melt temperature comparing with Fe^{3+} compounds.

CONCLUSIONS

A number of 56 samples from different types of pottery, and from different periods (from Roman time until the Early Medieval period) were analysed using petrographic and physical analysis.

The colour of the analysed potsherds suggest both reducing, respectively oxidizing atmosphere. Macroscopically, quartz grains, micas, and ceramoclast could be observed. The pore sizes vary from 0.5 x 1.5 mm to1.5 x 2.0 mm. According to the microscopic grain size, two types of ceramics can be separated: semifine, and coarse. Different types of fabric were described in the ceramic matrix based on the ratio between crystalline *vs.* amorphous phases: microcrystalline, and microcrystalline-amorphous.

As non-plastic materials (temper), crystalloclasts (quartz, micas, feldspars, iron oxi-hydroxides, amphibole, garnets, epidote, zircon), lithoclasts (quartzite, micaschist, gneiss, limestones), and ceramoclasts were identified. The high birefringence of the micas and of the whole matrix beside its characteristics indicates low firing conditions. The presence of the carbonates confirms these firing conditions. The bioclasts are represented by algae, and foraminifera remnants, typical for the geological Eocene deposits in the Mera– Suceag – Baciu area.

The presence of the elongated pores and the preferred orientation of mica lamellae suggest both a plastic shaping and potter's wheel.

The X-Ray diffraction patterns of some selected samples confirm the microscopic observations revealing a relatively simple mineralogical composition.

Samples compaction (water absorption capacity) varies between 9.09 % - 23.10 %.

Based on the microscopic features, mineralogical composition, and the compaction characteristics, the firing temperature of the studied potsherds could be estimate to be between 800°-900°C. The archaeological information (three documented kilns and other three presumed) and the performed analyses suggest that the Suceag pottery is a local product. Based on the analysed ceramic fragments, at this time, no connection between the three overlapping settlements could be determined.

EXPERIMENTAL SECTION

The macroscopic investigation was performed by using a Nikon SMZ 645 binocular. The microscopic study was performed on thin sections (< 25 μm) in polarized light by using a Nikon Eclipse E200 microscope. The microphotographs were taken with a NIKON FDX-35 camera.

The XRD patterns were obtained with a Bruker D8 Advance (Bragg-Brentano geometry) diffractometer, with Co anticathode (Co-K_a, λ_{Co} = 1.79026 Å), 35kV, 40 mA, in the 5°–65° 2Theta interval, $\Delta 2\theta = 0.02°$.

The physical characteristics (apparent density, water absorption, apparent porosity) were measured after water saturation, by boiling of the ceramic fragments. From every ceramic sample three fragments were collected for physical characterization.

ACKNOWLEDGEMENTS

The study was supported by PN-II-ID-PCE-2011-3-0881 and PN-II-ID-PCE-2011-3-0158 project funds (UEFISCDI-CNCS/Romanian Ministry of Education).

REFERENCES

1. S. Cociş, A. Paki, *ActaMN*, **1989**-**1993**, 26-30, *I/2*, 477.
2. C. H. Oprean, S. Cociş, Cercetările arheologice de la Suceagu (1991-1992). In: Situri arheologice cercetate în perioada 1983-1992, Bucureşti, **1996**, *251*, 109.
3. C. H. Oprean, *Ephemeris Napocensis*, **1992**, *2*, 159.
4. C. H. Oprean, S. Cociş, *CCA*, **1994**, 62.

5. C.H. Oprean, Eine spätrömische Riemenzunge aus der Siedlung von Suceag (Kreis Cluj). Beiträge zur Chronologie der Völkerwanderungszeit in Siebenbürgen. In: C. Cosma, D. Tamba, A. Rustoiu (Eds.), „Studia archaeologica et historica Nicolao Gudea dicata. Omagiu profesorului Nicolae Gudea la 60 de ani“, Zalău, **2001**, 467-478.
6. C.H. Oprean, Transilvania la sfârşitul antichităţii şi în perioada migraţiilor. Schiţă de istorie culturală, Ed. Nereamia Napocae, Cluj-Napoca, **2003**, 137-146.
7. C.H. Oprean, S. Cociş, *CCA*, **1996**, 116.
8. C.H. Oprean, S. Cociş, Die Töpferwerkstätten aus dem 5. Jh. n. Ch. aus der Siedlung von Suceag (Kr. Cluj). In: A. Rustoiu & A. Ursuţiu, „Interregionale und kulturelle Beziehungen im Karpatenraum (2. Jht. v. Chr. – 1. Jhr. n. Chr.)“, Cluj-Napoca, **2002**, 267-295.
9. C.H. Oprean, V.-A. Lăzărescu, *Ephemeris Napocensis*, **2013**, *23*, 339.
10. S. Scarcella (Ed.), Archaeological Ceramics: A Review of Current Research, Oxford, **2011**, BAR S2193.
11. W.Y. Adams, E.W. Adams, Archaeological typology and practical reality. A dialectal approach to artefact classification and sorting, Cambridge, **1991**, 427.
12. L.S. Klejn, Archaeological typology, Oxford, **1982**, BAR153.
13. V.-A. Lăzărescu, V. Mom, Pottery Studies of the 4th-Century Necropolis at Bârlad-Valea Seacă, Romania. In: S. Campana, R. Scopigno, G. Carpentiero, M. Cirillo (Eds.), The 43rd Computer Applications and Quantitative Methods in Archaeology: Keep the Revolution Going (CAA 2015), Oxford, **2016**, 875-888.
14. D.E. Arnold, Ceramic theory and social process, Cambridge, **1985**.
15. M.S. Tite, *Journal of Archaeological Method and Theory*, **1999**, *6(3)*, 181.
16. M.S. Tite, *Archaeometry*, **2008**, *50(2)*, 216.
17. R. Gindele, Ein im Römerzeitlichen Töpferzentrum von Medieşu Aurit‑Şuculeu Entdeckter Römischer Militärischer Beschlag. In: R. Madyda-Legutko & J. Rodzińska-Nowak, “Honoratissimum assensus genus est armis laudare. Studia dedykowane Profesorowi Piotrowi Kaczanowskiemu z okazji siedemdziesiątej rocznicy urodzin”, Krakow, **2014**, 337-343.
18. C. Ionescu, L. Ghergari, O. Tentea, *Cercetări arheologice*, **2006**, *XIII*, 387.
19. C. Ionescu, L. Ghergari, Caracteristici mineralogice şi petrografice ale ceramicii romane din Napoca. In: V. Rusu-Bolindeţ, “Ceramica romană de la Napoca. Contribuţii la studiul ceramicii din Dacia romană,” Bibliotheca Musei Napocensis, XXV, Ed. Mega, Cluj-Napoca, **2007**, 434-462.
20. M. Benea, M. Gorea, *Rom. J. Materials*, **2007**, *37(3)*, 219.
21. M. Benea, M. Gorea, N. Har, *Rom. J. Materials*, **2010**, *40(3)*, 228.
22. M. Benea, R. Ienciu, V. Rusu-Bolindeţ, *Studia Universitatis Babeş-Bolyai, Chemia*, **2013**, *LVIII (4)*, 147.
23. M. Benea, V. Diaconu, Gh. Dumitroaia (2015), *Studia Universitatis Babeş-Bolyai, Chemia*, **2015**, *LX (1)*, 89.
24. C. Ionescu, L. Ghergari, *Cercetări arheologice*, **2006**, *XIII*, 433.
25. C. Orton, P. Tyers, A. Vince, Pottery in Archaeology, Cambridge, **1993**.
26. P.M. Rice, Pottery Analysis. A Sourcebook, Chicago-London, **1987**.
27. A.O. Shepard, Ceramics for the Archaeologist, Washington D.C., **1976**.
28. N. Cuomo di Capri, La ceramica in archeologia, Roma, **1985**.

Plate 1. General plan of the site at Suceag

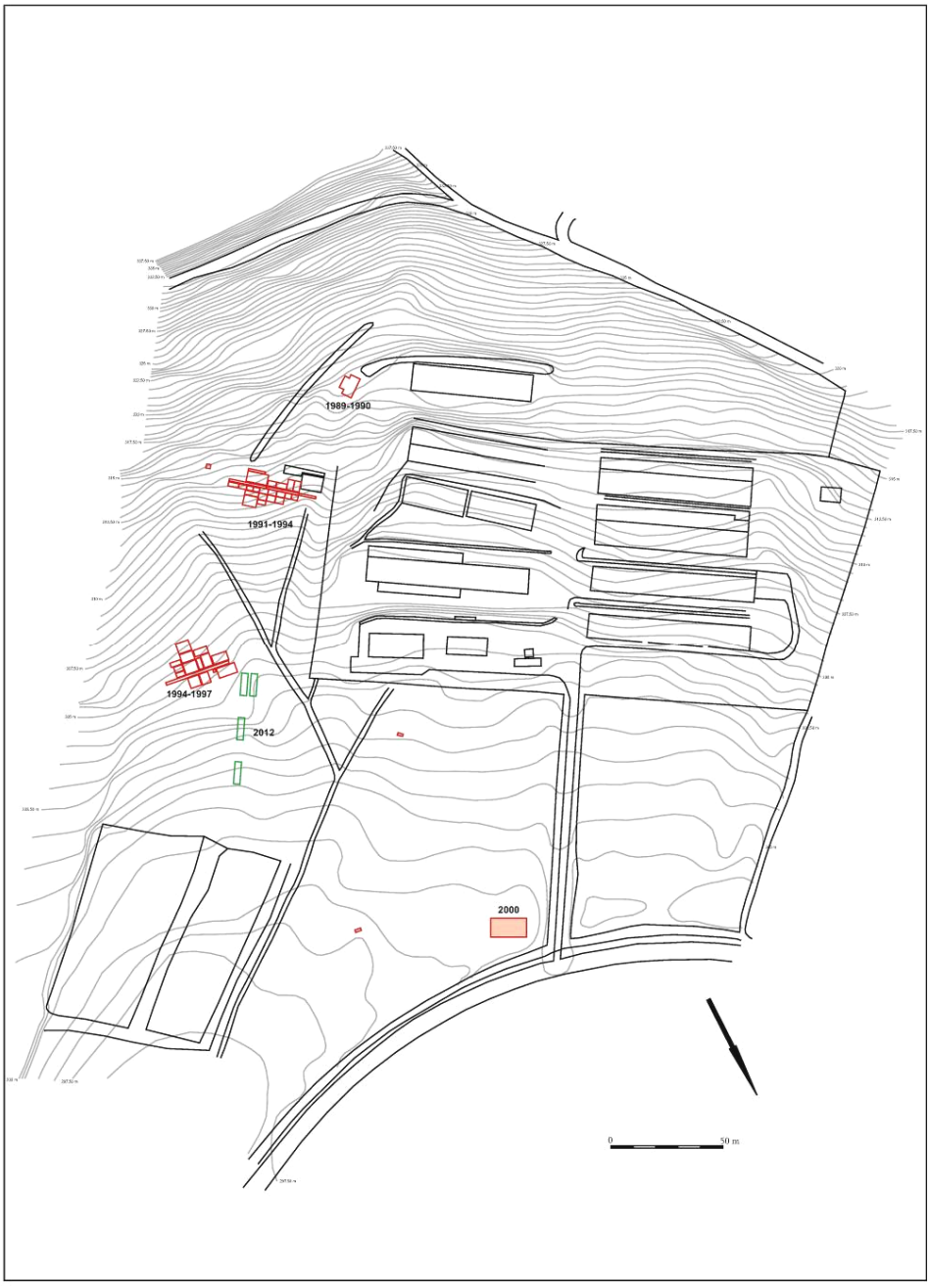

Plate 2. Electrical resistivity tomography; a. – 3D Inversion of the P1 ÷ P5 profiles at 0.40 m depth; b. – location of the 3D ERT slice on the magnetic map illustrating a pottery kiln.

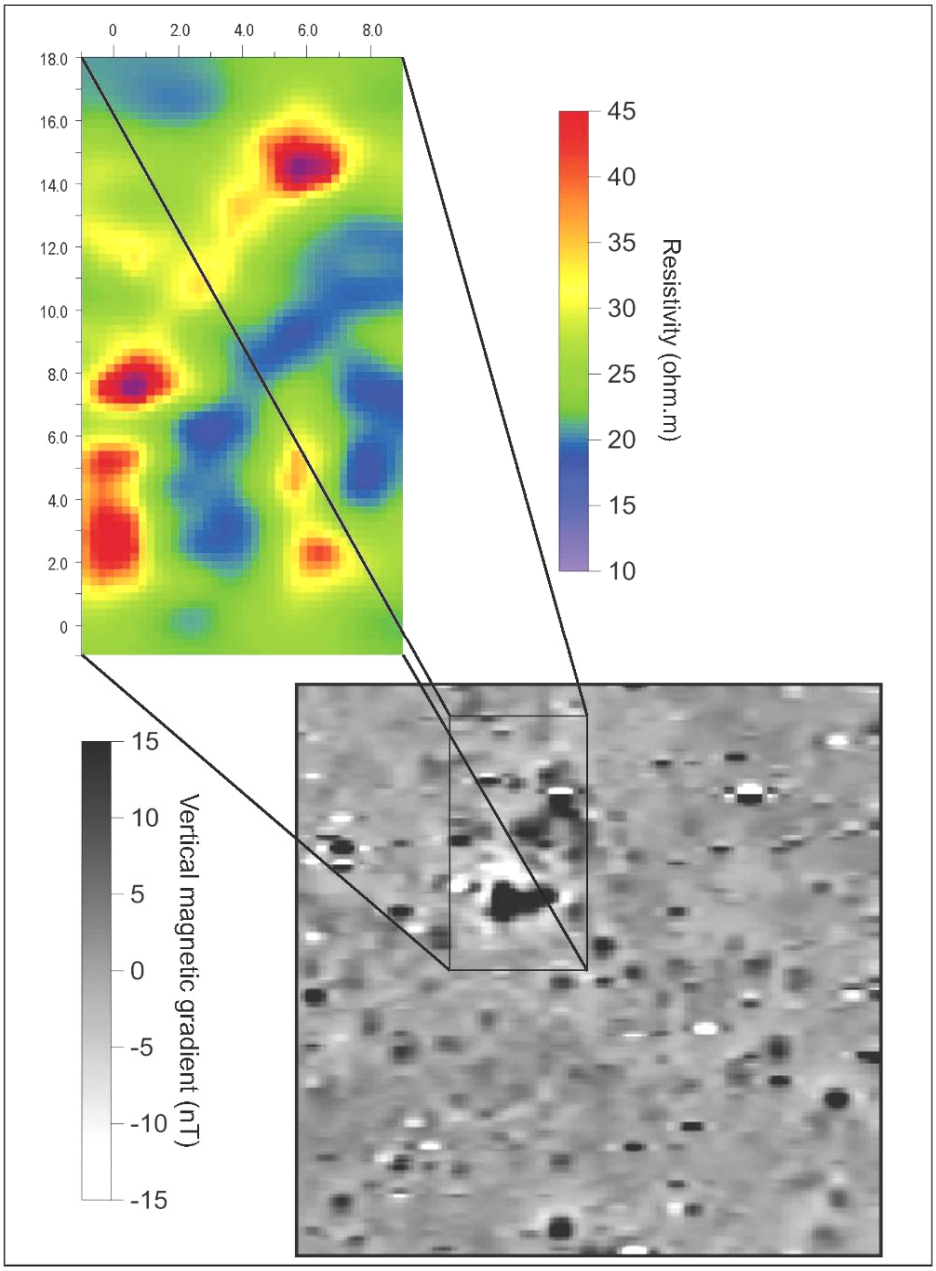

Plate 3. Pottery fragments from which the samples were taken (see Table 1).

Plate 4. Pottery fragments from which the samples were taken (see Table 1).

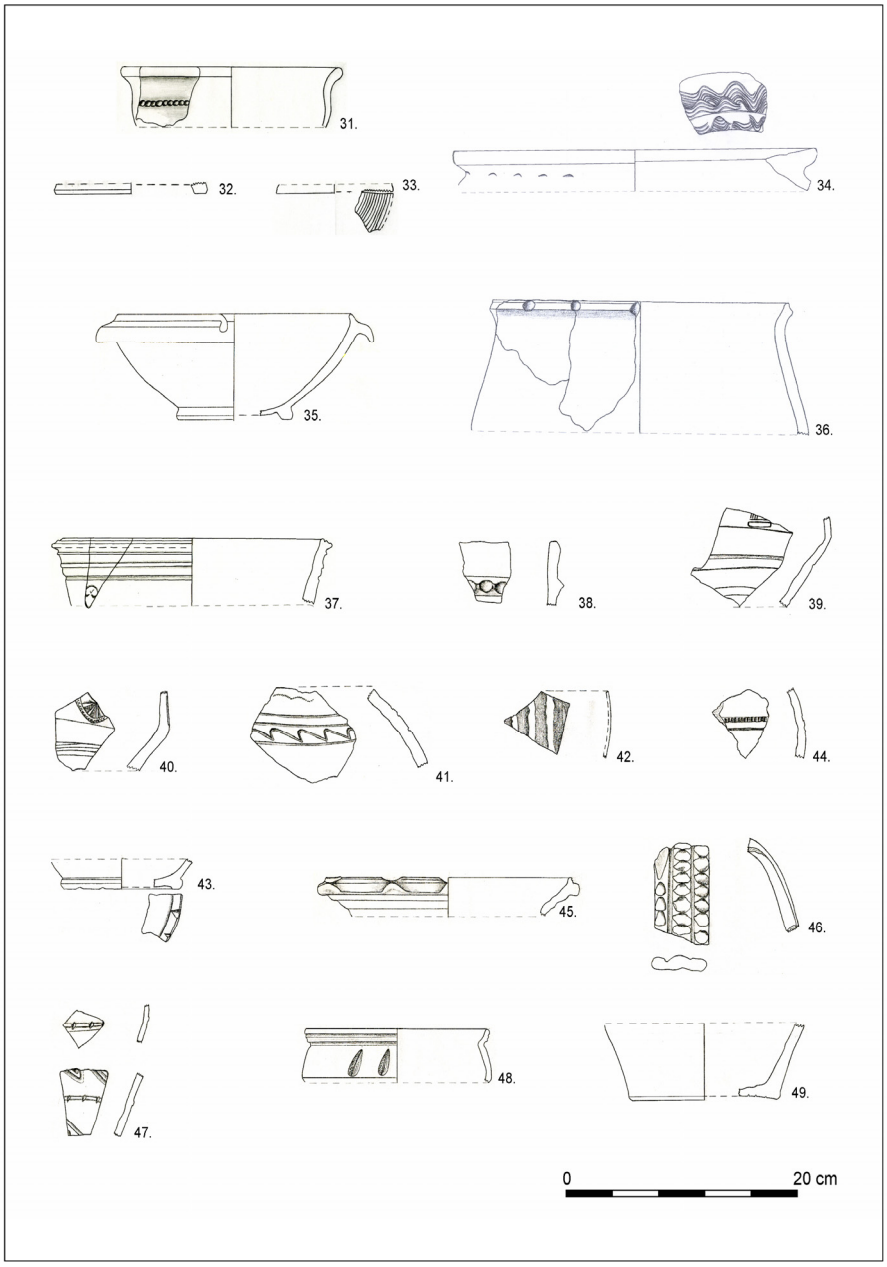

STUDIA UBB CHEMIA, LXI, 2, 2016 (p. 89-102)
(RECOMMENDED CITATION)

HUMAN HEALTH RISK ASSOCIATED WITH THE TRANSFER OF HEAVY METALS INTO THE TROPHIC CHAIN BY CATTLE GRAZING ON THE AREA IN THE VICINITY OF THE TAILING PONDS IN THE EAST OF BAIA MARE CITY, ROMANIA

IRINA SMICAL[a*], ADRIANA MUNTEAN[b], ZOLTÁN TÖRÖK[c]

ABSTRACT. In order to assess the potential human health risk associated with the transfer of heavy metals from contaminated soil to the trophic chain, several studies were conducted regarding the contaminants known to be associated to the non-ferrous ores processing industry in Eastern Baia Mare: Cu, Mn, Zn, Pb, Cd, Cr and Ni. The transfer of heavy metals into the trophic chain has the following order: from soil to vegetation: Zn>Cd>Cu>Mn>Pb>Cr>Ni and from vegetation to milk: Zn>Cu>Cd>Pb>Ni>Cr>Mn, respectively.

Based on the human risk index (HRI) calculated for each element, it was demonstrated that the ingestion of milk from the cows grassed on the contaminated area does not pose a significant risk for human health.

Keywords: *milk, heavy metals, food chain, human health risk*

INTRODUCTION

The presence of heavy metals in the soil and their accumulation in vegetables represents a major risk for human safety [1]. In order to evaluate the risk degree associated with the concentration of heavy metals in vegetables and their transfer into the human organism, a lot of research has been carried out [2-7]. Soils in the vicinity of mining exploitations and tailings ponds are usually characterized by high concentrations of heavy metals, such as Pb, Cd, Zn, Cu, Cr, Ni, Mo [8-9].

[a] *Technical University of Cluj-Napoca, North University Centre of Baia Mare, Faculty of Engineering, 62A Victor Babeş Street, Baia Mare City, Maramureş County, Romania*
[*] *Corresponding author: Irina.smical@yahoo.com*
[b] *Maramureş Water Management System, Someş-Tisa Basinal Water Administration, 2 Aleea Hortensiei, Baia Mare City, Maramureş County, Romania*
[c] *Faculty of Environmental Science and Engineering, Babeș-Bolyai University of Cluj-Napoca, 30 Fântânele St., Cluj County, Romania*

The studies carried out by Zhuang et al. (2009) [10] regarding the accumulation and transfer of heavy metals from a certain mining area into the trophic chain (plants-insects - chicken) demonstrated an increase in the bioaccumulation rate for Zn and Cu as compared with the bioaccumulation of Pb and Cd.

The study carried out by Póti et al, (2012) [11] regarding the transfer of heavy metals, such as Pb, Cd and Cr in sheep milk showed that the maximum threshold allowed in the European legislation for Pb and Cd was exceeded.

Other researches on the transfer of heavy metals (Cu, Zn, Cd, Cr, Ni and Pb) from grass into cow milk, carried out by Gougoulias et al., (2014) [12] demonstrated the highest bioaccumulation for Ni, Cu and Zn.

Temiz and Soylu, (2012) [13], studied the transfer of heavy metals: Cu, Fe, Zn, Cr, Ni, Cd and Pb from vegetation into milk, considering the summer and winter season, and the results showed that Cu, Pb and Cd had the highest transfer rate during summer. The results obtained by Ogundiran et al., (2012) [14] regarding the bioaccumulation of Pb, Cd, Cu and Zn in cow milk indicated a high transfer of lead into the milk of the cows fed with grass from a heavy metals contaminated site.

Studies carried out by Akbar Jan et al., (2011) [5], on the age and gender categories, regarding the transfer of heavy metals from milk to the blood of inhabitants from a polluted area, revealed high transfer of Cu, Zn and Mn. The highest concentrations of heavy metals were accumulated by the elderly male population.

This paper intends to emphasize the risks associated with the ingestion of milk contaminated with heavy metals analyzing their transfer from the soil polluted by metallurgic and mining activities into the trophic chain. The obtained results and observations may represent a reference source for other researches on health risks associated to the ingestion of food contaminated with heavy metals.

The study area

In order to assess the health risk associated with heavy metals from mining waste deposits, the grazing land located south of the „Iaz Central" tailings pond was chosen, situated at approximately 3 km East of Baia Mare city and less than 1 km North-East of Satu Nou de Sus (Figure 1). The study area is situated in the close vicinity of the tailings pond and it is used as a grazing ground for the cows in Satu Nou de Sus, therefore representing a risk source for the trophic chain. Furthermore, while tearing the grass, the cows also ingest a part of the soil, and in this case, the soil represents the source with the highest concentration in heavy metals.

In Satu Nou de Sus village there are approximately 360 milk cows, of which 70% are Romanian Piebald and 30% Holstein cow breeds. Most of these cows graze 120 – 150 days/year on the grazing ground situated in the vicinity of the mining waste deposit.

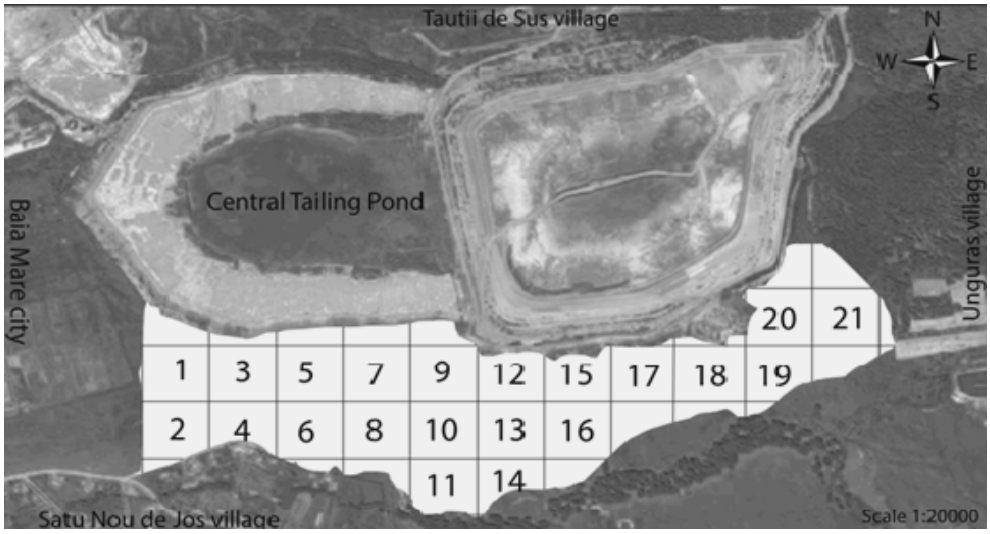

Figure 1. The map of the study area

This tailings pond contains more than 10 million tonnes mining tailings, produced during 25 years of processing activity of complex and gold ores coming from the mines of Şuior, Cavnic, Herja and Turţ [15-16].

Major pollution sources of the studied area were also SC Cuprom SA metallurgic plant and the Central Flotation Plant Baia Mare, due to the predominant wind directions, from West to East and South-West to North-East [17].

RESULTS AND DISCUSSION

The soil elements in the study area are included in the Luvisol class, white luvisol type, on a clay layer, with Ao-Ea-EB-Bt profile, characterized by good drainage [18].

21 soil samples from 0-20 cm depth and 21 grass samples were sampled from the investigated area. pH reaction, humus and total nitrogen content, metal in pseudo-total and bioavailable (in DTPA extraction) forms were determined for the soil samples. The heavy metals were determined for the grass sample, as well. The elements for primary statistics are presented in table 1.

Table 1. Primary statistical elements for the characterization of soil and vegetation

Indicators	Order 756/1997 [20]			Mean	Median	Minimum	Maximum	Standard Error	Standard Deviation	Confidence level (95.0%)
	N	A	I							
pH, pH units	-	-	-	5.622	5.630	5.170	6.200	0.071	0.324	0.148
Humus, %	-	-	-	1.397	1.420	1.080	1.680	0.036	0.165	0.075
N total, %	-	-	-	1.08	1.06	0.91	1.32	0.03	0.12	0.05
Cu T, mg kg^{-1} d.w.	20	100	200	35.03	32.00	16.70	52.60	2.42	11.10	5.05
Cu DTPA, mg kg^{-1} d.w.	-	-	-	4.389	4.100	2.110	7.190	0.349	1.598	0.728
Cu Grass, mg kg^{-1} d.w.	-	-	-	1.153	1.130	0.403	2.030	0.096	0.440	0.200
MnT, mg kg^{-1} d.w.	900	1500	2500	1118	1096	677	1465	46.0	209	95
Mn DTPA, mg kg^{-1} d.w.	-	-	-	142.1	131.0	86.0	206.0	6.2	28.6	13.0
Mn Grass, mg kg^{-1} d.w.	-	-	-	20.9	20.00	12.00	41.00	1.27	5.83	2.66
Pb T, mg kg^{-1} d.w.	20	20	100	46.2	39.60	16.30	105.6	5.72	26.21	11.93
Pb DTPA, mg kg^{-1} d.w	-	-	-	12.2	9.11	3.38	30.80	1.86	8.51	3.87
Pb Grass, mg kg^{-1} d.w.	-	-	-	1.683	1.220	0.641	4.420	0.240	1.098	0.500
ZnT, mg kg^{-1} d.w.	100	300	600	312.9	296.0	180.0	595.0	23.64	180.0	49.31
Zn DTPA, mg kg^{-1} d.w.	-	-	-	90.9	91.50	46.40	145.0	5.56	25.47	11.59
Zn Grass, mg kg^{-1} d.w.	-	-	-	26.2	26.60	13.30	44.70	1.82	8.34	3.80
CdT, mg kg^{-1} d.w.	1	3	5	1.187	1.06	0.656	2.868	0.1005	0.4608	0.209
Cd DTPA, mg kg^{-1} d.w.	-	-	-	0.417	0.281	0.164	1.620	0.076	0.350	0.159
Cd Grass, mg kg^{-1} d.w.	-	-	-	0.111	0.088	0.043	0.358	0.017	0.0790	0.036
Cr T, mg kg^{-1} d.w.	30	100	300	77.11	76.40	36.40	129.2	6.02	27.59	12.56
Cr DTPA, mg kg^{-1} d.w.	-	-	-	13.04	7.98	2.90	129.2	5.83	26.74	12.17
Cr Grass, mg kg^{-1} d.w.	-	-	-	0.790	0.769	0.476	1.28	0.047	0.2186	0.099
Ni T, mg kg^{-1} d.w.	20	75	150	40.1	36.80	24.10	70.10	2.90	13.27	6.04

Indicators	Order 756/1997 [20]			Mean	Median	Minimum	Maximum	Standard Error	Standard Deviation	Confidence level (95.0%)
	N	A	I							
Ni DTPA, mg kg^{-1} d.w.	-	-	-	7.06	3.85	1.92	38.8	2.287	10.48	4.772
Ni Grass, mg kg^{-1} d.w.	-	-	-	0.595	0.311	0.223	3.17	0.179	0.822	0.374
Note: N- normal value of the metal; A – alert threshold value; I– intervention threshold value; d.w. -dry weight; M - T - the total form of the metal; M - DTPA- the bioavailable form of metal after its extraction in DTPA; M - Grass - the total form of metal in vegetation										

According to those mentioned above, one may say that the pH reaction of the soil in the investigated area falls in the moderate acid range with a very low humus content and low level of assurance with potential accessible nitrogen [19].

Furthermore, the mean concentrations of the pseudo-total form of the metals of interest exceed the normal value in the Order 756/1997 [20], cadmium by at least 1.2 times and zinc by maximum 3.1 times.

Principal factor analysis (PCA) with Pearson correlation (n) identifies significant positive correlations between the soil pH reaction and most metallic elements (Cd, Cr, Cu, Mn, Pb) in soil and vegetation (Figure 2), thus demonstrating their common source. Strong negative correlations (Figure 2) have been identified between the total available nitrogen and the studied metallic elements.

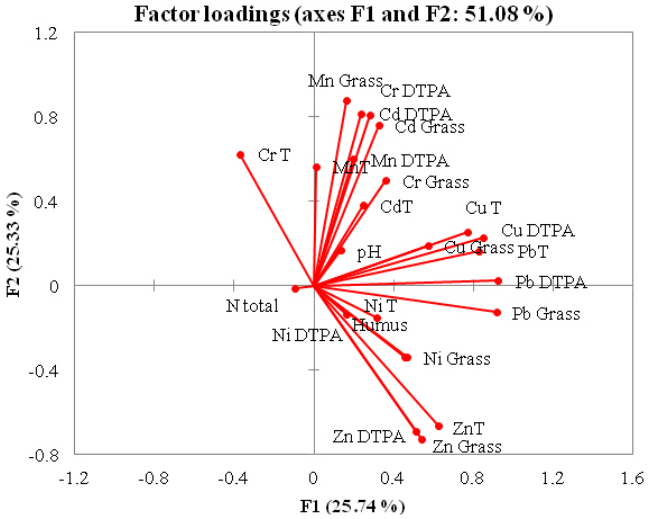

Figure 2. Principal factor analysis with Pearson correlation (n)

In order to assess the soil pollution level, the soil pollution index (PI_i) for each metal was calculated (eq. 2) [1].

$$PI_i = \frac{C_i}{S_i} \tag{2}$$

This demonstrates the highest value for zinc, followed by chromium, lead, nickel, copper, manganese and cadmium (Figure 3).

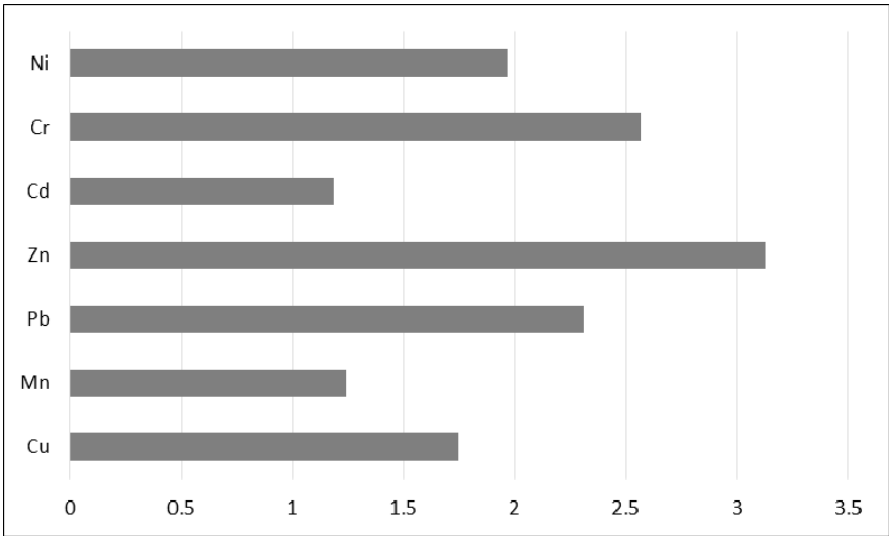

Figure 3. The pollution index for the soils in the grazing ground

According to studies carried out by Hu et al. (2013) [21], Yang et al. (2013) [22], Cheng (2007) [23], the Nemerow global pollution index for the investigated area (PI_N) was calculated using the equations 2-4 [1, 21 - 23]

$$P_{ave} = \frac{1}{7}\sum_{i=1}^{n} PI_i \tag{3}$$

$$PI_N = \sqrt{\frac{PI_{ave}^2 + PI_{i\max}^2}{2}} \tag{4}$$

where

PI_i – pollution index for each metal;
C_i – determined concentration of metals in soil;
S_i – metal concentration, considered normal values in soils, according to the current Romanian legislation (Order 756/1997);

PI_{ave} –the mean pollution index;
PI_{imax} – the maximum pollution index of the 7 studied metals (in this case, Zn=3.129);
PI_N – the Nemerow global pollution index.

For the studied area, the value of the Nemerow pollution index of 2.998 shows a moderate to severe pollution of the soils with heavy metals [22].

The European regulation no. 1881/2006 provides 0.020 mg kg^{-1} (wet weight) as maximum allowed limit for Pb in raw milk. Thus, the determined concentrations for all 10 raw milk samples, exceed the maximum allowed limit at least by 1.65 times and at most by 3.80 times. Identically, in all mentioned studies, the lead concentration was exceeded. For Cu, Mn, Zn, Cd and Ni the determined values were between the limits reported in several studies [24-27] (table 2).

Table 2. Heavy metals in raw cow milk

Metal	The present study mg l^{-1}	Enb et al., (2009) [24], mg kg^{-1}	Ogabiela et al, (2011) [25] mg l^{-1}	Bilandžić et al., (2011) [26] µg l^{-1}	Rahini, (2013) [27] mg l^{-1}
Cu	0.086 - 0.211	0.108 - 0.194	0.252 - 0.214	1.0 – 20.0	nr
Mn	0.057 - 0.130	0.040 - 0.084	0.179 - 0.219	nr	nr
Pb	0.033 - 0.076	0.040 - 0.960	0.550 - 0.710	1.0 - 476	1.84 – 20.7
Zn	3.086 - 4.117	3.001 - 3.940	3.239 - 5.521	nr	nr
Cd	0.0021-0.0053	0.070 - 0.112	0.163 - 0.099	1.0 – 20.0	0.28 –3.43
Cr	0.039 -0.085	0.028 - 0.066	1.757 - 1.568	nr	nr
Ni	0.0018-0.0062	0.002 - 0.009	nr	nr	nr
Note: nr – not reported					

According to equation (5) proposed by Khan et al., (2008) [1] and Cui et al., (2005) [28], they calculated the transfer factors (Ft) of the investigated metals from soil to vegetation and from vegetation to milk.

$$Ft = \frac{C_{grass(milk)}}{C_{bioavailablefromsoil(grass)}} \quad (5)$$

The transfer factors are sub-unitary, the highest values being recorded at the transfer from the pseudo-total form to bio-available form in soil and at the transfer from vegetation to milk (Figure 4).

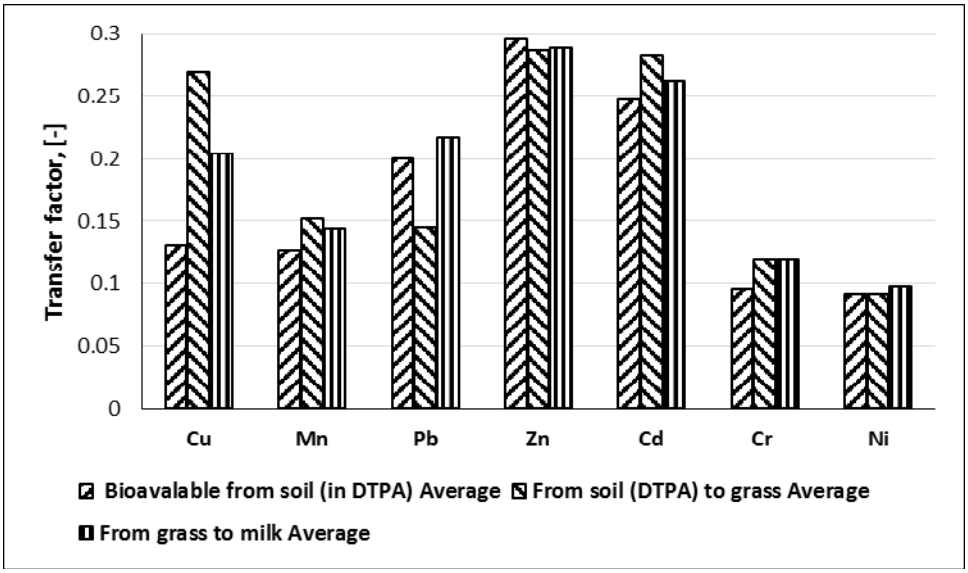

Figure 4. Mean values of the transfer factor for metals in soil-vegetation-milk

As shown in the graphic in Figure 5, the transfer factor of mean concentrations of heavy metals from soil to plant and from plant to milk, has the highest value for zinc, cadmium and copper, and the lowest value for nickel, chromium and manganese. In the case of lead, there is a significant difference between the values of the transfer factor from soil to grass and from grass to milk. The same situation is for copper, the difference demonstrating the higher transfer from soil to grass. One must notice that the identified transfer factor for zinc has almost identical values for each analyzed segment (0.296, 0.286 and 0.288), according to the results obtained by Kabata-Pendias, (2001) [29], and Kabata-Pendias and Mukherjee, (2007) [30].

The transfer of metallic elements allowed the establishing of the order of transfer from soil to vegetation: Zn>Cd>Cu>Mn>Pb>Cr>Ni and from vegetation to milk: Zn>Cu>Cd>Pb>Ni>Cr>Mn, in accordance with the studies carried out by Miclean et al., (2013) [31], Şenilă et al. (2012) [32].

The risks associated to human ingestion of milk from the cows that graze in the vicinity of the tailings pond were determined by calculating the Daily Oral Intake of Heavy Metals (DIM) through milk and the human risk index (HRI).

The determination of Daily Oral Intake of Heavy Metals (DIM) (equation 6) was done using the formula proposed by Khan et al. (2008) [1], considering that an adult with an average body weight of 65 kg intakes 1 litre milk/day.

$$DIM = \frac{C_{metal} \times D_{food\ intake}}{B_{average\ weight}} \quad (6)$$

where:

C_{metal} - the heavy metal concentration in milk (mg·l^{-1}),
$D_{food\ intake}$ - the daily intake of milk (l);
$B_{average\ weight}$ - the average human body weight (kg).

The human risk index (HRI) was calculated for each studied metal, as the ratio between the Daily Oral Intake of Heavy Metals (DIM) and the oral reference dose (RfD) (eq. 7) [1].

$$HRI = \frac{DIM}{RfD} \quad (7)$$

The reference doses for heavy metals Cu, Mn, Pb, Zn, Cd, Cr, Ni were taken from the Integrated Risk Information System [33], except for lead, which is not brought under regulation (table 1).

The human risk index (HRI), the Daily Oral Intake of Heavy Metals (DIM) and the oral reference dose (RfD) are presented in table 3.

Table 3. Average values for metal concentrations in milk, DIM and HRI

Metal	RfD (mg kg^{-1}-day) [33]	Mean±std (mg l^{-1})	DIM (mg kg^{-1})	HRI
Cu	4x10^{-2}	0.141±0.014	0.002	0.054
Mn	1.4x10^{-1}	0.089±0.007	0.001	0.010
Pb	-	0.051±0.004	0.001	-
Zn	3x10^{-1}	3.702±0.097	0.057	0.190
Cd	1x10^{-3}	0.003±0.0004	0.000	0.051
Cr	5x10^{-3}	0.057±0.0044	0.001	0.176
Ni	2x10^{-2}	0.004±0.0004	0.000	0.003
std – standard deviation				

Even if the limit value for Pb in raw milk, provided by the Regulation no. 1881/2006, is exceeded by 2.55 times in our study, the risk associated to the Pb presence in the ingested milk could not be determined because no reference dose was regulated for this metal [33], so far.

Because HRI has sub-unitary values [1, 3], one may say that the ingestion of milk coming from the cows that graze in the vicinity of the Central tailing pond does not pose a significant risk for human health.

CONCLUSIONS

In the Eastern part of Baia Mare city, there are grazing grounds in the close vicinity of mining waste tailing ponds, in an anthropic modified area, with acidic soil reaction and poor in nitrogen and humus. Thus, the sustainable development of this area requires the elaboration of a strategy for soil quality improvement, which will use the natural resources of the area.

The transfer of heavy metals from the soil of an industrial area, with mining characteristics from the Baia Mare area, has the following order: from soil to vegetation: Zn>Cd>Cu>Mn>Pb>Cr>Ni, and from vegetation to milk: Zn>Cu>Cd>Pb>Ni>Cr>Mn.

Although the presence of metallic elements in their pseudo-total form is abundant, the values of transfer factors for the studied elements are sub-unitary.

In order to assess the level of trophic risk, the pollution index, as well as the transfer factor from soil to vegetation for each studied metal were taken into account.

The human risk index is sub-unitary and has the following order: Zn>Cr> Cu>Cd>Mn>Ni. The risk associated to lead was not determined, because there is no reference dose established. Without taking into account the sub-unitary values, the highest health risk may be associated to zinc and cadmium.

In order to assess the human health risk associated to the presence of heavy metals in the milk of cows grazing on a contaminated area, the human risk index (HRI) was calculated. The sub-unitary value obtained for the risk index demonstrates that there is no significant risk for human health, due to milk intake.

EXPERIMENTAL SECTION

Sampling, processing and sample analysis

In order to identify the health risk associated to milk ingestion (fresh and/or processed) from the cows that graze on the grazing ground situated in the close vicinity of the ”Iaz Central” mining waste tailings pond, several studies regarding the contaminants known to be associated to non-ferrous ore processing industry were performed: copper, manganese, zinc, lead, cadmium, chromium and nickel. Their concentrations were analyzed in all the levels of the trophic chain; soil (the pseudo-total and bioavailable form),

grazed grass vegetation and milk. For soils, elementary physical – chemical characteristics were also determined (pH reaction, hummus content and total nitrogen).

The 21 ha of the grazing land were divided into 21 squares, each with a total area of 1 ha. Soils were sampled 60 days after grazing period began, from a depth of 0 – 20 cm, following the grass sampling, by cutting grass with a Teflon knife. The final soil sample was obtained by gathering 5 samples from each square, 0.5 kg each. Each soil and grass sample was sampled in polyethylene bags, according to standard STAS 7184/1-1984 [34] and Figure 1.

The milk samples were taken from 10 cows which grazed on the investigated area. Every morning and evening milking, an amount of 500 ml milk was sampled from every cow and put in labelled glass bottles. Then the samples were mixed to obtain a homogenous milk sample which was subjected to laboratory analyses. Every indicator, from every sample, was analyzed in 3 replicates and the mean values were calculated.

Soil samples were prepared for physical-chemical analyses according to the requirements in ISO 11464:2006 [35]; the foreign objects were removed, the soil was dried at room temperature, for 1 week. After drying, soil samples were grinded and sieved out through the 200 μm polyethylene sieve; from each sample, the pH, humus, total nitrogen and metals – the pseudo-total form [36] and DTPA extractible form [37] were determined.

The grass samples were moved entirely in Petri dishes and dried in an oven, at 105 °C, to reach the constant mass, afterwards being grinded.

The milk samples were cold preserved (2-4 °C) and analyzed within 24 hours since sampling.

In order to determine the pseudo-total forms of metals from soil, vegetation and milk samples were mineralized in a microwave oven, in Teflon capsules, in acidic medium (aqua regia for soil - 21 ml HCl 12M+7 ml HNO_3 15.8M and 7 ml HNO_3 15.8M +1 ml H_2O_2 30 % - for vegetation and milk samples), for 20 minutes at 160 °C and 800 W. The wet residues were decanted, after filtration, in 100 ml flasks and HNO_3 0.5M was added [36].

The bioavailable metallic fractions in the soil were determined by extraction in a buffer solution (at pH = 7.3 ± 0.2) of diethylene triamine pentaacetic acid (DTPA), at a temperature of (20 ± 2) ^oC in specific shaking conditions and at a ratio between soil: extraction solution of 1:2 (m/v) [37].

The atomic absorption spectrometry analysis (Perkin Elmer A Analyst 700, with flame and graphite atomization techniques) of interest metals was performed according to the following conditions: on calibrating pilot with a correlation factor of $R^2 \geq 0.990$, developed through the least squares method, from reference materials with NIST traces (Merck producer)

and with internal conditions of assuring the quality of results (control diagrams, quantification limit checking, repeatability and recovery check, by using a certified reference material).

The soil pH reaction was electrochemically determined, by using a WTW pH meter, InoLab 730, with Sentix probe – metrologically calibrated and verified, in aqueous solution, in m/v 1:2.5 ratio [38].

The humus content was determined through calculus, after determining the organic carbon, by using the method provided by the Romanian standard [39].

The total nitrogen was determined through the Kjeldahl method [40], by distillation in alkaline environment of the previous mineralized samples with a strong acid and the absorption of ammonia discharged in a solution of boric acid with a mix colour indicator, using a digestion system and with automatic distillation unit, ProNitro-Selecta type.

REFERENCES

[1]. S. Khan, Q. Cao, Y.M. Zheng, Y.Z. Huang, Y.G. Zhu, *Environmental Pollution,* **2008**, *152*, 686.
[2]. G. Dziubanek, A. Piekut, M. Rusin, R. Baranowska, I. Hajok, *Ecotoxicology and Environmental Safety*, **2015**, *118*, 183.
[3]. K. Khan, H. Khan, Y. Lu, I. Ihsanullah, S. Khan, N.S. Shah, I. Shamshad, A. Maryam, J. Nawab, *Ecotoxicology and Environmental Safety*, **2014**, *108*, 224.
[4]. X. Liu, Q. Song, Y Tang, W. Li, J. Xu, J. Wu, F. Wang, P.C. Brookes, *Science of the Total Environment*, **2013**, *463*, 530.
[5]. F. Akbar Jan, M. Ishaq, S. Khan, M. Shakirullah, S.M. Asim, I., Ahmad, F. Mabood, *Journal of Environmental Sciences*, **2011,** *23*, 2069.
[6]. S. Khan, R. Farooq, S. Shahbaz, M.A. Khan, M. Sadique, *World Applied Sciences*, **2009**, 6, 1602.
[7]. N. Sridhara Chary, C.T. Kamala, D. Samuel Suman Raj, *Ecotoxicology and Environmental Safety*, **2008**, *69*, 513.
[8]. L.M. Cai, Z.C. Xu, J.Y. Qi, Z.Z. Feng, T.S., Xiang, *Chemosphere*, **2015**, *127*, 127.
[9]. D. Xu, P. Zhou, J. Zhan, Y. Gao, C. Dou, Q. Sun, *Ecotoxicology and Environmental Safety*, **2013**, *90*, 103.
[10]. P. Zhuang, H. Zou, W. Shu, *Journal of Environmental Sciences*, **2009**, *21*, 849.
[11]. P. Póti, F. Pajor, A. Bodnár, L. Bárdos, *Journal of Microbiology, Biotechnology and Food Sciences*, **2012**, *2*, 389.
[12]. N. Gougoulias, S. Leontopoulos, Ch., Makridis, *Emirates Journal of Food and Agriculture*, **2014**, *26*, 828.
[13]. H. Temiz, and A. Soylu, *International Journal of Dairy Technology*, **2012**, *65*, 516.

[14]. M.B. Ogundiran, D.T. Ogundele, P.G. Afolayan, O. Osibanjo, *International Journal of Environmental Research*, **2012**, *6*, 695.
[15]. I. Smical, I. Bud, S. Duma, *Revista Minelor*, Petroșani, **2015**, *21*, 2.
[16]. Romaltyn Mining Ltd., (2012), Site Report, http://romaltyn.ro/assets/Raport_de_amplasament_Romaltyn.pdf
[17]. National Meteorological and Hydrological Institute (NMHI), (2012), Meteorological data, hydrological and water management needs for Aurul evacuation-sizing system, Baia Mare, Bucharest (in Romanian).
[18]. Soil and Agrochemical Studies Office (SASO) of Baia Mare, (2015), Data on climatic conditions and pedogenetical in eastern Baia Mare (in Romanian).
[19]. N. Florea, V. Balaceanu, C. Rauta, A. Canarache, et. al., "Methodology of Pedological Studies Development (MPSD)", Research Institute for Soil and Agrochemistry, Bucharest (in Romanian) 1987.
[20]. Order no. 756 of 3 November 1997 approving the regulation on environmental pollution assessment, published in Of.M. no. 303 bis/6 nov. 1997.
[21]. Y. Hu, X. Liu, J. Bai, K. Shih, E.Y. Zeng, H. Cheng, *Environmental Science and Pollution Research*, **2013**, *20*, 6150.
[22]. C.L. Yang, R.P. Guo, Q.L. Yue, K. Zhou, Z.F. Wu, *Environmental Earth Sciences*, **2013**, *70*, 1903.
[23]. J. Cheng, Z. Shi, Y. Zhu, *Journal of Environmental Science*, **2007**, 19, 50.
[24] A., Enb, M.A., Abou Donia, N.S., Abd-Rabou, A.A.K., Abou-Arab and M.H., El-Senaity, *Global Veterinaria*, **2009,** *3*, 268.
[25] E.E, Ogabiela, U.U, Udiba, O.B, Adesina, C.,Hammuel, F. A, Ade-Ajayi, G.G, Yebpella, U.J., Mmereole and M., Abdullahi, *Journal of Basic and Applied Scientific Research,* **2011**, *7*, 533.
[26] N. Bilandžić, M. Dokić, M. Sedak, B. Solonum, I. Varenina, Z., Knežević and M., Benić, *Food Chemistry,* **2011**, *127,* 63.
[27] E., Rahini, *Food Chemistry*, **2013**, *136,* 389.
[28]. Y.J. Cui, Y.G. Zhu, R. Zhai, Y. Huang, Y. Qiu, J. Liang, *Environment International*, **2005**, *31*, 784.
[29]. A. Kabata-Pendias, "Trace elements in soils and plants" CRC Press, Third Edition, USA, **2001,** 331.
[30]. A. Kabata-Pendias, B.A. Mukherjee, "Trace Elements from Soil to Human", Springer, Berlin, **2007**, 193-268.
[31]. M. Miclean, E. Levei, O. Cadar, M. Șenilă, I.S. Groza, *Carpathian Journal of Earth and Environmental Sciences*, **2013**, 8 (4) 93.
[32]. M. Şenilă, E.A. Levei, R.L. Şenilă, M.G. Oprea, M.C., Roman, *Journal of Environmental Science and Health*, **2012**, *47*, 614-621.
[33]. United States Environmental Protection Agency (USEPA), Integrated Risk Information System (IRIS), 2015, http://cfpub.epa.gov/ncea/iris/compare.cfm
[34]. SR 7184-1: 1984 Soils. Sampling for pedologycal and agrochemical investigations.
[35]. ISO 11464:2006 Soil quality -- Pretreatment of samples for physico-chemical analysis.
[36]. SR ISO 11466:1999 Soil quality. Extraction of trace elements soluble in aqua regia.

[37]. SR ISO 14870:2002 Soil quality. Extraction of trace elements in a buffered solution diethylenetriamine pentaacetic acid (DTPA).
[38]. SR 7184-13:2001 Soils. Determination of pH in water and saline suspensions (mass/volume) and in saturated paste.
[39]. STAS 7184/21-82 Soils. Humus content determination.
[40]. SR ISO 11261:2000 Soil quality. Determination of total nitrogen. Kjeldahl modified method.

STUDIA UBB CHEMIA, LXI, 2, 2016 (p. 103-118)
(RECOMMENDED CITATION)

WHEAT GERM BREAD QUALITY AND DOUGH RHEOLOGY AS INFLUENCED BY ADDED ENZYMES AND ASCORBIC ACID

ADRIANA PAUCEAN[a*], SIMONA MARIA MAN[a], SONIA ANCUŢA SOCACI[a]

ABSTRACT. Wheat germs are valuable bread making ingredients, but their addition in bread loaf negatively influences the bread quality by increasing the hardness and decreasing the volume. In the context of modern baking industry, with high demands for bread with superior nutritional and sensorial quality, it clearly appears to be necessary to modulate the rheological properties of dough by using additives. In this study the influence of amylase, xylanase, glucose-oxidase and ascorbic acid on the wheat/ wheat germ flours dough and bread properties was studied. Initially, the assessment of wheat germ flour substitution (0-4%) on rheological properties and bread quality of three commercial wheat flours was determined. A substitution of 4% wheat germ flour was found to be acceptable. Secondly, the effect of improvers on dough rheology and on bread quality obtained by wheat flour/wheat germ flour blends was studied. Xylanase markedly improved the elasticity and porosity. Amylase significantly increased the crust color, the porosity and the bread specific volume. Glucose-oxidase effect is related to a higher bread specific volume, an improvement of the bread shape and crumb porosity. Ascorbic acid caused a significant increment of specific volume. Enzymes and ascorbic acid can be used to improve wheat germ bread quality.

Keywords*: breadmaking improvers, farinographic and alveographic parameters*

INTRODUCTION

Wheat (*Triticum aestivum L.*) is one of the most important crops and has been used worldwide as a main ingredient in bread making. The increasing mechanization of the baking industry and the demand for a wide range of bread types have determined the necessity to modulate structure and viscoelastic properties of dough. In order to improve bread making performance,

[a] *Faculty of Food Science and Technology, University of Agricultural Sciences and Veterinary Medicine, Department of Food Technology, 3-5 Mănăştur street, 400372, Cluj-Napoca, Romania*
[*] *Corresponding author: adriana.paucean@usamvcluj.ro*

chemical compounds and enzymes are usually included in bread formulas [1]. On the other hand, nowadays consumers are aware about the relationship between diet and diseases and from this point of view it is a great challenge for bakers to obtain nutritious bread, rich in bioactive compounds, with high quality in terms of bread specific properties (volume, crumb and crust texture, firmness, color, taste etc). In this context, wheat germs have been proposed as valuable baking ingredients due to their nutritional interest and due to the possibility of using a by-product from the milling industry. The addition of raw wheat germ or its derivate to baking products has been studied using various approaches [2]. Some of those studies were based on the addition of raw wheat germ [3,4], but others incorporate defatted wheat germ [5], heated wheat germ [6], extruded wheat germ [2] or a combination of the two to obtain products with a longer shelf life and better functional properties than raw wheat germ [7]. Wheat germs are rich in bioactive substances such as antioxidants (tocopherols, tocotrienols, phenolics, carotenoids), sterols [8,9], unsaturated fatty acids (oleic, linoleic and α-linoleic acids) and essential amino acids [10]. As for human health benefits, it is reported that the processed wheat germ can be applied in prevention and treatment of cancers [11]. Studies showed that the raw wheat germ loaves had superior nutritive value but also a reduction of quality mainly due to the increase in bread hardness and decrease in bread volume [12]. On the contrary, heat treated and extruded wheat germ addition had a smaller effect on the gluten matrix than raw wheat germ [2,6]. More recently, Sun et al., 2015 [8] reported that the addition of wheat germ flour could be an effective way of producing functional white flour but caution should be paid to addition level of wheat germ because of the adverse increase in solid-like properties of the dough. Many local bakeries are confronted with such issues due to the supplementation of wheat flour with wheat germ flour and the solution could be the adjusting of the flour blends properties by using enzymes and chemical additives. The enzymatic treatment of wheat flours is an interesting alternative to generate changes in the structure of the dough and consequently, for improving functional properties of flours. They are generally recognized as safe (GRAS) and do not remain active in the final product after baking. Therefore, enzymes do not have to appear on the label, which is an additional commercial advantage [13]. Between enzymes used usually as bread-making improvers are gluten cross-linking enzymes and polysaccharides degrading enzymes [14]. Glucose oxidase is an oxidative enzyme that catalyzes the oxidation of β-d-glucose to δ-d-gluconolactona and hydrogen peroxide. Disulfide bond interchange and the gelation of pentosans promoted by hydrogen peroxide action are the most widespread theories to explain the strengthening effect of the glucose oxidase. Furthermore, it has been related with the formation of non-disulfide covalent intermolecular bonds in the gluten proteins [13]. Amylases, xylanases are hydrolytic enzymes able to change physicochemical and structural properties of polysaccharides, making

dough softer and viscous and increasing the availability of fermentable sugars. α-amylase prolongs oven rise and results in an increased loaf volume [15]. An increase in loaf volume and an improvement of bread crumb structure can be pursued with the addition of ascorbic acid that acts on the redox systems of wheat dough. In particular, the improver action of the ascorbic acid is due to its oxidation by gaseous oxygen to dehydroascorbic acid which determines the rapid oxidation of glutathione present in flour thus minimizing the SH/SS interchange reactions of reduced glutathione with intermolecular SS bonds of gluten molecules [16].

To the best of our knowledge the influence of additives (enzymes and ascorbic acid) on wheat flour/ wheat germ flour blends properties has not been studied. This study aimed to test several bread making improvers and evaluated their effects on dough rheology and bread quality of wheat germ supplemented wheat flours by two objectives: (I) assessment of wheat germ flour substitution on rheological properties and bread quality of three commercial wheat flours and (II) evaluation of improvers effect on dough rheology and bread quality obtained by wheat flour/wheat germ flour blends.

RESULTS AND DISCUSSION

Table 1 shows the mean values of psysico-chemical and rheological parameters for the three sets of wheat flours (WF1, WF2, WF3) used in the study. For all analyzed samples the wet gluten content was higher than 22%, minimum value indicated by SR ISO 7970/2001 for the bread making wheat. Zeleny sedimentation value (SDS) ranged between 30-40. This parameters was used to estimate the bread loaf volume [18] and the quality of the gluten. The Falling number (HFN) for the tested flours did not go below 200s. HFN ranged between 290s and 354s meaning that the wheat flour with lower extraction rates obtained by wheat milling most probably needs to be supplemented with amylases during bread making to get high-quality baking products [19]. The alveographic P value is the parameter that can differentiate particular flours and the baking volume could be significantly correlated with flour water absorption and protein content [20]. For the tested WF, P ranged between 84 and 93, with the higher value for WF2. Bread volume is positively correlated with farinograph dough development time and flour water absorption [21]. With respect to the maturograph characteristics, the wheat flour WF2 recorded the longer average proofing time 46 min, while WF3 samples showed shorter average proofing time 40 min. This parameter is important from technological point of view. Generally, shorter proofing time is more suitable for technological purposes [22]. Values of maturograph dough resistance ranged from 424 to 516 BU. Variety with the lowest protein content in the set (WF3)

had technologically optimal time of final proofing (40 min) and low dough resistance (440 BU). By assessing all parameters for the tested wheat flours we concluded their quality to be medium to good for baking purpose.

Table 1. Mean values of wheat flours psysico-chemical and rheological parameters

Parameters	WF1	WF2	WF3
Moisture (%)	14.43	13.89	14.91
Protein (%)	12.29	11.72	10.52
Ash (%)	0.545	0.56	0.554
Wet gluten content, %	28.1	26.6	25.2
Falling Number HFN (s)	351	320	294
Sedimentation value SDS (mL)	38	39	31
FWA (%)	60.8	61.75	57.3
DDT (s)	3.2	3.5	3.1
ST (s)	3.5	3.7	4.12
DS (BU)	61	71	100
P (mm H_2O)	84	93	88
L (mm)	80	80	61
P/L	1.05	1.16	1.44
W (x 10^{-4} J)	200	234	204
Proofing time (min)	42	46	40
Dough resistance (BU)	505	510	440
Baking volume (BU)	420	430	485
Oven rise (BU)	80	80	180

I. Influence of WGF addition on rheological properties

I.1. The Falling number (HFN)

The HFN decreased as the level of WGF increased in blends for all WF used in the study. 329s, 298s and 282s were the HFN average values recorded in blends with 4% WGF, compared to the controls (Tab.1). Results indicated that partial substitution of WF by WGF decreased the HFN. This trend could be explained by the higher α-amylase content founded in germ [8,23]. The presence of amylases increases the level of fermentable and reducing sugars in the flour and dough, thereby promoting yeast fermentation [24], which suggested that α-amylase activity might improve bread quality in terms of volume and crust color.

I.2 Farinograph and Alveograph characteristics

Farinograph characteristics of WF1, WF2, WF3 and those of blends obtained with WGF addition at 0, 2 and 4% level are shown in Table 2. A slight increment (non-significant, $p>0.05$) in FWA with the increased addition of

WGF was found, with a higher value for WF2. Incorporation of WGF had weakening effect on rheological characteristics of the dough (DDT, ST, DS). This tendency was observed for all tested blends.

Results for alveograph characteristics of WF:WGF blends are shown in Table 3. Incorporation of 4% WGF slightly decreased the tenacity value (P) in the case of WF1 samples, while a more marked decrement was observed for samples WF2, WF3.

Table 2. Farinographic properties of dough obtained by blending WGF:WF

Wheat flour	Addition level of WGF, %	FWA, %	DDT, min	ST, min	DS, BU
WF1	0%	60.8(0.01)	3.2(0.1)	3.8(0.2)	61.02(0.2)
	2%	61.0(0.01)	3.1(0.2)	3.71(0.1)	61.4(0.2)
	4%	61.2(0.02)	2.9(0.14)	3.45(0.13)	62 (0.1)
WF2	0%	61.75(0.02)	3.5(0.2)	4.2(0.2)	71(0.15)
	2%	60.8(0.02)	3.2(0.1)	4.09(0.15)	71.3(0.15)
	4%	63.8(0.01)	3.0(0.15)	3.88(0.1)	71.9(0.2)
WF3	0%	57.3(0.01)	3.1(0.2)	5.12(0.2)	100.0(0.2)
	2%	58.12(0.03)	3.1(0.1)	5.04(0.14)	100.45(0.2)
	4%	58.6(0.02)	2.9(0.12)	4.9(0.2)	100.91(0.1)

This tendency could be explained by the presence of pre-gelatinized starch in the heat treated WGF which, increase dough consistency [2] and its ability to retain gas. Dough extensibility (L) decreased with the level of WGF addition. Decrease in values of extensibility (L) caused reduction in energy value of dough. In consequence, dough strength (W) decreased with increasing proportions of WG, for all tested blends. These effects of WGF addition on rheological parameters can be attributed to the dilution of the gluten matrix, responsible for dough extensibility and to a competition to a certain extent with other WF components for water, creating a dough strengthening. Gomez et al., 2012 [2] showed that by measuring dough strength after 3h of resting the value was similar to the initial strength, suggesting that despite of the high level of enzyme activity in this part of the grain, these enzymes do not modify dough rheology, due probably to enzyme inactivation during heating [23,26]. The presence of glutathione- a reducing agent in WGF, was reported as an influencing factor on rheological properties [2,8,23]. These findings suggest that raw wheat germ and heat-treated germ did have significantly different effects on dough stability. By roasting or steaming WG the effect on dough stability is minimized. The type of thermal treatments partially inactivate the glutathione and produce different degrees of starch gelatinization [2,7,25].

I.3. Influence of WGF addition on bread quality and sensory characteristics

Increasing WGF from 0% to 4% in WF:WGF blends, decreased the specific volume (SV) with an average value of 11.20% and increased the elasticity of bread compared to the control sample. The crumb porosity had an opposite trend compared with the elasticity, lowered scores were obtained as the WGF addition increased in the blends. The use of WGF leaded to an intense and appreciated color of the crust, due to a higher α-amylasic activity leading increased amounts of sugars for Maillard reaction and caramelization during baking. All the samples of WGF breads scored marked higher in terms of flavor and dryness than the control, increasing substitution levels increased the flavor and dryness scores. This behavior is due to the special flavor of WGF while the improvement in dryness is due to the higher water absorption of WGF:WF blends than wheat flour. WGF addition caused an improvement of taste and sweetness for all tested bread samples. Results are consisting with [2,8,10].

Table 3. Alveographic properties of dough obtained by blending WGF:WF

Wheat Flour	Addition level of WGF, %	P (mm H_2O)	L (mm)	P/L	W ($x10^{-4}$ J)
WF1	0%	84(0.2)	80(0.14)	1.05(0.1)	200(0.1)
	2%	82(0.25)	74(0.25)	1.10(0.2)	198(0.1)
	4%	81(0.1)	71(0.2)	1.14(0.25)	175(0.15)
WF2	0%	93(0.4)	80(0.1)	1.16(0.2)	234(0.2)
	2%	90(0.3)	78(0.3)	1.15(0.3)	212(0.1)
	4%	87(0.1)	73(0.4)	1.19(0.2)	203(0.1)
WF3	0%	88(0.2)	61(0.1)	1.44(0.1)	204(0.1)
	2%	84(0.2)	58(0.2)	1.45(0.2)	188(0.2)
	4%	81(0.13)	55(0.1)	1.47(0.1)	167(0.2)

Considering the results obtained on the WGF influence on dough rheological parameters and bread quality of wheat flour, we selected blends with 4% WGF as acceptable and it were subjected to the second stage experiment to study the effect of enzymatic and chemical improvers. The codifications B1C, B2C, B3C were used for blends of WF1, WF2, WF3 with 4% WGF. This concentration mimics the percentage of wheat germ in the kernel, while higher concentrations of wheat germ (e.g.,6–8%) favored an excessive sweet taste which seemed to be rather far from the main sensory attributes [10].

II. Influence of additives on dough properties

II.1. Hagberg Falling Number (HFN)

As we expected the addition of AMYL at the levels of 100 and 200 mg/kg caused a significant ($p<0.05$) decrease of HFN for all tested blends. For AMYL2 treatments HFN reached values as for normal content in α amylase. 245s, 232s and 223s were the HFN values recorded for the AMYL 2 treatments of wheat/wheat germs blends. In the case of the other enzymes used no changes in HFN values were recorded.

II.2. Farinograph and alveograph characteristics

Effects of single treatment enzymes and AA on farinographic parameters of dough obtained from blends with 4% WGF addition is shown in Figure 1. The addition of AMYL lowered the FWA of each blends tested with lowest FWA for treatment AMYL2. A value of 59,8% FWA was recorded for B1C blend when AMYL2 treatment was applied, while for the other blends the water absorption recorded about of 62.9% (B2C) and 58.1% (B3C). Both, XYL and GOX increased FWA of each tested blends as compared to the controls. Non-significant differences ($p>0.05$) between the two level of addition of XYL (1,2) and GOX (1,2), respective, were recorded. By comparing the effects of XYL and GOX addition on the water absorption, it could be noticed that both levels of XYL (50 and 60 mg/kg) had the highest influence on increasing the FWA for all tested blends than GOX levels (30 and 60 mg/kg). FWA values changed very little with the addition of either XYL or GOX; our results are consistent with [27]. AA addition had a slight, non-significant ($p>0.05$), increasing effect on FWA for both levels of addition as compared to control blends. Comparing to the GOX effect, AA addition caused smaller increase in FWA for all tested blends. The complex mechanism by which this enzyme increase water absorption is attributed to the drying effect of GOX on dough and explained as being caused by hydrogen peroxide resulted from the oxidation of β-D-glucose catalyzed by glucose oxidase [30-32]. Hydrogen peroxide induces the oxidative gelation of water soluble pentosans and a greater water sequestration that should explain the increase in water absorption [16].

AMYL at both level of addition, significantly ($p<0.05$) decreased the DDT for all dough samples. The lowering effect on DDT was higher for AMYL2 treatments of all samples. The lowest value was recorded in the case of blend B2C (1.7 min) with a control value of 3.0 min. This tendency could be explained by the presence of a low molecular weight dextrin produced from damaged starches by amylase hydrolysis [16]. Similar results

were reported by [28,29]. XYL, GOX and AA induced an increase in DDT, without significant differences ($p>0.05$) between level of addition inside the same enzyme. Addition of XYL at 60 mg/kg caused the highest increment of DDT. XYL prevents the interference of pentosans with gluten formation [33, 34]. Addition of GOX at 30, 60 mg/kg and AA at 40,50 mg/kg led to similar effect on DDT for all tested blends. Similar results were reported by other studies concluding that addition of GOX or XYL increased the DDT [27, 34].

The lowest ST was measured on dough supplemented with AMYL and AA, without significant differences between levels of addition. GOX at both levels of addition significantly ($p<0.05$) increased the dough ST. Our results are consistent with [27,35]. All treatments increased the softening index except GOX. AMYL2 induced the highest increment of DS for all tested blends. The high hydration capacity of starch decreases as the amylolytic attack starts, particularly when water is added to the flour and mixing begins. This resulted in a decrease in dough stability and an increase in the dough softening [36].

With respect to the alveographic parameters, for all tested blends, both oxidative agents (GOX and AA) had strengthening effect, as we expected (Fig.2). By adding GOX at both level, dough tenacity (P) and energy (W) increased while dough extensibility decreased (L) in all tested blends. The effect of GOX is especially clear from the significant decrease in extensibility [37], producing stiffer and less extensible dough [38]. Similar results were obtained by [35, 39]. GOX action is related to the hydrogen peroxide produced which promoted the formation of disulphide linkages in gluten protein [16,40]. Results show (Fig.2) that AA significantly ($p<0.05$) influenced the dough extensibility (L) for all tested blends.

For both treatment with AA, L decreased, while the P and W parameters increased. AA acts by inhibiting the cleavage of the intermolecular SS bonds of the gluten [16]. Addition of AMYL caused a slight reduction in dough tenacity (P) and energy (W) in all blends at both levels of addition. Dough extensibility increased with the level of added AMYL in all tested blends. XYL addition had an opposite effect than amylase on dough alveographic parameters causing increment in P, W value and a slight decrement in extensibility. These enzymes can influence the gluten properties by changing the water distribution in the dough and also by having covalent interactions with gluten [16]. According to literature [15, 27, 28] they are also responsible for several changes in dough properties including decrease of the absorption capacity, slackening of dough consistency and development of a stickier dough. The rate at which these changes occur is directly proportional to the amount of starch damage and α-amylase level of the flour [16].

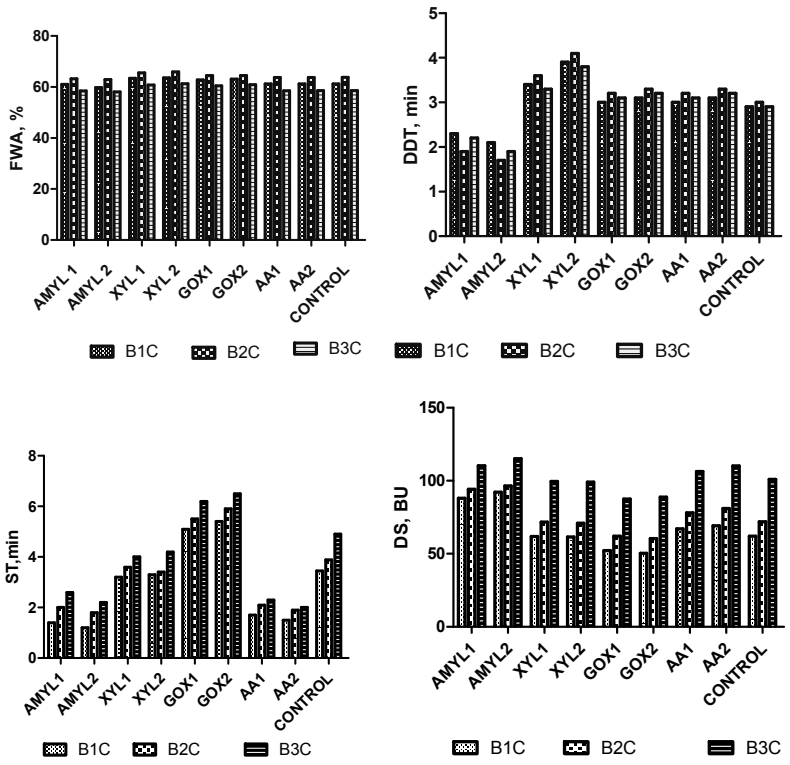

Figure 1. Effects of single treatment enzymes and ascorbic acid on farinographic parameters (FWA, DDT, ST, DS) of dough (4% WGF)

II.3. Influence of additives addition on wheat germ bread quality and sensory characteristics

When the influence of enzyme-supplementation on blends with 4% WGF was analyzed the SV of the control bread (without enzymes) prepared by using blends B1C, B2C, B3C were 3.02, 3.12, 3.09. All tested enzymes lead to bread with higher SV. Nevertheless, in the case of treatment GOX2 the SV was quite similar to the control sample for all tested blends meaning that for good quality flour, high dose of GOX increase dough strength causing an over-reinforcement of dough [28]. This effect hampers expansion during proofing and, consequently, negatively affects bread volume [28,41]. GOX2 treatment effect was moreover in shape improvement. Similar effect was reported by [13]. Lower dose of glucose oxidase (GOX1) lead to higher loaf

height improving the bread loaf volume. Supplementation with AMYL and XYL also caused significant improvement of bread loaf SV for both added doses. Ravi et al., 2000 [42] reported considerable increase in volume of amylase supplemented loaf. Amylase effect is explained by the presence of some deformed starch granules due to the action of α-amylase on long starch chains [27] and a slight leakage of amylose [13]. XYL supplementation, in both doses, lead to higher SV than AMYL supplementation. By scanning electron microscopy studies, it was observed thinning of some protein fibrils and a slight distortion of starch granules in the micrograph of dough with XYL addition [27].

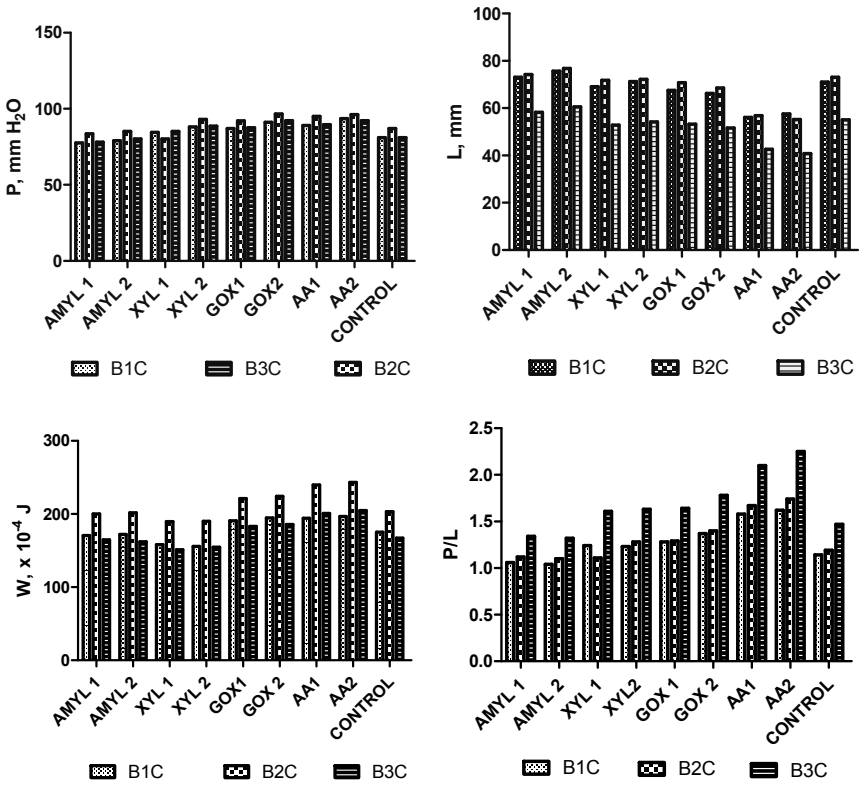

Figure 2. Effects of single treatment enzymes and ascorbic acid on alveographic parameters (P,L, W, P/L) of dough obtained from blends with 4% WGF addition

Also this effect could be explained by a delay in the crumb formation during baking giving better oven spring and larger bread volume and softer crumb [43]. AA addition caused also a significant increment of SV independently

of the added dose. By PCA studies it was showed that the effects of the addition of ascorbic acid is independent of its concentration [16], result consistent with ours.

The sensory scores for elasticity, porosity, color, mouth satisfaction increased with all improvers treatments in case of all tested blended (WGF:WF) breads. The highest improvement in the total overall quality was brought about by XYL2 recording an average value of 37.06, followed by AMYL2 with an average value of 35.63 and GOX 2 with the average value of 31.36 very close to AA2 with average value of 31.13. XYL caused a marked improvement of elasticity and porosity scores. Xylanase have a positive effect on dough properties and bread quality because they stabilize gas cells, improving its expansion capacity during proofing and baking and consequently improving bread characteristics, such as specific volume and firmness [28, 44]. AMYL significantly increased the crust color and the porosity while elasticity was less influenced. Amylases are able to change physicochemical and structural properties of polysaccharides, making dough softer and viscous and increasing the availability of fermentable sugars. α-amylase prolongs oven rise and results in an increased loaf volume [16] while the increased amount of fermentable sugars intensify bread color, taste and aroma. Glucose-oxidase effect is related especially to a greater specific volume, a better shape, an improving effect in the crumb grain and is attributed to the hydrogen peroxide released from the GOX reaction [39].

II.4 Relationship between rheological properties and wheat germ-enzyme supplemented bread quality parameters

Data were subjected to a Pearson correlation analysis in order to determine significant ($p<0.05$) relationships between rheological and bread quality parameters. The coefficients of significance are shown in Tab.4. The alveograph parameters W, P and P/L were found to be positively and significantly ($p< 0.01$) correlated to the SV, while among farinograph parameters only FWA was positively and significantly ($p< 0.01$) correlated to the SV. Dough extensibility L and DDT were negatively correlated to the SV. Flour strength is a measure of the gluten quality whereas tenacity is a predictor of the ability of the dough to retain gas and this lead to a better balance between elasticity and extensibility [16]. The correlation between water absorption and bread specific volume is related to the contribution of the evaporated water to increasing of bread volume [45]. P, P/L and FWA values were negative correlated to the H/W ratio, while L –dough extensibility was positively correlated to the H/W ratio.

Table 4. Coefficients of significant correlations ($p<0.05$) between rheological and bread quality parameters of dough

Rheological Parameter	SV (cm^3/g)	H/W ratio
P (mm H_2O)	0.554	-0.619
L (mm)	-0.501	0.615
W (x 10^{-4} J)	0.621	0.524
P/L	0.561	-0.603
FWA, %	0.756	-0.492
DDT, min	-0.488	-

CONCLUSIONS

Wheat flour replacement at different levels by WGF changed the rheological characteristics of the dough as well as the bread quality (SV, H/W ratio, sensory properties). A decrement of bread volume and H/W ratio was found with the increment of WGF in bread formulation. A substitution of 4% WGF was found as acceptable. The addition of bread making improvers (enzymes and ascorbic acid) improved the WGF:WF dough rheological parameters as well as the quality indices of wheat germ bread. Xylanase caused a marked improvement of elasticity and porosity. Amylase significantly increased the crust color, the porosity and the bread specific volume. Glucose-oxidase effect is related to a higher bread specific volume, an improvement of the bread shape and crumb porosity. Ascorbic acid addition caused also a significant increment of SV independently of the added dose. In the case of WGF:WG dough, the alveograph parameters W, P and P/L were found to be positively and significantly ($p< 0.01$) correlated to the SV, while among farinograph parameters only FWA was positively and significantly ($p<0.01$) correlated to the SV. Dough extensibility L and DDT were negatively correlated to the SV.

EXPERIMENTAL SECTION

Materials

Three types of commercial wheat flour (WF1,WF2,WF3) were used in this study. Wheat flour samples produced by local mills were sold as type 550 according to ash content by Romanian classification. Wheat germs (WG) were brought from a specialized local store and processed after method described by [8]. Dried yeast (Pakmaya) and salt were brought from the local market. Ascorbic acid (AA), fungal α-amylase (AMYL, 50000 SKBU/g), fungal xylanase (XYL, 2700 FXU/g) and glucose oxidase (GOX, 10000 GU/g) were procured from Enzymes & Derivates, Neamt, Romania.

Blends, dough formulations, bread making procedure and optimization

In the first step, blends of wheat flour (WF1,WF2,WF3) and wheat germ flour (WGF) were obtained by substituting the same amount of wheat flour with 0%, 2% and 4% WGF. A straight dough method for bread preparation and the following formula (for control bread) was used: wheat flour 100%, dried yeast 2%, salt 2% (amount of ingredients in reference to flour) and water needed for preparation of dough with farinograph consistency of 500 BU. Wheat germ bread were prepared using blends describe forementioned; a total of nine type breads were baked in triplicate. In the second step, for each type of blends composed by wheat flour (WF1, WF2, WF3) and the selected optimum level of WGF (as found by dough rheological and bread quality evaluation from the first step) four additives were included in the bread formulas one by one. Samples codification, based on additive and amount were: AA1-ascorbic acid 40mg/kg, AA2- ascorbic acid 50 mg/kg, XYL1-xylanase 50 mg/kg, XYL2- xylanase 60 mg/kg, AMYL1- amylase 100 mg/kg, AMYL2- amylase 200 mg/kg, GOX1-glucose oxidase 30 mg/kg, GOX2-glucose oxidase 60 mg/kg. Enzymatic and chemical additives were tested at different levels of addition chosen on the basis of preliminary tests (data not shown) and included in the ranges usually applied in bakery industry. Control bread samples were prepared without using additives. Dough was kneaded using a single spiral mixer (type Hobart) for 12 min; dough with 24˚C temperature was divided into pieces of 1000g and the following steps were used: rounding, first pre-proofing (20 min, 25˚C, relative humidity (RH) 60%), second rounding, second pre-proofing (30 min, 25˚C, 60% RH), final shaping, final proofing (70 min, 30˚C, 80% RH), baking in electrical oven (40 min, 225˚C), cooled and packed. Two hour after baking, the loaves were weighed, the height and width of the central slice was measured and bread volume was determined according to AACC Approved Method 10-05 (American Association of Cereal Chemistry, 2000) procedure. Specific volume (SV) of bread was expressed as the volume ⁄ weight ratio (cm^3/g) of finished bread and H/W ratio was calculated.

Physicochemical and Rheological Characteristics

Wheat flour samples were subjected to physicochemical analyses (moisture, ash, protein content). Also, Hagberg's Falling number (HFN), Zeleny's sedimentation value (SDS) and rheological –farinograph and alveograph-characteristics were determined. The American Association of Cereal Chemists (AACC 2000) methods were used to determine all these parameters. Farinograph (Brabender, Duisburg, Germany) was used and the following results were

expressed as flour water absorption (FWA, %), dough development time (DDT, min), dough stability (ST, min) and the degree of softening (DS, BU). The viscoelastic properties of the dough were assessed using an Alveograph MA 82 (Chopin). The following parameters were automatically recorded: tenacity or resistance to extension (P, mm H_2O), dough extensibility (L, mm), curve configuration ratio (P/L) and the deformation energy (W x 10^{-4} J). In addition, in order to obtain more information about rheological characteristics of the fermented dough the maturograph and oven spring apparatus (Brabender, SRN) was used for recording the proofing time (min), the dough resistance (BU), the baking volume (BU), the oven rise (BU). All measurements were performed in triplicate and the average values were used.

Sensory evaluation

Sensory analysis of bread was carried out according to the method described by [17], with minor modifications. Elasticity, color, porosity, flavor, sweetness, dryness, taste and mouth satisfaction were evaluated using a scale from 0 to 10 points, with 10 being the highest score. The panel group was composed of 25 bread usual consumer volunteers from 20 to 57 years of age and from various socioeconomic backgrounds, consisting of Faculty of Food Science and Technology staff and students from Cluj-Napoca, Romania. The sensory evaluation was performed in both steps of experiment fore mentioned. All breads were analyzed in the same session.

Statistical analysis

The results of three independent assays (performed with replicates each) were expressed as mean value (SD). All data were compared by one-way analysis of variance (ANOVA) followed by Duncan test and Pearson's correlation coefficient. The statistical evaluation was carried out using Graph Prism Version 5.0 (Graph Pad Software Inc., San Diego, CA, USA).

REFERENCES

1. B. Dunnewing, T. van Vliet, R. Orsel, *Journal of Cereal Science*, **2002**, *36*, 357.
2. M. Gómez, J. González, B. Oliete, *Food Bioprocess Technol*, **2012**, *5,* 2409.
3. J.S. Sidhu', S.N. Al-hooti', J.M. Al-Saqer', Amani al-Othmav, *Journal of Food Quality*, **2001**, *2,* 235.
4. S.N. Al-Hooti, J.S. Sidhu, J.M. Al-Saqer, A. Al-Othman, *Nahrung-Food*, **2002**, *46(2),* 68.

5. M.U. Arshad, F.M. Anjum, T. Zahoor, *Food Chem*, **2007**, *102*, 123.
6. Srivastava Alok, K. Sudha, M.L. Baskaran, V. Leelavathi, *European Food Research Technology*, **2007**, *42*, 358.
7. Y. Pomeranz, M.J. Carvajal, M.D. Shogren, R.C. Hoseney, K.F. Finney, *Cereal Chemistry*, **1970**, *47(4),* 429.
8. Sun Ru, Zhengmao Zhanga, Xinjuan Hua, Qinhui Xinga, Wuyan Zhuo, *Journal of Cereal Science*, **2015**, *64*,153.
9. N. Gelmez, N.S. Kıncal, M. E. Yener, *J. Supercrit. Fluid*, **2009**, *48*, 217.
10. C.G. Rizzello, L. Nionelli, R. Coda, R. Di Cagno, M. Gobbetti, *Eur Food Res Technol*, **2010**, *230*, 645.
11. A. Zalatnai, K. Lapis, B. Szende, E. Rásó, A. Telekes, A. Resetár, Hidvégi M.*Carcinogenesis*, **2001,** *22*, 1649.
12. M. Majzoobi, S. Farhoodi, A. Farahnaky, M.J. Taghipour, *J. Agr. Sci. Tech*., **2012**, *14*, 1053.
13. P.A. Caballero, M. Go´mez, C.M. Rosell, *European Food Research and Technology*, **2007**, *224*, 525.
14. V. Stojceska, P. Ainsworth, *Food Chemistry*, **2008**, *110*, 865.
15. P.A Caballero, M. Go´mez, C.M. Rosell, *Journal of Food Engineering*, **2007**, *81*, 42.
16. A. Baiano, C. Terracone, *CyTA - Journal of Food*, **2001**, *9(3)*, 180.
17. Å. Haglund, L. Johansson, L. Dahlstedt, *J. Cereal Sci*., **1998**, *27*, 199.
18. J.L. Ward, K. Poutanen, K. Gebruers, V. Piironen, A.M. Lampi, L. Nystrom, A.A. Andersson, P. Aman, D. Boros, M. Rakszegi, *J Agric Food Chem*., **2008**, *56*, 9699.
19. I. Banu, I. Aprodu, *International Journal of Food Science and Technology*, **2015**, *50*, 1644.
20. I. Konopka, L. Fornal, D. Abramczyk, J. Rothkaehl, D. Rotkiewicz, *International Journal of Food Science and Technology*, **2004**, *39*, 11.
21. M.S. Butt, F.A. Anjum, D.J. van Zuilichem, M. Shaheen, *International Journal of Food Science and Technology*, **2001**, *36*, 433.
22. M. Hrušková, I. Švec, O. Jirsa, *Journal of Food Engineering*, **2006**, *77(3),* 379.
23. D. Every, S. C. Morrison, L. D. Simmons, M. P. Ross, *Cereal Chem.,* **2006**, *83* 57.
24. S. Hamada, K. Suzuki, N. Aoki, Y. Suzuki, *J. Cereal Sci*., ***2013***, *57*, 91.
25. M. Miyazaki, N. Morita, *Food Research International,* **2005**, *38(4),* 369.
26. M.L. Sudha, A.K. Srivastava, K. Leelavathi, *Eur Food Res Technol*, **2007**, *225*, 351.
27. D. Indrani, P. Prabhasankar, J. Rajiv, R. Venkateswara, *Journal of Food Science*, **2003**, *68(9),* 2804.
28. M.E. Steffolani, P.D. Ribotta, G.T. Pérez, A.E. León, *International Journal of Food Science and Technology*, **2012** ,*47*, 525.
29. T. Maeda, T. Hashimoto, M. Minoda, S. Tamagawa, Morita, *Cereal Chemistry*, **2003**, *80*, 722.
30. V. Vemulapalli, K.A. Miller, R.C. Hoseney, *Cereal Chemistry*, **1998**, *75*, 439.
31. H.S. Gujral, C.M. Rosell, *Food Research International*, **2004**, *37*, 75.
32. A.D. Bettge, C.F. Morris, *Cereal Chemistry*, **2007**, *84*, 237.

33. M. Wang, T. van Vliet, R.J. Hamer, *Journal of Cereal Science*, **2004**, *39*, 341.
34. J.C. Pescador-Piedra, A. Garrido-Castro, J. Chanona-Pérez, R. Farrera-Rebollo, G. Gutiérrez-López, G. Calderón-Domínguez, *International Journal of Food Properties*, **2009**, *12(4)*, 748.
35. P. Prabhasankar, D. Indrani, R. Jyotsna, R.G. Venkateswara, *Journal of the Science of Food and Agriculture*, **2004**, *84(15)*, 2128.
36. I.S. Doğan, *International Journal of Food Science and Technology*, **2003**, *38*, 209.
37. C. Primo-Martín, J. Mingwei Wang, W. J. Lichtendonk, J.J. Plijter, R. J. Hamer, *J Sci Food Agric*., **2005**, *85*, 1186.
38. A.F. Dagdelen, D. Gocmen, *Journal of Food Quality*, **2007**, *30*, 1009.
39. C.M. Bonet, P.A. Rosel, M. Caballero, I. Gómez, Pérez-Munuera, M.A. Lluch, *Food Chemistry*, **2006**, *99*, 408.
40. C.H. Poulsen, P.B. Hostrup, *Cereal Chemistry*, **1998**, *75*, 51.
41. C.M. Rosell, J. Wang, S. Aja, S. Bean, G. Lookhart, *Cereal Chemistry*, **2003**, *80*, 52.
42. R. Ravi, R. Sai Manohar, P. Haridas Rao, *Eur Food Res Technol.,* **2000**, *210*, 202.
43. B. Polderman, P. Schoppink, *Cereal Foods World*, **1999**, *44*, 132.
44. T. Jiménez, M.A. Martínez-Anaya, *Food Science and Technology International*, **2001**, *7*, 5.
45. I. Švec, M. Hrušková, *Scientia Agriculturae Bohemica*, **2009**, *40*, 58.

STUDIA UBB CHEMIA, LXI, 2, 2016 (p. 119-126)
(RECOMMENDED CITATION)

ADSORPTION OF PALM OIL CAROTENES ON NATURAL AND ACID ACTIVATED MONTMORILLONITE CLAYS

ORLÉANS NGOMO[a,b,c], JEAN BAPTISTE BIKE MBAH[a*], RICHARD KAMGA[a], RODICA DINICA[c]

ABSTRACT. The adsorption behavior of natural and acid activated Montmorillonite clays from Maroua (Far North region of Cameroon) were studied by batch adsorption method. Carotene adsorption was monitored by measuring the absorbance of the mixture before and after adsorption experiments. The effect of contact time, temperature and initial carotene concentration were analyzed. It was found that the amount of carotene adsorbed increases with contact time and the adsorption equilibrium was attained after 30 min irrespective of the adsorbent used. Temperature has little effect on the adsorption process. The amount of β-carotene adsorbed at equilibrium increased with the initial carotene concentration. Kinetic modeling shows that experimental data follows pseudo-first order, pseudo-second order and intraparticle diffusion models. The line best fit was obtained with the pseudo second order diffusion model. Langmuir, Freundlich, and Temkin isotherms models were used to adjust the equilibrium data. The line best fit was obtained with the Freundlich model. The small values of the Freundlich constants and that of the energy constant of Temkin model revealed that the adsorption of carotene on clays is a physical process.

Keywords*: Montmorillonite, carotene, palm oil, adsorption modelling.*

INTRODUCTION

Crude palm oil is the world's richest natural plant source of carotene in term of retinol. The orange-red color of palm oil is due to the relatively high content of these carotenes. The major carotenes in palm oil are α and β carotenes, which account for 90% of the total carotenes [1].

[a] *Department of Applied Chemistry, National School of Agro-Industrial Sciences, University of Ngaoundere, P.O. Box 455 Cameroon.*
[b] *Department of Chemistry, Faculty of Sciences, University of Yaoundé I, P.O. Box 812 Yaoundé, Cameroon*
[c] *Department of chemistry, Faculty of Sciences, Universitatea "Dunarea de Jos'' din Galati, Str. Domneasca nr. 47. 800 008 Galati, Romania*
[*] *Corresponding author: jbmbahgm@gmail.com / jbmbah@yahoo.fr*

Due to their antioxidant properties, carotenes are usually used in food industries and in cosmetic formulations. It has been found that carotene improves the general aspect of skin [2]. However, carotenes have been considered as undesired compounds in the palm oil refining processes [2, 3, 4]. Adsorption on suitable material has been preferred for the removal of pigments from vegetable oils [5-9]. The most effective adsorbent for pigment removal from vegetable oils are montmorillonite base activated clay and activated carbon [5, 4, 10]. Montmorillonite clay is preferred to activated carbon for the vegetable oil refining due the high cost of the latter adsorbent [3, 4, 9].

The purpose of this work is to study the mechanism of adsorption of palm oil carotenes on natural and activated montmorillonite in hexane. Therefore, kinetic and isotherm data will be fitted with theoretical models.

RESULTS AND DISCUSSION

1. UV-visible Spectrum of palm oil

The absorption spectrum of crude palm oil (Fig. 1) presents a maximum absorption band at 445 nm, with shoulder at 420 nm. The reduction of the optical density to this maximum of absorption was used to follow the adsorption of carotene.

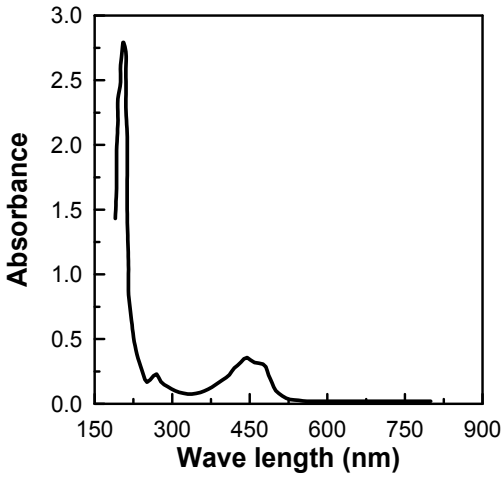

Figure 1. Adsorption spectrum of crude palm oil.

2. Adsorption kinetics

Fig. 2 shows the time evolution of the amount of β-carotene adsorbed on natural clay (a: M0M) and modified clay (b: M0.5M) for different initial concentration of carotenes (20 mg/L, 40 mg/L and 50 mg/L).

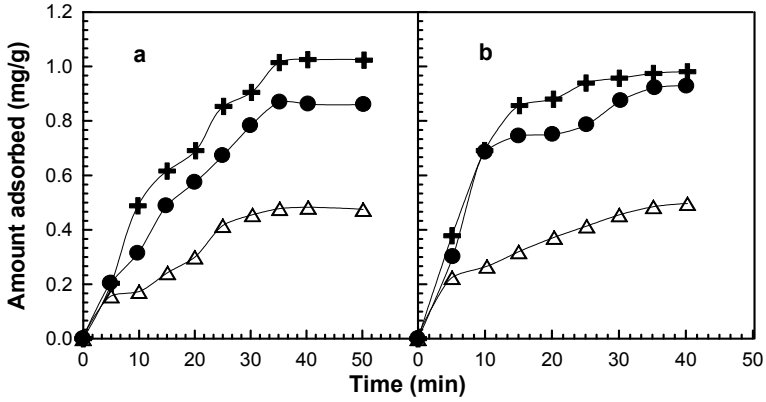

Figure 2. Time evolution of the amount of β-carotene adsorbed on clay for different initial concentrations: 20 mg/L (Δ), 40 mg/L (●) and 50 mg/L (✚). a: M0M, b: M0.5M

It is observed that the amount of carotenes adsorbed increased rapidly with time, and then slowed down for a contact time greater than 30 min. It can also be observed that the amount of carotenes adsorbed increased with the initial concentration, independently of the nature of clay used. This increase is rather fast in the first minutes and is stabilized after a contact time greater than 30 minutes.

At equilibrium, the amount of carotenes adsorbed (table 1) is proportional to the initial concentration for natural clay. This relation of proportionality does not hold after modification of clay.

Table 1. Amount of carotene adsorbed (μmol/g) at equilibrium for different initial concentrations

	Initial concentration (mg/L)		
	20	40	50
M0M	0.89±0.02	1.63±0.03	1.94±0.04
M05M	0.91±0.02	1.73±0.04	1.85±0.04

The effect of the temperature on the adsorption process was studied by carrying out experiments at different temperatures (25, 45 and 65° C). The increase in the amount of carotene adsorbed was less than 2% when temperature increased from 25°C to 65°C (Table 2). Hence temperature has little effect on adsorption kinetics.

Table 2. Amount of carotene adsorbed (µmol/g) at equilibrium for different temperatures

	Temperature (°C)		
	25	45	65
M0M	1.63±0.03	1.67±0.03	1.75±0.04
M05M	1.73±0.04	1.75±0.04	1.77±0.04

The adsorption data were analyzed by using three kinetic models, in particular intraparticle diffusion, pseudo-first order and pseudo-second order models. The respective linear equations of these various models are as follows:

$$q_t = k_{int}\sqrt{t} + \alpha\ ;\ \ln(q_e - q_t) = \ln q_e - k_1 t\ ;\ \frac{t}{q_t} = \frac{1}{k_2 q_e^2} + \frac{1}{q}t$$

where k_{int}, k_1 and k_2 are the respective intraparticle diffusion, pseudo-first and pseudo-second order kinetic constants, q_e and q_t are the respective amount of carotene adsorbed at equilibrium and at time t, α is a constant.

The experimental data follows the pseudo-first model if R^2 of the regression line of $\ln(q_e-q_t)$ as function of t is greater than 0.90. Similarly the experimental data follows the pseudo-second model if R^2 of the regression line of $1/q_t$ as function of t is greater than 0.90. For the intraparticle diffusion model de R^2 for q_t as function of $t^{1/2}$ should be greater than 0.90.

The R^2 values are greater than 0.90 for the three kinetic models, for natural and acid activated clays (Table 3).

Table 3. Kinetic parameters for adsorption of carotene on Montmorilonite

		Clays	
		M0M	M05M
Pseudo first order	k_1	0.07	0.08
	q_e	1.82	1.31
	R^2	0.94	0.92
Pseudo second order	k_2	0.04	0.05
	q_e	2.17	1.81
	R^2	0.91	0.98
Intraparticle diffusion	k_{int}	0.15	0.14
	q_{ei}	0.05	0.05
	R^2	0.97	0.97
$q_{e\ exp}$		1.63	1.73

k_1 (min^{-1}); k_2 ($\mu molg^{-1}min^{-1}$); q_e ($\mu molg^{-1}$), $q_{e\ exp}$ ($\mu molg^{-1}$)

These results show that the experimental data follows the three kinetic models. The amount of carotene adsorbed at equilibrium i.e. q_e, for intraparticle diffusion model is 25 times of magnitude lower than the experimental value

(q_e exp), thus this model is not applicable to the experimental data. The q_e values for the pseudo-first and pseudo-second models are close to the experimental values.

The main steps in adsorption from solution are diffusion from solution to the adsorbent surface, diffusion at adsorbent surface and diffusion inside the pores of adsorbent [2, 10, 11]. The pseudo first order kinetic model assume that the adsorption is a one step elementary reaction; while the pseudo second order kinetic model assumes that the adsorption occurs in two steps; that is diffusion of adsorbate and adsorbate–adsorbent interaction [11, 12]. These results suggest that the adsorbate interaction with clay surface is a quick reaction, and that the diffusion is the limiting step as it has a very small kinetic constant. This explains why this data follows both pseudo first and pseudo second kinetic models.

3. Adsorption isotherms

The isotherms express the amount adsorbed per unit mass of clay (mg/g) as function of the equilibrium concentration in solution (mg/L) (Fig. 3).

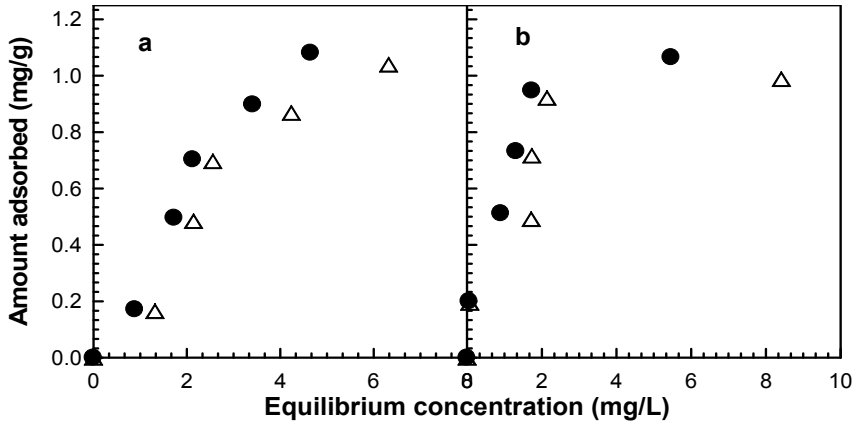

Figure 3. Adsorption isotherms of carotenes on clays at 25°C (Δ) and 45°C (●) a) M0M; b) M0.5M

The isotherms with acid activated clays are characterized by a large increase in the amount adsorbed at low equilibrium concentration, and then followed by a tendency of the formation of a plateau when the concentration is higher. Adsorption isotherms on natural clay are quite different, being characterized by a smaller adsorption in the range of low concentration, while almost a linear increase is observed in the range of higher concentration. Temperature has little effect on the adsorption isotherms; this is in accordance with the results of kinetics experiments.

In order to optimize the design of an adsorption system to remove the carotene from solution, it is important to establish the most appropriate correlations of the equilibrium data with theoretical models. Using different adsorption models to analyze adsorption isotherm data is also an interesting approach to have more information on the carotene-clay interaction. The most usually used isotherm models have been tested in the present study [13, 14, 15]. The respective linear equations of Langmuir, Freundlich and Temkin are:

$$\frac{C_e}{q_e} = \frac{1}{K_L b} + \frac{1}{b} C_e \quad ; \quad q_e = B\ln A + B\ln C_e \quad ; \quad \ln(q_e) = \ln K_F + \frac{1}{n}\ln C_e$$

where C_e is the concentration of carotene at equilibrium; q_e and q_m are the amount of carotene adsorbed per gram of adsorbent at equilibrium and at the monolayer, K_L is the Langmuir constant related to adsorption energy; K_F is a Freundlich constant, indicative of the adsorption capacity of the adsorbent; n_F is a constant indicative of adsorption intensity; B is the Temkin constant indicative of adsorption energy and A is the Temkin isotherm constant.

The results of the application of these equations to the adsorption of carotene on natural and acid activated clays are presented in table 4. Most of the R^2 values exceeded 0.90. However Freundlich isotherm suits the experimental data better than the other 2 models. This suggests that the surface heterogeneity of clay play a major role in the carotene adsorption. Similar results were reported in the literature for adsorption of phenol on different adsorbents [2, 10, 16].

Table 4. Langmuir, Freundlich and Temkin isotherm parameters

		Clays			
		M0M		M05M	
T (K)		298	318	298	318
Langmuir	K_L	0,32	0,61	0,56	0,38
	R_L	0,07	0,04	0,04	0,06
	b	0,24	1,37	1,35	1,32
	R^2	0,90	0,95	0,90	0,97
Freundlich	K_F	0,09	0,26	0,47	0,85
	1/n	0,40	0,54	0,84	2,13
	R^2	0,96	0,96	0,95	0,96
Temkin	A	1,31	1,41	7,91	56,90
	B	0,41	0,84	0,31	0,20
	R^2	0,98	0,99	0,91	0,90

b (µmol/g) ; B (J/mol)

All the n_F value of the Freundlich equation were lower than 1, indicating that carotene molecules are unfavorably adsorbed by clays [16]. This is in accordance with the small value of K_L the Langmuir equilibrium constant. This is also in agreement with the monolayer capacity q_m. The

poor values of the Temkin energetic constant B, shows that carotene are loosely bound to adsorbent surface. The overall analysis of the isotherm parameters shows that the adsorption of carotene on clays at temperatures lower than 60°C is a physical phenomenon. Therefore the clay–carotene material is suitable for cosmetic application.

CONCLUSION

Adsorption of carotene from hexane solution on natural and acid activated clays was studied at different initial concentrations (20 mg/L, 40 mg/L and 50 mg/L) and at different temperatures (25°C, 45°C and 65°C). It was observed that the amount of carotene adsorbed increased with an increase in the initial carotene concentration. Temperature and acid activation have limited effects on the adsorption process. Kinetic studies reveal that diffusion of the adsorbate is the limiting step. Freundlich isotherm fitted the experimental data better than Langmuir and Temkin isotherm. Adsorption of carotene on clays at 25°C was found to be a physical process.

EXPERIMENTAL SECTION

Palm oil was provided by SOCAPALM Co (Cameroon). The standard β carotene used as reference for the calibration curve was purchased from Sigma-Aldrich Ltd. It is a dark red compound of chemical formula $C_{40}H_{56}$ and molecular weight of 536.89 g/mol. A LAMBDA 35, UV visible spectrophotometer was used for carotene analysis. Calibration was performed by measuring the absorbance of a series of standard β- carotene solution at 450 nm. A 1 cm optical path quartz cell was used and hexane was used as reference.

Clay materials used in the present study were sampled in Maroua of the far north region of Cameroon. Clay fraction (<2 μm) was obtained by sedimentation. Monmorillonite was identified as the main clay mineral of the sample.

Acid activation was carried out by mixing clays and 0.5M analytical grade HCl solution for 24 hours at room temperature (≈25°C); the solid to liquid ratio was 1:10w/w ratio. Upon activation, the clay was washed several times with distilled water until negative test of Cl^-. The resulting slurry was filtered under vacuum. The acid activated clay was dried in an oven at 105°C for 8 hours and crushed in an agate mortar.

An initial solution of carotene was made by mixing 2 g of palm oil with 40 mL of hexane (analytical grade). Samples of this initial solution were further diluted drop wise to have the desire initial concentration of carotene. Carotene solutions with initial concentrations of 20, 40 and 50 mg/L were then prepared.

Adsorption of carotene on clay fraction was studied using batch experiments. A fixed amount of dry adsorbent (0.2 g) and 5 mL of β- carotene solution were placed into caped erlenmeyer flasks (100 mL). The flasks were agitated with a magnetic agitator (250 rpm) at the desired temperature for a predetermined contact time. After centrifugation at 1500 rpm, the absorbance of carotene solution was measured at 450 nm. The amount of carotene adsorbed per gram of adsorbent, was calculated according to the mass balance equation as follows:

$$q_t = \frac{(C_0 - C_t)V}{W}$$

where C_0 and C (mg/L) are initial and final concentrations of carotene; V is the volume of the carotene solution used and W is the mass of dry adsorbent used (g).

ACKNOWLEDGEMENTS

Orléans Ngomo is very thankful to the AUF "Eugen Ionescu" program for providing the fellowship.

REFERENCES

1. Y.M. Choo, S.C.Yap, C.K. Ooi, A.S.H. Ong, S.H. Goh, *Elaeis*, **1997**, *3*: 309.
2. B.J. Nde-Aga, R. Kamga and J.P. Nguetnkam, *Journal of applied Sciences*, **2007**, *7,* 2462.
3. M. Rossi, M. Gianazza, C. Alamprese, F. Stanga, *Food Chemistry*, **2003**, *82*, 291.
4. J.B. Bike Mbah, E. Ngah, M. Praisler, R. Kamga, *International Journal of Biosciences*, **2013,** *3*, 15.
5. A.L. Ahmad, C.Y. Chan, S.R. Adb Shukor, M.D. Mashitah, *Chemical Engineering Journal*, **2009,** *148*, 978.
6. E. Sabah, M. Cinar, M.S. Celik, *Food Chemistry*, **2007**, *100*, 1661.
7. J.B. Bike Mbah, R. Kamga, J.P. Nguetnkam, J. Fanni, *European Journal of Lipid Science and Technology*, **2005**, *107*, 387.
8. G.E. Christidis and S. Kosiari, *Clays and clay Minerals*, **2003**, *51*, 327.
9. P.A.M. Mourao, P.J.M. Carrott, M.M.L. Ribeiro Carrott, *Carbon*, **2006**, *44*, 2422.
10. A. Proctor and C. Palianiappan, *Journal of the American Oil Chemists' Society*, **1990**, *67*, 572.
11. W. Plazinski, J. Dziuba, and W. Rudzinski, *Adsorption*, **2013**, *19*: 1055.
12. F.C. Wu, R.L. Tseng, S.C. Huang, R.S. Juang, *Chemical Engineering Journal,* **2009,** *151*, 1.
13. W. Plazinski, J. Dziuba, W. Rudzinski, *Adsorption,* **2013,** *19,* 1055.
14. A. Derylo-Marczewska, A.W. Marczewski, S. Winter, D. Sternik, *Applied Surface Sciences,* **2010**, *256,* 5164.
15. J. Febrianto, A.N. Kosasih, J. Sunarso, Y.H. Ju, N. Indraswati, S. Ismadji, *Journal of Hazardous Materials*, **2009**, *162*, 616.
16. B.H. Hameed, *Colloids and Surfaces A: Physicochemical Engineering Aspect,* **2007**, *307*, 45.

STUDIA UBB CHEMIA, LXI, 2, 2016 (p. 127-136)
(RECOMMENDED CITATION)

COMPARATIVE CHEMICAL ANALYSIS OF ESSENTIAL OILS FROM LAVENDER OF DIFFERENT GEOGRAPHIC ORIGINS

MIOMIR ŠOŠKIĆ[a,b,*], DRAGICA BOJOVIĆ[b], VANJA TADIĆ[c]

ABSTRACT. The purpose of this study was to determine and analyse the chemical composition of essential oils of dry lavender flowers from the area of Budva and Rovinj and to compare to the results obtained in the commercially available sample in Montenegro. Based on gas chromatography (GC and GC/MS) analysis approximately 100 components were identified in the analysed samples, which makes 96.95% to 99.74% of the components present in essential oils. The analysis has shown that oxygenated monoterpenes were the dominant group of compounds. The significant difference in oxygenated monoterpene content between the samples from the area of Budva (71.74%) and Rovinj (91.79%) and the commercially available sample (87.63%) was noted. The most abundant oxygenated monoterpenes in the lavender oil sample from Budva region were linalool and borneol (27.32% and 20.24% respectively); the sample from Rovinj contained linalool and camphor (47.67% and 11.82% respectively) and commercial sample camphor and linalool (21.23% and 19.92% respectively). Monoterpene hydrocarbons were present in a significantly lower percentage in the commercial sample (2.64%) and in a sample from Rovinj (3.57%), while the high content occurred in the sample from the climate of Montenegrin seaside (Budva) (23.74%) with the dominant constituent β-phellandrene (19.1%). The oxygenated sesquiterpenes were slightly less present in the sample from Rovinj (1.14%) and Budva (1.88%), and almost twice as much present in the commercial sample (4.37%) represented with caryophyllene oxide as the dominant ingredient in all three samples; the samples from Rovinj, Budva and commercial ones contained 0.36%, 0.43% and 2.78% respectively. Hydrocarbon sesquiterpenes were insignificantly present in the analysed samples. Hydrocarbon sesquiterpenes were insignificantly presented in the commercial sample (0.83%); the sample from Budva (1.38%) and in a sample from Rovinj (1.66%). As the dominant constituent was sesquisabinen (1.0%) in the sample from Budva and *trans*-(*E*)-caryophyllene in a sample from Rovinj (0.58%) and commercial sample (0.22%).

Keywords: *lavender, essential oil, isolation, identification, chemical composition.*

[a] *Clinical Center of Montenegro, Ljubljanska bb, 81000, Podgorica, Montenegro*
[b] *University of Montenegro, Faculty of Pharmacy, Kruševac bb, 81000, Podgorica, Montenegro*
[*] *Corresponding author: misos@t-com.me*
[c] *Institute for Medicinal Plant research "Dr Josif Pančić", Tadeuša Koščuška 1,11000, Belgrade, Serbia*

INTRODUCTION

Lavandula angustifolia Mill. syn. *Lavandula officinalis* Chaix was commonly known as lavender is a species of the genus *Lavandula* from *Lamiaceae* family [1]. Lavender species are grown worldwide primarily for their essential oils, which are used in the food processing, aromatherapy products, cosmetics and perfumes [2, 3].

L. angustifolia is a perennial herbaceous plant being one of the most loved aromatic and medicinal plants in the world. Lavender is the term, which comes from Latin word "lavando" derived as a part of the verb "lavare" which means “to wash”. The Romans used lavender for obtaining a pleasant smell in their bath, as well as for its beneficial effect on health [1].

The plant grows as a small shrub up to 60 cm high with the blue-violet flowers, which contain essential oil, responsible for the plant’s beautiful scent. It is native to the Mediterranean areas [1, 4]. The dried incompletely developed blossoms of the lavender plant have been used, as an official drug [5].

According to the European Pharmacopoeia, 8th Edition (Ph. Eur. 8.0), lavender flowers should contain at least 13 ml / kg of anhydrous essential oil [6]. The main constituents of lavender dried blossoms essential oil are linalool, linalyl acetate, cineole, camphor and β-ocimene. The plant also contains a high percentage of tannins up to 12 %. The essential oil extracted from the fresh blossoms of lavender contains in high percentage linalool and linalyl acetate [5].

Lavender essential oil can be used externally and internally for various purposes. Externally the essential oil is used in salves, balms, cosmetics, perfumes and topical skin preparations. Taken internally essential oil of lavender is believed to have a beneficial effect on many health impairments, including anxiety, stress, depression, irritability, nervousness, exhaustion, insomnia, headaches, migraines, colds, flatulence, upset stomach, digestion, loss of appetite, liver and gallbladder problems. In addition, it has been known as a breath freshener and mouthwash [7].

Dried lavender flowers have been used for tea-like preparation for improving the mood disorder, insomnia and lassitude, also with beneficial effects on abdominal complaints. Lavender essential oil has its application as a corrector of the taste and odour for pharmaceutical preparations, also as a rubefacient and insecticide [8].

According to the U.S. Food and Drug Administration, *L. officinalis* has been classified as safe and has been included on the safe substances list, commonly known as “Generally Recognised as Safe” (GRAS) [5].

RESULTS AND DISCUSSION

The yield of essential oils (% v/w) amounted to approximately 3 % of dry lavender flowers.

According to the Ph. Eur. 8.0 requirements, dried lavender flowers should contain at least 13 ml / kg of anhydrous essential oil [6]. Essential oil yields found in our samples were in accordance with literature data.

The qualitative and quantitative chemical composition assessment were done using both gas chromatography (GC) and gas chromatography/ mass spectrometry (GC/MS) analysis. Using the GC/MS analysis approximately 100 components were identified in the analysed samples, which makes 96.95% to 99.74% of the components present in essential oils (Table 1).

Table 1. The chemical composition of essential oils from *L. angustifolia* Mill. of different geographic origins

GC Peak No.	Compound	Budva %	Rovinj %	Commercial sample %
1.	tricyclene	0.15	-	0.05
2.	thujene	0.16	0.12	-
3.	α-pinene	0.72	0.35	0.26
4.	camphen	0.70	0.43	0.64
5.	thuja-2-4(10)-diene	0.28	-	-
6.	sabinene	0.50	0.09	0.06
7.	β-pinene	0.11	0.29	0.26
8.	3-octen-1-ol	0.42	0.41	-
9.	3-octanone	-	0.13	-
10.	myrcene	0.62	0.75	0.53
11.	dehydroxy-*trans*-linalool oxide			0.15
12.	α-phellandrene	0.03	0.05	-
13.	δ-3-carene	0.13	0.18	-
14.	α-terpinene	0.09	0.04	-
15.	*p*-cymene	0.08	0.04	0.19
16.	limonene	-	-	0.28
17.	β-phellandrene	19.1	0.16	-
18.	1-8-cineole		9.60	14.89
19.	*(Z)*-β-ocimene	0.38	0.47	0.19
20.	*(E)*-β-ocimene	0.18	0.46	0.08
21.	γ-terpinene	0.14	0.09	0.10
22.	*cis*-sabinene hydrate	0.39	0.22	0.11
23.	*cis*-linalool oxide	0.80	0.61	4.20
24.	camphenylon	-	-	t
25.	*trans*-linalool oxide	0.73	0.66	3.09
26.	terpinolene	0.37	0.05	
27.	linalool	27.32	47.67	19.92
28.	3-*(Z)*-hexenyl isobutanoate			0.64
29.	1-octen-3-yl acetate	-	-	0.55
30.	*(Z)*-*p*-menth-2-en-1-ol	0.39	-	-
31.	α–campholenal	0.13	-	-
32.	*(Z)*-*p*-menth-2,8-dien-1-ol	t	-	-
33.	nopinon			0.14

GC Peak No.	Compound	Budva %	Rovinj %	Commercial sample %
34.	camphor	7.52	11.82	21.23
35.	*trans*-verbenol	0.15		0.31
36.	nerol oxide	-	-	0.10
37.	hexyl isobutanoat	t	0.03	t
38.	pinocarvone	t	0.05	0.14
39.	borneol	20.24	8.11	5.33
40.	lavandulol	-	-	0.48
41.	terpinene-4-ol	4.60	3.08	0.74
42.	*p*-cymene-8-ol	t	-	-
43.	cryptone	2.69	0.85	-
44.	α–terpineol	0.85	1.86	2.01
45.	dihydrocarveol	-	-	0.35
46.	myrtenol	0.24	-	t
47.	4-*cis*-caranone	-	-	t
48.	verbenone	0.20	-	0.32
49.	*trans*-carveol	0.44	-	-
50.	β–cyclocitral	-	-	0.09
51.	nerol	0.33	0.40	0.52
52.	hexyl-2-methyl-butanoate	0.17	-	0.09
53.	isobornyl formate	-	-	0.10
54.	cymine aldehyde	0.64	-	-
55.	carvone	0.31	-	0.14
56.	hexyl isovalerate	-	0.42	0.13
57.	carvotanacetone	-	0.20	-
58.	linalool acetate	1.50	4.56	9.73
59.	geraniol	-	-	t
60.	bornyl acetate	0.06	t	0.05
61.	lavandulyl acetate	1.26	0.49	1.83
62.	*p*-cymene-7-ol	0.20	-	-
63.	hexyl tiglate	0.08	0.18	0.07
64.	neryl acetate	0.06	0.45	0.46
65.	α-copaene	-	t	-
66.	geranyl acetate	-	0.98	0.95
67.	hexyl hexanoate	0.33	-	-
68.	sesquithujene	0.05	0.09	-
69.	α-*cis*-bergamotene	-	0.15	-
70.	*trans*-(*E*)-caryophyllene	0.04	0.58	0.22
71.	santalene	0.05		0.33
72.	lavandulyl isobutanoate	0.07	0.05	t
73.	linalool butanoate			t
74.	α–*trans*-bergamoten	0.14	0.02	t
75.	β-*(Z)*-farnesene	-	t	-
76.	α-humulene	-	t	-
77.	β-*(E)*-farnesene	0.05		t
78.	sesquisabinene	1.0	0.44	-
79.	7-epi-1,2-dehydro-sesquicineol	0.04	-	-
80.	geranyl propanoate	0.10	-	-

GC Peak No.	Compound	Budva %	Rovinj %	Commercial sample %
81.	neryl isobutanoate	-	0.13	t
82.	*trans*-muurola-4(14),5-diene	0.05	0.38	0.07
83.	γ-amorphene	-	t	-
84.	isodaucene	-	t	-
85.	cuparene	t	-	-
86.	lavandyl isovalerate	0.52	-	0.25
87.	γ-cadinene	-	-	0.21
88.	longipinalol	-	-	0.19
89.	caryophyllene oxide	0.43	0.36	2.78
90.	davanone	-	t	-
91.	Fokienol	-	-	t
92.	humulene epoxide II	-	-	0.06
93.	1,10-di-epi-cubenol	-	-	0.08
94.	curcumen	-	-	t
95.	davanol	-	t	-
96.	caryophylla-4(12),8(13)-dien-5α -ol	-	-	t
97.	epi-α-cadinol	0.20	t	0.55
98.	α-bisabolol oxide B	0.17	0.05	-
99.	*(E)*-14-hydroxy-9-epi-caryophyllene	-	t	0.16
100.	*(Z)*-14-hydroxy-caryophyllene	-	-	0.40
101.	epi-α-bisabolol	1.04	0.73	-
102.	α-germacra-4(15),5,10(14)-trien-1-ol	-	-	0.08
103.	*(Z,Z)*-2,6-farnesol	-	t	-
104.	*(R,R)*-6,7-bisabolone	t	-	-
105.	cyclocolorenone	-	-	0.07
	% of total	**99.74**	**99.33**	**96.95**
	* % - Percentage * t – Compounds with percentage less of 0.05%			

The analysis showed that oxygenated monoterpenes were the dominant group of compounds. The significant difference between the quantitative and qualitative chemical patterns in the investigated samples from the area of Budva (71.74%), Rovinj (91.79%) and the commercially available sample (87.63%) was noted. The most abundant oxygenated monoterpenes in the lavender oil sample from Budva region were linalool and borneol (27.32% and 20.24% respectively); the sample from Rovinj contained linalool and camphor (47.67% and 11.82% respectively) and commercial sample camphor and linalool (21.23% and 19.92% respectively).

Monoterpene hydrocarbons were present in a significantly lower percentage in the commercial sample (2.64%) and in a sample from Rovinj (3.57%), while the high content occurred in the sample from the climate of Montenegrin seaside (Budva) (23.74%) with the dominant constituent being β-phellandrene (19.1%).

The investigated samples contained oxygenated sesquiterpenes in small quantity, with the percentage of 1.14%, 1.88% and 4.37% (the samples from Rovinj, Budva and the commercial sample respectively). Caryophyllene oxide was found to be the dominant ingredient in all three investigated samples (samples from Rovinj, Budva and commercial sample, representing 0.36, 0.43 and 2.78%, respectively).

Hydrocarbon sesquiterpenes were insignificantly present in the commercial sample and the samples from natural origin from Budva and Rovinj (0.83%, 1.38% and 1.66% respectively) with sesquisabinen (1.0%) in the sample from Budva, *trans-(E)*-caryophyllene in the sample from Rovinj (0.58%) and commercial sample (0.22%) as the dominant constituent within this group of compounds.

The percentage distribution of different classes of chemical compounds present in the essential oils of lavender *L. angustifolia* Mill. of different geographic origins was presented in Table 2 below.

Table 2. The chemical composition of essential oils from lavender of different geographic origins

The different classes of the compounds usually present in essential oils	**Budva**	**Rovinj**	**Commercial sample**
Monoterpene hydrocarbons	23.74	3.57	2.64
Oxygenated monoterpenes	71.74	91.79	87.63
Hydrocarbon sesquiterpenes	1.38	1.66	0.83
Oxygenated sesquiterpenes	1.88	1.14	4.37
Other compounds	1.0	1.17	1.48
% of total	**99.74**	**99.33**	**96.95**

The major constituent of lavender oils from the samples from Budva and Rovinj was linalool (27.32% and 47.67% respectively). The commercial sample has been shown to be abundant in camphor, as the major constituent (21.23%) (Table 1).

As presented in Table 3, comparing the obtained results to the Ph. Eur. 8.0 requirements for the representative and chosen components (limonene, 1,8-cineole, camphor, linalool, terpinen-4-ol, lavandulyl-acetate, lavandulol and α-terpineol), the certain undesirable difference might be observed. For example, the percentage of camphor and 1,8-cineole (known

as eucalyptol), deviated from the requirements of Ph. Eur. 8.0 in all investigated samples. On the other side, the content of linalool conformed to the requirements of Ph. Eur. 8.0 in the sample from Budva and commercial sample, but did not meet the corresponding requirements in the sample from Rovinj.

Table 3. Comparison of the obtained chemical analysis to Ph. Eur. 8.0 monograph requirements

Terpenoid Components	Ph. Eur. 8.0 [6]	Budva	Rovinj	Commercial sample
Limonene	Maximum 1.0 %	-	-	0.28 %
1,8-cineole	Maximum 2.5 %	-	9.6 %	14.89 %
Camphor	Maximum 1.2%	7.52 %	11.82 %	21.23 %
Linalool*	From 20 to 45 %	27.32 %	47.67 %	19.92 %
Terpinen-4-ol	From 0.1 to 8.0 %	4.6 %	3.08 %	0.74 %
Lavandulyl-acetate*	Minimum 0.2 %	1.26 %	0.49 %	1.83 %
Lavandulol	Minimum 0.1 %	-	-	0.48 %
α-terpineol	Maximum 2.0 %	0.85 %	1.86 %	2.01 %

* The components responsible for antibacterial and antifungal properties [1,11].

Numerous previous studies and results obtained in this study indicated the difference in the chemical composition of terpenoid compounds.

Variability in the chemical composition was most probably dependent on numbers of factors such as genetics (species or variety) of the plant, environmental conditions (geographical, climatic or seasonal) and processing of plant material [9].

In the literature, the major components of the lavender essential oil were reported to be linalool and linalyl acetate. It was stated that it also contained α-thujene, camphene, α- and β-pinene, sabinene, p-cymene, eucalyptol (1,8-cineole), myrcene, limonene, camphor, lavandulol, β-caryophyllene, lavandulyl acetate, γ-terpinene, terpinen-4-ol, *(Z)*- and *(E)*- β-ocimene etc. [1].

The chemical composition of the essential oils in this study indicated the presence of linalool and linalyl acetate in all analysed samples. Percentage of these compounds corresponded to the literature data. Limonene and lavandulol were not found in the samples from Budva and Rovinj. In commercial sample limonene and lavandulol were present in a percentage of 0.28% and 0.48%, respectively, being in accordance with the requirements of Ph. Eur. 8.0. In the samples from Budva, Rovinj and commercial sample, camphor was found to represent 7.52%, 11.82% and 21.23%, respectively, in investigated samples, being the most abundant component in the commercial sample. Taking into account the Ph. Eur. 8.0 requirements for this compound for lavender essential

oil (maximum 1.2%) it is obvious that the determined concentration extended the limits. Comparing the content of 1,8-cineole (found in the quantity of 9.6% and 14.9% in the sample from Rovinj and commercial sample, respectively, and being not present in the sample from Budva) to the Ph. Eur. 8.0 requirements (maximum 2.5%), the statement could be made that the sample from Budva met this requirement. The concentration of terpinen-4-ol in all investigated samples conformed to the Ph. Eur. 8.0 requirements (from 0.1 to 8.0%) (Table 3).

CONCLUSIONS

Lavender essential oils were analysed using gas chromatography techniques (GC and GC/MS). The yield of essential oils (% v/w) amounted to approximately 3 % of dry lavender flowers. Essential oils yields were in accordance with literature data.

Based on GC/MS analysis approximately 100 components were identified in the analysed samples, which makes 96.95% to 99.74% of the components present in essential oils. Linalool was the main constituent of lavender essential oil in the samples from Budva (27.32%) and Rovinj (47.67%), followed by borneol, β-phellandrene, camphor and 1,8-cineole. In the commercial sample, camphor was dominant compound (21.23%) followed by linalool, 1,8-cineole, linalool acetate and borneol.

Previous studies and obtained results in this study indicated the existence of differences in the terpenoid chemical composition. Variability in the qualitative and quantitative composition most probably depended on the genotype of the plant and the influence of different environmental factors. The application of lavender essential oil for therapeutic purposes depends on its qualitative properties. The obtained results might be significant in order to evaluate the quality of the plant raw material.

EXPERIMENTAL SECTION

Plant material and extraction procedure

Plants' material was collected in the initial flowering stage in Budva and Rovinj during summer 2014. Dried plant material was packed in paper bags and stored in a cool and dry place. The commercially available sample was purchased in a community pharmacy in typified package in Podgorica.

The essential oil of lavender was obtained by applying the method of hydro-distillation in the Clevenger type apparatus, according to Procedure I of the Yugoslav Pharmacopoeia IV. Hydro-distillation was performed for a period of 150 minutes (2,5 h) [10].

Each hydro-distillation was performed in 5 replicates. Lavender oil was separated by decantation from the remaining water and then dried on anhydrous sodium sulphate (Na_2SO_4). The essential oil was packaged and stored in dark glass phials until gas chromatography analyses.

Qualitative and Quantitative analysis of essential oils (GC and GC/MS)

GC analysis. Oil samples were analysed by gas chromatography technique (GC) on Hewlett-Packard (Model 5890 II) with a split-splitless injector connected to an HP-5 column (25 m x 0.32 mm, 0.52 μm) and flame ionising detector (GC/FID). Operated was using the following conditions: injector temperature, 250 °C; column temperature changes in column temperature programmed linearly from 40 to 260 °C with a rate of change of the 4 °C / min; carrier gas, H_2; injection volume, 1 ml / min, with a split ratio of 1:30; temperature detector 300 °C, while the isothermal conditions were bracketed at 260 °C for 10 minutes. The amount of the injected sample, dissolved in methylene chloride (CH_2Cl_2), was 1 μl. Surface percentages obtained in the range as a result of the determination of standard chromatogram are used for quantitative analysis.

GC/MS analysis. The analysis was performed on HP 1800 C II, GCD system (Hewlett-Packard, Palo Alto, CA, USA), equipped with a column HP-SMS (30 m x 0.25 mm x 0.25 μm). As the carrier gas used helium. Transfer line was heated to 260 °C. The mass spectra were obtained in the Ei mode (70 eV), in the range of from 40 to 450 m/z. The amount of the injected sample, dissolved in methylene chloride (CH_2Cl_2) was 0.2 μl. The components of the oil were identified by comparing the mass spectra with those in the database Wiley 275 and NIST/NBS (NIST–National Institute of Standards and Technology/ NBS-National Bureau of Standards) libraries, without using the various search engines. Identification of the components was achieved by comparing their retention indices and mass spectra with those found in the literature and compared with those obtained with the help of an automatic mass spectral analysis and software system for the identification (The Automated Mass Spectral Deconvolution and Identification System - AMDIS ver. 2.1), GC/MS library. The percentage of the constituents of the essential oil was obtained by normalising the surface of the corresponding peak and all the relative response factors were entered as 1.

ACKNOWLEDGMENTS

This research was supported by Serbian Ministry of Education, Science and Technological Development Project No. III45017.

REFERENCES

1) M.L. Balchin, “Lavender: The Genus Lavandula”, Taylor and Francis, Inc., London, **2002**.
2) C. Jianu, G. Pop, A.T. Gruia, F.G. Horhat, *International Journal of Agriculture and Biology,* **2013**, 15, 772.
3) L.L. Meessen, M. Bou, J.C. Sigoillot, C.B. Faulds, A. Lomascolo, *Applied Microbiology* and *Biotechnology*, ***2015****, 99(8), 3375.*
4) M. Saadatian, M. Aghaei, M. Farahpour, Z. Balouchi, *Global Journal of Medicinal Plant Research,* **2013**, 1(2), 214.
5) V. Schulz, R. Hansel, M. Blumenthal, V.E. Tyler, “Rational Phytotherapy”, Springer Verlag, Berlin, Heidelberg, New York, **2004**.
6) European Pharmacopoeia, 8th Edition, European Directorate for Quality Medicines, Council of Europe, Strasbourg, **2014**.
7) L. Hui, L. He, L. Huan, L. Xiaolan, Z. Aiguo, *African Journal of Microbiology Research*, **2010**, 4, 309.
8) N. Kovačević, “Bases of Pharmacognosy”, Serbian school book, Belgrade, **2004**.
9) V.D. Zheljazkov, C.L. Cantrell, T. Astatkie, E. Jeliazkova, *Journal of Oleo Science*, **2013**, 62, 195.
10) Yugoslavian Pharmacopoeia IV, Pharmacopoea Jugoslavica edition quarta, National Institute for Health Protection, Belgrade, **1984**.
11) H.M.A. Cavanagh, J.M. Wilkinson, *Phytotherapy Research*, **2002**, 16, 301.

STUDIA UBB CHEMIA, LXI, 2, 2016 (p. 137-154)
(RECOMMENDED CITATION)

PROMOTED ALUMINA SUPPORTED Ni CATALYST FOR ETHANOL STEAM REFORMING

MONICA DAN[a], MARIA MIHET[a], MIHAELA DIANA LAZAR[a*], LIANA MARIA MURESAN[b*]

ABSTRACT. The catalytic behavior of Ni/γ-Al_2O_3 catalyst modified with Cu, Ag, and Au was investigated in the process of ethanol steam reforming. The catalysts were prepared by co-impregnation and were characterized by specific surface area determination (S_{BET}), Inductively Coupled Plasma Mass Spectrometry (ICP-MS), X-ray diffraction (XRD), temperature programmed reduction (TPR), temperature programmed desorption (TPD) The data obtained from the experiments revealed that even at temperature as low as 350°C the ethanol is converted entirely, showing high selectivity for H_2 and CH_4.The activity of the Ni/γ-Al_2O_3 is only slightly increased by the addition of the supplementary metals. Nevertheless, the addition of metals to Ni/γ-Al_2O_3 has a positive effect in diminishing the quantity of CO_2 produced in the reaction. The promoted alumina Ni catalysts present a higher stability in some experimental conditions.

Keywords: *Ethanol steam reforming, Ni-catalysts, hydrogen production*

INTRODUCTION

Hydrogen is involved in many chemical and petrochemical processes, being considered as a promising clean energy vector [1,2]. Due to the increasing concern regarding environmental issues, an alternative to the fossil fuels it's demanded by the global society. New renewable energy sources which include H_2 are investigated by the research community. H_2 is mainly produced in industry from steam reforming of natural gas, a process who contributes to the greenhouse effect [3].

[a] *National Institute for Research and Development of Isotopic and Molecular Technologies, 67-103 Donath Street, 400293 Cluj-Napoca, Romania*
[*] *Corresponding authors: diana.lazar@itim-cj.ro, limur@chem.ubbcluj.ro*
[b] *Babeş-Bolyai University, Faculty of Chemistry and Chemical Engineering, 11 Arany Janos str., RO-400028, Cluj-Napoca, Romania*

Therefore, renewable sources like biomass for the production of hydrogen attract increased interest [4,5]. Among various bio-derived feedstocks, ethanol has the advantage of high hydrogen content, low toxicity and easiness in storing and handling. The ethanol can be transformed in hydrogen in conditions of relative low temperature and pressure (through steam reforming).

The reaction scheme of the ethanol steam reforming (ESR) is composed of a main reaction:

$$C_2H_5OH + 3H_2O \rightarrow 2CO_2 + 6H_2 \quad (1)$$

and a series of other parallel reactions, the most common of them being: [6–8]

- ethanol decomposition $C_2H_5OH \rightarrow CH_4 + CO + H_2$ (2)
- ethanol dehydrogenation $C_2H_5OH \rightarrow CH_3CHO + H_2$ (3)
- ethanol dehydration $C_2H_5OH \rightarrow C_2H_4 + H_2O$ (4)

The acetaldehyde can further decompose to form CH_4 and CO or can undergo steam reforming:

$$CH_3CHO \rightarrow CH_4 + CO \quad (5)$$
$$CH_3CHO + H_2O \rightarrow 2CO + 3H_2 \quad (6)$$

The CO formed in (eq.2) and (eq.5) can further be oxidized to CO_2 through water gas shift (eq.7) or to form carbon through Boudouard reaction (eq.8):

$$CO + H_2O \rightarrow CO_2 + H_2 \quad (7)$$
$$2CO \leftrightarrow C + CO_2 \quad (8)$$

Also, the ethylene can polymerize and form coke [9]:

$$nC_2H_4 \rightarrow \text{polymers} \rightarrow C \quad (9)$$

It is relatively obvious that the reactions involved in ethanol steam reforming process are many and complex and their relative occurrence depend on the nature of the catalytic material and of the reaction conditions.

The catalyst is crucial in order to obtain a good hydrogen production. According to the literature, different types of catalyst were tested in the process of ethanol steam reforming: oxides [10,11], noble and non noble metals [12–15]. Noble metals such as Ru, Rh, Pt, and Pd on various supports are well known for their high catalytic activity and stability. The main drawback of these catalysts is their high cost and relatively low availability.

Nickel and cobalt are mostly used as catalysts in ESR process [16,17] presenting good catalytic activity and low cost. The values recorded for ethanol conversion and for hydrogen selectivity in the process of ESR

using supported Ni catalyst are relatively high. However, there is a major drawback for this type of catalyst, mainly the poor stability in time, the catalyst deactivation occurring due to carbon deposition. The promotion of the supported Ni catalysts with other elements can improve the catalysts stability but also the catalytic activity. There are studies that suggest that carbon deposition on Ni catalysts for steam reforming of hydrocarbons can be strongly suppressed by adding promoters such as Ag or Au [18,19].

Catalysts based on copper are most interesting for ESR process. The catalytic properties of this type of catalyst depend strongly on the interaction of the metal with the support [20]. Copper is shown to act as a promoter on the catalytic activity and stability of the catalyst [21][22]. Alumina is one of the most used supports in ESR process having a high thermal stability.

The aim of this paper was to study the catalytic performances of alumina supported Ni catalysts promoted with Cu, Ag and Au at low temperature and high S/C ratio in the process of steam reforming of ethanol. The effect of addition of supplementary metals was studied in terms of structural modification, ethanol conversion, hydrogen yield, and catalyst stability.

RESULTS AND DISCUSSION

Catalyst characterization

Determined by ICP-MS method, the nickel content of the prepared catalysts is similar for Ni/Al and Ni-Au/Al with a value of 6.8 wt% and lower for Ni-Ag/Al and Ni-Cu/Al (Table 1).

The recorded N_2 adsorption-desorption isotherms for all studied catalysts show a type IV isotherm usually associated with a mesoporous structure [23]. The total surface area (S_{tot}), pore volume and pore size are not significantly affected by the addition of the supplementary metal (Table 1). The pore's radius varies between 20Å and 40Å for all the catalysts.

Table 1. Structural characteristics of Ni catalysts

Catalyst	S_{tot} (m^2/g)	S_{Ni} (m^2/g)	C_{Ni} (%)	C_{metal} (%)	$D_{Ni\text{-}XRD}$ (nm)
Ni/Al	102	2.4	6.8	-	10.0
Ni-Ag/Al	105	1.2	6.0	0.9	7.2
Ni-Au/Al	109	2.2	6.8	1.0	8.7
Ni-Cu/Al	104	1.3	6.1	0.8	5.9

From Ni chemisorption measurements we were able to calculate the surface of catalytic active area (Table 1). The values of the Ni surface area for Ni/Al and Ni-Au/Al are similar and are lower for Ni-Ag/Al and Ni-Cu/Al.

TPR experiments were performed on the calcinated catalysts precursors in order to evaluate the type and strength of interaction between NiO_x species and the support in correlation with the addition of the second metal. In order to clearly identify the reduction peaks, the TPR recorded profile was subjected to a mathematical analysis using a Gaussian function. Thus, for Ni/Al, three major peaks situated at 673°C, 735°C and 802°C were identified (Figure 1). It is generally accepted that the lower temperature peaks are associated with the presence of NiO_x particles with weak interaction to the support, while the high temperature peaks correspond to NiO_x species in close contact with the support [24]. The peaks situated below 673°C prove the existence of NiO_x species with low and medium interaction to the alumina support. The peaks situated above the 700°C are in general associated with the reduction of highly dispersed $NiAlO_4$.

The shape of the recorded TPR profile of the bimetallic catalysts is different from the TPR profile corresponding to Ni/Al. The addition of the noble metals (Ag, Au) to Ni/Al has the effect of lowering the main reduction peak from 735°C for NI/Al to 534°C for Ni-Ag/Al and 557°C for Ni-Au/Al. Also low intensity peaks are observed with values situated between 140°C-300°C associated to NiO_x species with low interaction with the support.

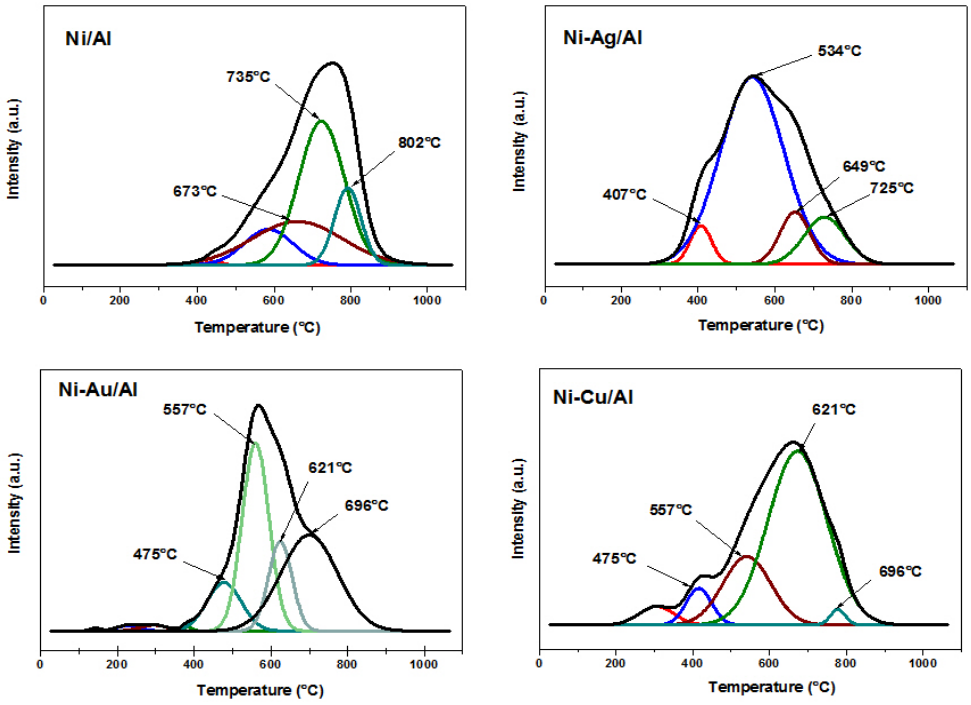

Figure 1. TPR profile of alumina supported nickel catalysts

The addition of copper to Ni/Al has a similar effect by lowering the temperature of the main reduction peak to 672°C from 735°C. Also, around 430°C a supplementary peak is present which could correspond to the reduction of CuO or to a NiO species as well. The peaks situated at 320°C correspond entirely to the reduction of CuO species [25]. In conclusion the addition of all three studied metals to Ni/Al_2O_3 decreases the strength of NiO_x interaction with the support increasing thus the reducibility of catalyst precursor.

From the XRD patterns of the prepared Ni catalysts, it was possible to determine the support crystallinity and the size of Ni crystallites (Figure 2). For all the catalysts the presence of the Ni corresponding diffraction peaks were observed at 44.5°, 51.8° and 76.5°. The Bragg reflexions situated at 37.3° and 43.3° and associated with NiO are not present, suggesting thus the presence of Ni only in the metallic state [26]. The presence of metallic Au, Ag and Cu could not be confirmed, probably due to the low quantity of the metal. The spectral lines associated with the presence of CuO at 20°, 33° also could not be confirmed. From XRD patterns the nickel crystallites size was calculated for all samples using Scherrer's equation (Table 1). The addition of all three studied metals decreases the Ni crystallites size in the following order: Ni-Cu/Al < Ni-Ag/Al < Ni-Au/Al < Ni/Al. The strongest effect was observed for Cu which produced the decrease of Ni crystallites size at almost half, inducing thus a much higher dispersion of active metal on the catalyst surface. For Ni-Cu/Al and Ni-Ag/Al the decrease of Ni nanoparticles is not correlated with variation of Ni surface area. Normally, a higher Ni dispersion is associated with higher metal surface area, which is not the case here. The only explanation would be that for these two catalysts a fraction of additional metal is deposited on the top of Ni nanoparticles. For Ni-Au/Al the addition of Au does not significant influence the catalyst structure.

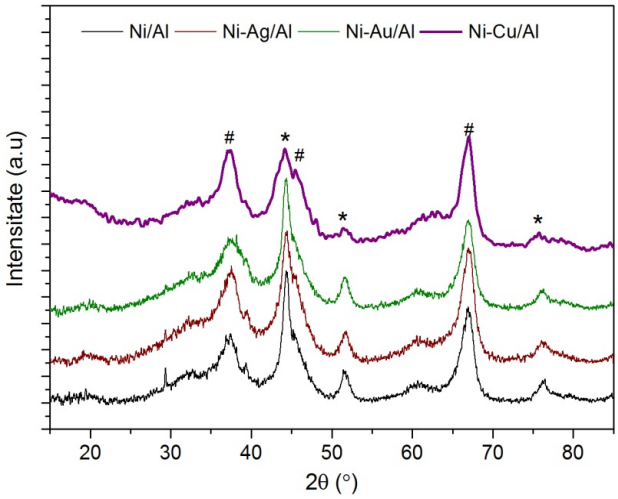

Figure 2. XRD pattern of the fresh prepared supported Ni catalyst: *- Ni, #-Al

H_2-TPD investigations were performed in order to obtain information regarding the type and strength of catalytic active sites for hydrogen chemisorption and activation and also on the influence that the additional metals might have on the nature of the catalytic active sites. The recorded profile shows in general two domain of hydrogen desorption peaks: one situated at lower temperature denoted as type I peaks, and one situated at higher temperature denoted as type II peaks. Type I peaks correspond to hydrogen desorbed form Ni nanoparticles and is in direct correlation with the number of Ni catalytic active sites [27, 28]. The hydrogen which is originally located on subsurface layers and/or the spillover hydrogen is usually associated with type II peaks [24].

The recorded TPD profile of the investigated catalytic material presents an asymmetric shape for all the alumina supported Ni catalyst. In order to distinguish between these two types of peaks the TPD profile were deconvoluted using a Gaussian type function (Figure 3).

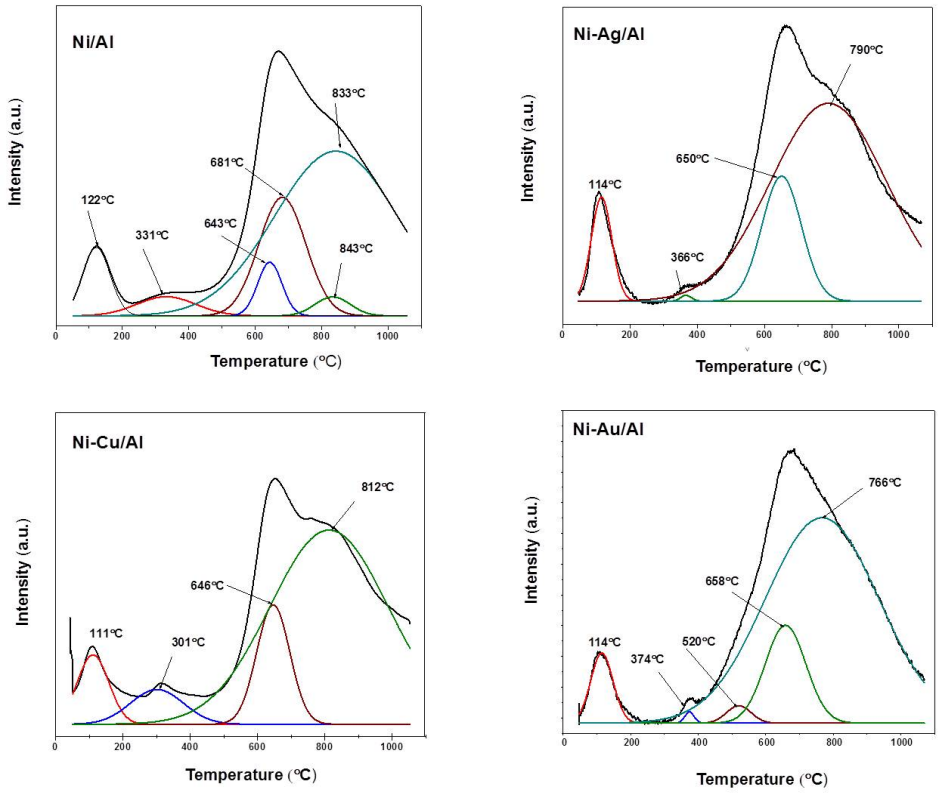

Figure 3. H_2-TPD profile of alumina supported Ni catalysts

From the deconvolution of the desorption curves it has been observed the presence of both type I and type II peaks. For all the investigated catalysts the distinction between the type I (below 500°C) and type II (above 500°C) desorption regions is very clear. For all the catalysts the identified peaks are mainly type II which suggest that all of the investigated catalyst have a high capacity to store hydrogen subsurface and/or on the support. For Ni/Al and Ni-Cu/Al two types of peaks were distinguished in region I: type Ia situated at temperature values <200°C, and types Ib with values 200°C<T<500°C, which indicates the presence of two different Ni catalytic active sites with different strength of H-Ni bonds. For Ni-Ag/Al and Ni-Au/Al the intensity of the Ib type peak is very low, demonstrating the prevalence of only one type of Ni catalytic sites.

The conclusion of the catalysts characterization section is that the addition of the supplementary metals (Ag, Au and Cu) to the alumina supported Ni catalyst leads to better reducibility of the catalyst precursor and better dispersion of Ni on the catalyst surface. The addition of Cu, Ag and Au does not change the mesoporous structure of the alumina supported catalysts and has a only a small influence on the type and strength of catalytic sites for hydrogen chemisorption.

Catalyst activity and selectivity

The Ni catalysts supported on alumina were tested in ethanol steam reforming at low temperature (150°C - 350°C) and high water-ethanol ratio (EtOH - H_2O = 1:30 molar ratio). The low temperature used in this study tries to improve the energy costs of the hydrogen production process. Another important aspect that was taken into consideration is the possibility of improving the water gas shift reaction and diminishing the concentration of CO, by working at low temperature (eq. 7) [29]. Also, we have chosen such a high water-ethanol ratio in order to try to reduce the carbon deposition on the catalyst surface of the studied catalyst.

Each catalyst was tested for 24 h at each temperature with 133 ml/min flow of carrier gas. The liquid (ethanol-water mixture) feed rate was varied between 0.1-0.6 ml/min.

The ethanol conversion function of temperature and liquid feed is presented in (Figure 4). At the lowest studied temperature - 150°C, regardless of the liquid feed, the ethanol conversion is around or less than 50%. At this temperature the addition of the supplementary metal to Ni/Al does not seem to have a significant positive effect on the ethanol conversion except for 0.3 ml/min feed rate.

At the highest temperature (350°C) for 0.1 ml/min and 0.3 ml/min liquid feed rate the maximum conversion is attained for all studied catalysts. For 0.6 ml/min liquid feed rate a decrease in ethanol conversion is recorded regardless of the imposed working temperature. In these working conditions a positive effect of metal addition upon ethanol conversion was attained, especially in the case of Ag and Cu. At lower reagents flow the 100% conversion observed for all catalysts impede the observation of any possible influence of additional metal to the catalyst performance.

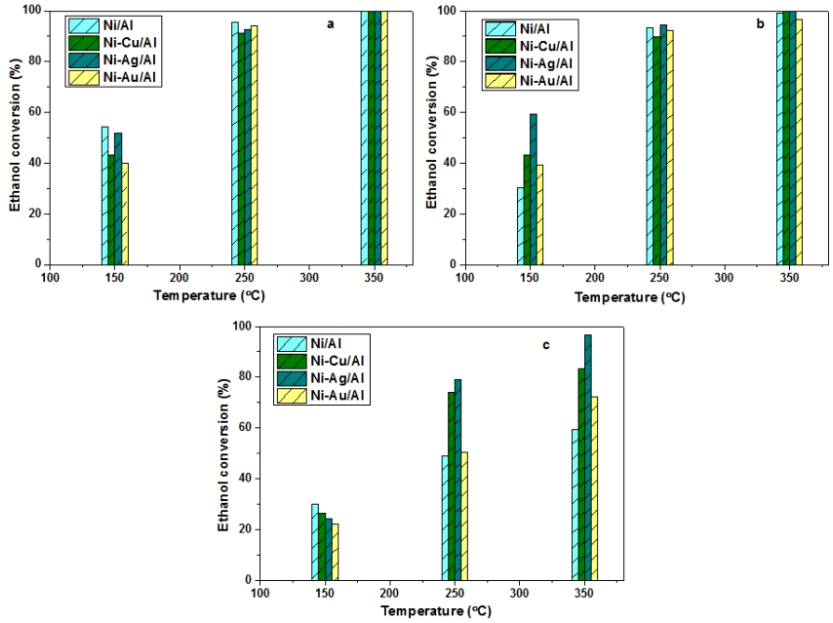

Figure 4. Ethanol conversion with temperature and liquid feed rate in ethanol steam reforming reaction: a-0.1ml/min; b-0.3ml/min; c-0.6ml/min

The TOF number (turn over frequency) was calculated in order to estimate the influence of metals on the intrinsic catalytic activity of Ni active sites. The TOF results (Table 2) at 150°C and 0.1 ml/min feed rate suggest a similar catalytic activity for Ni/Al and Ni-Ag/Al and a lower one for Ni-Au/Al. Although the TOF number for Ni-Cu/Al is higher than the one obtained for Ni/Al this is not reflected in a higher ethanol conversion. One possible explanation for this is that Ni/Al has a higher surface area, higher Ni dispersion which leads to a higher number of Ni catalytic active sites and therefore to a better overall catalytic activity.

At 150°C and 0.3 ml/min liquid feed rate it can be observed a direct correlation between high values of TOF number and high values for ethanol conversion for Ni-Ag/Al and Ni-Cu/Al, compared to the values recorded for Ni/Al.

Table 2. Catalytic parameters for all tested catalysts in ethanol steam reforming

Catalyst	TOF x 10^{-2} (s^{-1})						N x 10^{18} (at/g cat)
	Liquid flow ml/min						
	0.1		0.3		0.6		
	150°C	350°C	150°C	350°C	150°C	350°C	
Ni/Al	2.5	4.6	4.2	13	8.3	16	37
Ni-Cu/Al	3.7	8.6	11	25	13.6	42	20
Ni-Ag/Al	4.8	9.3	16	28	13.4	53	19
Ni-Au/Al	2	5.1	5.9	14	6.7	22	34

TOF-turnover frequency; N-number of catalytic active sites per g catalyst

The results obtained at 350°C and 0.6 ml/min feed rate, revealed high values for TOF for all the bimetallic catalyst compared to Ni/Al. This is reflected also in the conversion of ethanol which is higher for all the tested catalysts with additional metal.

The liquid products are removed from the mixture through condensation at the reactor exit. Besides water, the liquid mixture also contains unreacted ethanol (depending on ethanol conversion) and traces of acetaldehyde and acetone. The gaseous phase is dried by passing it through a silica trap and then analyzed on line. The identified products are: H_2, CO, CH_4, and CO_2. No traces of other light alkynes or alkenes were identified, although these compounds are mentioned in other studies [30]. At low experimental temperature H_2 is the main compound in the gaseous mixture regardless of liquid feed rate and of the investigated catalyst (Figure 5).

The distribution of products in the gaseous mixture is modified due to the various reactions that are favoured by increasing the temperature. At 350°C we observe that hydrogen selectivity at a given value of liquid feed is not significantly influenced by the addition of the supplementary metals. By increasing the reagents flow the relative concentration of H_2 in the exhausted gases increase with almost 20% reaching around 70% values (Figure 6). This is only partially due to the decrease of relative concentration of methane, which would imply an increase of catalyst selectivity for hydrogen production, and mainly to the decrease of carbon oxides concentrations. At 0.1 ml/min liquid feed and 350°C the values of the CO_2 selectivity are drastically decreased by the addition of the supplementary metals to Ni/Al. Important concentrations of CO were recorded especially for Ni-Au/Al catalyst. By raising the liquid feed rate to 0.6 ml/min the relative concentration of CO_2 is lower, as mentioned before, but the same trend of decreasing of the CO_2 selectivity is observed for promoted catalysts (Figure 6).

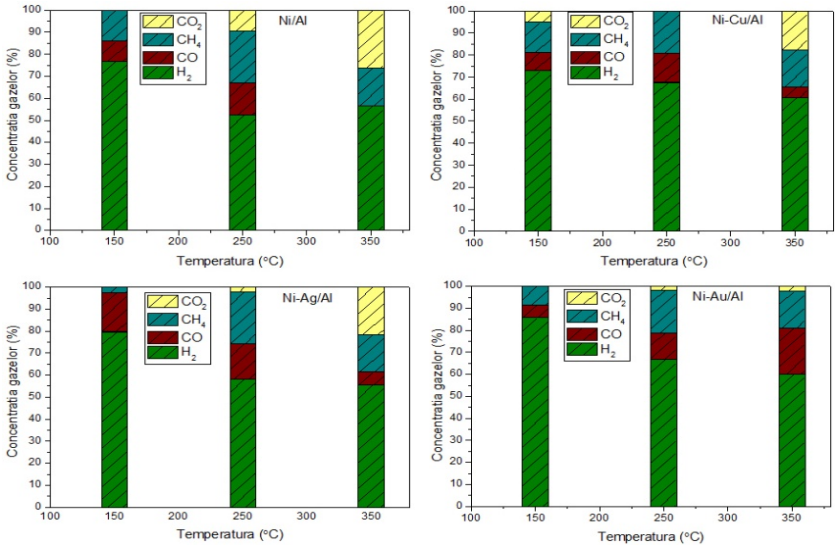

Figure 5. Composition of effluent gases (mol %) in ethanol steam reforming at 0.1 ml/min liquid feed rate

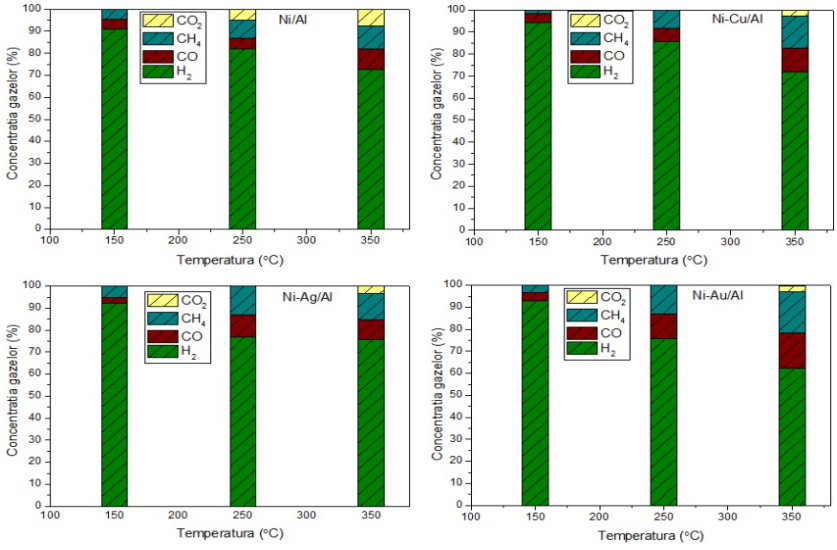

Figure 6. Composition of effluent gases (mol %) in ethanol steam reforming at 0.6 ml/min liquid feed rate

The hydrogen yield is an important catalytic parameter (calculated according to (eq. (10)) which characterizes the catalyst efficiency to obtained hydrogen from the raw material in ESR reaction (Figure 7). At the lowest

working temperature the obtained values are low due to low conversion of ethanol. Increasing the temperature to maximum (350°C) we obtained higher values for this parameter. Its value is situated around 30% being not significantly influenced by the metal addition or the reagents flow.

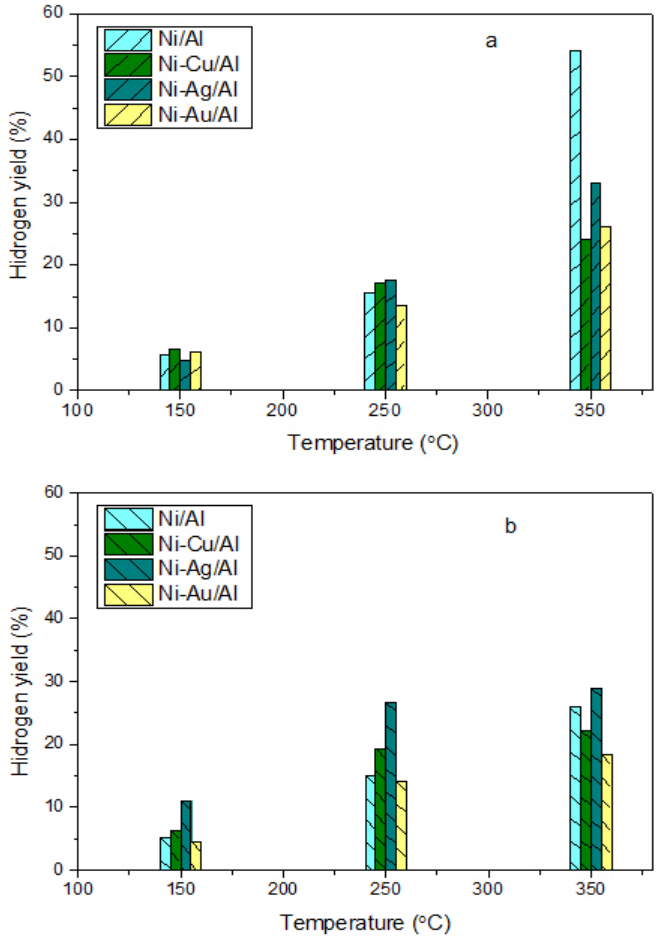

Figure 7. The variation of hydrogen yield with temperature and liquid feed rate in ethanol steam reforming reaction: a - 0.1 ml/min; b - 0.6 ml/min

The stability of the catalyst was evaluated during 24h on stream by measuring on line the ethanol conversion. It was observed at lower experimental temperature and lower feed rate a decrease in ethanol conversion higher than the one recorded for ESR experiments at higher temperature.

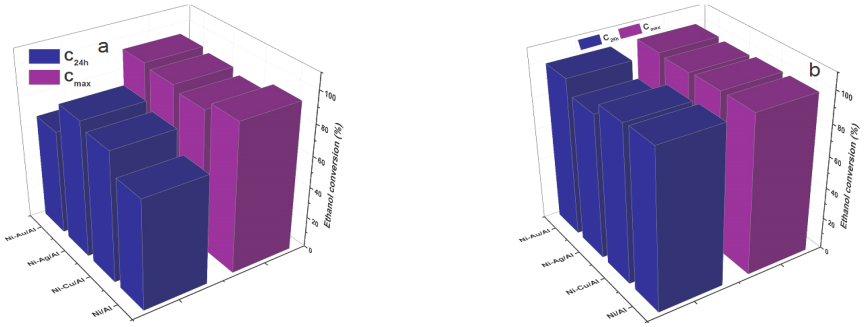

Figure 8. Catalyst stability for alumina supported Ni catalysts in ESR reaction at 0.1 ml/min liquid feed rate a-250°C; b-350°C; C_{max}-maximum ethanol conversion, C_{24h}- ethanol conversion after 24h

The addition of metals (Au, Ag, and Cu) to Ni/Al seems to have a positive effect by diminishing the catalyst deactivation in most of the tested experimental conditions. Thus, the promoted catalysts tested at the 0.1 ml/min flow rate at 250°C and 350°C present lower deactivation, except Ni-Au/Al at 250°C for which a drop of almost 30% from the initial value of ethanol conversion is recorded (Figure 8a).

With the increase of liquid feed rate to 0.6 ml/min at 250°C a deactivation of all the catalysts was observed: Ni-Au/Al deactivates almost completely and Ni/Al at ≈50% from the maximum values of ethanol conversion. Contrarily, for Ni-Ag/Al and Ni-Cu/Al a beneficial effect of additional metal is clearly observed (Figure 9a). For the same liquid feed rate and 350°C the recorded deactivation for all the tested catalyst is even more pronounced, Ni-Au/Al being the catalyst for which the recorded deactivation is the highest (Figure 9). It can be concluded that the stability of all catalysts at 0.6 ml/min liquid flow and 350°C is very poor despite their good initial catalytic activity.

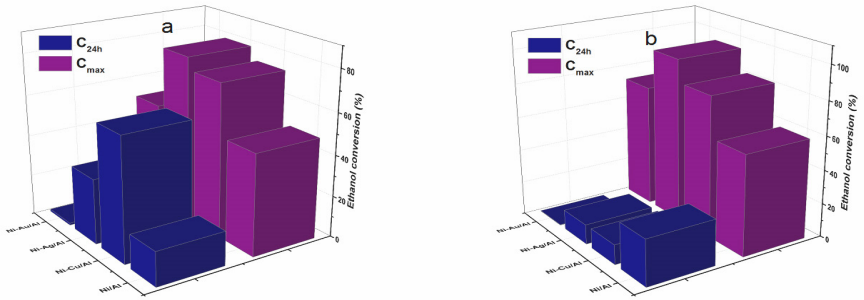

Figure 9. Catalyst stability for alumina supported Ni catalysts in ESR reaction at 0.6 ml/min liquid feed rate a-250°C; b-350°C; C_{max}-maximum ethanol conversion, C_{24h}- ethanol conversion after 24h

The deactivation of the catalyst in ESR reaction is mainly due to the formation of carbon and its deposition on the catalyst surface [31]. In order to investigate the catalysts deactivation for 0.6 ml/min liquid flow, XRD techniques were used.

The XRD analysis of the used catalyst revealed that the lines that should be attributed to Cu, Ag and Au do not appear in the spectra, due to the low amount of the metal deposited on the support. The recorded spectra did not contain any peak in the area of 2θ = 26.5° [33] that could be assigned to graphitic carbon. Besides the lines attributed to Al_2O_3 and Ni, the presence of NiO at 2θ= 43°, was also revealed for Ni/Al and the Cu and Ag promoted catalysts (Figure 10). NiO is not active for ESR and is a cause of catalysts deactivation. In this case, the high flow rate and high water: ethanol ratio provide an oxidizing environment at 350° which lead to Ni oxidation to NiO with subsequent loose of catalytic activity. The addition of another metal does not strongly influence this phenomenon. At 250° the addition of Cu and Ag interfere in the process and reduce the catalyst deactivation (Figure 9a).

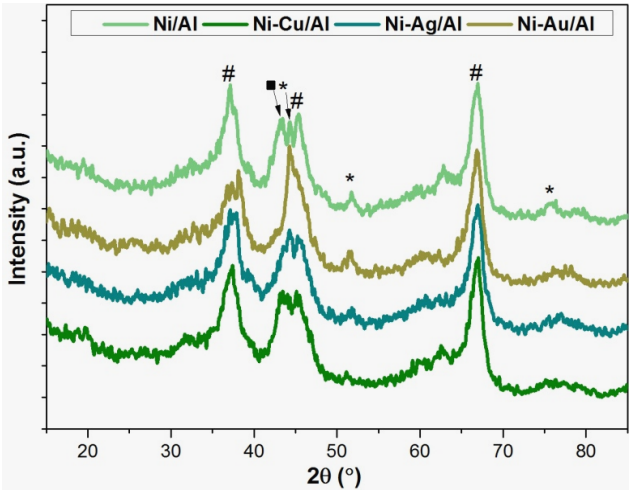

Figure 10. XRD spectra of the alumina-Ni supported catalysts used in the ESR reaction at 350°C and 0.6 ml/min liquid feed flow

CONCLUSIONS

An investigation of group Ib belonging metals promoted on alumina supported Ni catalysts (Ni/Al, Ni-Ag/Al, Ni-Au/Al, Ni-Cu/Al) used in the process of ethanol steam reforming at low temperature and high water:ethanol ratio was carried out. The catalysts were prepared by co-impregnation and characterized by ICP-MS, XRD, TPR and H_2-TPD.

The addition of the supplementary metal to Ni/Al improves the reducibility of the catalyst precursor and the Ni dispersion, but does not change the mesoporous structure of the catalyst. The maximum ethanol conversion is obtained at temperature of 350°C and 0.1 ml/min and 0.3 ml/min of liquid feed rate. Better catalytic activity was recorded for the bimetallic catalyst at 350°C and 0.6 ml/min compared to Ni/Al, but the stability is very poor for all tested catalysts on these experimental conditions.

The reaction products mixture contains high proportion of hydrogen and low proportion of methane alongside the carbon oxides; the values of CO_2 selectivity are lower for the bimetallic catalysts compared to those for Ni/Al. The highest hydrogen yield was recorded for Ni/Al at 350°C and 0.1 ml/min liquid feed rate. The addition of metals (Ag, Au, Cu) to Ni/Al proves to have a positive effect by diminishing the catalyst deactivation only in some experimental conditions.

EXPERIMENTAL SECTION

Catalysts preparation

The Ni/Al_2O_3 (denoted Ni/Al) catalyst was prepared by wet impregnation of γ-alumina (Merck, Germany, S_{tot}= 135 m^2/g) with an aqueous solution of $Ni(NO_3)_2 \cdot 6H_2O$. The co-impregnation method was used to prepare the promoted alumina supported nickel catalysts. Thus $Ni\text{-}Cu/Al_2O_3$ (denoted Ni-Cu/Al), $Ni\text{-}Ag/Al_2O_3$ (denoted Ni-Ag/Al), $Ni\text{-}Au/Al_2O_3$ (denoted Ni-Au/Al) were prepared by impregnation of γ-alumina with a mixture of aqueous solution of $Ni(NO_3)_2 \cdot 6H_2O + Cu(NO_3)_2 \cdot 6H_2O$, $Ni(NO_3)_2 \cdot 6H_2O + AgNO_3$, $Ni(NO_3)_2 \cdot 6H_2O + HAuCl_4$.

The impregnated catalysts samples were dried at room temperature overnight, calcinated in Ar at 550°C for 4h followed by reduction with H_2 at 550°C for another 4h. All reagents unless other specified were purchased from Alfa Aeser, Germany and used with no further purification.

Catalyst characterization

Metal content was determined by ICP-MS analysis using an ELAN DCR-e instrument (Perkin-Elmer, USA). The metals were removed from the support by treating 0.1 g catalyst sample with 5 ml of concentrated HNO_3 for nickel, copper and silver containing samples. In order to determine the gold content, the catalyst sample was treated with 5 ml of "*aqua-regia*".

Adsorption desorption isotherms obtained using a Sorptomatic 1900 (Thermo Electron Corporation, USA) instrument were used to determine the total surface area (S_{tot}), pore volume (V_p) and pore radius (r_p).

X-ray powder diffraction (XRD) spectra were recorded using a Brucker D_8 advanced diffractometer with $CuK_{\alpha 1}$ radiation source, operated voltage 40 kV and 40 mA current. The diffraction patterns were recorded in the range $20° < 2\theta < 85°$ with a step size of 0.01°/s. The size of Ni crystallites was determined using Scherrer's equation.

The active surface area of the catalysts was measured by H_2 chemisorption in conventional volumetric equipment. The sample (≈ 2.5 g) was reduced overnight at 350°C in hydrogen flow and degassed at the same temperature until a final pressure lower than 10^{-5} torr was attained. Adsorption of hydrogen was carried out at room temperature. The metallic surface area was calculated assuming a stoichiometry of 1:1 H to Ni atom and that each nickel atom occupies 6.5 $Å^2$.

Using as equipment TPRO 1100 (Thermo Scientific, USA) it was possible to record the profile obtained from H_2 temperature programmed reduction (TPR) and H_2 temperature programmed desorption (TPD) experiments of every prepared catalyst. For TPR experiments 0.35 g of calcinated catalyst precursor was placed in the reactor with Ar for 30 min and then heated from room temperature to 1100°C, with a rate of 10°C/min with a 20 ml/min (H_2 +Ar) mixture (10 vol% H_2).

For TPD experiments, about 0.35 g of catalyst was activated in the same mixture (H_2+ Ar) at 550°C for 4 h and then cooled down to 50°C in Ar (20 ml/min). Hydrogen chemisorption was performed at 50°C in (H_2+Ar) mixture for 1h followed by cleaning in Ar for 30min. Hydrogen desorption were made by heating the catalyst sample in Ar (20 ml/min) from 50°C to 1100°C, with a temperature rate of 10°C/min.

Catalyst activity testing

The catalytic activity of the prepared catalyst was evaluated in the process of ethanol steam reforming. The experimental setup is described in detail (Figure 11). The experiments were performed at ambient pressure in a stainless steel (i.d. 9 mm) fixed bed reactor placed in a temperature controlled oven. The carrier gas (Ar) is controlled by a mass flow controller and the liquid mixture (ethanol-water) is introduced in the reaction system through LC-6A (Shimadzu, Japan) pump. At the reactor outlet, the liquid phase is removed from the outcoming mixture through condensation. The effluent gas is further dried by passing it through silica gel. Furthermore the gas is analyzed on-line using a gas chromatograph (Sferocarb column, 2m, 80-100 mesh and Ar as carrier gas at 120°C) equipped with a TCD detector.

The catalyst (1g) is mixed with alumina support (1g) with the same granulation (100-200 μm) and placed in the reactor. Prior to catalytic activity test, the catalyst is reduced in H_2 at 350°C for 3h. The temperature

range of the experiments is set between 150°C and 350°C at atmospheric pressure. The H_2O: EtOH volumetric ratio was 9:1 (10 vol% solution of EtOH in water) which gives an H_2O: EtOH molar ratio of 30:1.

Ethanol conversion was calculated using the following formula:

$$C_{EtOH} = \frac{[EtOH]_{in} - [EtOH]_{out}}{[EtOH]_{in}} x100 \quad (10)$$

where $[EtOH]_{in}$ and $[EtOH]_{out}$ are ethanol molar concentrations in the initial solution and in the outlet condensed liquid, respectively.

Hydrogen yield was calculated according to the formula:

$$H_2 \text{ yield} = \frac{\text{moles } H_2 \text{ produced}}{6 \text{ x (moles EtOH converted)}} \text{ x } 100 \quad (11)$$

The identified compounds in the gas mixture are expressed in mol %, taking into consideration only the reaction products and not the carrier gas.

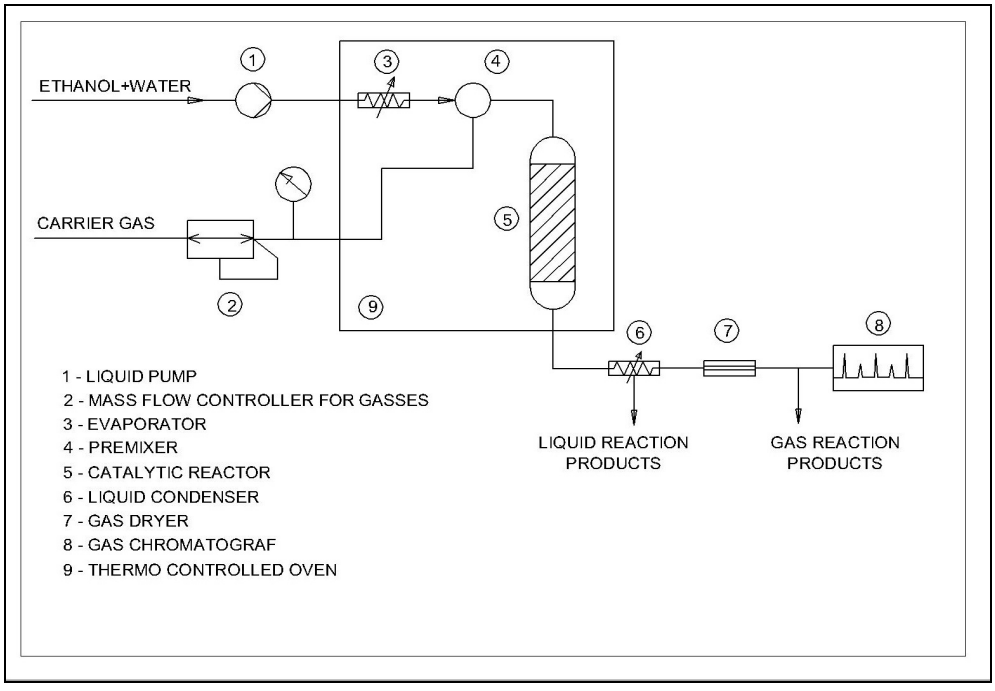

Figure 11. The schematics of the experimental setup for the ethanol steam reforming process

ACKNOWLEDGMENTS

This work was supported by a grant of the Romanian National Agency for Scientific Research, Project Number PN-II-PT-PCCA-2011-3.2-0452

REFERENCES

1. A. Züttel, A. Remhof, A. Borgschulte, O.Friedrichs, *Philosophical Transactions Series A Mathematical, physical, and engineering sciences,* **2010**, 368, 3329–3342.
2. C. Pirez, M. Capron, H. Jobic, F. Dumeignil, L. Jalowiecki-Duhamel, *Angewandte Chemie International Edition,* **2011**, 50, 10193–10197.
3. L. He, J.M.S. Parra, E.A. Blekkan, D.Chen, *Energy Environmental Science,* **2010**, 3, 1046–1056.
4. P.R. Piscina, N.Homs , *Chemical Society Reviews,* **2008**,37, 2459–2467.
5. D.M. Alonso, S.G. Wettstein, J.A. Dumesic, *Chemical Society Review*, **2012**, 41, 8075–8098.
6. W. Xu, Z. Liu, A.C. Johnston-Peck, S.D. Senanayake, G. Zhou, D. Stacchiola et al., *American Chemical Society Catalysis,* **2013**, 3, 975–984.
7. G. A. Deluga, J.R. Salge, L.D. Schmidt, X.E. Verykios, *Science* **2004**, 303, 993–997.
8. A. Therdthianwong, T. Sakulkoakiet, S. Therdthianwong, *Science Asia*, **2001**, 27,193–198.
9. A.N. Fatsikostas, X.E. Verykios, *Journal of Catalysis*, **2004**, 225, 439–452.
10. M. Skotak, Z. Karpinski, W. Juszczyk, J. Pielaszek, L. Kepinski, D. Kazachkin et al., *Journal of Catalysis,* **2004**, 227, 11–25.
11. M.C. Sánchez-Sánchez, R.M. Navarro, J.L.G Fierro, *International Journal of Hydrogen Energy,* **2007**, 32, 1462–1471.
12. P.Y. Sheng, H.Idriss, *Journal of Vacuum Science Technology A*, **2004**, 22, 1652-1658.
13. J. Raskó, A. Hancz, A. Erdőhelyi, *Applied Catalysis A General*, **2004**, 269, 13–25.
14. Z. Wang, C. Wang, S. Chen, Y. Liu, *International Journal of Hydrogen Energy,* **2014**, 39, 5644–5652.
15. R. Buitrago-Sierra, J. Ruiz-Martínez, J.C. Serrano-Ruiz, F. Rodríguez-Reinoso, A. Sepúlveda-Escribano, *Journal of Colloids and Interface Science*, **2012**, 383, 148–154.
16. S. Li, M. Li, C. Zhang, S. Wang, X. Ma, J. Gong, *International Journa of Hydrogen Energy,* **2012**, 37, 2940–2949.
17. R. Padilla, M. Benito, L. Rodríguez, A. Serrano, G. Muñoz, L.Daza, *Internatioanl Journal of Hydrogen Energy*, **2010**, 35, 8921–8928.
18. H.S. Bengaard, J.K. Nørskov, J. Sehested, B.S. Clausen, L.P. Nielsen, A.M. Molenbroek, et al., *Journal of. Catalysis*, **2002**, 209, 365–384.
19. N.V. Parizotto, K.O. Rocha, S. Damyanova, F.B. Passos, D. Zanchet, C.M.P. Marques, et al., *Applied Catalysis A General*, **2007**, 330, 12–22.
20. A. Kubacka, M. Fernández-García, A. Martínez-Arias, *Applied Catalysis A General.,* **2016**, in press, doi:10.1016/j.apcata.2016.01.027
21. C. Ratnasamy, J.P. Wagner, *Catalysis Reviews,* **2009**, 51, 325–440.

22. F. Wang, Y. Li, W. Cai, E. Zhan, X. Mu, W. Shen, *Catalysis Today* **2009**,146, 31–36.
23. S.J. Gregg. Adsorption, Surface area and Porosity, *Academic Press*, **1982**.
24. S. Velu, S.K. Gangwal, Solid State Ionics **2006**,177, 803–811.
25. H. Wang, R.T.K Baker, *The Journal Physical Chemistry B,* **2004**, 20273–20277.
26. Y. Matsumura, T. Nakamori, *Applied Catalysis A General,* **2004**, 258,107–114.
27. A.G. Boudjahem, S. Monteverdi, M. Mercy, M.M. Bettahar, *Journal of Catalysis,* **2004**, 221, 325–334.
28. Y. Cesteros, P. Salagre, F. Medina, J. Sueiras, *Applied Catalysis B Environmetal,* **2000**, 25, 213–227.
29. L. García, Compendium of Hydrogen Energy, **2015**.
30. G. Rabenstein, V. Hacker, *Journal of Power Sources,* **2008**,185,1293–1304.
31. L.V. Mattos, G. Jacobs, B.H. Davis, F.B. Noronha., *Chemical Reviews,* **2012**, 112, 4094–4123.
32. Z.L. Zhang, Verykios XE., *Catalysis Today,* **1994**, 21, 589–595.
33. A. Tanksale, J.N. Beltramini, G.M. Lu., *Renewable Sustainable Energy Reviews.,* **2010**, 14, 166–182.

STUDIA UBB CHEMIA, LXI, 2, 2016 (p. 155-166)
(RECOMMENDED CITATION)

A MACROKINETIC STUDY OF THE OXIDATION OF METHANOL TO FORMALDEHYDE ON Fe_2O_3 – MoO_3 OXIDE CATALYST

SIMION DRĂGAN[a*], IVETTE KULIC[a]

ABSTRACT. In this paper, a kinetic study about the oxidation of methanol to formaldehyde on Fe_2O_3-MoO_3 oxide catalyst was investigated. Results about the changes of the conversion at different contact times and the way the composition of the mixture respectively temperature influence the oxidation process, is submitted. The parameters were elected so that they match with those of the existing industrial reactors. We analyzed the influence of the above mentioned parameters on the rate of the process. Processing the experimental results in $\ln k - T^{-1}$ coordinates allowed the determination of the activation energy and the establishment of the corresponding mechanisms. The results, E_a=57.23 kJ/mol, indicate that under 520K the mass transformation processes (chemical reaction, adsorption – desorption) are the limiting ones the oxidation process. At temperatures higher than 535K the value of the activation energy, E_a=9.39 kJ/mol, emphasizes that limiting are the inner/outer diffusion phenomena. In the temperature range 520K – 535K, when E_a=25 – 42 kJ/mol, the process is carried out after a combined macrokinetic model (mass transfer –transformation).

Keywords: *methanol oxidation process, kinetic study, macrokinetic model.*

INTRODUCTION

Formaldehyde (FA) is a product of the organic chemical industry with many practical applications [1-3]. Big amounts of formaldehyde are used in the manufacture of ureo-, melamino- and fenaldehydical resins, which are used as adhesives or impregnating agents. The synthesizing of polyacetates and of 1,4-butandiol is based also on formaldehyde [4]. Another industrial branch which requires large amounts of formaldehyde is the production of fertilizers with the gradual solubility in time. Formaldehyde

[a] *"Babeş-Bolyai" University, Faculty of Chemistry and Chemical Engineering, Arany Janos 11, RO-400028 Cluj-Napoca, Romania*
[*] *Corresponding author: sdragan@chem.ubbcluj.ro*

finds practical use also as a disinfectant of the agricultural lands or for the warehouses infected with pathogenic agents. In all these practical applications formaldehyde is used in the form of diluted solutions with a concentration of 38-40 %. World production of formaldehyde has an average annual growth rate of 3-4 % [2,5].

Formaldehyde has great importance in the economic since its production is in full development, what justifies the continuation of studies in order to improve its manufacturing technology.

The first industrial methods for formaldehyde synthesis used high purity methane gas as a raw material, which was oxidized on silver catalysts [6,7]. The high proportion of secondary reactions, the low yields in formaldehyde, the large and complicated installations for the purification of the product, made this procedure to have only historical importance. Over 90 % of the world production of formaldehyde is currently done after techniques which use methanol as a raw material [3,4], [6-10].

The production of formaldehyde from methanol was carried out in two different technologies which differ only in the used catalyst. In the first applied industrial method, the oxidation of methanol is performed on silver catalysts [9] at high temperature (500-600 °C) and pressure (1.3-1.5 atm.), in complex industrial systems, with large power consumption. The advantage of the method is the high concentration of methanol in the reaction mixture which defines less gas flow and higher concentration of formaldehyde in the final product.

The second method is based on the reactions discovered in 1931 by Adkins and Peterson [11] who oxidized for the first time methanol with molecular oxygen on Fe_2O_3 – MoO_3 oxide catalyst, in much milder conditions: range of temperature between 200-300 °C and atmospheric pressure. Although the process was industrialized since 1950, the composition of the catalyst remains almost unchanged up to the present time. Due to the economical efficiency of the method, did it to become more common on an industrial scale, therefore, studies have been reinforced for the improvement of the selectivity of the catalysts and of the industrial technology [12-20].

The studies for the improvement of the catalysts led to the conclusion that the catalytic activity and selectivity to formaldehyde are determined by the presence of two phases in the structure: a prevailing phase of $Fe_2(MoO_4)_3$ and one amorphous of MoO_3 located on the surface of the $Fe_2(MoO_4)_3$ spinel [21-26]. The presence of MoO_3 on the surface of the spinel is because it volatilizes during the operation, and facilitates the formation of Fe_2O_3, compound that catalyzes the oxidation to CO_2 [22-24, 27-29]. On the other hand Fagerazzi [30] shows that actually Mo^{6+} replaces Fe^{3+} in the crystalline

network of the spinel and through this the catalyst retains both its activity and selectivity.

Massarotti [31] justifies the high activity and selectivity of Fe_2O_3 – MoO_3 catalyst trough the presence of MoO_3 dissolved in the dominant phase of the $Fe_2(MoO_4)_3$ spinel thereby providing the regeneration of the active surface.

As a result of the studies about the relationship between the catalytic activity, selectivity and the chemical composition of the catalyst, is established that the maximum activity for the $Fe_2(MoO_4)_3$ spinel corresponds to a Mo:Fe ratio of 1.5. In industrial practice the Mo:Fe ratio is 2.2-2.6 [28], the excess of Mo ensures a selectivity of 92-94 %, at a total conversion in methanol of 95-98 %.

The most of the worldwide conducted researches had as a goal establishing the causes what determines the deactivation of catalyst. It has been shown, that the deactivation is determined by the volatilization of MoO_3 [21-24], by the sintering [32-37] or forming of inactive Fe_2O_3 $FeMoO_4$ phases [22,23,33]. All phenomena what determines the deactivation of the catalyst are under the influence of the high operating temperature.

Obviously, many studies were made about catalysts used in the process but very little designed for the kinetic of the oxidation on industrial catalysts [12,21,38]. Productivity growth of the existing oxidation technologies of methanol to formaldehyde supposes, in addition to the improvement of the catalysts with the help of various additives of V_2O_5 and Co_2O_3 [12,38], the knowledge of the laws after which the overall process of oxidation is carried out, which is more complicated than the chemical reaction.

The overall process of oxidation must take into account, besides the mass transformation phenomena (chemical reaction, adsorption, desorption) those of internal and external diffusion [39-42]. Depending on the working conditions (temperature, concentration of the reactant mixture) the oxidation process of methanol to formaldehyde can be carried out after any of the possible macrokinetic models:

- mass transformation (chemical reaction, adsorption – desorption of reactants or of the reaction products);
- mass transfer of the reactants through the gaseous phase to the surface of the catalyst or of the reaction products from the surface in volume and diffusion through the pores of the catalyst;
- combined macrokinetic model mass transfer – transformation.

In this work a macrokinetic study is performed regarding the oxidation of methanol to formaldehyde on Fe_2O_3 – MoO_3 industrial catalyst in which we examined the effect of the reaction mixture and of the temperature on the global rate of reaction of the process.

RESULTS AND DISCUSSION

In order to highlight the influence of initial reaction mixture composition and temperature on the global rate of the oxidation process, measurements were conducted on which bases the conversion of methanol (Me) and the rate of oxidation, appropriate for different contact times, were calculated. The experimental results regarding the influence of the concentration of Me, O_2 and FA on the global conversion and on the oxidation rate of Me for different contact times are shown in fig. 1-6.

The data from fig. 1 underlines the strong influence of Me concentration in the reaction mixture on the global conversion. Thus, it is clear that at a content of 7.5 % vol. Me and 4 % vol. O_2 in the reaction mixture, the final conversion reaches the value of 70 % and increases till 84 % when the concentration of Me is reduced to 1.5 % vol. From fig. 2 it can be concluded that simultaneously with the reduction of Me content in the reaction mixture, the rate and rate constant of the oxidation process is decreasing, sinks from $1.35 \cdot 10^{-4}$ to $1.321 \cdot 10^{-7}$ mol/g·s·torr even though the excess in O_2 is growing from a ratio of O_2: Me=2.67 to O_2: Me=13.35. If we work with O_2 excess (over the stoichiometric ratio) the rate of the oxidation process does not depend anymore on the concentration of O_2, this only affects the final value of the conversion.

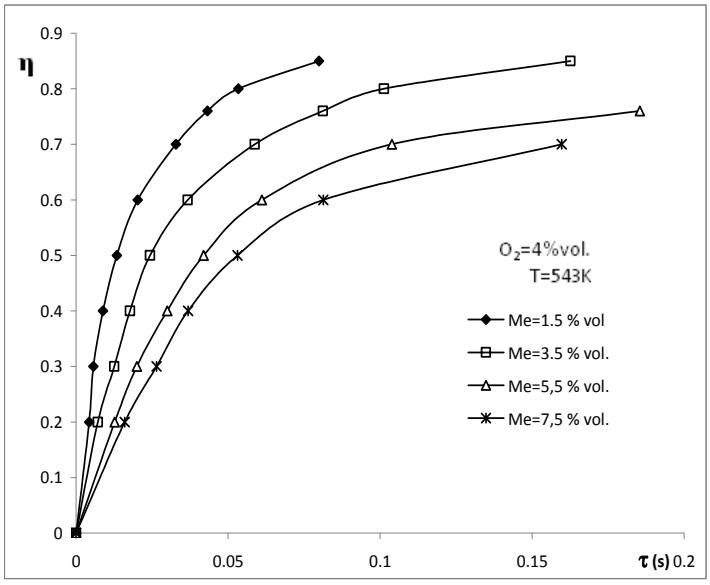

Fig.1. The conversion of methanol - contact time at different concentrations of Me

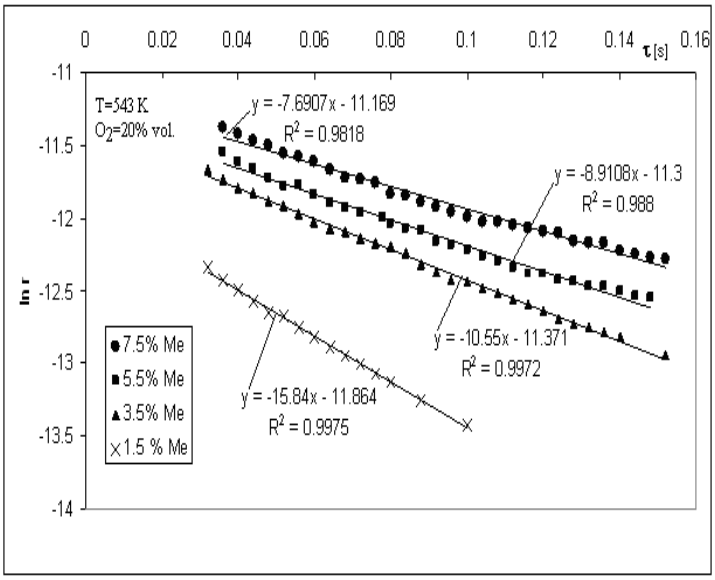

Fig. 2. The effect of concentration in Me on the rate of oxidation

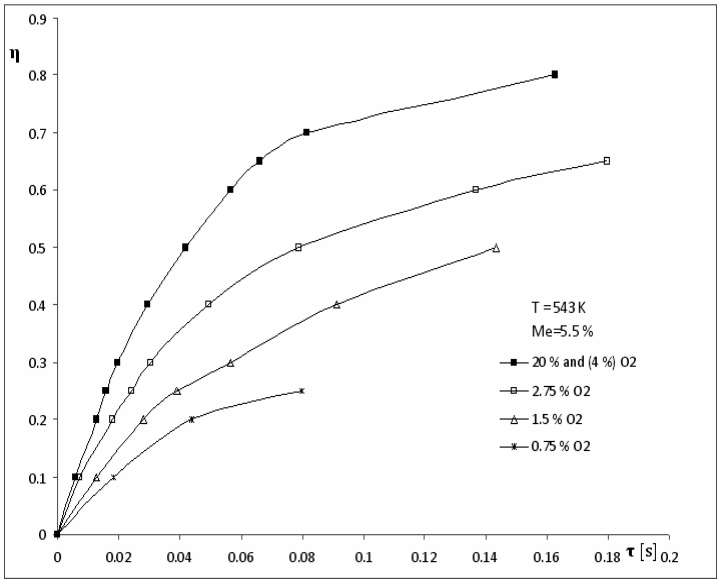

Fig.3. The conversion of methanol - contact time at different concentrations of O_2

In fig. 3 is presents the influence on the conversion of the O_2 concentration in the reaction mixture at a constant concentration of Me = 5.5 % vol. . There is a strong influence of the O_2 concentration (respectively of the ratio O_2:Me) in

the reaction mixture over the conversion. At a ratio below the stoichiometric one (O_2:Me = 1:5) the final conversion of methanol barely reaches the value of 24 %. As the O_2 concentration increases (1.5 % vol.), which corresponds to a molar ratio of O_2:Me close to the stoichiometric one, the conversion increases significantly reaching the value of 50 %. When the concentration of O_2 equals the stoichiometric ratio O_2:Me = 0.5, more precisely 2.75 % O_2 in the reaction mixture, the conversion grows over 60 %. At a concentration of 4 % vol. O_2 which corresponds to a ratio O_2:Me = 4:5.5, the conversion of Me has a value around 80 %. It can be noticed that this value is identical with the conversion the corresponding to a great excess of O_2 in the reaction mixture (20 % vol. O_2) with a ratio of O_2:Me = 20:5.5.

In fig. 4 it is shows the influence of O_2 concentration over the oxidation rate.

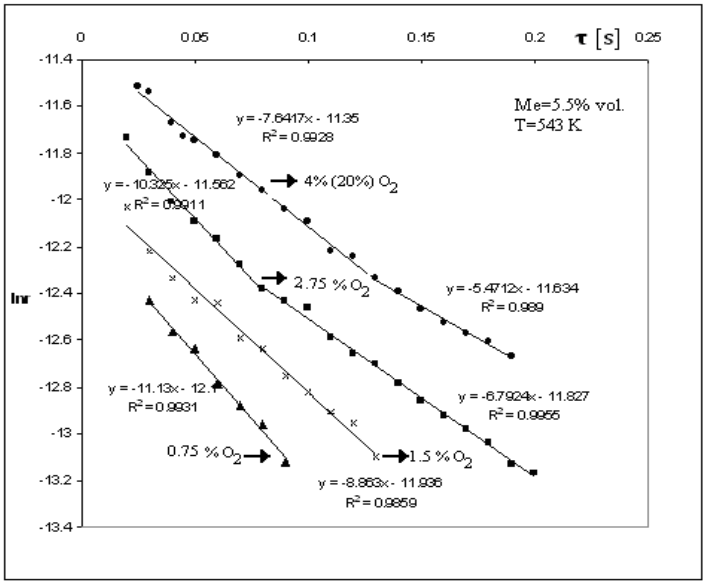

Fig.4. The effect of O_2 concentration on the rate of oxidation

At low concentration of O_2 in the reaction mixture (0.75 % vol.), which corresponds to a ratio of O_2:Me = 0.75:5.5, the angle coefficient is constant throughout the process and corresponds with the value of the rate constant equal with $k=1.466 \cdot 10^{-5}$ mol/g·s·torr. As the concentration of O_2 in the reaction mixture is growing, the rate and the rate constant of the process is increasing reaching at 1.5 % vol. O_2 a value of $1.415 \cdot 10^{-4}$ mol/g·s·torr. When the concentration of O_2 in the reaction mixture is 2.75 % vol. O_2 that corresponds to the stoichiometric ratio, it is seen that the points doesn't settle on one line. The

rate constants for the two plots have the following values $3.28 \cdot 10^{-5}$ mol/g·s·torr, respectively $1.122 \cdot 10^{-3}$ mol/g·s·torr, which show that there is a change in the macrokinetic mechanism of the process. At concentrations of O_2 over the stoichiometric ratio the rate constants have higher values $4.80 \cdot 10^{-4}$ mol/g·s·torr, respectively $4.206 \cdot 10^{-3}$ mol/g·s·torr, indicating that also here we have a change in the macrokinetic mechanism, even if the excess of O_2 is much higher than the stoichiometric ratio O_2:Me = 20:5.5.

The Data in fig. 5 shows the influence of the FA concentration on the conversion. It is established that with the growth of the concentration of FA, the final conversion of Me decreases from 76 % (when the concentration of FA is 0 %) to 65 % (when the reaction mixture contains 6.3 % FA).

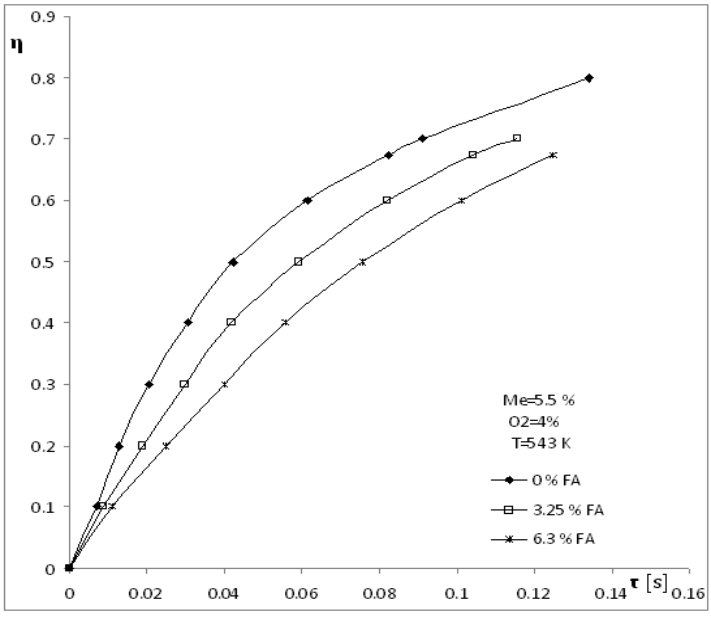

Fig.5. The conversion of methanol - contact time at different concentrations of FA

With increasing the content of FA in the reaction mixture, the reaction rate of the process is decreasing (fig. 6). At higher concentrations than 6.3 % vol. FA there is a change in the macrokinetic mechanism. The decrease of the oxidation rate with the growth of the FA content can be explained as follows: at high concentration of FA in the gaseous phase the driving force of the desorption process decreases and through this the normal movement of O_2 to the catalyst surface and the recovery of the $Fe_2(MoO_4)_3$ spinel is impeded, knowing that the oxidation is performed with O_2 from the spinel.

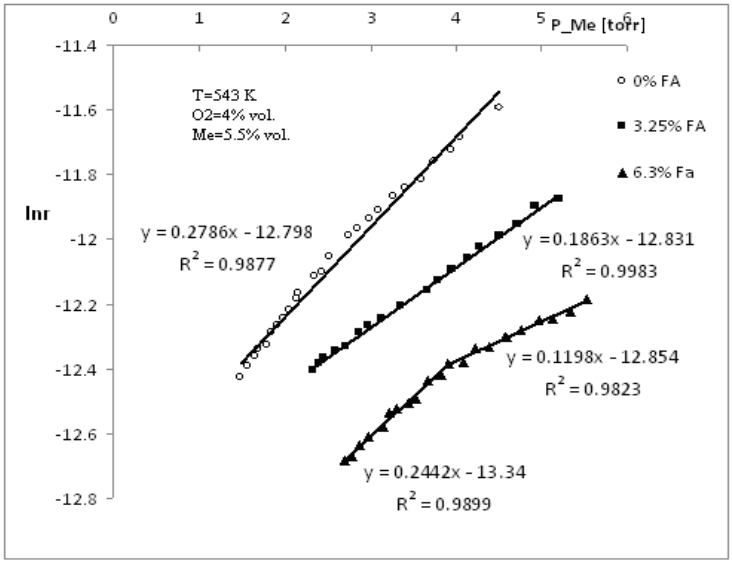

Fig.6. The effect of FA concentration on the rate of oxidation

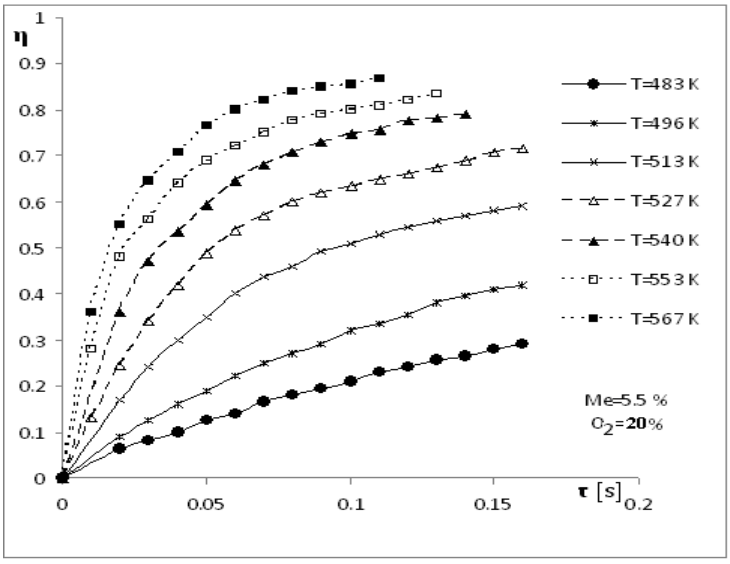

Fig.7. The conversion of methanol - contact time at different temperatures

As the temperature strongly influences the reaction rate, measurements were conducted, through which the influence of this parameter on the final conversion in the temperature range 475-567 K is revealed, which meets the working conditions of the current industrial reactors. The results are presented in fig. 7 and 8.

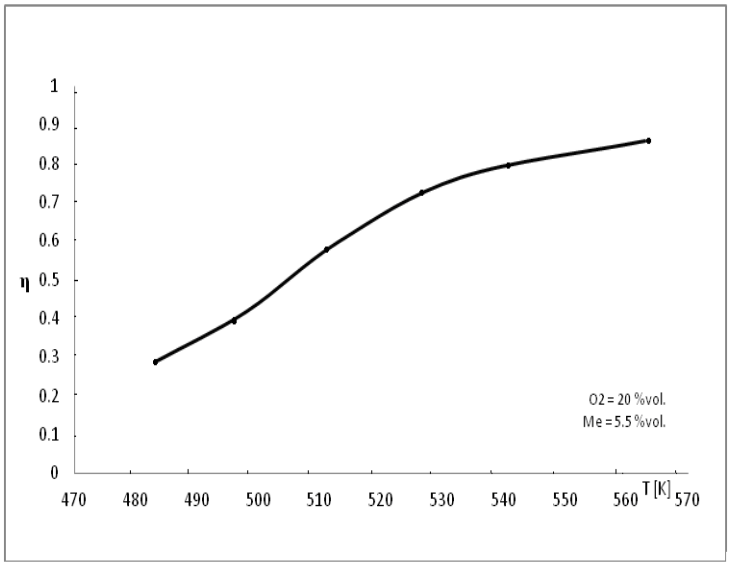

Fig. 8. The final conversion of Me at different temperatures

In fig. 7 it is seen that at temperatures under 513 K the conversion changes linearly with the contact time, reaching a value of 30 % at 475 K and increases until 55 % at 513 K. At temperatures above 513 K the conversion increases grows faster with the contact time to the value of 86 % at 567 K.

In fig. 8 we can see the change of the final conversion with the temperature at the same contact time. There is a linear increase of the conversion in the temperature range 475-500 K. After that the conversion increases faster, reaching a value of more than 75 % at 530 °K. Above this temperature, while maintaining approximately the same contact time as in the temperature range of 500-530 K, the final conversion continues to grow linearly to 85 % but with a significantly slight slope.

Table 1. The values of the rate constant

$k \cdot 10^7$ [mol/g·s·torr]	3.1	4.50	7.14	8.74	9.16	9.56	10.2
ln k	-14.989	-14.614	-14.152	-13.95	-13.903	-13.86	-13.796
T [K]	483	496	513	527	540	553	567

The graphical representation in $\ln r - T^{-1}$ coordinates of the data from table 1. is presented in fig. 9.

The diagram from fig. 9 shows a change in the slope around 515 K which leads to the conclusion that there is a change of the macrokinetic mechanism after which the oxidation process is carried out. From the slopes of the lines the activation energy was calculated. In the temperature range 475-515 K the

value of the activation energy is 57.23 kJ/mol specific for the case when limitative are the mass transformation processes (chemical reaction, adsorption – desorption). In the temperature range 530 -567 K the activation energy has a small value, 9.39 kJ/mol, what suggests that limitative in this part of the process are the external or internal diffusion phenomena. It may also be noticed a narrow temperature region 530-540 K in which the value of the activation energy is in the range of 25-42 kJ/mol corresponding to a combined macrokinetic model: mass transfer – transformation.

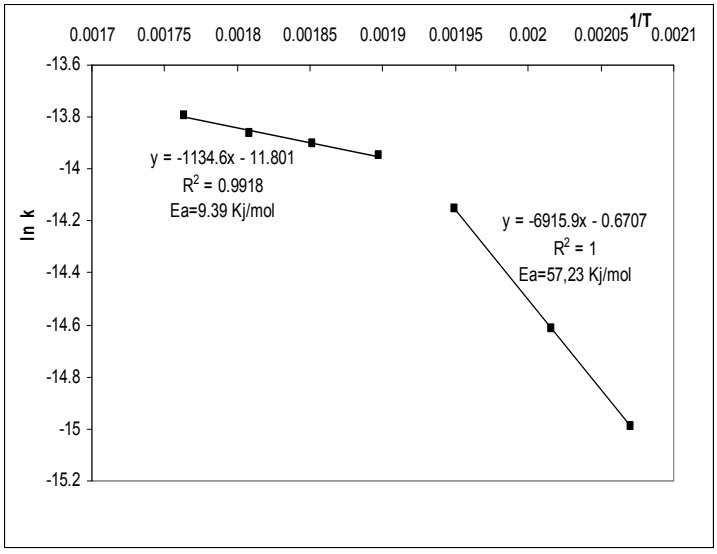

Fig. 9. $\ln\ \mathrm{k} - T^{-1}$ diagram

CONCLUSIONS

1. It was pointed out how the main parameters influence the conversion and the reaction rate.
2. It is noted that at a ratio of O_2:Me above the stoichiometric value neither the conversion nor the rate does depend on the concentration of O_2 in the reaction mixture.
3. The formaldehyde in the reaction mixture reduces significantly both rate and especially the conversion of Me.
4. The rate constants at different temperatures and from the $\ln k - T^{-1}$ diagram the activation energies were calculated.
5. It was pointed out that the process highly depends on the temperature being limited by the mass transformation phenomena under 518 K and by the external or internal diffusion phenomena above 523 K, which is indicated by the low values of the activation energy.

EXPERIMENTAL SECTION

The measurements were done on an industrial catalyst with the size of 5X5X2 mm and with the specific surface of 5.5 m^2/g determined by the BET method with nitrogen. The chemical composition of the catalyst corresponds to a ratio of Mo:Fe = 2.6 , the hole ratio and the density of the particle is ε = 0.5, respectively $\rho_{particol}$ = 1100 kg/m^3. The reagents were of analytical purity: methanol of 94 % and formaldehyde solution of 38 % supplied by the company "Nordic". The used oxidizing agent was molecular oxygen from the air. For the achievement of necessary concentrations ratios, respectively, of the Me:O2 ratio was used N2 and O2 from cylinders. The effect of the temperature and of the reaction mixture (O_2, Me, FA) on the oxidation rate was examined in a reactor with recycle, with a diameter of 21 mm, made out of stainless steel put into an oven with automatic temperature adjustment. The formation of the reaction mixture Me–O_2, Me–O_2–FA was made by gurgling air through the saturator with Me respectively in two saturators: one for Me and another for FA. The heating of the mixture to the operating temperature was made in an oven with automatic adjustment. For a uniform distribution of the reaction mixture on the entire cross section of the reactor, the catalyst was covered with a 5 cm thick layer of inert material. The flow rate of the air, N_2 respectively O_2 was measured with a rotameter. The chemical composition of the output was determined using gas chromatography.

REFERENCES

1. Reuss G., Disteldorf W., Grundler O., Hilt A. (**1988**) In: *Ullmann's encyclopedia of industrial chemistry*, 5th edn, vol. A11,VCH Publishers, Weinheim, chapter 6, 651.
2. Chrichton B. (**2006**) In: Informally speaking (*newsletter from Perstorp Formox*), spring/summer 2006, 2-8. http://www.perstorpformox.com
3. S.A.R.K. Deshmukh, M.van Sint Annaland, J.A.M. Kuipers, *Appl. Catal. A*., **2005**, *289*, 240.
4. Qian M., Liauw M.A., Emig G., *Appl. Catal. A.,* **2003**, *238*, 211.
5. Părăuşanu V., Corobea M., Muscă G., *Economia hidrocarburilor*, Ed. Ştiinţifică şi Enciclopedică, Bucureşti, **1980**, chapter 4.
6. Părăuşanu V., *Procese tehnologice în industria chimică*, Ed. Did. şi Ped., Buc., **1978**, chapter 3.
7. McCormick R.L., Al-Sahali M.B., Alptekin G.O., *Applyed Catalysis A.,* **2002**, *226*, 129.
8. Adkins H., Peterson W.R., *Journal of American Chemical Society*, **1931**, *53*, 1512.
9. Soares A.P.V, Portela M.F, Kiennemann A., *Catalalysis Reviews*, **2004,** *47*,125.
10. Wade L.E., Gengelbach R.B., Trumbley J.L., Hallbauer W.L., *Encyclopedia of Chemical Technology* (Eds: H. Mark, D.F. Othmer, C.G. Overberger, G.T. Seaborg), John Wiley & Sons, New York, **1981**, chapter 5.
11. Andersson A., Hernelind M., Augustsson O., *Catalysis Today*, **2006**, *112*, 40.

12. Soederhjelm E., House M.P., Cruise N., Holmberg J., Bowker M., Bovin J.O., Andersson A., *Top Catalysis*, Springer Science, **2008**, *11*, 244.
13. Santacesaria E., Morbidelli M., Carra S., *Chememical Engineering Science,* **1981**, *36* (5), 909.
14. Alessandrini G., Cairati L., Foryatti P., Villa P.L., Trifiro F., *J. Less - Comm Met.,* **1977**, *54*, 373.
15. Ulukardesler A.H., Atalay S., Atalay F.S., *Chemical Engineering Technology*, **2010**, *33* (1), 167.
16. Dente M., Collina A., *Chemical Ind.*, **1964**, *46*, 752.
17. Bowker M., House M., Alshehri A., Brookes C., Gibson E.K., Wells P.P., *Catalysis Structure & Reactivity*, **2015**, *1* (2), 95.
18. Khorshidi J., Kalbasi M., *The 12th Int. Conf. On Fluidization – New Horizons in Fluidization Engineering*, **2007**, 615.
19. Bowker M., Holroyd R., Elliott A., Morrall P., Alouche A., Entwistle C., Toerncrona, A., *Catalysis Letters*, **2002**, *83* (3-4), 165.
20. Bjoerk V., Depart. Of Chem. Eng., Lund. Univ., Sweden, **2011**, 1.
21. Andersson A., Hernelind M., Augustsson O., *Catal Today*, **2006**, *40*, 112.
22. Soares A.P.V., Portela M.F., Kiennemann A., *Catal. Commun*, **2001**, *2*, 159.
23. Soares A.P.V., Portela M.F., Kiennemann A., Hilaire L., *Chem. Eng. Sci.*, **2003**, *58*, 1315.
24. Ma Z.H., Kmiotek S.J., *J. Catal*, **1988**, *109*, 132.
25. Trifiro F., Carbucicchio M., Villa P.L., *Hyperfine Interact*, **1998**, 111.
26. Sun-Kou M.R., Mendioroz S., Fierro J.L.G., Palacios J.M., Guerro-Ruiz A., *J. Mater. Science*, **1995**, *30*, 496.
27. Boreskov G.K., Kolovertnov G.D., Kefeli L.M., Plyasova L.M., Karakchiev L.G., Mastikhin V.N., Popov V.I., Dzisko V.A., Tarasova D.V., *Kinet Katal*, **1966**, *7*, 144.
28. Okamoto Y., Morikawa F., Oh Hiraki K., Imanaka T., Teranishi S., *J. Chem Soc Chem. Comm.*, **1981**, 1018.
29. Bowker M., Holroyd R., Elliott A., Morrall P., Alouche A., Entwistle C., Toernerona A., *Catal. Lett*, **2002**, *83*, 165.
30. Fagherazzi G., Pernicone N., *J Catal*, **1970**, *16*, 321.
31. Massarotti V., Flor G., Marini A., *J. Appl. Cryst*, **1981**, *14*, 64.
32. Popov B.I., Bibin V.N., Boreskov G.K., *Kinet. Katal*, **1976**, *17*, 371.
33. Buriesci N., Garbassi F., Petrera M., Petrini G., Pernicone N., *Stud. Surf. Sci. Catal.*, Elsevier, Amsterdam, **1980**, *6*, 115.
34. Aruanno J., Wanke S., *Can. J. Chem. Eng.*, **1975**, *53*, 301.
35. Aruanno J., Wanke S., *Can. J. Chem. Eng.*, **1977**, *55*, 93.
36. Dente M., Poppi R., Pasquon J., *Chim. Ind., Milan*, **1964**, *46*, 1326.
37. Wichterlova B., Jiru P., *Chem. Prumysl*, **1965**, *4*, 198.
38. Soares A.P.V., Farinha Portela M., Kiennemann A., *Catal. Rev.*, **2005**, *47* (1), 125.
39. Levenspiel O., *Tehnica Reactiilor în Industria Chimică*, Ed. Tehnica Bucureşti, **1967**, chapter.4.
40. Calistru C., Leonte C. *Tehnologia substantelor anorganice*, Ed. Did. si Ped., Buc., **1972**, chapter 2.
41. Satterfield C.N., Sherwood T.K., *The Role of Diffusion in Catalysis*, Addison-Wesley, Reading, MA, **1963**, chapter 3**.**
42. G.F. Froment, K.B. Bishoff, *Chemical Reactor Analysis and Design*, Wiley, New York, **1990**, chapter 6.

STUDIA UBB CHEMIA, LXI, 2, 2016 (p. 167-175)
(RECOMMENDED CITATION)

DETECTION OF OCHRATOXIN A IN INSTANT COFFEE BY UPLC-MS/MS

MANUELA MINCEA[b], COSMIN IONASCU[b], KATALIN KIS[a,b], VASILE OSTAFE[a,b*]

ABSTRACT. A rapid, accurate and economic procedure has been applied to extract and analyze trace level of ochratoxin A (OTA) in instant coffee. The OTA was extracted and cleaned-up by methanol extraction followed by retention on IRA-400 anion exchanger and quantified by Ultra Performance Liquid Chromatography (UPLC) with MS/MS detection. Under optimum conditions, the detection limit (S/N = 3) was 0.05 ng/g and recoveries of OTA at spiking levels of 5, 10, and 20 ng/mL, were 82.67 ± 8.05%, 96.87 ± 4.63%, and 98.25 ± 4.46% respectively.

Keywords: *ochratoxin A; mycotoxin; instant coffee; contamination; UPLC-MS.*

INTRODUCTION

Ochratoxin A (OTA) is one of the most dangerous secondary metabolite from out of more than 300 mycotoxins that have been isolated and described. OTA is a substituted isocumarin derivative of phenylalanine and is produced in temperate climates especially by species of *Penicillium* and in tropical and subtropical regions mostly be *Aspergillus* species [1,2]. This mycotoxin contaminate a large variety of food and feed products being a major concern for the international trade. Studies made in different countries from all over the world have pointed out the presence of OTA in numerous products with vegetal origin: peanuts, cereals, coffee, beer, wine and fruit juice [3-10]. OTA was reported to be present in dangerous levels in animal products like milk [11], pork and poultry meat [12-13].

The international legal bodies have established very low limits of permitted levels of OTA in products designated to human consumption due to the fact that a lot of studies have shown OTA to be a teratogenic, carcinogen and a foetotoxic

[a] *Advanced Environmental Research Laboratories, Multidisciplinary Research Platform "Nicholas Georgescu - Roegen", 4 Street Oituz, Timisoara 300086, Romania*
[b] *Department of Biology – Chemistry, Faculty of Chemistry, Biology, Geography, West University of Timisoara, 16 Street Pestalozzi, Timisoara 300115, Romania*
[*] *Corresponding author: vasile.ostafe@e-uvt.ro*

agent [14-15]. Also, OTA was advocated to be nephrotoxic, being associated with Balkan endemic nephropaty [14-16]. The International Agency of Research on Cancer (IARC) classified OTA as a possible carcinogen for humans - 2B group [17], based on sufficient evidence in animals and for kidney carcinogenicity of OTA but inadequate evidence in humans. The presence of OTA was signaled in human milk [18] and in human blood [19].

Many countries have established maximum levels for OTA in cereals and other products but only a few have rules for coffee and coffee derived products despite the extensive studies regarding the presence of OTA in green, roasted and instant coffee [6, 20-25].

The European Union has established the highest permitted level of OTA in roasted coffee beans at 5 ng/g and in instant coffee at 10 ng/g [26]. The European Commission had established a Tolerable Weekly Intake (TWI) for OTA at 120 ng/kg b.w./week [27].

RESULTS AND DISCUSSION

Sample extraction and purification

The first step in optimization was to select an appropriate extraction solvent. The suitability of methanol, chloroform, acetone, cold and hot water was tested. The results (see Figure 1) showed that the highest extraction efficiency was obtained with methanol.

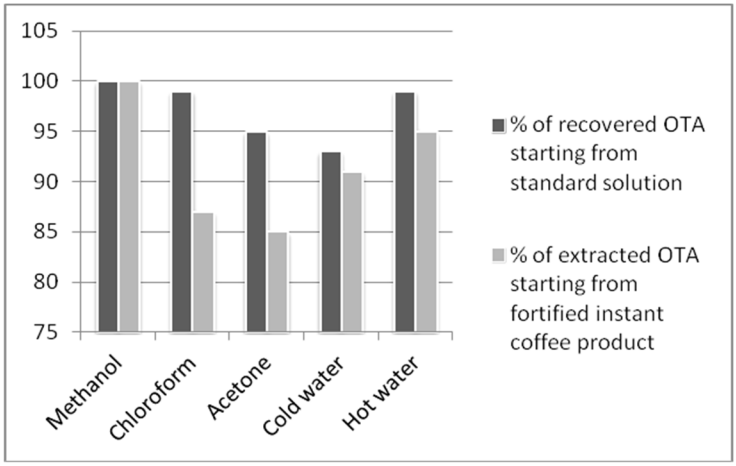

Figure 1. The influence upon the yield of extraction of OTA following the same extraction protocol except for the nature of the extraction solvent (the recovery values for each solvent are normalized, considering the best yield 100%).

The influence of the matrix upon the yield of the extraction of OTA is also presented in Figure 1. There were compared the results obtained when a solution of 20 ng/mL OTA prepared in the extraction solvent was subjected to the extraction procedure with those obtained when 2.5 g of instant coffee product free of OTA was subjected to the extraction procedure starting with 20 mL extraction solvent containing 20 ng/mL OTA.

Qualitative analysis

The analytical characteristics of the UPLC-MS/MS method including the calibration curve, repeatability, limits of detection and quantitation were investigated under the optimized conditions.

Calibration curve was prepared for the target analyte after the extraction of a standard series of spiked fresh instant coffee samples with the regression equation being y = 402.773x + 975.965 and the determination coefficient of 0.999. The precision of the proposed method was calculated by 3 replicated extractions and analysis using 3 levels of fortification of spiked sample (5, 10 and 20 ng OTA/g coffee), and the relative standard deviations (RDSs) of OTA were between 4 and 8 % (see Table 1). The limits of detection (LOD, S/N = 3) and quantitation (LOQ, S/N = 10) for the processed spiked fresh instant coffee were 0.05 and 0.2 ng/g, respectively.

Validity of the method

To assess the applicability of the proposed method, commercial instant coffee samples were obtained and analysed; the extraction procedure followed by separation with UPLC-electrospray tandem MS being applied.

Table 1. Recovery of OTA from spiked instant coffee samples.

Concentration Added (ng/g)	Concentration Detected (ng/g)	Mean (ng/g)	Recovery (%)	Relative Standard Deviation (%)
5.00	4.51	4.17	82.67	8.05
	4.12			
	3.88			
10.00	10.8	9.69	96.87	4.63
	9.21			
	9.75			
20.00	19.01	19.65	98.25	4.46
	20.65			
	19.29			

Confirmation

The results showed that the presence of OTA was confirmed in over 90% of the analyzed samples of instant coffee, always being below the European legal limit. The identity of OTA in samples was confirmed by the fragmentation patterns obtained in MS2 spectra of the key ion at *m/z* 239 Da. These patterns were similar to those found in the MS2 spectra of the standard of OTA (see Figure 2).

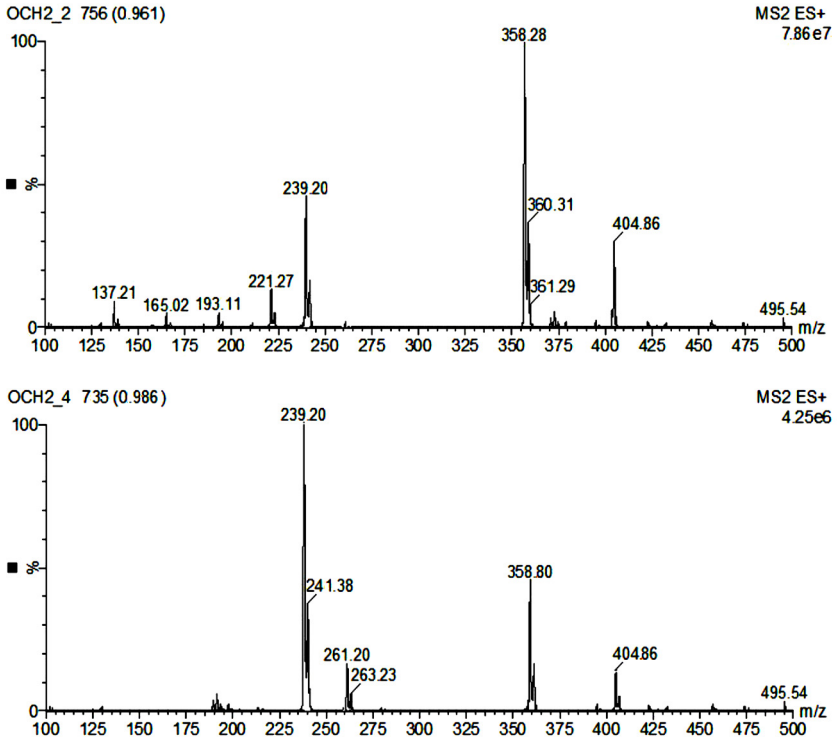

Figure 2. The MS2 spectra of an OTA standard solution obtained at 15V collision energy (upper panel) and used for quantification (404.8> 358.7 m/z) and at 23 V (lower panel) used for confirmation (404.8> 239.6 m/z) of the presence of the analyte in the sample

In Figure 3 there are presented the two chromatograms of the same instant coffee product, subjected to the sample preparation procedure, but the sample corresponding to the chromatogram B was fortified with 10 ng OTA/g instant coffee product before the sample preparation. For comparison, in the lower panel there is presented the chromatogram of a standard solution of OTA (100 ng/mL).

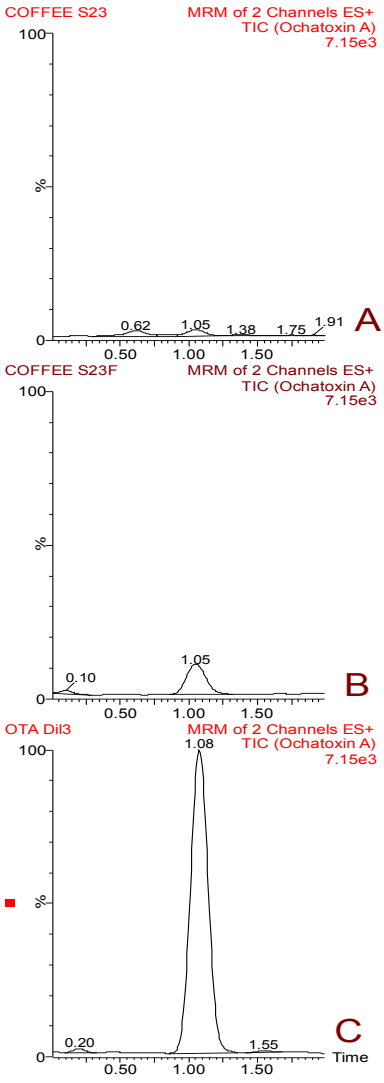

Figure 3. UPLC chromatograms (A) instant coffee sample naturally contaminated with 2.5 ng OTA/g product, injection 10 µL, (B) the same instant coffee sample, fortified with 10 ng OTA/g product before starting the sample preparation procedure, injection 10 µL, (C) a standard solution containing 100 ng/mL of OTA

CONCLUSIONS

This study reports the successful analysis of OTA in instant coffee samples based on UPLC-MS/MS technique. The presented method offers suitable features of merit such as low detection limit (0.05 ng OTA/g product), good recovery (over 82%), and relative standard deviation lower than 8%, together with other advantages such as rapidity (less than 15 min), low cost of analysis and minimal use of organic solvents.

EXPERIMENTAL SECTION

Sample collection

Instant coffee products were processed in 24 h after purchase. Quantities of 10 g of samples were grounded, mixed and sub-sampled prior to analysis.

Reagents

The OTA standard was purchased from Sigma (Redox Lab Supplies Com S.R.L. Bucharest, Romania). A stock solution of 0.5 mg/mL OTA was prepared in methanol and stored at -20 ºC and protected from light. Methanol, formic acid and Amberlite® IRA-400 chloride form were also purchased from Sigma-Aldrich.

Working solutions (in the range 0.2 – 200 ng/mL) for the recovery tests and calibration curve were prepared by appropriate dilution of the OTA stock solution in 0.1% formic acid in 30% methanol.

Sample preparation

In 20 mL methanol was added 2.5 g instant coffee product and vortexed for 3 min at 2.500 rpm. For OTA extraction other solvents, like chloroform, acetone, cold and hot (boiling) water were also tested. The samples were centrifuged for 5 min at 5.500 rpm (Rotofix 32A, Hettich). From the supernatant were collected 16 mL (equivalent to 2 g of initial coffee product) and mixed with an equal quantity of 1 mM $NaHCO_3$. This solution was percolated on a small column filled with 0.5 mL Amberlite IRA-400 (previously washed with 5 mL methanol and further with 10 mL of 1 mM $NaHCO_3$). The column was washed with 5 mL of 1 mM $NaHCO_3$. The analyte was eluted with 0.5 mL methanol (containing 0.1% HCOOH), followed by 0.5 mL of 0.1% HCOOH. From the eluate, 10 µL were injected in UPLC system after filtration on 0.2 µm membrane filter.

UPLC analysis

The chromatographic analysis was carried out on a Waters Acquity UPLC-MS system (Binary Solvent Manager, Xevo TQD MS-detector equipped with an electrospray ionization interface) with a UPLC BEH C18, 1.7 µm (2.1×100 mm) column, using a gradient elution procedure. Mobile phase A consisted in 0.02% formic acid in 5% methanol and mobile phase B

was 0.02% formic acid in methanol. The gradient profile was: 0 – 0.2 min, 30% A and 70% B; 0.2 – 1 min, linearly increase until 100% B; 1 – 1.5 min, hold 100% B; 1.5 – 1.6 min, linearly decrease until 70% B (initial condition). The column temperature was set at 30°C. The analyses were run at a flow rate of 0.3 mL/min, and the sample volume injected was 10 µL.

Calibration

To prepare the calibration curve, appropriate volumes of OTA stock solutions were diluted with 0.1% formic acid in 30% methanol to prepare a series of working solutions containing 0.02–500 ng/mL. A calibration curve was constructed by plotting the peak area for each standard against the mass of OTA injected. Slope and intercept data of the calibration curve were used to compute the quantity of the analyte in coffee extracts.

For quantitative determination of OTA peak areas of the sample, chromatograms were correlated with the concentrations according the calibration curve. Standard solutions and sample volumes of 10 µL were injected in triplicate. The linearity was determined in the range of 0.2-200 ng/mL of OTA using 7 calibrators. The retention time was 1.08 min. An OTA standard solution at 10 ng/mL was daily injected at the beginning of the analysis.

Validation

The coffee samples, spiked with various concentrations of standard solutions, were analyzed. Limits of detection were based on a signal to noise (S/N) ratio with 3:1 as the minimum. Recovery tests were performed in triplicate by spiking standards at 3 different levels into OTA-free samples: 5, 10, and 20 ng/mL in coffee. The spiked samples and blank samples without standard were analyzed by UPLC.

Confirmation and quantification

The ESI parameters for Xevo TQD MS detector were fixed as follows: capillary voltage at 3 kV, source temperature at 150°C, desolvation temperature at 300°C, and desolvation gas at 500 L/h. Nitrogen was used as the desolvation gas, and argon was employed as the collision gas. The detailed MS/MS detection parameters for the analyte are presented in Figure 4 and Table 2 and were optimized by direct injection of a 1 µg/mL OTA standard solution into the detector at a flow rate of 10 µL/min.

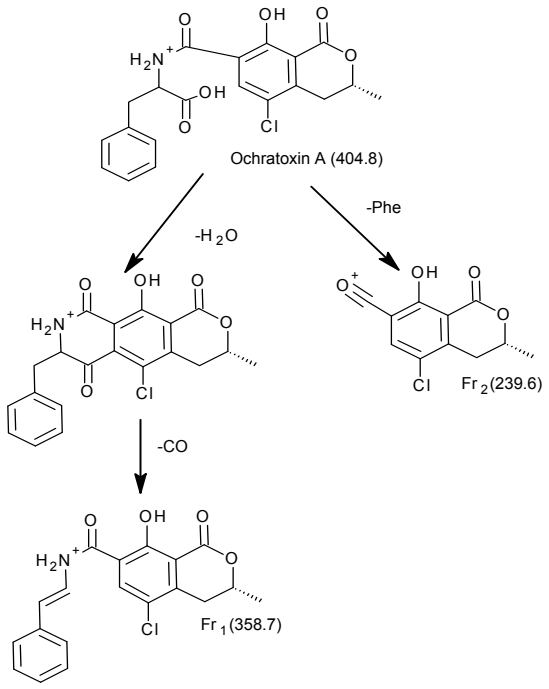

Figure 4.
Fragmentation pattern of ochratoxin A, obtained at cone voltage 30 V and collision energy 15 V, for daughter fragment with m/z 358 and 23 V for the fragment with m/z 239

Table 2. Mass spectrometer parameters for OTA detection.

Transition monitored	Precursor ion (*m/z*)	Fragment ion (*m/z*)	Cone voltage (V)	Collision voltage (V)
Quantification	404.8	358.7	30	15
Confirmation	404.8	239.6	30	23

Analyses were carried out in multiple reactions monitoring mode (MRM), using two specific transitions for the analyte and the detector was fixed at maximum Extended Dynamic Range with peak mass widths of 2 and 1.5 Da for the first and third quadrupole, respectively. The dwell time for all transitions was 0.01 seconds.

REFERENCES

1. J. I. Pitt, *Medical Mycology*, **2000**, *38(1)*, 17.
2. J. I. Pitt, J. C. Basilico, M. L. Abarca, C. Lopez, *Medical Mycology*, **2000**, *38(1)*, 41.
3. P. M. Scott, S. R. Kanhere, *Food Additives and Contaminants*, **1995**, *12*, 591.
4. K. Jorgensen, G. Rasmussen, I. Thorup, *Food Additives and Contaminants*, **1996**, *13*, 95.

5. B. Zimmerli, R. Dick, *Food Additives and Contaminants*, **1996**, *13*, 655.
6. S. Patel, C. M. Hazel, A. G. Winterton, A. E. Gleadle, *Food Additives and Contaminants*, **1997**, *14*, 217.
7. N. Karagözlü, M. Karapinar, *Turkish Journal of Biology*, **2000**, *24*, 561.
8. S. C. Duarte, A. Pena, C. M. Lino, *Food Microbiology,* **2010**, *27*, 187.
9. M. Maham, V. Kiarostami, S. Waqif-Husain, R. Karami-Osboo, M. Mirabolfathy, *Czech Journal of Food Science*, **2013**, *31(5)*, 520.
10. C. Ionascu, V. Ostafe, *Studia Universitatis Babeş-Bolyai Chemia*, **2014**, *59*, 17.
11. A. Breitholtz-Emanuelsson, M. Olsen, A. Oskarsson, I. Palminger, K. Hult, *Journal of AOAC International*, **1993**, *76*, 842.
12. K. Jorgensen, *Food Additives and Contaminants*, **1998**, *15*, 550.
13. L. M. Sorensen, J. Mogensen, K. F. Nielsen, *Analytical and Bioanalytical Chemistry*, **2010**, *398*, 1535.
14. E. O'Brien, D. R. Dietrich, *CRC Critical Reviews in Toxicology*, **2005**, *35*, 33.
15. T. Vrabcheva, T. Petkova-Bocharova, F. Grosso, I. Nikolov, I. N. Chernozemsky, M. Castegnaro, S. Dragacci, *Journal of Agricultural and Food Chemistry*, **2004**, *52*, 2404.
16. A. P. Grollman, B. Jelakovic, *Journal of the American Society of Nephrology*, **2007**, *18*, 2817.
17. IARC (International Agency for Research on Cancer) “Evaluation of carcinogenic risks to humans: some naturally occurring substances, food items and constituents, heterocyclic aromatic amines and mycotoxins”, Geneva, **1993**, Monograph 56**,** 489-521.
18. G. Biasucci, G. Calabrese, R. Di Giuseppe, G. Carrara, F. Colombo, B. Mandelli, M. Maj, T. Bertuzzi, A. Pietri, F. Rossi, *European Journal of Nutrition*, **2011**, *50*, 211.
19. M. B. Coronel, V. Sanchis, A. J. Ramos, S. Marin, *Food and Chemical Toxicology*, **2011**, *49*, 2697.
20. G. v.d. Stegen, U. Jorissen, A. Pittet, M. Saccon, W. Steiner, M. Vincenzi, M. Winkler, J. Zapp, C. Schlatter, *Food Additives and Contaminants*, **1997**, *14*, 211.
21. L. A. Leoni, L. M. Soares, P. L. Oliveira, *Food Additives and Contaminants*, **2000**, *17*, 867.
22. G. A. Lombaert, P. Pellaers, M. Chettiar, D. Lavalee, P. M. Scott, B. P. Lau, *Food Additives and Contaminants*, **2002**, *19*, 869.
23. L.-C. Lin, P.-C. Chen, Y.-M. Fu, D.Y.-C. Shih, *Journal of Food and Drug Analysis*, **2005**,*13(1)*, 84.
24. L. R. Batista, S. M. Chalfoun, G. Prado, R. F. Schwan, A. E. Wheals, *International Journal of Food Microbiology*, **2003**, *85*, 293.
25. M. B. Coronel, S. Marin, G. Cano-Sancho, A. J. Ramos, V. Sanchis, *Food Additives and Contaminants*, **2012**, *29*, 979.
26. EU (European Commission Regulation) “No 105/2010 of 5 February 2010 amending Regulation (EC) No 1881/2006 setting maximum levels for certain contaminants in foodstuffs as regards ochratoxin A”, *Official Journal of the European Union,* **2010**, *L35*.
27. EFSA, *European Food Safety Authority Journal*, **2006**, *365*, 1.

STUDIA UBB CHEMIA, LXI, 2, 2016 (p. 177-193)
(RECOMMENDED CITATION)

HPLC MONITORING OF CURCUMIN IN PREVENTIVE AND THERAPEUTIC TREATMENT OF RATS TO DIMINISH ACUTE INFLAMMATION AND OXIDATIVE STRESS

CONEAC ANDREI[a], ORĂSAN MEDA SANDRA[b*], CRIŞAN MARIA[a], MARE CODRUŢA[c], DECEA NICOLETA[d], MIHU CARMEN MIHAELA[a], MUREŞAN ADRIANA[d], LAZAR LEORDEAN VIORICA[e], FILIP MIUŢA[f]

ASTRACT. Curcumin [1,7-bis(4-hydroxy-3-methoxyphenyl)-1,6- heptadiene - 3,5-dione] is a phenolic substance derived from the root of the *Curcuma longa* L plant. It is used as antiproliferative, anti-invasive and antiangiogenic agent with anti-inflammatory functions, cancer chemopreventive activity and antioxidant properties.

The aim of the study was to assess curcumin in rat plasma by HPLC with 425 nm UV detection at specified time intervals (15, 30, 60, 90, 120, 150, 180 minutes) in a treatment plan containing Curcumin in order to diminish acute muscular inflammation and oxidative stress.

The concentration of curcumin in rat plasma was evaluated comparatively in a preventive plan (curcumin administration first, then induced inflammation) versus a therapeutic plan (induced inflammation followed by curcumin administration) on 6 adult female Wistar-Bratislava albino rats assigned to three groups.

The HPLC results showed a decrease of curcumin concentration, with time, in all study groups. The statistical analysis (MANOVA) of the obtained data certified that the treatment plan applied to each group influenced the evolution of curcumin concentration in a significant way. A decrease in the amount of curcumin was noticed when inflammation occurred in the body, most probably determined by the accelerated metabolism in the presence of inflammation.

[a] *Iuliu Hatieganu University, Faculty of General Medicine, Histology Department, 8 Victor Babeş str., RO-400012, Cluj-Napoca, Romania*
[b] *Iuliu Hatieganu University, Faculty of General Medicine, Physiopathology Department, 8 Victor Babes str., RO-400012, Cluj-Napoca, Romania,*
[*] *Corresponding author: meda2002m@yahoo.com*
[c] *Babes-Bolyai University, Faculty of Economics and Business Administration, Department of Statistics – Forecasts - Mathematics, 58-60 Teodor Mihali str., RO-400591, Cluj-Napoca, Romania*
[d] *Iuliu Hatieganu University, Faculty of General Medicine, Physiology Department, 8 Victor Babes str., RO-400012, Cluj-Napoca, Romania*
[e] *Vasile Goldis Western of University Faculty of General Medicine,* 86, Liviu Rebreanu, 310045, Arad, *Romania*
[f] *Babeş-Bolyai University, Raluca Ripan Institute for Research in Chemistry, 30 Fântânele str., RO-400294 Cluj-Napoca, Romania*

The study of oxidative stress levels measured by the variables MDA and PC was performed in different rat tissues: muscle, liver *and* kidneys, for each study group and the highest results were registered in the muscle.
The results obtained in both our research directions validated the anti-inflammatory and antioxidant effect of curcumin.

Keywords: *Curcumin, inflammation, HPLC, oxidative stress*

INTRODUCTION

Curcumin [1,7-bis(4-hydroxy-3-methoxyphenyl)-1,6- heptadiene-3,5-dione] is a phenolic substance derived from the root of the *Curcuma longa* L plant [1]. It is the yellow pigment in turmeric or curry powder, commonly known as a dietary Indian spice and a natural coloring agent for food [1,2]. Curcumin is one of the most highly researched phytochemicals because it has been shown to be an antiproliferative, anti-invasive and antiangiogenic agent, which exhibits numerous activities [3,4].

Over the last half century studies focused on the important anti-inflammatory function of curcumin, which is based on the downregulation of inflammatory transcription factors (NF-kB and AP-1), enzymes (COX-1 cyclooxygenase, MMPs or glutathione S-transferases) and important cytokines (tumor necrosis factor, interleukin 1 and 6), adhesion molecules, proliferation (EGFR and Akt) and cell survival proteins and pathways (ß-catenin and adhesion molecules) [2-4]. Curcumin inhibits the activity of various kinases, downregulates cell cycle arrest (cyclin D1, E and MDM2) and, on the other hand, it upregulates the proteins *p21*, *p27* and *p53* [3].

Besides suppressing specific inflammatory factors, following oral and topical administration, curcumin has cancer chemopreventive activities, that also include the activation of apoptotic mechanism by the up-regulation of the caspase family proteins and by the downregulation of anti-apoptotic genes (Bcl-2 and Bcl-XL)([4-8]. It is also considered a mediator of chemoresistance and radioresistance due to the molecular response of cancer cells to curcumin at genomic level, an aspect which was explored by cDNA microarrays analysis [3,4].

Several articles underlined its antioxidant properties as Curcumin reduces the reactive oxygen species (ROS) (including superoxide anions and hydroxyl radicals) and *diminishes* oxidative damage [9-12]. As a result of its important role in different physiopathological mechanisms, the potential of Curcumin was evaluated in neoplastic, neurological, cardiovascular, pulmonary

and metabolic diseases [2]. Several studies considered Curcumin a therapeutic agent in wound healing, diabetes, Alzheimer disease, Parkinson disease, cardiovascular disease and arthritis. Some clinical trials also showed its benefits in familial adenomatous polyposis, inflammatory bowel disease, ulcerative colitis, colon cancer, pancreatic cancer, hypercholesterolemia, atherosclerosis, pancreatitis, psoriasis, chronic anterior uveitis and multiple mieloma [3-5].

Despite its promising biological effects, some studies reported low systemic bioavailability of curcumin after oral dosing [1,13]. Although investigated so far in both animal models and human subjects in phase I clinical studies, the pharmacodynamics and pharmacokinetics of Curcumin lack important information and the research in the field is still open [2,14].

Several methods have been developed to determine curcumin in biological samples, high performance liquid chromatography (HPLC) with UV detection [1,7,13,15,16], tandem mass spectrometric (MS) detection [17-20] or ultra performance liquid chromatography (UPLC) [21].

The results of similar studies encouraged us to develop our own model and to investigate curcumin therapy on an animal model: Wistar adult rats [22,23,24,25,26,27].

The aim of the study was monitoring curcumin in rat plasma by HPLC with UV detection at specified time intervals (15, 30, 60, 90, 120, 150, 180 minutes) in a treatment plan in order to diminish acute muscular inflammation and oxidative stress. We assessed comparatively the concentration of curcumin in rat plasma in a preventive (first curcumin administration and then induced inflammation) versus a therapeutic plan (induced inflamation followed by curcumin administration). It was also our purpose to evaluate oxidative stress in muscles and some internal organs (liver and kidney) by MDA (Malondialdehyde) and PC (protein carbonyl).

RESULTS AND DISCUSSION

HPLC analysis

The initial trials for curcumin determination from plasma were performed based on literature information [1,15]. We developed a simple, rapid and sensitive HPLC method to determine curcumin levels from rat plasma. According to the chemical characteristics, the maximum UV adsorption of curcumin was 425 nm and set as detection wavelength. The mobile phase was optimized for good resolution and symmetric peak shape for analysis, as well as a short run time of 6 min. Thus we designed a mobile phase consisting of a mixture of methanol – 0.1% formic acid (90-10, v/v) and a

Lichrosorb RP-C18 column (25 x 0.46 cm) at 30 ºC column temperature. The flow rate was set at 1.2 mL min^{-1}. Because of the complex nature of plasma, a pre-treatment procedure was needed to remove protein and potential interferences prior to HPLC analysis. Thus, methanol was used for the precipitation of proteins from rat plasma.

The linear regression analysis of curcumin was developed by plotting the peak area of curcumin versus the concentration of curcumin in ng mL^{-1}. The regression coefficient of calibration curve was R^2 = 0.996 within the range 100–2000 ng/mL for curcumin, extracted from rat plasma samples. The linear equation for curcumin was Y = 0.00062 X - 0.0143 (n=15 points). The limit of quantification (LOQ) of curcumin detected in rat plasma was 7 ng mL^{-1}.

A 2007 American study described the bioavailability of curcumin in rodents and humans and reported that the amount of free curcumin detected in the serum collected at 1 hour postgavage administration of curcumin in mice, fell below the limit of quantification of 5 ng mL^{-1}at HPLC determination [20].

In Figure 1 HPLC chromatograms of blank plasma, curcumin standard and Sample I are presented.

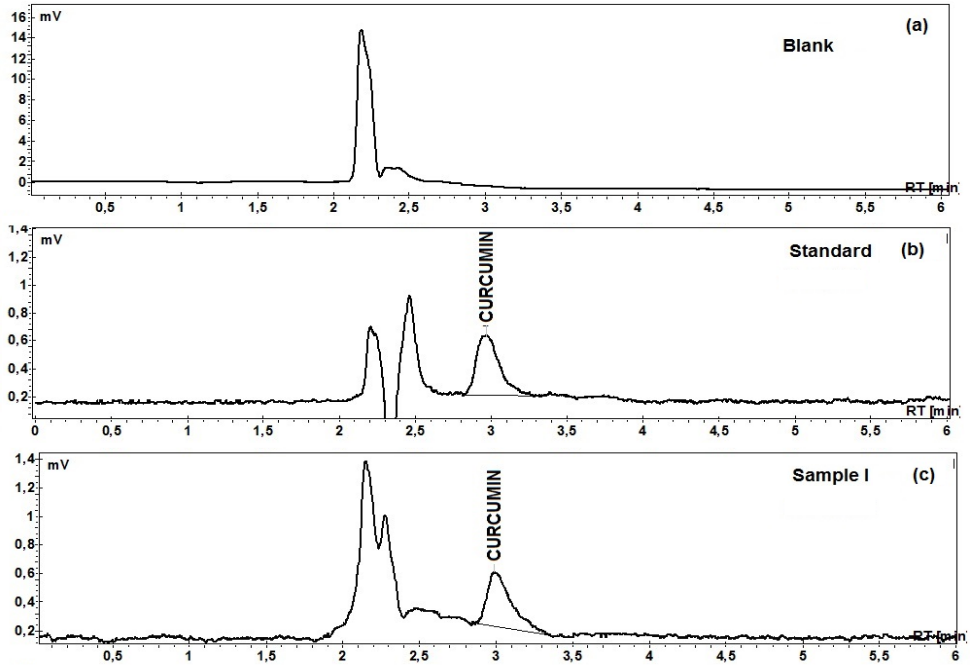

Figure 1. HPLC chromatograms **of: (a)** blank plasma. **(b)** standard curcumin at 40ng/mL in blank plasma, expressed as a peak at the retention time of 2,89 min. **(c)** Sample I (rat plasma from Group I obtained at 15 min after oral administration of curcumin suspension of 150 mg Curcumin / rat kg body weight.

The HPLC analysis was performed on plasma samples from different study groups (Groups I-III) collected at 15, 30, 60, 90, 120, 150, 180 minutes. The animals in Group I (Samples I and IB) were treated with curcumin only. Those in Group II (Samples II and IIB) received preventive curcumin followed by induced inflammation, while animals in Group III (Samples III and IIIB) received induced inflammation followed by curcumin treatment.

The HPLC results are included in Figure 2, that displays the concentration of curcumin in the study groups, collected at the specified time intervals. Three HPLC determinations were performed for each sample and the mean value was calculated individually for the mentioned time intervals.

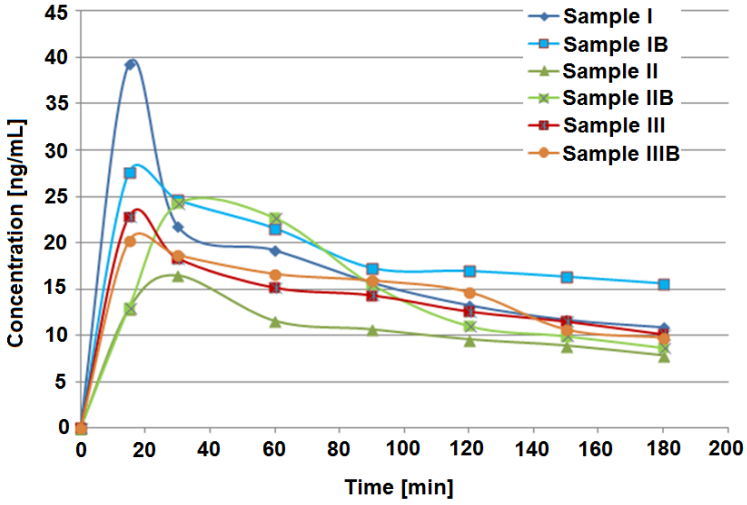

Figure 2. HPLC curcumin concentration in plasma samples for Study Groups I-III.

The results obtained showed a decrease of curcumin concentration with time, in the majority of cases, in all study groups. Exception is made by Group II which recorded, on average, higher concentration values at 30 min assessment than at 15 min. After this span time, the same decreasing tendency was recorded also by Study Group II. We noticed the sudden increase of curcumin concentration in Group II in the sample prelevated at 30 min versus 15 min, followed by a normal decrease, as the one seen in Groups I and III.

All three study groups present a maximum of curcumin quantity, present in rat plasma in the first 40 minutes of the sample assessments. We noticed that the higher quantities correspond to the Group I (treated orally with curcumin, without inflammation). By comparison to literature results, curcumin was found in maximum quantities in the first hour of assessment, which confirms our results.

Also, a study that used administration of curcumin-loaded HPC nanoparticles to rats, showed significant improvement in pharmacokinetic parameters at one hour following the sampling when (is) compared with administration of curcumin suspension [15].

For the statistical analysis of data, the significance of influences was tested and we took into consideration a single influence factor - the group the samples belonged to: Group I, II or III.

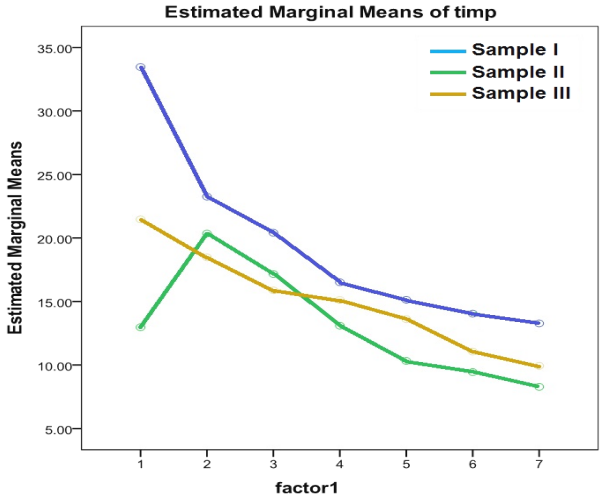

Figure 3. Mean curcumin concentration–time profiles in the three study groups. Factor 1 represents the time of sampling for the 7 samples prelevated at 15-30-60-90-120-150-180 minutes.

By taking into account that the constant factor (intercept) as well as the variable factor (the sample) have values lower than 0,05 (even 0.000), we can conclude that both factors contribute significantly to the model. The type of treatment applied influences considerably the variations illustrated by curcumin concentrations.

Table 1. Parameters of statistical analysis

Tests of Between-Subjects Effects **Measure: time.** **Transformed Variable: Average**					
	Type III Sum of Squares	**df**	**Mean Square**	**F**	**Sig.**
Intercept	31741.587	1	31741.587	2658.196	0.000
Proba	886.995	2	443.498	37.141	0.000
Error	179.115	15	11.941		

We applied the multivariate analysis of variance (MANOVA) and used all the data (all three HPLC determinations for one time frame) not only group mean scores. This analysis certified that the type of the treatment applied to each group, influenced in a significant way the evolution of curcumin HPLC concentration.

The presence of a significant influence was also supported by the 4 multivariate tests (Pillai's Trace, Wilk's Lamba, Hotelling's Trace and Roy Largest Root) included in the table below.

Table 2. Multivariate Tests performed on the HPLC results for Groups I-III.

Effect		Value	Error df	Sig.
factor1 (time)	Pillai's Trace	0.981	10.000	0.000
	Wilks' Lambda	0.019	10.000	0.000
	Hotelling's Trace	51.205	10.000	0.000
	Roy's Largest Root	51.205	10.000	0.000
factor1 * Proba	Pillai's Trace	1.413	22.000	0.001
	Wilks' Lambda	0.082	20.000	0.002
	Hotelling's Trace	5.184	18.000	0.005
	Roy's Largest Root	3.401	11.000	0.005

During the experiment both the singular effect of the passing of time and the compound effect of the passing of time and time of the testing (sampling) were considered. In both cases, all 4 tests registered values of acceptance probability of the nul hypothesis <0.05, which meant that both effects taken into consideration (time and sample) performed a positive influence on curcumin concentration.

For a more precise assessment during the experiment, the estimation of the regression parameters was performed for each separate dependent variable (in our case - each measuring) depending on the analyzed factor. From the statistical analysis point of view, the constant in the model was the mean value of the treatment group (Group III) used as comparison for each measuring.

The coefficients of the other samples showed if, on average, the value of curcumin concentration was higher or lower than that of treatment Group III. Reasonably, it must be interpreted if Sig <0.05.

At 15 min, curcumin concentration recorded in Group I was higher with 11.995 than in Group III. This difference was statistically significant. At 30 min and 60 min, the concentration in Group I was statistically significant and higher with 4.77 and 4.53, than in Group III. On the determination performed at 90 min and 120 min, curcumin concentration in Group I was

higher, with 1.39 and 1.51 than in Group III. By comparing Group I with Group III at 150 min, curcumin concentration in Group I was higher, with 2.98, the difference being statistically significant. With the last measuring with a time frame of 180 min, curcumin concentration in Group I was higher with 3.34 than in Group III, the difference being statistically significant.

In conclusion, in Group I (rat treated only with oral curcumin) the plasmatic concentration of curcumin was higher at any moment of sampling (at 15-30-60-90-120-150-180 min) as compared to Group III (rat with induced inflammation and treated with oral curcumin afterwards). Curcumin concentrations in Group III were lower, probably because of the accelerated metabolism in the presence of inflammation. These values validated the anti-inflammatory effect of the tested substance.

While assessing Group II values at15 minutes we noticed significantly lower curcumin values, with 8.497 than in Group III. Surprisingly, at 30 minutes, and 60 minutes, curcumin concentration in Group II was higher with 1.87 and 1.28 than in Group III. At 90 minutes, curcumin concentration in Group II was lower, with 2.02, than in Group III, and at 120 minutes, curcumin concentration in Group II was lower, with 3.29 than in Group III, the difference being statistically significant. At 150 min and 180 min, curcumin concentration in Group II was lower, with 1.61 and 1.65 on average, than in Group III.

By comparative analysis of Group II (rat to which curcumin was preventively administered and then inflammation was induced) with Group III, we noticed that curcumin concentration was generally lower than in the Group III (rat with induced inflammation and treated with oral curcumin afterwards). In Group II, there were two values higher than in Group III, at 30 min and 60 min respectively, after induced inflammation.These values followed then a descending line, in agreement with the anti-inflammatory effect exercised.

Carboxymethyl cellulose (CMC) is a food additive used as a viscosity thickener and an emulsifier for high concentrations of curcumin in oral administration [22, 28]. A study performed in 2010 on a mouse model proved that both oral curcumin and its CMC emulsifier have anti-inflammatory effects. It also pointed out that curcumin has both preventive and therapeutic effects in the studies with induced murin colitis models [29-32].

Recent curcumin studies described an action of blocking inflammatory pathways, effectively preventing the launch of proteins triggering swelling and pain. Therapeutic effects of curcumin are due to its reduced production of potent proinflammatory mucosal cytokines, as well as the inhibitor effect performed on: phospholipase, lipooxygenase 2, leukotrienes, tromboxane, prostaglandins, nitric oxide, collagenase, elastase, hyaluronidase, monocyte chemoattractant protein-1 (MCP-1), interferon-inducible protein, tumor necrosis factor (TNF) and interleukin 12 (Il-12) [33]. Mercola study showed that the

subjects treated with curcumin had lower levels of blood markers of inflammation such as C-reactive protein (CRP). Phase 1 human trials found no toxicity from curcumin intake and demonstrated the safety of administration [33].

Previous reports from literature on another type of inflammation (colitis) sustain our results based on an acute inflammation model (miositis in rats) underlining the important effect of curcumin in both preventive and therapeutic plans. Even research performed on human subjects concluded that short-term supplementation with bioavailable curcumin significantly improves the inflammatory and oxidative status of patients, suggesting the benefits of preventive administration [34].

Our research protocol did not intend to clarify the nature of curcumin metabolites through the HPLC analysis of plasma. We knew from previous findings that curcumin-glucuronoside, dihydrocurcumin-glucuronoside, tetrahydrocurcumin (THC) and THC-glucuronoside are the major metabolites of curcumin *in vivo* [35].

Several studies showed that orally administered curcumin is absorbed from the alimentary tract and is present in the general blood circulation after being metabolized to the form of glucuronide/sulphate conjugates. Pan study proved that 99% of these curcumin metabolites, in plama were present as glucuronide conjugates [20].

Oxidative Stress

Our study aimed to evaluate oxidative stress determination in muscles of the thigh and in organs such as liver and kidney. The samples were collected from the two rats included in the study of Groups I, II and III, as well as from a witness group: two healthy rats who were not exposed to inflammation and did not receive oral Curcumin.

Oxidative stress reflects the level of oxidative damage in a cell, tissue, or organ, caused by the *reactive oxygen species* (ROS), which can be of endogenous sources (energy generation from mitochondria or the detoxification reactions involving the *liver cytochrome P-450 enzyme system*) and exogenous sources: environmental pollutants, alcohol or cigarette exposure, to ionizing radiation, and bacterial, fungal or viral infections [36,37].

Reactive oxygen species, such as free radicals (superoxide and hydroxyl radicals) as well as peroxides (hydrogen peroxide), represent a class of molecules that are derived from oxygen metabolism [38].

Oxidative stress leads to many pathophysiological conditions in the body such as neurological syndromes, gene mutations and cancer, cardiovascular disorders and inflammatory diseases [39,40].

Curcumin has been cited as a natural phenolic compound, with important anti-inflammatory and anti-oxidant properties. It is reported to inhibit production of inflammatory cytokines by peripheral blood monocytes

and alveolar macrophages. It also decreases the inducible nitric oxide synthase (iNOS), cycloxygenase and lipoxygenase and it easily penetrates into the cytoplasm of cells, accumulating in membranous structures such as plasma membrane, endoplasmic reticulum and nuclear envelope [41].

Malondialdehyde (MDA), protein carbonyl (PC) were the oxidizing agents studied in this research. MDA, an important biomarker for oxidative stress, is the end-product of radical-initiated oxidative decomposition of polyunsaturated fatty acids. Its presence is predictive for the occurrence of cardiovascular events or metabolic diseases [42,43].

Proteins are important targets of oxidative changes, too. The changes in the constituent amino acids, caused by oxygen radicals or other activated oxygen species lead to functional or structural protein alterations [44]. The direct oxidation of lysine, arginine, proline and the reactions with MDA produced by lipid peroxidation, determine protein carbonyls to be formed [45].

The oxidation of proteins by reactive oxygen species can be emphasized by determining the PC content [46]. Reactive oxygen species and reactive carbonyl species cause DNA, protein and lipid damage. Collagen structures in the skin are important targets for carbonyl stress, too [45]. Figure 5 presents the results of oxidative stress markers, MDA and PC from blank samples 1 and 2 compared to the sample of Groups I, II, III.

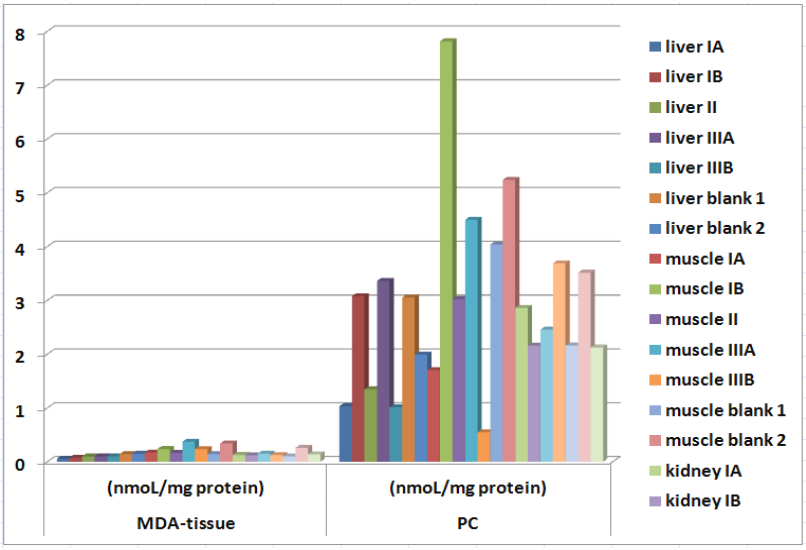

Figure 5. Results of the oxidative stress markers (MDA and PC).

For the statistical analysis of the oxidative stress results we took into consideration the small number of observations and we evaluated the normality of MDA distribution and PC. MDA was not normally distributed

(Sig.=0,007) and PC was (Sig =0,064). In both instances, we also performed parametric tests (Student-t) as well as non parametric ones.

When evaluating the 3 types of samples (Groups I to III) ANOVA analysis provided very high values of Sig., which demonstrated that the type of sample did not influence significantly oxidative stress, measured by the variables MDA and PC. Although MDA levels and PC levels assessed from the same sample (muscle, liver or kidney) seemed to be higher in one group, the difference was not statistically significant, probably due to the small number of samples.

Table 3. ANOVA analysis of oxidative stress expressed by MDA and PC.

ANOVA						
		Sum of Squares	**df**	**Mean Square**	**F**	**Sig.**
MDA	Between Groups	0.066	2	0.033	8.398	0.003
	Within Groups	0.071	18	0.004		
	Total	0.137	20			
PC	Between Groups	10.610	2	5.305	2.206	0.139
	Within Groups	43.283	18	2.405		
	Total	53.893	20			

In the case of MDA, ANOVA provided significant results, indicating that the tissue origin (from muscle, liver or kidney) had a significant influence on the level of oxidative stress. The results were also confirmed by the non-parametric Chi-Square or Kruskal Wallis Test.

Our study results pointed out that oxidative stress was the highest in the muscle.

With reference to PC assessment it can be concluded that there were no significant differences among the tissues examined.

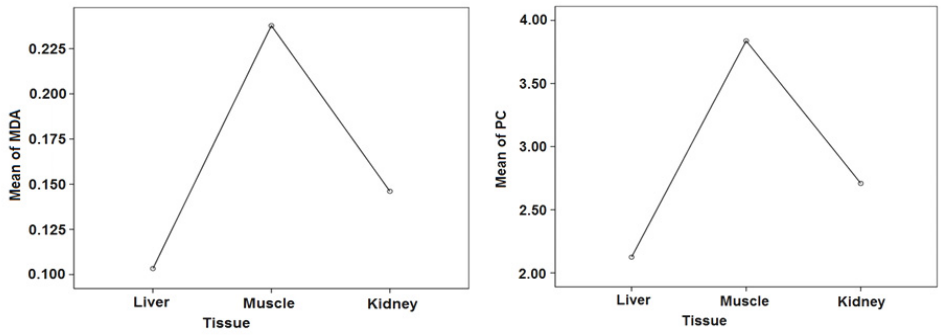

Figure 6. MDA and PC results in the three types of tissue

CONCLUSIONS

Our paper describes a specific and high-performance liquid chromatography (HPLC) method for the determination of curcumin in rat plasma. After protein precipitation performed for each sample, a throughput bioanalysis was done. The assay method was successfully applied to the study of pharmacokinetics of curcumin in the rats included in our study groups. The results obtained by HPLC suggest a decrease of curcumin concentration, with time, in the majority of cases, in all study groups.

The multivariate analysis of variance (MANOVA) certified that the type of the treatment applied to each group, influenced the evolution of curcumin HPLC concentration in a significant way.

Our results based on an acute inflammation model (miositis in rats) underline the important effect of curcumin in both preventive and therapeutic treatment plans. Curcumin concentrations in the study Group III were lower than in Group I, probably because of the accelerated metabolism in the presence of inflammation. The values thus validated the anti-inflammatory effect of the tested substance.

The type of sample from the study groups (Group I-III) did not influence significantly oxidative stress, measured by the variables MDA and PC.

Our study results pointed out that oxidative stress was the highest in the muscle. As far as PC assessment was concerned, it was concluded that there were no significant differences among tissues examined.

EXPERIMENTAL SECTION

Instrumentation

The analyses were carried out on a HPLC Jasco Chromatograph (Japan) equipped with an intelligent HPLC pump (Model PU-980), a ternary gradient unit (Model LG-980-02), an intelligent column thermostat (Model CO-2060 Plus), an intelligent UV/VIS detector (Model UV-975) and an injection valve equipped with a 20µL sample loop (Rheodyne). The samples were injected manually with a Hamilton Rheodyne Syringe (50 mL). The system was controlled and the experimental data analyzed were performed with the ChromPass software. Separation was carried out on a Lichrosorb RP-C18 column (25 x 0.46 cm) at 30 ºC column temperature. The mobile phase was a mixture of methanol and 0.1% formic acid (90:10, v/v). The flow rate was 1.2 mL min^{-1} and the UV detection was 425 nm. The mobile phase and samples were filtered through a 0.45 µm membrane.

Materials and reagents

Curcumin (1E,6E)-1,7-Bis(4-hydroxy-3-methoxyphenyl)-1,6-hepta-diene-3,5-dione, purity > 98%) was purchased from Abcam (BioZyme, Romania). Methanol and formic acid were purchased from Merck (Darmstadt, Germany) and analytical grade water was obtained from Milli-Q Ultrapure water purification system (Millipore, USA). 0.45 µm PTFE filters Syringe were purchased from Nordic Invest (Cluj, Romania). Carboxymethyl cellulose (CMC) was obtained from Abcam (BioZyme, Romania). All reagents used in this study were of analytical grade.

Standard solutions and spiked samples

Stock solution of curcumin was prepared in methanol at a concentration of 100 mg/mL and stored in amber coloured bottle at 4°C. The curcumin stock solution was diluted with methanol to obtain working solutions of concentration ranging from 1 to 20 µg/mL. All the prepared solutions were protected from light using amber-coloured volumetric flasks. Standard solutions (0.1, 0.2, 0.5, 1, 2 µg/mL) were prepared by spiking 100 µL of each working solution (1, 2, 5, 10 and 20 µg/mL) into 100 µL of blank plasma and 800 µL of methanol. These standards were used to construct calibration curves for the quantification of curcumin in rat plasma concentrations ranging from 100 to 2000 ng/mL.

Experimental design for drug administration

The experiments were performed on 6 adult female Wistar-Bratislava albino rats (mean age 17 weeks), weighing 200-250 g, bred in the Animal Facility of “Iuliu Hatieganu” University of Medicine and Pharmacy. The animals were housed under controlled conditions (on a 12 hours light-dark cycle, at an average temperature of 22±2°C and ca. 55% relative humidity). They had free access to standard pellets, as basal diet, and water ad libitum, except for 12 hours of fasting before the experiment. 150 mg of Curcumin (Abcam, BioZyme, Romania) was dissolved in carboxymethyl cellulose (CMC) 0.5% and then administered in oral suspension (150 mg curcumin/ kg rat weight). The rats were randomly assigned to three groups (Group I) (n=2). The first group received 0.5 ml / animal oral curcumin suspension (150 mg Curcumin / rat kg body weight) and blood was prelevated at 15, 30, 60, 90, 120, 150 and 180 min. The second group (Group II) was administered curcumin by gavage (preventively) and one hour later terebenthine was injected i.m., followed by blood prelevation at the same time intervals. The rats in the third

group (Group III) received Terebenthine i.m. and after 2 hours curcumin was given by gavage (treatment), then blood prelevation was performed as specified for the other two experimental groups.

After the experiment animals were sacrificed by cervical dislocation. The study protocol was approved by the Institutional Animal Ethical Committee (IAEC) of *Iuliu Hatieganu* University of Medicine and Pharmacy Cluj-Napoca. Experiments were performed in triplicate following the Animal Testing Regulations.

Plasma sample preparation

Blood (approx. 1 ml) was collected from the rat retro orbital plexus in an EDTA test tube at 15, 30, 60, 90, 120, 150 and 180 min post dosing of curcumin suspension. Immediately after collection, blood samples were gently inverted several times to ensure complete mixing with the EDTA solutions. The samples were left at room temperature for more than half an hour and then centrifuged at 4500 rpm for 10 minutes. After centrifugation, the upper organic layer was aspirated with a pipette and inserted into a clean Eppendorf tube, resulting a quantity of 0.5 ml plasma (containing three types of proteins: albumins, globulins and fibrinogen) and the curcumin.

For HPLC analysis the rat plasma samples were prepared by using protein precipitation. At each sample of 200 µL rat plasma 800 µL of methanol was added and it was shaken for a few minutes in order to precipitate the plasma protein. The filtrate was then passed through 0.45 µm PTFE filters Syringe and injected into the HPLC system.

Oxidative stress assessment

Tissue samples from liver, kidney and muscles were collected from each rat. Biopsy samples helped to determine MDA (nmoL/mg protein), PC levels (nmoL/mg protein) as markers of oxidative stress.

Tissue homogenization was performed using a PT 1200E Polytron homogenizer. The homogeneous medium was obtained using 50 mM Tris-buffered saline + 10 mM EDTA, pH 7.5. A given volume of Tris-buffered saline was added to a tissue sample while stirring in an ice bath. The content was centrifuged for 10 minutes at 1000 x g, 400C, and the supernatant was separated. The total protein concentration of the supernatant was determined using the Bradford method.

MDA was determined by fluorescence lipid peroxidation. Through this process, the resulting MDA reacts with thiobarbituric acid to form a fluorescent adduct. For the determination of tissue homogenate, the sample was boiled for one hour with 10 mM of 2-thiobarbituric solution in 75 mM K_2HPO_4, pH 3.

After quenching, the reaction product was extracted with n-butanol. The concentration was measured in the organic phase after its separation by centrifugation. Emission intensity was measured at 534 nm with a Perkin Elmer spectrofluorimeter using the synchronous fluorescence technique to a 14 nm difference between the excitation and emission wavelengths (Δλ). MDA concentration was determined based on a calibration curve consisting of common MDA concentrations using the same measurement technique [47].

The determination of protein carbonyl was carried out by means of a technique which is based on the reaction with a classic carbonyl reagent: 2,4-dinitrophenylhydrazine. The reaction leads to the formation of 2,4-dinitrophenylhydrazone, yellow in color, that can be determined spectrophotometrically. Serum samples were reacted with 10 mM of 2,4-dinitrophenylhydrazine solution in 2.5 N HCl for 1 hour at room temperature in the dark. After being treated with 20% trichloroacetic acid and after the separation of the precipitate obtained by centrifugation, the sample was washed three times with a 1:1 mixture of ethyl acetate and absolute ethanol (v/v). Then, the precipitate was dissolved in 6 M guanidine hydrochloride. From the samples obtained, protein concentration was determined by measuring the extinction at 280 nm. Later, on the same samples, the extinction at 355 nm was also read (wavelength corresponding to the absorp- tion spectra of hydrazones). The protein concentration of the samples analyzed was determined based on a calibration curve consisting of common concentrations of albumin solutions in 6 M guanidine hydrochloride. Simultaneously with the samples treated with 2,4-dinitrophenylhydrazine, blank samples were also processed, only treated with 2.5 N HCl. Extinction was read based on these samples. Carbonyl concentration assessment was done according to the following formula: C = Abs 355 x 45.45 nmoL/mL. Results were expressed as nmol/mg protein, taking into account the protein concentration of the sample expressed in milligrams [46,48].

ACKNOWLEDGMENTS

This paper was published under the frame financed by the University of Medicine and Pharmacy “Iuliu Hatieganu” Cluj-Napoca, internal grant no. 1491/14/28.01.2014.

REFERENCES

1. J. Li, Y. Jiang, J. Wen, G. Fan, Y. Wu, C. Zhang, *Biomedical chromatography*, **2009**, *23*(11), 1201.
2. B.B. Aggarwal, B. Sung, *Trends in pharmacological sciences*, **2009**, *30*(2), 85.
3. P. Anand, H.B. Nair, B. Sung, A.B. Kunnumakkara, V.R. Yadav, R.R. Tekmal, B.B. Aggarwal, *Biochemical pharmacology*, **2010**, *79*(3), 330.
4. B.T. Kurien, A. Singh, H. Matsumoto, R.H. Scofield, *Assay and drug development technologies*, **2007**, *5*(4), 567.
5. R.A. Sharma, A.J. Gescher, W.P. Steward, *European Journal of Cancer*, **2005**, *41*(13), 1955.
6. G.P. Lim, T. Chu, F. Yang, W. Beech, S.A. Frautschy, G.M. Cole, *The Journal of Neuroscience*, **2001**, *21*, 8370.
7. Y. Pak, R. Patek, M. Mayersohn*, Journal of Chromatography B*, **2003**, *796*, 339.
8. T. Atsumi, Y. Murakami, K. Shibuya, K. Tonosaki, S. Fujisawa, *Anticancer Research,* **2005**, *25*, 4029.
9. H.P. Ammon, M.A. Wahl, *Planta Medica*, **1991**, *57*, 1.
10. Y.J. Surh, *Nature Reviews Cancer*, **2003**, *3*(1), 768.
11. F. Payton, P. Sandusky, W.L. Alworth, *Journal of Natural Products*, **2007**, *70*, 143.
12. W. Yang, J.F.M. Yu, D. Wang, Y. Rong, P. Yao, A.K. Nüssler, H. Yan, L. Liu, *Cellular Physiology and Biochemistry*, **2015**, *35*, 789.
13. V.O. Gutierres, M.L. Campos, C.A. Arcaro, R.P. Assis, H.M. Baldan-Cimatti, R.G. Peccinini, S. Paula-Gomes, I.C. Kettelhut, A. Martins Baviera, and I.L. Brunetti, *Evidence-Based Complementary and Alternative Medicine*, **2015**, *2015*, 1.
14. R.A. Sharma, W.P. Steward, A.J. Gescher, *Springer US*, **2007**, *1*, 453.
15. D. Gugulothu, P. Desai, V. Patravale, *Journal of Chromatographic Science*, **2013**, *1*, 1.
16. S.P. Singh, S. Wahajuddin, G.K. Jain, *Journal of Bioanalysis & Biomedicine*, **2010**, *2*(4), 79.
17. Y. Li, K. Bi, *Biomedical Chromatography*, **2003**, *17*, 543.
18. J-L. Jiang, X-L. Jin, H. Zhang, X. Su, B. Qiao, Y-J Yuan, *Journal of Pharmaceutical and Biomedical Analysis,* **2012**, *70*, 664.
19. X-M. Wang, Q-Z. Zhang, J. Yang, R-H. Zhu, J. Zhang, L-J. Cai and W-X. Peng, *Tropical Journal of Pharmaceutical Research*, **2012**; *11*(4), 621.
20 P. Anand, A.B. Kunnumakkara, R.A. Newman, B.B. Aggarwal. *Molecular Pharmaceutics*, **2007**, *4*(6), 807.
21. Z. Jin, Z. Jiang, H. Wang, L. Bian, J. Lei, G. Hu, *Latin American Journal Of Pharmacy*, **2015**, *34*(2), 301.
22. R. Ravichandran, *Journal of Biomaterials and Nanobiotechnology*, **2013**, *4*, 291.
23. I. Khalaf, L. Vlase, B. Ivanescu, D. Lazar, A. Corciova, *Studia UBB Chemia*, **2012**, *LVII(2)*, 113-118.
24. D. Benedec, I.E. Popica, I. Oniga, et al., *Studia UBB Chemia*, 2015, *LX*(*4*), 257-266.
25. A. Dragus, M.S. Beldean-Galea, *Studia UBB Chemia*, **2015**, *LX(2),* 117-124.

26. Z.I. Szabo, T Szabo, R. Emoke, E. Sipos, *Studia UBB Chemia*, **2014**, *LIX(4),* 195-203.
27. M. Muresan, D. Benedec, L. Vlase, R. Oprean, A. Toiu, I. Oniga. *Studia UBB Chemia*, **2015**, *LX(1),* 127-138.
28. V.L. Ung, B.C. Sydora, R.N. Fedorak, *Digestive Diseases and Sciences*, **2010**, *51*, 1272.
29. H. Jiang, C.S. Deng, M. Zhang, J. Xia, *World Journal of Gastroenterology*, **2006**, *12*, 3848.
30. K. Sugimoto, H. Hanai, K. Tozawa, A. Aoshi, M. Uchijima, T. Nagata, Y. Koide, *Gastroenterology*, **2002**, *123*, 1912.
31 Y.T. Jian, G.F. Mai, J.D. Wang, Y.L. Zhan, R.C. Luo, Y.X. Fang, *World Journal of Gastroenterology*, **2005**, *11*, 1747.
32. H.M. Arafa, R.A. Hemeida, A.I. El-Bahrawy, F.M. Hamada, *Food and Chemical Toxicology,* **2009**, *1*, 1311.
33. N. Chainani-Wu, *Journal of Alternative and Complementary Medicine*, **2003**, *9*(1), 161.
34. V.P. Menon, A.R. Sudheer, *Advances in Experimental Medicine and Biology*, **2007**, *595*, 105.
35. M.H. Pan, T.M. Huang, J.K. Lin, *Drug metabolism and disposition*, **1999**, *27*(4), 486.
36. C. Kala, S. Ali-Syed, M. Abid, S. Rajpoot, N.A. Khan, *International Journal of Pharmacognosy and Phytochemical Research*, **2015**, *7*(2), 383.
37. B. Halliwell, *Biochemistry*, **2007**, *401*(1), 1.
38 A. Ramond, D. Godin-Ribuot, C. Ribuot, P. Totoson, I. Koritchneva, S. Cachot S.P. Levy, M. Joyeux-Faure, *Fundamental & clinical pharmacology*, **2011**, 27(3), 252.
39. N. Singh, A.K. Dhalla, C. Seneviratne, P.K. Singal, *Molecular and Cellular Biochemistry*, **1995**, *147*(1), 77.
40. M. Valko, D. Leibfritz, J. Moncol, M.T. Cronin, M. Mazur, J. Telser, *International Journal of Biochemistry & Cell Biology*, **2007**, *39* (1), 44.
41. J. Amer, H. Ghoti, E. Rachmilewitz, A. Koren, C. Levin, E. Fibach, *British Journal of Haematology*, **2006**, *132*(1), 108.
42. T. Grune, M.M. Berger, *Current Opinion in Clinical Nutrition & Metabolic Care*, **2007**, *10*, 712.
43. C.E. Pippenger, R.W. Browne, D. Armstrong, "Regulatory antioxidant enzymes" in "Methods in Molecular Biology", vol. 108, Free Radicals and Antioxidant Protocols, D. Armstrong (ed.), Humana Press Inc., Totowa, NJ, **1993**, 299-311.
44. E.R. Stadtman, *Science*, **1992**, *257*, 1220.
45. B.S. Berlett, E.R. Stadtman, *Journal of Biological Chemistry*, **1997**,*272*, 20313.
46. S. Dimon-Gadal, P. Gerbaud, P. Therond, J. Guibourdenche, W.B. Anderson, D. Evain-Brion, F. Raynaud, *Journal of Investigative Dermatology,* **2000**, *114*, 984.
47. M. Conti, P.C. Morand, P. Levillain, A. Lemonnier, *Clinical Chemistry,* **1991**, *37*(7), 1273.
48. A.Z. Reznick, L. Packer, *Methods in enzymology*, **1994**, *233*, 357.

STUDIA UBB CHEMIA, LXI, 2, 2016 (p. 195-203)
(RECOMMENDED CITATION)

REACTIVITY OF OVARIECTOMISED FEMALE RATS AFTER ADMINISTRATION OF INJECTABLE OESTROGENS BY TEM MICROSCOPY

MOCAN-HOGNOGI RADU FLORIN[a*], COSTIN NICOLAE[a], CONSTANTIN CRACIUN[b], MALUTAN ANDREI[a], TRIF IOANA[a], CIORTEA RAZVAN[a], MIHU DAN[a]

ABSTRACT. The purpose of this electrone microscopy study was to identify and specify structural and ultrastructural changes occurring in the vulvar epithelium of ovariectomised female rats, as well as their reactivity to the administration of injectable oestrogens. We used 30 female Wistar white rats, distributed in four groups with 1 control group, to which oestrogenic treatment was administered. The hormone replacement therapy with injectable oestrogens (Estradiol, Estradurin, Sintofolin), at a dose of 0.2 mg/rat/day was administered for 14 days. Afterwards, all animals were sacrificed and vulvar biopsies were taken, which were then processed using optical microscopy (the semithin section technique) and transmission electron microscopy (TEM) techniques. This study showed that injectable oestrogen treatment over a period of 14 consecutive days enables the recovery of each tissue layer, with regard to the structural and ultrastructural modifications arising in ovariectomised female rats.

Keywords: *oestrogens, optical microscopy, transmission electron microscopy, structure, atrophy, vulvar hyperplasia*

INTRODUCTION

Variations in estrogen levels strongly affect cell growth and metabolism in a variety of tissues including the vulvo-vaginal epithelium, the ovary and uterus.

Estradiol is biosynthesized from progesterone, also produced from cholesterol, via intermediate pregnenolone. One principal pathway then converts progesterone to its 17-hydroxy derivative, 17-hydroxyprogesterone,

[a] *Second Clinic of Obstetrics and Gynaecology of the "Iuliu Hatieganu" University of Medicine and Pharmacy 32 Clinicilor Str., RO-400006*
[*] *Corresponding author: radumocan@yahoo.com*
[b] *Center of Electron Microscopy of "Babes-Bolyai" University* Str. Kogălniceanu, Nr. 1, RO-400084 Cluj-Napoca, Romania

and then to Δ4-androstenedione via sequential cytochrome P450-catalyzed oxidations. The action of an aromatase on Δ4 -androstenedione generates estrone, which is then metabolized by a dehydrogenase to the final compound, 17β-estradiol [1].

The reaction to injectable oestrogen therapy is quick, due to the presence of a large number of oestrogenic receptors, either ER-α or ER-β, in the genital tract, especially in the vulvar area [2,3].

The lack of of estrogen production characteristic to menopause is responsible for the various signs and symptoms, which frequently compromise the quality of life [4,5]. Of these, vulvar atrophy is highly prevalent and does not resolve spontaneously in time unlike other symptoms such as the vasomotor ones [6,7].

The vulvar epithelium reacts to various hormonal influences, much like the entire female genitive tract, i.e. the cells at this level have a specific type of receptivity to female sexual hormones and suffer structural and functional modifications due to the decrease and, even more, lack of such hormones [8,9].

During the metabolism of female hormones, many enzymes catalyse reactions such as aromatisation, oxidation, reduction, sulfonation, desulfonation, hydroxylation and methoxylation. These enzymes must all recognise and bind oestrogen but they have diverse structures [10].

Figure 1 shows the chemical structure of the injectable substances used in this study.

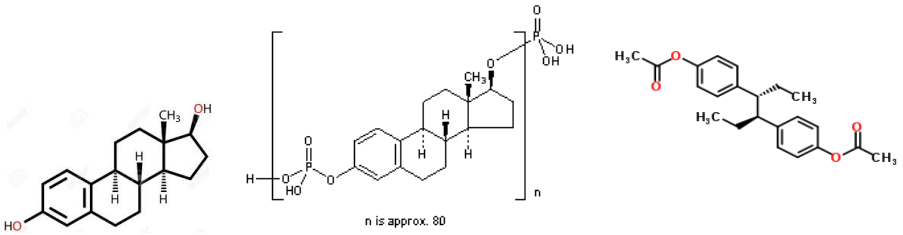

Figure 1. Structure for: a) Estradiol; b) Estradurin, (polyestradiol phosphate); c) Sintofolin (Hexestrol diacetate)

The novelty of this study is the possibility to investigate by new modern methods and a proprietary protocol the effects of estrogen injection on the vulvar structure.

In this study, we attempted to identify the structural and ultrastructural changes of the vulvar epithelium of ovariectomised female rats through optical microscopy and transmission electron microscopy, as well as their response to the administration of injectable oestrogens.

RESULTS AND DISCUSSION

Surgically induced menopause was demonstrated through postoperative estradiol level measurements, with statistically significant differences between the study groups. (Fig.2.)

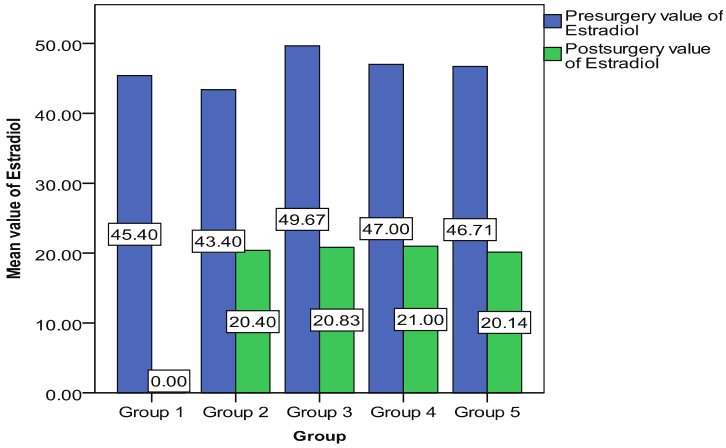

Figure 2. Comparing pre/postoperative estradiol values

The vulvar epithelium of group 1 had a normal structure on the semi thin section technique (Fig.3A).

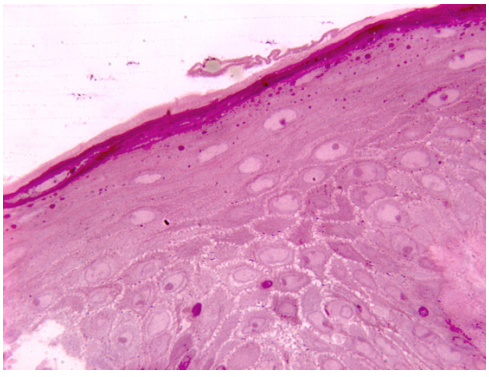

Figure 3A. Light microscopy micrograph showing a normal aspect of vulvar epithelium, containing partially keratinized cells of the basal, spinosum and superficial layers. Ob X 100.

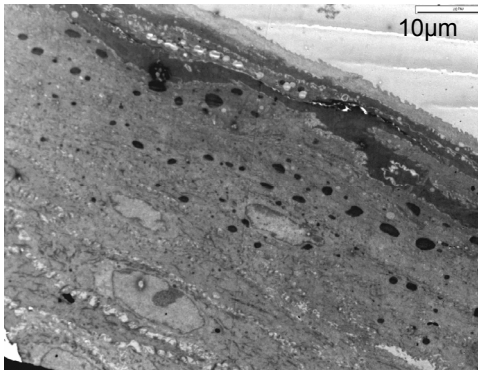

Figure 3B. Electron micrograph (TEM) image of vulvar epithelium showing normal ultrastructural aspects of cells components. Keratohyalin granules are apparent in superficial layer.

In group 2, however, we found both structural and functional changes of the vulvar epithelium due to ovariectomy. Cells in division are relatively scarce, or may even lack in some areas of the basal layer, suggesting the poor regenerative activity of the cells in this layer. In some areas we even found alterations of the entire epithelium, including the destruction of some cells of the basal layer. The superficial layer per se was absent. We even found some signs of destruction of the spinous layer. It is typical for the intercellular space of the spinous layer to be very dilated and include numerous damaged desmosomes, which leads to weak cohesion between cells and the potential disruption or destruction of the entire spinous layer. Of note is the presence of numerous blood vessels, especially veins, most of which are congested or overburdened with erythrocytes (Fig.4A).

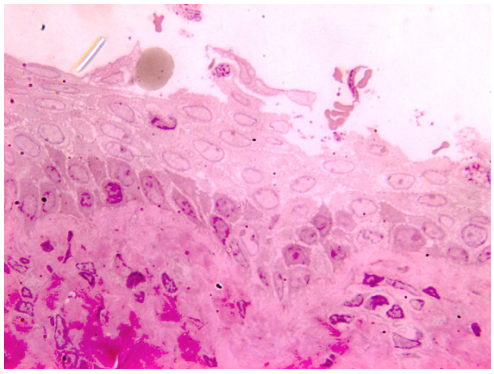

Figure 4A. Micrograph of vulvar (labia minor) epithelium from ovariectomized rats showing structural alterations with partially desquamated cells of the superficial layer and the disappearance of keratohyalin granules. Ob. X 100.

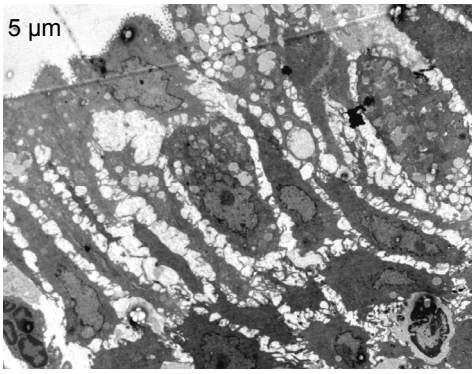

Figure 4B. Electron micrograph picture of labium minor (vulvar) epithelium from ovariectomized rats. Ultrastructural alterations of desmosomes between cells leading to larger intercellular spaces and loss of cohesion between epithelial cells.

In groups 3, 4 and 5, contrary to group 2, the semithin sections reveal hyperplasia of all cellular layers of the vulvar epithelium. Such findings indicate hyperplasia occurring in the vulvar tissues, with the regeneration and, respectively, preservation of structures in similar conditions to those of animals from group 1. We found relatively numerous cells in division, suggesting that the administration of injectable oestrogens had the ability to stimulate cell regeneration in the basal layer. We also noted the presence of Merkel cells, indicating the fact that this layer of cells not only had a normal structure, but that their metabolic activity had actually been stimulated. The granular layer was poorly represented in the normal epithelium and lacked completely in group 2, of ovariectomised rats. On the other hand, it appears that in this case, the administration of oestrogens

stimulated the synthesis of keratin granules and their accumulation in the form of a distinctive granular layer, and then as a keratinised superficial layer, even slightly horned in the external, apical area of the vulva. In the upper part of the chorion, towards the basal membrane of the epithelium, we found several elastic and collagen connective fibres, as well as a relatively numerous cell population, including fibroblasts, fibrocytes, eosinophils and mast cells (Fig.5A).

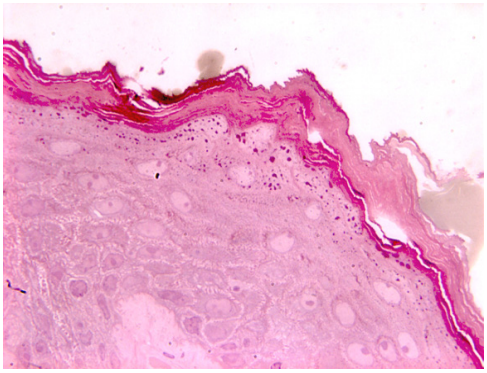

Figure 5A. Micrograph of vulvar epithelium from ovariectomized rats treated with oestrogen showing the protective effects of oestrogens. All cells in the epithelium appear to have a normal structure. Keratohyaline granules and the keratin layer are evident. Ob. X 100.

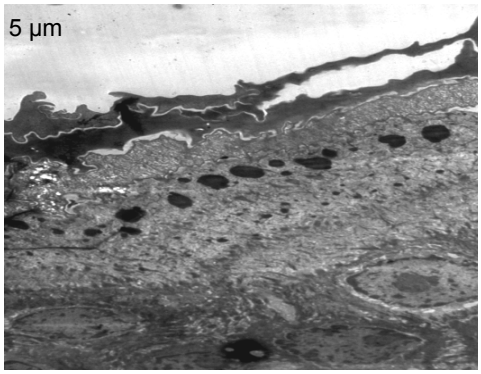

Figure 5B. Electron micrograph of labia minor (vulvar) epithelium from ovariectomized rats treated with oestrogen showing the protective effects of oestrogens. All cells have almost normal ultrastructure and the keratohyaline granules and keratin layer are present.

The ultrastructural studies using transmission electron microscopy (TEM) in group 1 revealed a normal ultrastructure of all layers of the vulvar epithelium (Fig.3B).

In group 2, the electron microscopy images showed multiple complex changes brought on by ovariectomy, visible in all cells of the vulvar epithelium, as well as in all components of the chorion. In the spinous layer, it was apparent that intercellular spaces were expanded due to the depletion of desmosomes, leading to a weakened intercellular cohesion. There were no granular or keratinised superficial layers, and the last row of cells in the spinous layer reached the surface of the epithelium. The entire chorion was congested, to the extent that all its cellular and fibre components had a dense aspect, with several alterations. It is interesting, however, that some of the eosinophils and neutrophils were in a process of alteration, with a ruptured cell membrane and granules scattered in their vicinity. Smooth muscle cells were rare and separated by large spaces, occupied chiefly by eosinophils and neutrophils, but also by mast cells (Fig .5B).

In all groups treated with oestrogens, i.e. groups 3, 4 and 5, we found that the injectable oestrogen treatment lead to the protection and regeneration of the vulvar structures affected by ovariectomy, but not in all areas. Hyperplasia was present more evidently in the chorion than in the epithelium. It is certain that in the epithelium, the oestrogen treatment led to an increase in keratin synthesis, suggested by the presence of an evident granular layer. The cytoplasm of cells appeared dense because of the abundance of ribosomes, small granules of keratin, mitochondria, tonofilaments and even the presence of lipid droplets. In the chorion, there were abundant elastic and collagen fibres, along with a large number of fibroblasts, fibrocytes, mast cells and eosinophils. Furthermore, we found blood vessels and myelinated and non-myelinated nerve fibres of sensitive formations, probably Meissner corpuscles. Such nerve fibres were also present in areas of lipid accumulation, either in large deposits or in small droplets, belonging to sebaceous glands and probably located on the external and basal side of the vulva (Fig.4B).

Optical microscopy and transmission electron microscopy are particularly useful methods in the study of the microanatomy of the genital tract, facilitating the in-depth understanding of the structural and ultrastructural modifications occurring at this level during menopause [11,12].

This experimental study showed that bilateral ovariectomy triggers important and complex changes in the vulvar epithelium [13,14]. The experimental model of hormone replacement therapy with surgically induced menopause through bilateral ovariectomy in female rats is well known [15,16].

Our results on the study of semithin sections from a normal vulvar epithelium, found multiple and complex changes induced by ovariectomy in group 2 rats. These changes, both structural and functional, occurred in every layer of the vulvar epithelium: relatively scarce cells in division, sometimes completely absent in some areas of the basal layer, suggesting a poor regenerative activity of the cells of this layer. In certain areas we even found alterations of the entire epithelium, including the destruction of some cells of the basal layer. The superficial layer per se was absent. The rats in groups 3, 4 and 5, when compared to group 2, had hyperplasia of all cell layers of the vulvar epithelium on the semithin sections.

The ultrastructural investigations confirm the results of the structural study based on semithin sections, showing that the injectable oestrogen treatment helped protect and rebuild the structure of the vulvar epithelium, the chorion and the muscle layers affected by ovariectomy.

Based on these results, we concluded that all three types of injectable oestrogens used helped to treat vulvar atrophy [17,18].

This study showed that injectable oestrogen treatment over a period of 14 consecutive days enables the recovery of structural and ultrastructural modifications occurring in each layer in ovariectomised female rats, similar to other results published in literature [19,20].

CONCLUSIONS

Experimentally-induced menopause causes important and polymorphic changes in the entire vulvar epithelium, with various degrees of ultrastructural alterations.

The injectable oestrogen treatment had a stimulating effect on the structural and functional regeneration of the vulvar epithelium.

This study showed that Optical Microscopy and Transmission Electron Microscopy can be used as complex complementary diagnostic methods, useful in the understanding and clinical assessment of vulvar changes occurring during menopause, as well as in their adjuvant therapy.

EXPERIMENTAL SECTION

This study used a total of 30 female Wistar white rats, with an average weight of 200 g, obtained from the laboratory animal facility of the "Iuliu Hatieganu" University of Medicine and Pharmacy of Cluj-Napoca. Throughout the experiment, the rats were given standard food and water ad libitum, thus observing the standard conditions required by the current legislation on the protection of laboratory animals.

The following study groups were created:

- Group 1 - control group (no surgical intervention, no oestrogenic treatment, premenopausal), including 5 subjects.
- Group 2 - operated, menopausal, without treatment, including 5 subjects.
- Group 3 - operated and treated with Estradiol, i.e. a natural oestrogen, at a dosage of 0.2 mg/day/rat, for a period of 14 days, including 6 subjects.
- Group 4 – operated and treated with Estradurin, i.e. a synthetic oestrogen, at a dosage of 0.2 mg/rat every 7 days, for a period of 14 days, including 7 subjects.
- Group 5 – operated and treated with Sintofolin treatment, i.e. a synthetic oestrogen, at a dosage of 0.2mg/day/rat, for a period of 14 days, including 7 subjects.

Estradiol (Biofarm, Bucharest, Romania, Zip code: 031212) was used for group 3; each 1 ml-vial of injectable oily liquid contained 2.5 mg estradiol, which was diluted in 9 ml neutralised and sterilised sunflower oil, so that for a dose 0.2 mg of estradiol/rat/day, we administered 0.8 ml of oily solution. Estradurin, (Pharmacia & Upjohn Company LLC (a subsidiary of Pfizer Inc.)), 7000 Portage Road Kalamazoo, MI 49001 United States, is a synthetic oestrogen which was used for group 4; each 2 ml-vial contained 80 mg of powdered polyestradiol phosphate, diluted in 38 ml of distilled water, so that for 0.2 mg of estradiol/rat/day, we administered 0.1 ml solution. Estradurin was administered at 7-day intervals since it is a powerful phosphatase inhibitor, with a particularly slow release, ensuring considerable

oestrogenic activity for a prolonged period of time, even weeks after the injection. Sintofolin (Terapia S.A, 400632, Cluj-Napoca, jud. Cluj, Romania) a synthetic oestrogen, was used for group 5; each 2 ml vial of injectable oily liquid contained 5 mg of hexestrol diacetate, which was diluted with 8 ml of neutralised and sterilised sunflower oil, so that 0.4 ml of oily solution was administered for 0.2 mg/rat/day.

Bilateral ovariectomy was performed in 25 of the 30 female rats included in the study. We considered menopause installed 15 days after surgery. For confirmation, the estradiol level was tested 15 days after surgery and compared with pre-surgery hormonal levels.

The bilateral ovariectomy in female Wistar rats was performed in accordance with the technique described by Waynforth et al [21]. The animals were anesthetized by intramuscular injection of a mixture of Xylasine (10 mg/kg, Xylocontact) and ketamine (100 mg/kg).

Once menopause was confirmed in all groups, we began administering various injectable oestrogen hormonal formulas, over a 14-day period. In the final stage of the study, 15 days after treatment, all animals were sacrificed, using the cervical dislocation method. Biopsies from the vulva and vagina were taken from all groups, and the samples were then processed using optical microscopy (the semithin section technique) and transmission electron microscopy (TEM) methodologies and techniques [22,23,24].

The study protocol was approved by the Ethics Committee of the “Iuliu Hatieganu” University of Medicine and Pharmacy of Cluj-Napoca (approval number no. 116/06.03.2015).

The tissue samples were immediately immersed into a 2.7% glutaraldehyde solution, in phosphate buffer 0.1 M. 7.2, so as to prefix them for 90 minutes at a temperature of +4°C. In the first stage, 500 nm-thick semithin sections were taken from the blocs obtained, and properly modelled for optical microscopy studies, followed by ultrafine 40-60 nm-thick sections from the selected areas of the same blocs, for electronic microscopy studies. The sections were made with a Leica UC 6 ultramicrotome, using DDK diamond knives, and then collected onto electrolytic grids and double-contrasted with uranyl acetate and lead citrate, prior to their examination under a Jeol JEM 1010 transmission electron microscope (TEM). We used a Megaview III camera for the capture of images which were then stored in a database using the Soft Imaging Analysis application.

The semithin section technique was used for optical microscopy studies, on sections 500 nm-thick obtained from the same blocs processed for electronic microscopy research with the same ultramicrotome. These sections were stained with Epoxy tissue stain, specific for epoxy synthetic resins. We used an Olympus BX 51 microscope to examine the sections and a CCD Media Cibernetics camera to capture the images, using the Image Pro Plus software.

REFERENCES

1. C.J. Saldanha, L. Remage-Healey, and B.A. Schlinger. *Endocrine reviews*, **2011**, *32(4),* 532
2. C.E. Skala, I.B. Petry, S.B. Albrich, A. Puhl, G. Naumann, H. Koelbl, *Eur J Obstet Gynecol Reprod Biol.*, **2010**, *153(1),* 99
3. J.S. Kang, B.J. Lee, B. Ahn, D.J. Kim, S.Y. Nam, Y.W. Yun, K.T. Nam, M. Choi, H.S. Kim, D.D. Jang, Y.S. Lee, K.H. Yang, *J Vet Med Sci.*, **2003**, *65(12),* 1293
4. M. DiBonaventura, M. Moffatt, A.G. Bushmakin, M. Kumar, J. Bobula, *J Womens Health (Larchmt)*, **2015**, *24(9*), 713
5. D.W. Sturdee, N. Panay, *Horm Metab Res.*, **2014**, *46(5),* 328
6. J. López-Belmonte, C. Nietro, J. Estevez, J.L. Delgado, J. Moscoso del Prado, *Maturitas*, **2012**, *72(4)*, 353
7. F.M. Lewis, *Post Reprod Health*, **2015**, *21(4),* 146
8. S. Mirkin, B.S. Komm, *Maturitas*, **2013**, *76(3),* 213
9. J. Cen, H. Zhang, Y. Liu, M. Deng, S. Tang, W. Liu, Z. Zhang, *Gynecol Endocrinol.*, **2015**, *31(7),* 582
10. S. Safe, K. Kim, *J. Mol. Endocrinol.*, **2008**, *41(5*), 263.
11. B. Larsen, A.J. Markovetz, R.P. Galask, *Appl Environ Microbiol.,* **1978**, *35(2),* 444
12. S.K. Adam, S. Das, K.A. Jaarin, *Int J Exp Pathol*., **2009**, *90(3),* 321
13. M. Unkila, S. Kari, E. Yatkin, R. Lammintausta, *J Steroid Biochem Mol Biol.,* **2013**, *138*, 107
14. M.E. Basha, S. Chang, L.J. Burrows, J. Lassmann, A.J. Wein, R.S. Moreland, S. Chacko, *J Sex Med.*, **2013**, *10(5),* 1219
15. H.N. Henriques, A.C. de Carvalho, P.J. Soares Filho, J.A. Pantaleão, M.A. Guzmán-Silva, *Int J Exp Pathol.,* **2011***, 92(4*), 266
16. F.F. Onol, F. Ercan, T. Tarcan, *J Sex Med.*, **2006**, *3(2),* 233-41
17. M.A. Mvondo, D. Njamen, S. Tanee Fomum, J. Wandji, *Phytother Res.*, **2012**, *26(7),* 1029
18. E. Damke, A. Storti-Filho, M.M. Irie, M.A. Carrara, M.R. Batista, L. Donatti, L.S. Gunther, E.V. Patussi, T.I. Svidzinski, M.E. Consolaro, *Microsc Microanal*., **2010**, *16(3),* 337
19. E. Damke, A. Storti-Filho, M.M. Irie, M.A. Carrara, M.R. Batista, L. Donatti, L.S. Gunther, E.V. Patussi, T.I. Svidzinski, M.E. Consolaro, *Microsc Microanal*., **2010**, *16(3),* 337
20. G. Magro, A. Righi, R. Caltabiano, L. Casorzo, M. Michal, *Hum Pathol.*, **2014**, *45(8),* 1647
21. T. Nevalainen, E. Berge, P. Gallix, B. Jilge, E. Melloni, P. Thomann, B. Waynforth, L.F. van Zutphenry, *FELASA Board of Management. Lab Anim.*, **1999**, *33(1*), 1
22. J. Kuo, "Electron Microscopy. Methods and Protocols", Second Edition. Humana Press, **2007**
23. M. Pavelka, J. Roth, "Functional ultrastructure. An atlas of tissue biology and pathology", Springer Wien-New York, **2005**
24. M.A. Hayat, "Principles and techniques of electron microscopy", Biological Appl. Fourth Ed.", Ed. Cambridge Univ. Press., **2000**

STUDIA UBB CHEMIA, LXI, 2, 2016 (p. 205-214)
(RECOMMENDED CITATION)

MICROSTRUCTURAL ANALYSIS OF THE INTERFACE BETWEEN SOME SUPERALLOYS AND COMPOSITE/CERAMIC MATERIALS

ALEXANDRU-VICTOR BURDE[a], STANCA CUC[b,c*], ADRIAN RADU[c], MIRCEA AURELIAN RUSU[c], COSMIN SORIN COSMA[c], RADU SEPTIMIU CÂMPIAN[a], DAN LEORDEAN[c]

ABSTRACT. The clinical success of aesthetic ceramic fused to metal or composite resin bonded to metal restorations depends on the quality and strength of composite/ceramic bonding. To investigate the ceramic and composite surface adhesion to the surface of the alloys, samples were prepared by metallographic techniques and then were analyzed by Scanning Electron Microscopy (SEM). We studied a total of four samples of superalloys, denoted S1, S2, S3, and S4. Each of these was treated with: Vita ceramic powders, Noritake ceramic powders, Premise Indirect composite and an indigenous composite C1. At a magnification level of x1500, the adherence between the layers and the surface irregularities of the layers that improve the adherence could be properly observed. It is worth noting that after the sample preparation procedure, samples S1, S2 and S4 were damaged, the only sample remaining in a good condition was sample S3.

Keywords: *Superalloys, Composite, Ceramic Materials, Microstructural Analysis, Scanning Electron Microscopy*

INTRODUCTION

Hybrid porcelain fused to metal (PFM) and metal-composite restorations are still the most popular type of fixed dental restorations [1,2] because of their good mechanical strength, high biocompatibility [3] and long-term satisfactory

[a] *University of Medicine and Pharmacy "Iuliu Haţieganu", Faculty of Dental Medicine, 32 Clinicilor Str., RO-400006, Cluj-Napoca, Romania*
[b] *"Babes Bolyai" University, "Raluca Ripan" Chemistry Research Institute, Department of Polymer Composites, 30 Fantanele Str., RO-400294, Cluj-Napoca, Romania*
[c] *Technical University, Faculty of Materials and Environment Engineering, Bd. Muncii 103-105, RO-400641, Cluj-Napoca, Romania*
[*] *Corresponding author: stancabobo@yahoo.com*

clinical performance [4]. Metal-composite restorations are not generally used for long spanning bridges because of their high fragility [5]. In such clinical situations, the restorative material requires a suitable mechanical strength, so conventional PFM bridges are still preferred to support the mastication forces for long-term clinical success. Their widely use has certified their clinical effectiveness due to many positive aspects of their properties, such as wetting behavior and interface adhesion that are directly linked to the bond-based metal and ceramic elements [6-8].

PFM restorations are comprised of a metallic framework, which confers mechanical resistance to the restoration, and a veneering ceramic layer which covers the metallic framework partially or completely [9]. The first non-noble alloys that have served in PFM restorations contained a composition of cobalt, chromium, iron, nickel and other metals [10,11]. Non-noble alloys show a lower resistance to corrosion by comparison to noble alloys, their fluidity is reduced and the mechanical processing is difficult, but they have a higher hardness and a high modulus of elasticity [12].

Co-Cr alloys have some advantages over Ni-Cr-Be alloys, due to their high degree of biocompatibility that derives from the lack of Ni, which is known to cause Ni-related allergic responses or Beryllium related toxic consequences [13], and greater resistance to corrosion generated by the higher concentration of chromium found in this type of alloys, which forms a protective oxide film on the surface of the framework [14]. The main causes of failure of PFM restorations are the corrosive degradation of alloys, mechanical wear and fatigue breakage [15].

The veneering ceramics used in PFM restorations convey optimum optical, mechanical and biocompatible properties to the final restoration due to their aesthetic color, low thermal conductivity, chemical resistance, high flexural strength, surface density and roughness, but these components also offer some disadvantages like: low tensile strength, further processing after glazing is nearly impossible because the machined surfaces become rough, the presence of internal and external cracks that lead to fracture and high cost [16-19].

The current investigations are aimed to study the way in which two commercially available feldspatic veneering ceramics, as well as a commercially available composite resin adhere onto the surface of Co-Cr superalloy frameworks, by comparison with an indigenous experimental composite C1 manufactured at ICCRR-Cluj-Napoca. The purpose of this study is to describe the adherence proprieties of the C1 composite by comparison with commercially available products that serve the same purpose in aesthetic hybrid restorations. For this purpose we are using scanning electron microscopy (SEM) which produces high-resolution images of sample surfaces. The images created by SEM have a three-dimensional black and white appearance, with a sharp focus over a great depth of field [20].

RESULTS AND DISCUSSION

After the preparation of the samples, it was observed that the deposited layers were peeling and cracking in samples S1, S2 and S4, while all the layers of sample S3 remained 90% intact.

Examination of samples in group S1 revealed that approximately 90% of the Vita ceramic layer was removed. Small portions that remained attached to the alloy indicate that Vita ceramic material (V1) is adherent to the support of the super alloy. Figure 1 indicates how the ceramic material V1 has adhered to the support. At the interface between the V1 layer and the alloy, the oxide layer can be distinguished. Note that some parts of the ceramic material did not adhere to the alloy, due to the presence of elongated cracks that formed parallel to the metal-ceramic interface. The difference between the oxide layer and the cracks can be observed in the form of a thin, white reaction layer that has formed only near the oxide layer.

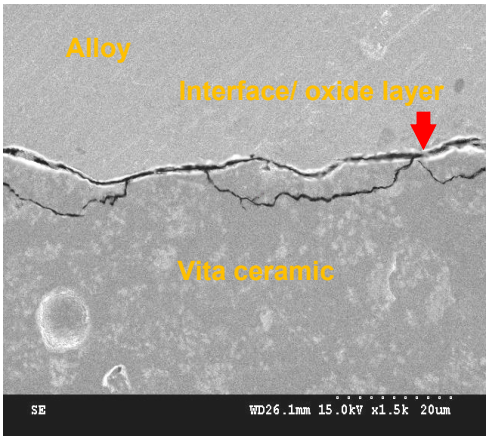

Figure 1. Adhesion of Vita ceramic material, sample group S1 X 1500. The super alloy is in the upper part of the image

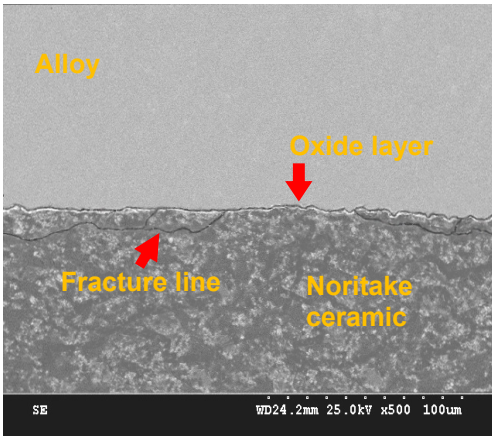

Figure 2. Appearance of the interface between Noritake- Alloy, sample S1 X 500

The Noritake ceramic (N1) layer was also removed from the S1 sample in approximately the same proportion as the V1 ceramic, as it can be observed in Figure 2. An oxide layer can be distinguished at the metal-ceramic junction. This layer has been formed during the oxide firing of the metal framework. For this sample, between the ceramic and the super alloy, a similar but thinner black belt that represents the space between the super alloy and the ceramic support was observed. Thin fracture lines can be observed in the ceramic veneering material near the metal-ceramic junction.

Aspects of composite adhesion to the metal framework are displayed in Figure 3, where the boundary between the two layers is shown- the Premise Indirect composite (P1), in the upper right of the image, presenting air pockets) and the indigenous composite (C1), on the left of the picture, presenting a uniform appearance. Detaching from the support alloy is clearly visible. In depth viewing of the border between the two composites and the metal framework shows that both composite materials have adhered to the supporting material in small areas, which are encircled in Figure 3. In Figure 4, a portion of Premise Indirect composite is shown penetrating the surface irregularities and massive peeling can be observed at the top of the image, due to the crack that propagates along the boundary.

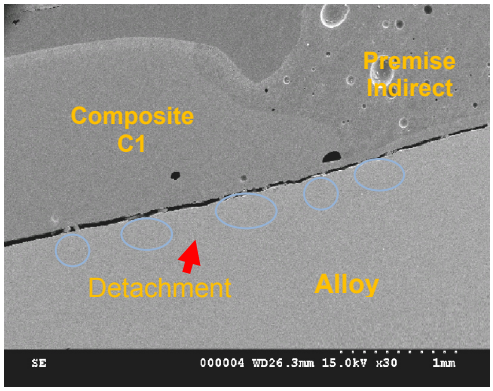

Figure 3. Adhesion of C1 and P1 composites to the surface of the alloy. Adherent areas are encircled, sample S1 X30

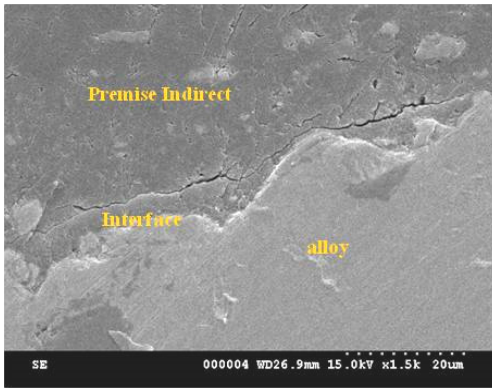

Figure 4. Adhesion of Premise Indirect to the metallic alloy, sample S1 X 1500

Adhesion was also revealed in the case of the indigenous composite, which besides peeling presented cracks, as displayed in Figure 5. Besides the peeling from the supporting layer, penetration of surface irregularities and patches of adherent composite material can be seen (metal framework is at the bottom of the image).

The procedure of sample preparation in the case of group S2 resulted in separation of the layers deposited on the metal frame. V1 veneering ceramic is detached from the metal framework on approximately 90% of the length of the layer and presents multiple surface cracks (Figure 6), however small patches of adherent ceramic material can also be observed.

At the interface between the V1 ceramic and the metal framework, small irregularities and air pockets are visible.

In the case of the N1 veneering ceramic, sample preparation resulted in peeling and cracking of the ceramic material from the surface of the super alloy, in a similar manner to the V1 veneering.

The composite materials have been affected in a small degree by the preparation procedure, as seen in Figure 7. The Premise Indirect composite (P1), which contains air pockets, is located in the upper right of image, while the indigenous composite (C1) is located on left. Adhesion-wise, both composites have adhered to the surface of the super alloy, discontinues and in thin layers.

Adherence to the metal frame has occurred only in a thickness of 2 to 8 μm, given the fact that the remaining thickness of the layer was separated by the cracks caused by the sample preparation technique. Adherence of the indigenous composite (C1) has also been discontinues, in a layer thickness of 2 to 8 μm, as seen in Figure 7.

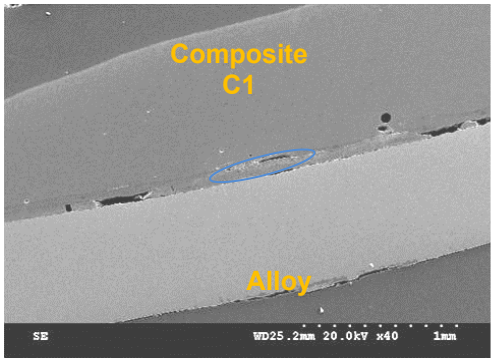

Figure 5. Boundry between C1 and alloy. Peeling area and fracture line is encircled. Sample S2 X40

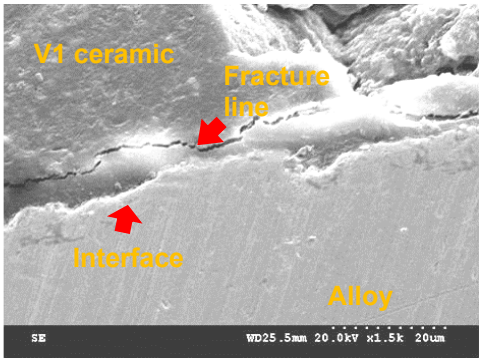

Figure 6. Interface between V1 ceramic and alloy. Sample S1 X1500

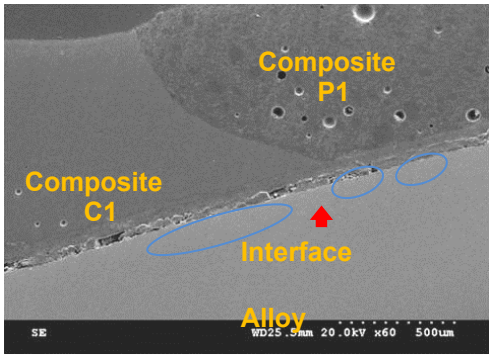

Figure 7. Adhesion of C1 and P1 compo-sites to the metal framework. Fracture lines and air pockets are encircled. Sample S2 x60

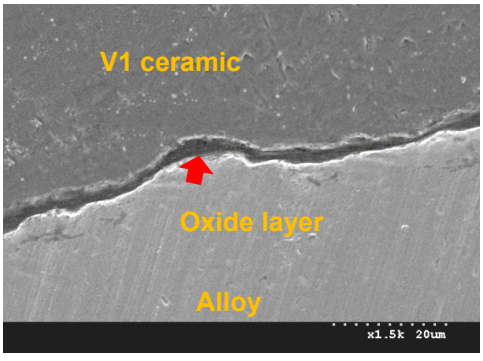

Figure 8. Interface between V1 ceramic and alloy. Sample S3 X1500

Examination of sample group S3 reveals that the prepartion technique used had a small effect on the adherence of the different veneering materials used, given the fact that the materials adherent to the alloy on almost the entire lenght. The layer of V1 veneering ceramic contains a small number of cracks and the adherence to the metal frame is proven to be good, as seen in Figure 8.

Similar results were obtained when using the Noritake ceramic veneering material (Figure 9). The layer of ceramic is continues and presents a good adherence to the surface of the super alloy with a small number of micron sized air-pockets present near boundary between the super alloy and the ceramic layer.

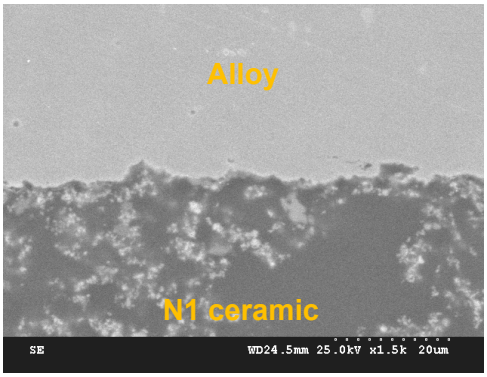

Figure 9. Boundary between N1 veneering ceramic and alloy. S3 X1500

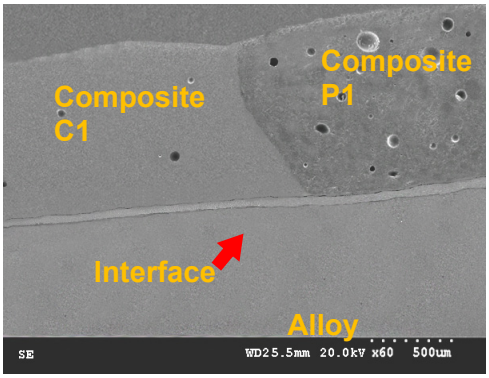

Figure 10. Adhesion of C1 and P1 composites to the surface of the alloy. S3 x60

The Premise Indirect composite and indigenous composite had a good and very good adherence to the super alloy. In Figure 10, the separation limit between the two types of composite is presented (composite C1 on the left and Bellglass composite on the right), with the metal support located at the bottom of the figure. The layer of Premise Indirect presented in this sample also contains embedded air pockets. Adherence of the two composites to the metal frame is illustrated in Figure 11 and 12. In both Figures the super alloy frame is located at the top of the image.

During sample preparation of group S4, about 90% of the thickness of the veneering materials has been removed. After sample preparation, approximately 10% of the thickness of the Vita ceramic veneering material has remained adherent to the surface of the super alloy, this remaining portion of the V1 layer contains micron sized voids and presents a similar adhesion to the metal frame as the samples in group S1 and S2.

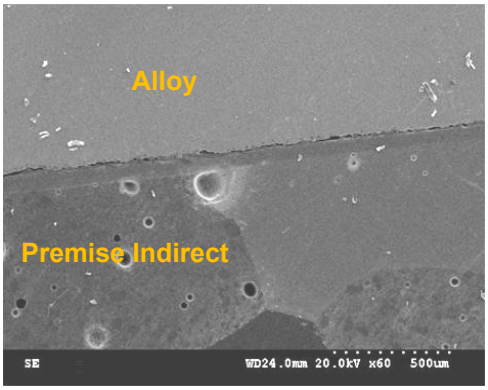

Figure 11. Separation limit between the composite materials- alloy. S3 X60

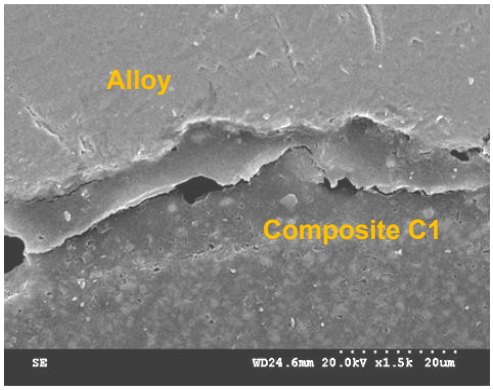

Figure 12. Adherence of indigenous composite to the super alloy sample. S3 X 1500

The Noritake veneering ceramic was removed in about 85% of thickness during sample preparation and presented similar appearance and characteristics with the samples in S1 and S2 groups.

The layers of P1 and C1 composite materials were also affected by the sample preparation procedure. The adherence of the two composite materials to the super alloy framework is presented in Figure 13 and 14. Good adherence of the P1 composite has been observed in a thin layer, separated from the much thicker layer by a crack formed parallel to the metal-composite boundary.

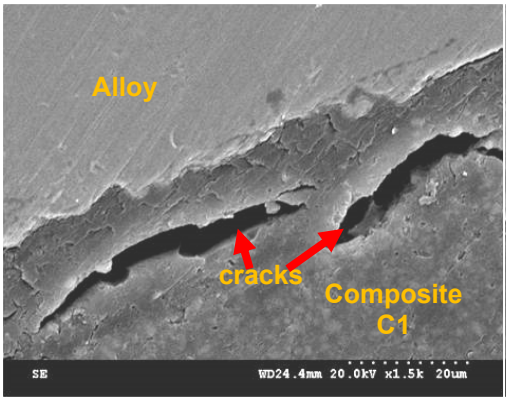

Figure 13. Boundary between C1 composite and alloy. Multiple cracks in the C1 layer. Sample S4 X1500

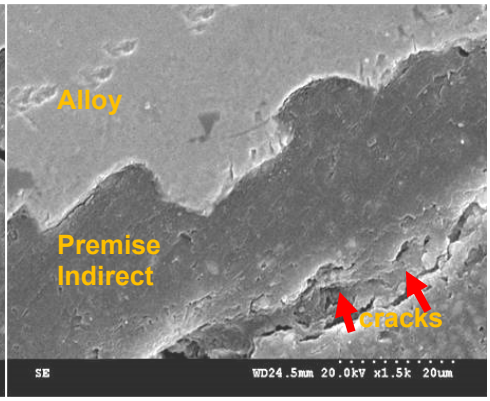

Figure 14. Adherence of the P1 layer to the metal framework. Sample S4 X1500

The adherence of the indigenous composite, which can be observed in figure 12, is observed only in a thinner layer, which is separated from the underlying layer by numerous cracks with lengths of about 40 microns and appreciable width of about 2-4 microns.

CONCLUSIONS

Scanning Electron Microscopy examination with a degree of magnification of between x30 to x1500 of the veneering ceramic and composite layers on the super alloy led to the conclusion that in all of the cases, the studied materials have adhered, in large or small quantities, to the surface of the super alloys.

At a magnification degree of X1500, the adherence between the layers and the irregularities present on the surface of the layers that improve the adherence could be best observed. In addition, the appearance of an oxide layer with a different structure and coloration from the rest of the metallic layer has been noted. The oxide layer may act as a buffer layer. It is worth noting that after the sample preparation procedure, samples S1, S2 and S4 were damaged, the only sample remaining in a good condition is sample S3.

EXPERIMENTAL SECTION

In order to investigate the morphological surface adhesion of the veneering materials to the superalloy frameworks, the Co-Cr superalloy specimens were fabricated by conventional casting technique. For this purpose, four groups consisting of four wax patterns (N=16) in the form of a bar with dimensions of 0.5 mm × 3 mm × 25 mm (IQ sticks, Yeti Dental) were invested with phosphate-bonded investment (BellaVest SH, BEGO). The indigenous composite C1 is manufactured at ICCRR, Cluj Napoca and based on glass with Zn (40% SiO_2; 30% ZnO; 10% Al_2O_3; 10% B_2O_3; 5% CaO; 5% Na_2O melting temperature: 1350^0C) and quartz, colloidal silica as inorganic phase. For organic phase: monomers mixture consists of BisGMA (ICCRR-synthesis, TEGDMA (Aldrich) and UDMA (urethane dimethacrylate, Aldrich) with photo-baro-thermo polymerization system.

The molds were heated at 1050 °C and cast with the superalloys at 1450°C using a centrifugal- induction casting machine (OrcaCast, п Dental)-one mold per superalloy-molds were left to cool down to room temperature and the specimens were then divested and cleaned by sandblasting with alumina particles (110 μm). The specimens were then coated with the four veneering materials, according to the manufacturers instructions.

After veneering, the samples were embedded in a self-curing acrylic resin and then they were mechanically polished with SiC sandpaper (220–2000 grit) under continuous water cooling using a diamond paste (DP Paste, Struers). Between each polishing step, the specimens are rinsed with distilled water and ultrasonically cleaned for 1 min in order to remove remnants of polishing debris and pastes. After polishing, a thin layer of 10 nm of gold coating was deposited on the samples using a sputter coater (B7341, Agar Scientific), before observation with the scanning electron microscopy SEM (HitachiS-2600N).

We studied a total of four groups, denoted S1, S2, S3 and S4. Each of these groups contained four samples which were treated with: Vita VMK Master ceramic (V1), Noritake EX-3 ceramic (N1) Kerr Premise Indirect- a commercially available composite (P1) and an indigenous composite –C1 (C1).

ACKNOWLEDGMENTS

This work was funded by: The Romanian Ministry of Education and Research, National Project TE no. 37/2015.

REFERENCES

[1]. D. Pettenò, G. Schierano, F. Bassi, M.E. Bresciano, S. Carossa, *The International Journal of Prosthodontics,* **2000**, *13*, 405
[2]. R.D. Douglas, M. Przybylska, *Journal of Prosthetic Dentistry*, **1999**, *82*(2), 143
[3]. M. Behr, F. Zeman, T. Baitinger, J. Galler, M. Koller, G. Handel, *The International Journal of Prosthodontics,* **2014**, *27*(2), 153
[4]. I. Sailer, N.A. Makarov, D.S. Thoma, M. Zwahlen, B.E. Pjetursson, *Dental Materials*, **2015**, *31*(6), 603
[5]. A. Della Bona, *Journal of Applied Oral Science*, **2005**, *13*(2), 101
[6]. G.C. Cho, T.E. Donovan, W.W.L. Chee, *Journal of the California Dental Association*, **1998**, *26*, 113
[7]. M. Bagby, S.J. Marshall, G.W. Marshall Jr., *Journal of Prosthetic Dentistry*, **1990**, *63*, 21
[8]. A. Bechir, R.M. Comăneanu, H.M. Barbu, *Tehnologia metalo-ceramică,* **2011**, Ed. Printech, Bucureşti
[9]. T.B. Ozçelik, B. Yilmaz, I. Ozcan, A.G. Wee, *Journal of Prosthetic Dentistry,* **2011**, *106*(1), 38
[10]. F.C. Giacomelli, C. Giacomelli, A. Spinelli, *Journal of the Brazilian Chemical Society,* **2004**, *15*(4), 541
[11]. H.W. Roberts, D.W. Berzins, B.K. Moore, D.G. Charlton, *Journal of Prosthodontics*, **2009**, *18*(2), 188

[12]. A.W.E. Hodgson, S. Kurz, S. Virtanen, V. Fervel, C.O.A. Olsson, S. Mischler, *Electrochimica Acta*, **2004**, *49*, 2167
[13]. L. Baldwin, J.A. Hunt, *Journal of Biomedical Materials Research Part A,* **2006**, *79*(3), 574
[14]. M. Moldovan, C. Prejmerean, M. Brie, V. Popescu, G. Furtos, *Studia UBB Chemia*, **2001**, *XLVI*(1-2), 207
[15]. P.A. Schweitzer, *Corrosion Engineering Handbook*, **2007**, CRC Press, New York
[16]. R. Hickel, J. Manhart, *Journal of Adhesive Dentistry*, **2001**, *3*, 45
[17]. N.M. Jedynakiewicz, N. Martin, *Biomaterials*, **2001**, *22*, 749
[18]. R.C. Pratt, J.O. Burgess, R.S. Schwartz, J.H. Smith, *Journal of Prosthetic Dentistry,* **1989**, *62*, 11
[19]. Z. Chen, J.J. Jr. Mecholsky, *Journal of Materials Research*, **1993**, *8*, 2362
[20]. A. Della Bona, R. van Noort, *American Journal of Dentistry,* **1998**, *11*, 276

STUDIA UBB CHEMIA, LXI, 2, 2016 (p. 215-223)
(RECOMMENDED CITATION)

THE INFLUENCE OF CHROMOPHORE PRESENCE IN AN EXPERIMENTAL BLEACHING GEL ON LASER ASSISTED TOOTH WHITENING EFFICIENCY

IOANA ROXANA BORDEA[a], PATRICIA ONDINE LUCACIU[a*], BOGDAN CRIȘAN[b], CAMELIA-MANUELA MÎRZA[c], DANIELA POPA[d], ANCA ȘTEFANIA MESAROȘ[e], STAVROS PELEKANOS[f], RADU SEPTIMIU CÂMPIAN[a]

ABSTRACT. The aim of this study was to assess the ability of chromophore to improve laser whitening procedures on bovine teeth. The teeth were previously stained with black tea. We evaluated the color change with the help of the Vita Easy Shade Spectrophotometer. Two batches of four teeth were prepared and immersed for 14 days in a solution of black tea. For the bleaching, an experimental gel was used. Batch I was kept in the gel without chromophore and batch II in the gel with chromophore. The teeth from both batches were kept for 30 sec in the gel and were afterwards irradiated with a diode laser (980nm). The statistical analysis showed significant differences between T1 (the measurement of the color after the staining process) and T2 (the measurement of color after the whitening process) for the first batch and T0 (the initial measurement of the color of the teeth) and T2 (the measurement of color after the whitening process) for the second batch.

Keywords: *dental bleaching, laser, bovine teeth, experimental gel*

INTRODUCTION

Due to recent increase of aesthetic expectations, the methods to achieve a brighter, whiter and beautiful smile have also seen a continuous development. Patients come more often to dental clinics in order to achieve

[a] *Iuliu Haţieganu University, Faculty of Dental Medicine, Department of Oral Rehabilitation, 15 Victor Babeș str., RO-400012, Cluj-Napoca, Romania*
[*] *Corresponding author: ondineluc@yahoo.com*
[b] *Iuliu Haţieganu University, Faculty of Dental Medicine, Department of Cranio-Maxillofacial Surgery, Dental Implantology, 37 Cardinal Iuliu Hossu str., RO-400029, Cluj-Napoca, Romania*
[c] *Iuliu Haţieganu University, Faculty of Medicine, Department of Pathophysiology, 2-4 Victor Babeș str., RO-400012, Cluj-Napoca, Romania*
[d] *Iuliu Haţieganu University, Faculty of Dental Medicine, Department of Prosthetic Dentistry, 32 Clinicilor str., RO-400006, Cluj-Napoca, Romania*
[e] *Iuliu Haţieganu University, Faculty of Dental Medicine, Department of Dental Propaedeutics and Esthetics, 32 Clinicilor str., RO-400006, Cluj-Napoca, Romania*
[f] *Athens University, Faculty of Dental Medicine, Department of Prosthodontics, 2 Thivon str., 115 27, Athens, Greece*

the results that make them feel more comfortable and more beautiful. The color of their teeth is a very important aspect so they try to achieve lighter shades. Studying the enamel, the shade change could be the result of two processes: the demineralization and the direct absorption of the food dye.

After the teeth eruption, their initial color also changes because of the interaction with different types of food dyes, smoking, and various chemicals found in drugs, bacteria, as well as other types of pigments. In time, the pigments start to infiltrate the dental structures, changing their shade. The main purpose of the chemical treatments used to obtain a lighter shade is to release chromophore compounds into the dental structure. The most commonly used dental bleaching agents are hydrogen peroxide (H_2O_2), hydrogen peroxide urea ($CH_6N_2O_3$), sodium perborate ($NaBO_3$). The hydrogen peroxide urea decomposes and determines hydrogen peroxide.

Polyphenols representing the coloring substances may determine two types of reactions. One of them is the binding reaction that is done by chelating with calcium ions found in the structure of the hydroxyapatite in the enamel and in the dentine. The second possibility is of forming compounds due to the reaction of collagen found at the level of the dentine.

The two types of bounds are attacked by compounds called free radicals. These are the result of decomposed hydrogen peroxide. The chromophores are later transformed into small-molecule compounds. This change makes them easier to be removed from dental structures.

The decomposing of peroxide leads to intermediary products such as the free radicals ($H_2O_2 \rightarrow H\cdot + \cdot OOH$) or ($H_2O_2 \rightarrow HO\cdot + \cdot OH$), it can also generate perhydroxyl anions ($H_2O_2 \rightarrow H^+ + :OOH^-$) or combinations between free radicals and anions, also basic ($\cdot HOO + OH^- \rightarrow O_2^{-}\cdot + H_2O$) or acidic ($HOO\cdot \rightarrow O_2^- + H^+$) solution. Under the effects of peroxides, the oxidation takes place ($C{=}C + O\cdot \rightarrow C{-}C + H_2O \rightarrow OH{-}C{-}C{-}OH$) [1].

\ /
O

The main reaction of the mechanism involved in the bleaching process is the redox reaction where the hydrogen peroxide performs a reduction of the organic pigments that are impregnated in the dentin and in the enamel, thus allowing its elimination. When in contact with the dental enamel, the hydrogen peroxide releases oxygen that is unstable, and that will form links with other substances that are free or unstable bounded to a substance, in order to obtain the stabilization. The reaction takes place because of the large electronegativity of the oxygen. The oxygen ions react with the molecules that stained the enamel. As a result they break them and generate single chains or smaller molecules, which are lighter and therefore are easier to eliminate [2].

Researches in the recent years were focused on improving the process of teeth whitening by combining the effects of whitening gels with lasers [3].

The activation of the bleaching agents can be done with light sources such as Er:YAG, Nd:YAG, diode, argon, Co_2 lasers, Led and halogen lamps. Colorless bleaching gels do not absorb significantly the light sources used for the activation and therefore a big amount of energy is reflected or transmitted. Using a colored bleaching agent provides the absoption of the light by the bleaching gel [4,5,6,7].

The diode laser is absorbed in precise chromophores found in the composition of beaching gels. Its absorption makes the reaction of bleaching to take place more rapidly, more effectively and more safe if we compare it with the conventional method [8].

The aim of this research was to assess and compare the efficiency of two formulas with and without chromophore for the same experimental gel during laser-assisted bleaching procedures on bovine teeth.

RESULTS AND DISCUSSION

1. Assessment of luminosity (L*) parameter indicated statistically significant differences between at least two stages for batch I ($p < 0.01$) and between at least two stages for batch II ($p < 0.001$).

As expected, for batch I, luminosity (L*) values were higher in T0 than in T1 or T2 and in T2 than in T1. All the differences were statistically significant. The same situation was observed for batch II: higher values in T0 than in T1 or T2, and higher values in T2 than in T1, all the differences being also statistically significant ($p < 0.001$).

There were no statistically significant differences between the two batches in any of the stages of this study ($p>0.05$).

2. For the red-green contrast (a*) values, statistically significant differences were observed between at least two stages for batch I ($p < 0.001$), and also for batch II ($p < 0.001$).

For batch I, the red-green contrast values (a*) were higher in T1 and T2 than in T0, the differences being statistically significant. Between T1 and T2, the differences were not statistically significant. For batch II, a* values were higher in T1 and T2 than in T0, and in T1 than in T2, the differences being statistically significant.

Between the two batches, statistically significant differences were observed during stage T_1 and T_2 ($p < 0.05$).

3. Assessment of the yellow-blue contrast (b*) indicated statistically significant differences between at least two stages for batch I ($p < 0.001$) and between at least two stages for batch II ($p < 0.05$).

For batches, I and II, the yellow-blue contrast values (b*) were higher in T1 and T2 than in T0, the differences being statistically significant only between T0-T2 and T1-T2.

Between the two batches, there were no statistically significant differences during the three stages ($p > 0.05$).

4. For the shade variation (ΔE*) values, statistically significant differences were observed between at least two variations for batch I ($p < 0.001$), and also for batch II ($p < 0.001$). We made the following abbreviations: ΔE*1 – the difference between T1 and T0, ΔE*2 – the difference between T2 and T0, ΔE*3 – the difference between T2 and T1.

For batch I, ΔE*1 had higher values than ΔE*2 or ΔE*3, the differences being statistically significant ($p < 0.001$). Between ΔE*2 and ΔE*3, the differences were not statistically significant. The same situation was observed for batch II. Between the two batches, there were no statistically significant differences ($p > 0.05$).

5. The statistical analysis for the brightness variation (ΔL*) values revealed statistically significant differences between at least two variations for batch I ($p < 0.01$) and for batch II ($p < 0.01$). We made the following abbreviations: ΔL*1 – the absolute value of the difference between luminosity in stage T1 and luminosity in stage T0, ΔL*2 – the absolute value of the difference between luminosity in stage T2 and luminosity in stage T0, ΔL*3 – the absolute value of the difference between luminosity in stage T2 and luminosity in stage T1. We found statistically significant differences between ΔL*1 - ΔL*3 ($p < 0.001$) in batch I, and statistically significant differences between ΔL*1 - ΔL*2 ($p < 0.001$) in batch II. Between the two batches, there were no statistically significant differences ($p > 0.05$).

6. The statistical analysis for the chroma (C*) values indicated statistically significant differences between at least two stages for both batches I and II ($p < 0.001$). For batch I, chroma (C*) values were higher in T1 and T2 than in T0, the differences being statistically significant between T0-T1, T1-T2 ($p < 0.05$) and T0-T2 ($p < 0.01$). For batch II, chroma (C*) values were also higher in T1 and T2 than in T0, the differences being statistically significant only between T0-T1 ($p < 0.01$) and T0-T2 ($p < 0.05$).

7. The correlation analysis between the values of the studied indicators showed during stage T0, for batch I, a positive correlation between a* and b* and a negative correlation between L* and b*. For batch II we observed a positive correlation between a* and b* and negative correlations between L* and a*, L* and b*, L* and C*.

During stage T1, for batch I we observed positive correlations between L* and b*, a* and b*, L* and C* and a negative correlation between L* and a*. For batch II we observed positive correlations between all the indicators.

During stage T2, for batch I we observed positive correlations between L* and b*, a* and b*, L* and C* and a negative correlation between L* and a*. For batch II we observed a positive correlation between a* and b* and negative correlations between the other indicators.

By applying the original gel obtained experimentally we observed an improvement in all parameters assessing the luminosity and colour, tested teeth turned from a darker shade to a lighter one after the experiment. The mean value for a* was in T1-14.60 and in T2-12.96 for batch I, T1 19.93 and T2 8.76 for batch II, for b* in T1 28.66 and in T2 44.86 for batch I, T1 30.86 and T2 43.50 for batch II, for C* in T1 6.82 and in T2 7.60 for batch I, T1 7.13 and T2 7.26 for batch II and for L* T1 21.30 and in T2 55.30 for batch I, T1 28.20 and T2 59.33 for batch II.

By sequential application of the gel and laser irradiation we obtained beneficial effects, favorable and valid results.

The review of Abdelfattah MM concluded that the use of lasers in teeth whitening is an effective way of bleaching the teeth. There are three dental lasers that have been cleared by Food and Drug Administration for tooth whitening: argon laser, CO_2 laser and diode laser. Other lasers have been tested for teeth bleaching, such as Alexandrite and Nd:YAG.

Another result indicated by Abdelfattah MM is that using the diode laser the enamel's surface was smoother [9].

Son et al. have concluded that teeth brightness was increased by laser assisted whitening, so to achieve the ultimate power bleaching process they used the most effective energy source, in order to avoid any adverse effect. They also showed that by combining the hydrogen peroxide with the diode laser it can not only improve the whitening effect but also protects the changes that take place in the enamel structure compared to the treatment accomplished without laser [10].

The review carried by De Moor et al. showed that from all bleaching wavelengths the diode wavelengths have been the most investigated ones because of the large range of wavelengths that can be used for performing the beaching [11].

The study of Fornaini et al. showed that the variable results on the dental bleaching procedures can be explained by considering that the effects of

whitening depend on various factors, such as the chromophore, the nature of the enamel and the wavelength [12].

Our study brings a plus in the research field because we used an original gel. This research is useful also in the clinical part after testing this gel also on human teeth. Commercial whitening products are very expansive, our original gel once introduced in clinical use will be easy to access for our patients. This is in accordance with the study conducted by Berger et al. [13].

A big number of studies were performed on bovine teeth because it is difficult to obtain human teeth, the source and age of the collected teeth are difficult to be controlled, they are small and have a curved surface that limit some specific tests and also because of the infection hazard. Another problem refers to the ethical requirements of their use. Bovine teeth are easily obtained in large quantities, they are in a good condition and have more uniform composition. The bovine teeth have been suggested as a possible substitute for human teeth for experiments because they have similar chemical and physical properties [14,15].

Yasen et al. showed in his review the advantages of using bovine teeth as a substitute to human teeth [16].

In 2009, Attia et al. demonstrated in an in vitro study that the bovine and human substrates behave similar while undergoing a bleaching process [17].

Further studies are necessary and are being conducted in order to confirm our theses and to define the interaction between the substances used for staining the teeth, the enamel, the gel and it's interaction with the laser.

CONCLUSIONS

Our research demonstrated that the use of chromophore in the experimental gel created by us had a better bleaching effect compared to the same gel without chromophore during laser-assisted bleaching procedures on bovine teeth.

Effects produced by using the lasers depend on two substances, the one that made the coloration and the one with which the bleaching process was made. This experimental trial demonstrates the action of lasers in influencing the bleaching result.

For the a* parameter representing the red-green contrast we observed that the variation of the colour is not depending on the modifications on the red-green axis.

For the b* parameter that gives the value for the yellow-blue contrast for batch I, the batch without chromophore, we did not achieve a significant colour change.

During the measurement of T2 that represented the measurement after the staining process the chromophore prevented the modification of b* according to the whitening gel without chromophore.

The variation of luminosity (L*) is not affected by the presence or absence of the chromophore in the gel. The modification of the parameter luminosity it is due strict to the combination of the whitening gel and the diode laser.

EXPERIMENTAL SECTION

We designed a case control study conducted on bovine teeth. The research was approved by the Ethical Committee of "Iuliu Hatieganu" University of Medicine and Pharmacy, Cluj Napoca.

Eight bovine teeth were selected. These types of teeth are very well suited for the spectrophotometric evaluation of colour, because of their large flatness and uniform composition compared to the human teeth.

The extracted bovine teeth were collected from a slaughter house, professionally cleaned (using Satelec P5 Newtron XS) and stored in saline solution.

For the tooth colour measurements we used a Vita Easy Shade Spectrophotometer, that uses the CIEL*a*b* evaluation, model that was proposed by the Commission International de l'Éclerage [18].

The teeth were stained by immersing them for 14 days in a black tea solution that was prepared using three bags of tea 1,7 gram/bag (Lipton Black Tea) in 250 ml of boiling water. After that the shade of the teeth was determined and this measurement represented the T1 value registered the same as for the T0 value with the same spectrophotometer.

Two gel samples were prepared: a reference sample (I) which contained propylene glycol, hydrogen peroxide (38 %), 1.1 % fluoride and 3 % potassium nitrate and a sample (II) which contained additionally methylene blue acting as a chromophore agent.

Both salts, ammonium fluoride (0.11 g) and potassium nitrate (0.3 g) were dissolved in distilled water and a certain concentration of hydrogen peroxide (35 %, ρ=1.13 g/cm^3) solution (3.36 ml) was added for the prepared saline solution. After complete dissolution of the solid component, propylene glycol was added (6.64 ml) to the prepared solution and left to react under magnetic stirring at room temperature for 1 h, until the solution was transformed in a semisolid gel. The gels were prepared by courtesy of dr.Oana Onija.

We divided the teeth in a control (batch I) and a study one (batch II). The teeth from the control batch were kept for 30 sec in the original gel without chromophore and the ones from the study batch in the gel with

chromophore. After that teeth from both batches underwent laser irradiation with continuous wave, using a diode laser (980nm, model Ceralas D15, Ceramoptec, Jena, Germany) for another 30 sec at 50 W.

The shade was determined after the irradiation and the measurement recorder as T2 value as described for the T0 and T1 with the same spectrophotometer.

The difference in color between the different recordings was calculated and obtained by applying the specific formulas [19].

The ΔE^* value represents the shade variation, ΔE^*_1 represents the shade variation between T1 and T0, ΔE^*_2 the shade variation between T2 and T0 and ΔE^*_3 the shade variation between T2 and T1.

The luminosity variation is represented by the ΔL^* value. For the three measurements of the color of the teeth we have ΔL^*_1 representing the absolute value of the difference between luminosity in stage T1 and in stage T0, ΔL^*_2 - the absolute value of the difference between luminosity variation between in stage T2 and in stage T0 and ΔL^*_3 - the absolute value of the difference between luminosity variation between in stage T2 and in stage T1.

All collected values were introduced in an Excel table and all the data collected was statistically analyzed.

Statistical indicators -Elements of descriptive statistics have been calculated and the data was presented using indicators of centrality, location and distribution.

Statistical analysis- Shapiro-Wilk test was used for testing the normal distribution. For data following a normal distribution, Student's *t*-test was used, while for non-normally distributed data, non-parametric tests such as Mann-Whitney (U) or Wilcoxon signed-rank were used. For the analysis of more than two samples, ANOVA or Kruskal-Wallis tests were used. The significance level was $\alpha = 0.05$ (5%), 0.01 (1%) or 0.001.

To measure the statistical dependence between two variables the Pearson (r) correlation coefficient or the Spearman's rank correlation coefficient (rho) were used. For the degree of association we used the Colton empirical rules.

Statistical analysis was performed using StatsDirect v.2.7.2 software, OpenEpi v.3.03 online software and the Excel application (from Microsoft Office 2010 suite).

ACKNOWLEDGMENTS

Dr. Bordea Ioana Roxana is a fellow of the POSDRU grant no.159/1.5/S/138776 entitled: "A collaborative institutional model for transferring biomedical scientific research to clinical practice-TRANSCENT".

REFERENCES

1. B. Touati, D. Nathonson, P. Miara, “Esthetic Dentistry and Ceramic Restoration”, Martin Dunitz Ltd, London, **1999**, chapter 6.
2. N. Lunardi, A. Correr, A. Rastelli, D. Lima, R. Consani, *Journal of Clinical and Experimental Dentistry*, **2014**, *6*, e 321.
3. J.F. Bortolatto, T.C. Trevisan, P.S. Bernardi, E. Fernandez, L.N. Dovigo, A.D. Loguercio, *Lasers in Medical Science,* **2016**, *1*, 1.
4. S.E.A. Camargo, P.E. Cardoso, M.C. Valera, M.A.M. de Araujo, A.N. Kojima, *The European Journal of Esthetic Dentistry*, **2009**, *4*, 82.
5. R. Blankenau, R.E. Goldstein, V.B. Haywood, *Compendium continuing education dentistry,* **1999**, *20*, 781.
6. J.W. Baik, F.A. Rueggeberg, F.R. Liewehr, *Journal of Esthetic and Restaurative Dentistry*, **2001**, *13*, 370.
7. K. Luk, L. Tam, M. Hubert, *Journal of the American Dental Association*, **2004**, *135*, 194.
8. S.N. Anaraki, S. Shahabi, N. Chiniforush, H. Nokhbatolfoghahaei, H. Assadian, B. Yousefi, *Lasers in Medical Science*, **2015**, *30*,1013.
9. M.M. Abdelfattah*, Journal of Medicine and Medical Sciences*, **2014**, *5*, 230.
10. J.H. Son, J.H. An, B.K. Kim, I.N. Hwang, Y.J. Park, H.J. Song, *Journal of Dentistry*, **2012**, *40*, 941.
11. R.J.G. de Moor, J. Verheyen, P. Verheyen, A. Diachuk, M.A. Meire, P.J. de Coster et al., *The Scientific World Journal*, **2015**, *2015*, 1.
12. C. Fornaini, G. Lagori, E. Merigo, M. Meleti, M. Manfredi, R. Guidotti et al., *Lasers in Medical Science*, **2013**, *28*, 1.
13. S.B. Berger, L.E.S. Soares, A.A. Martin, G.M.B. Ambrosano, C.P.M. Tabchoury, M. Giannini, *Brazilian Journal of Oral Sciences*, **2014**, *13*, 22.
14. F. Al Hano, M. Nayif, *Journal of Oral Research*, **2013**, *1*, 6.
15. T. Dostalova, H. Jelinkova, D. Housova, J. Sulc, M. Nemec, M. Miyagi et al., *Brazilian Dental Journal*, **2004**, *15*, SI 3.
16. G.H. Yassen, J.A. Platt, A.T. Hara, *Journal of Oral Science*, **2011***, 53*, 273.
17. M.L. Attia, F.H.B. Aguiar, P. Mathias*, American Journal of Dentistry*, **2009**, *22*, 175.
18. CIE (Commission Internationale de l’Eclairage). Colorimetry - technical report. CIE Pub, Vienna, **2004**.
19. S. Chu, A. Devigus, A. Mielezsko, "Fondamental of colour” Quintessence Book, Hanover, **2004**, chapter 3.

STUDIA UBB CHEMIA, LXI, 2, 2016 (p. 225-238)
(RECOMMENDED CITATION)

CONSIDERATIONS ON THE RELATIVE EFFICACY OF ALUMINUM SULPHATE VERSUS POLYALUMINUM CHLORIDE FOR IMPROVING DRINKING WATER QUALITY

ELENA CICAL[a,b], CRISTINA MIHALI[b], MIRCEA MECEA[a,b], ANCA DUMUŢA[b], THOMAS DIPPONG[b*]

ABSTRACT. This study presents the evolution of specific parameters of raw water quality from the Strâmtori-Firiza Lake, which is the raw water source of the water plant in Baia Mare town, Romania. Parameters such as temperature, turbidity, oxidability were recorded over a four years interval. A comprehensive database on the evolution of these water parameters was thus created showing the tendency of these parameters across time. The possible correlations among the parameters were investigated. Positive correlations were found for oxidability and Al content and also for turbidity and oxidability. Temperature and turbidity were found to be highly variable (2-17°C, 3-53 NTU) across seasons. In order to improve the turbidity of treated water, two coagulants were tested: basic polyaluminum chloride (PAC) and aluminum sulphate (SA) evaluating the efficiency of the two treatment methods. While the traditionally used aluminum sulphate was found to be effective only when the temperature and turbidity were high: temperature >10ºC, turbidity >10 NTU (nephelometric turbidity unit), PAC emerged as an efficient clarifying agent even at low temperature and turbidity.

Keywords: *treatment, drinking water, polyaluminum chloride, coagulation*

INTRODUCTION

The quality of raw water sources used for drinking water production must comply with strict requirements [1,2]. High quality drinking water is essential for optimal survival of human beings [3]. There are some important issues related to the drinking water sources: increasing of drinking water demand, shrinking water resources, more stringent water quality goals,

[a] *S.C. Vital S.A., 21 Gheorghe Sincai Street, 430011, Baia Mare, Romania*
[b] *Technical University of Cluj Napoca, North University Center of Baia Mare, 62A Dr. Victor Babeş Street, 430083, Baia Mare, Romania*
[*] *Corresponding author: dippong.thomas@yahoo.ro*

concerns related to the water disinfection by-products [4,5] and the presence of the organic micropollutants in drinking water sources and as well as in finished drinking water [6,7,8].

Aiming to provide high quality drinking water brings about huge challenges and guides the evolution of water supply systems [9,10,11]. The main source of raw water for drinking purposes is surface water. Lake water is preferred as a source for drinking water production because usually it contains less suspended and colloidal materials and its temperature is more constant than that of river water [12].

Several natural phenomena generate high turbidities of the raw water, leading to large amounts of colloidal substances. Such phenomena include melting of snow, alluvial deposits from the lake surrounding versants, abundant rainfall, lake water destratification and gathering of the mud deposited on the lake bottom during the time periods when the lake volume is low.

These colloidal substances that contribute to turbidity have the specific gravity similar to water and practically stay in suspension for a long time [13]. This phenomenon is due to their stability in aqueous solutions. It consists of the formation of a layer having electric charges with the same sign around these colloidal particles which determines them to repel each other, so their deposition is delayed for a long time or doesn't happen [14].

Due to the complex and highly variable physical and chemical composition and of the particularities of each raw water source, the problem of water treatment and the use of an efficient coagulant is not an easy one. Systematic studies should be conducted in the laboratory as well as at industrial scale [15]. The most commonly used coagulation agents for water treatment are aluminum and iron compounds, used especially as chlorides and sulphates [16].

The aluminum sulphate having the chemical formula $Al_2(SO_4)_3$* $18H_2O$ and containing 8,1 % Al, is an efficient coagulant in most cases, but in the case of natural water with low turbidities, temperatures and alkalinity, the results are not satisfactory due to low flocculation velocities [17]. Polyaluminum chloride (PAC) represents an alternative product for aluminum sulphate used in the treatment of residual and drinking water [18,19]. PAC is composed of polymers having different dimensions which contain aluminum ions bound by oxygen atoms [20]. The basic polyaluminum chloride is an acid product in a liquid form which can be dosed in diluted solution in the installation.

The Strâmtori-Firiza storage lake is a part of the Runcu Firiza hydrotechnical system and is currently the main water supply for Baia Mare city. Raw water is treated in the water plant of the organization Vital SA. Baia Mare. The quality of raw and drinking water is monitored in the laboratory of the plant. The water treatment plant also includes an industrial pilot where new technologies of water treatment could be tested. Several analyses are

performed in the central laboratory of SC Vital SA following the water quality control at its source, the potable water indicators, the monitoring program of the water quality in Baia Mare municipality and in county agencies. In addition, research studies aim to optimize the quality of drinking water whatever is the quality of raw water (even with high turbidity and low temperature) and to test new techniques of water treatment [12].

The water quality of the storage lake is influenced by the weather, having a pronounced seasonality. The hydrological and climatic parameters and also the water dynamics are ecological factors that impact the organisms living in or around the lakes [21]. The raw water quality was monitored during the 2011-2014 period.

Parameters of interest are temperature, turbidity, water oxidability and aluminum content. Temperature significantly influences the stages of the coagulation process by enhancing the rate of the hydrolysis process of aluminum compounds and diminishing the rate of their adsorption [22,23].

Turbidity is one of the most important indicators for the quality of drinking water and is a measure of its clarity [24]. Turbidity can provide food and protection for microorganisms. If not removed, turbidity can cause the multiplication of the pathogenic microorganisms in the distribution system, leading to waterborne disease outbreaks [25].

Water oxidability quantifies the amount of organic matters present in a liter of water that can be easily oxidized using a chemical oxidant such as potassium permanganate ($KMnO_4$). In aquatic ecosystems, such as a storage lake, natural organic matter comprises a heterogeneous mixture of organic compounds including high molecular compounds and small molecular substances: proteins, amino acids, lipids, polysaccharides and biopolymers [26-28].

Aluminum can occur in different forms in water: hydroxide species, colloidal polymeric solutions and gels, and precipitates. Also aluminum forms complexes with organic compounds like humic or fulvic acids [25].

Aluminum coagulants are widely used in water treatment plants to remove turbidity and the organic dissolved substances. Excessive aluminum in water is associated with adverse effects on human health and thus water plants concentrate their efforts towards controlling its concentration [22].

We created a comprehensive database that includes the variation of temperature, turbidity, water oxidability and aluminum content in order to establish the range of values for the registered parameters during four years, their tendencies across time and to investigate the possible correlation among the parameters. This database is useful in establishing the optimal coagulant doses for the treatment of raw water with varied compositions (oxidability, turbidity, pH, residual Al content etc.).

We aimed to find the best treatment method across all seasons and to maximize the quality of the drinking water in the treatment plant taking into account the significant variation of the parameters of raw water. The Strâmtori-Firiza storage lake is a water source with high turbidities and low temperatures during six months of the year when water treatment using aluminum sulphate was not efficient. The implementation of polyaluminum chloride as an alternative coagulation reagent in the case of Strâmtori Firiza raw water with highly variable temperature and turbidity needed extended studies in order to establish the optimum reagent doses. We performed a comparison with the coagulation method based on aluminum sulphate in the context of the variability of water parameters.

RESULTS AND DISCUSSION

This study was elaborated based on a mathematical calculation and on a database which monitors the values determined for the analyzed parameters. The monthly average values of the main parameters: temperature, turbidity, oxidability and aluminum content and their variation domains were determined in order to establish the evolution of raw water quality in the period 2011-2014. These data are presented in figures 1-3.

The monthly average turbidity (Fig. 1) of the raw water varied in the range 3.0-53.0 NTU according to the seasons: turbidities below 7.0 NTU are specific to winter periods while the ones below 20 NTU to the spring-autumn period. In particular, 2012 presented abundant rainfall and floods and as consequence higher turbidity levels were registered (about 50 NTU in May and around 30 NTU in August and September).

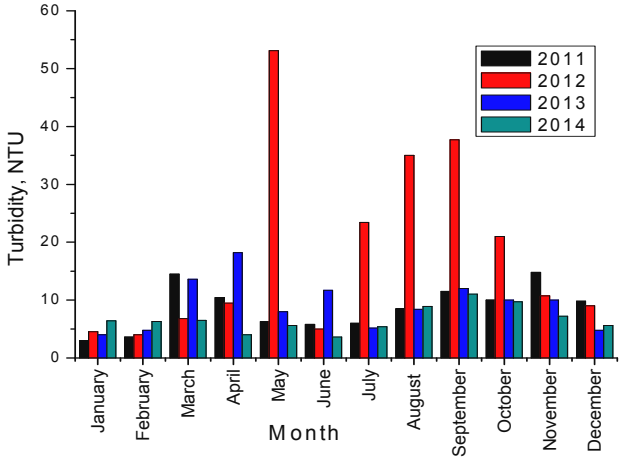

Figure 1. Average turbidity of the raw water during the period of the study

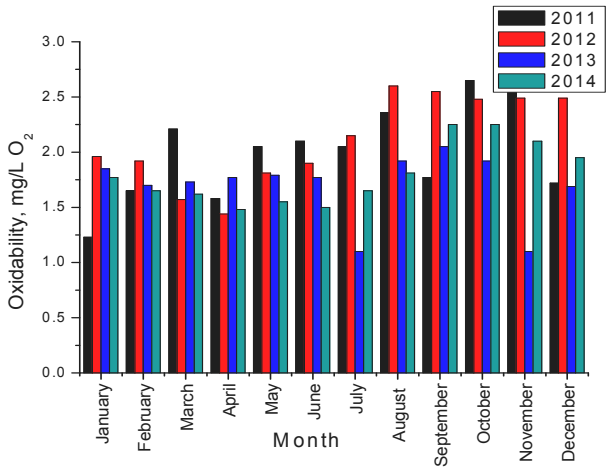

Figure 2. The average oxidability of the raw water during the period of the study

Figure 2 shows the dynamics of the oxidability parameter. During the period of the study, the organic matter that is globally quantified by the oxidability had monthly average values between 1.20 – 2.50 mg/L of O_2, with low values in the months characterized by low turbidity and with high values in the months of high raw water turbidity. Such a correlation between turbidity and oxidability is expected because the turbidity is higher especially in rainy days when there are leakages from the floods that flow in the lake from the versants that surround Strâmtori storage lake. The floods carry over the soil containing humic acids causing the increase of organic matter in raw water quantified by oxidability. Recent studies revealed the growing tendency of the natural organic matter content in the raw waters both in surface and ground waters [29].

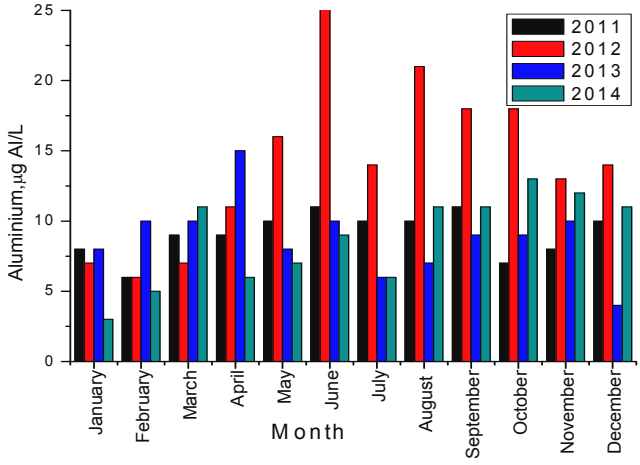

Figure 3. The average variation of aluminum in raw water during the studied period

Such two coagulation agents containing aluminum used for water treatment lead to differential increases of the aluminum content in the resulting drinking water. While research in this field is controversial, some studies claim that long-term excessive exposure to aluminum is related to the risk of Alzheimer's disease and dementia [30].

All other parameters equal, it is important to choose the coagulant agent that will result in the minimum residual aluminum content. The upper limit of aluminum content is set by Romanian legislation to 0.2 mg/L.

Table 1 shows the yearly average values and standard deviation of the studied parameters.

Table 1. The yearly average values of the main characteristics of raw water

Year/ Parameter	Temp., °C	Turbidity, NTU	Oxidability, mg/L O_2	Al, mg/L
2011	8.68±3.87*	8.62±3.81 *	2.01±0.45 *	9.17±1.53 *
2012	9.20±5.39	18.31±16.03	2.11±0.40	14.17±5.86
2013	9.03±5.24	9.22±4.27	1.70±0.30	8.83±2.69
2014	8.27± 5.47	6.68±2.21	1.80±0.28	8.75±3.22

*standard deviation of the average value

Table 2. Correlation coefficients between the studied parameters of raw water during the four years (Temp-temperature, T-turbidity, O-oxidability, Al content-Al)

	Temp	T	O	Al
Temp	1			
T	0.340	1		
O	0.340	0.376	1	
Al	0.411	0.578	0.426	1

Positive correlation coefficients were found for turbidity and oxidability and also for oxidability and Al content. These correlations indicate the likely sources of turbidity: organic matter derived from the runoff. The runoff contains both organic matter and Al in soluble and colloidal forms. The highest correlation coefficient was found for Al content and turbidity. Therefore it is a worthwhile pursuit to find an efficient way to reduce the Al dose of the coagulant by finding a coagulant that requires a lower Al dose to ensure a low turbidity, instead of good turbidity.

In order to obtain a better quality for drinking water (low turbidity and low aluminum content) basic polyaluminum chloride was tested during a month and compared with the classical coagulant aluminum sulphate.

Figures 4 and 5 present the comparison of the optimal aluminum doses experimentally obtained in the laboratory for the two coagulants: aluminum sulphate (SA) and basic polyaluminum chloride (PAC) and the calcium hydroxide doses corresponding for achieving the optimal precipitation pH for raw water turbidities of 10.0-200.0 NTU.

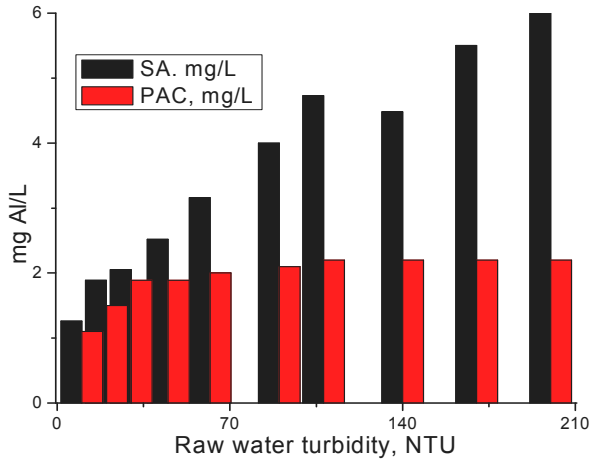

Figure 4. Optimal doses of aluminum depending on the turbidity of the raw water (coagulants: aluminum sulphate SA and polyaluminum chloride PAC)

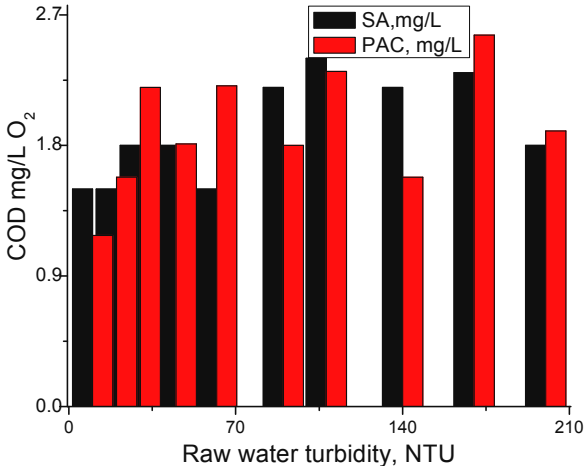

Figure 5. The treated water oxidability at optimal doses of Al depending on the turbidity of the raw water (aluminum sulphate SA, polyaluminum chloride PAC)

By using aluminum sulphate the values of the optimal doses are in the range of about 2- 4 mg Al/L being higher compared with the ones obtained in the case of basic polyaluminum chloride which are around 1 - 2 mg Al/L. Both coagulants need alkalinization with $Ca(OH)_2$ to obtain an adequate pH. The results of water quality monitoring during 2011-2014 period show that, except 3-4 months per year, when high values were registered for turbidity and oxidability, the quality of this source is appropriate to be used as drinking

water source considering the main parameters. In order to evaluate the performances of the two coagulants, the characteristics of the treated water (turbidity) were compared with the optimal coagulant reagent expressed as Al doses and OH^- doses. In the case of PAC lower reagent doses were necessary for both Al and OH^-. Thus, at low turbidity the doses of reagent used for PAC were reduced with 30-50 % compared with those used for aluminum sulphate while at high turbidity the aluminum dose for PAC was approximately half of that used for the water treated with aluminum sulphate. That means lower reagent consumption and a lower residual Al in the drinking water.

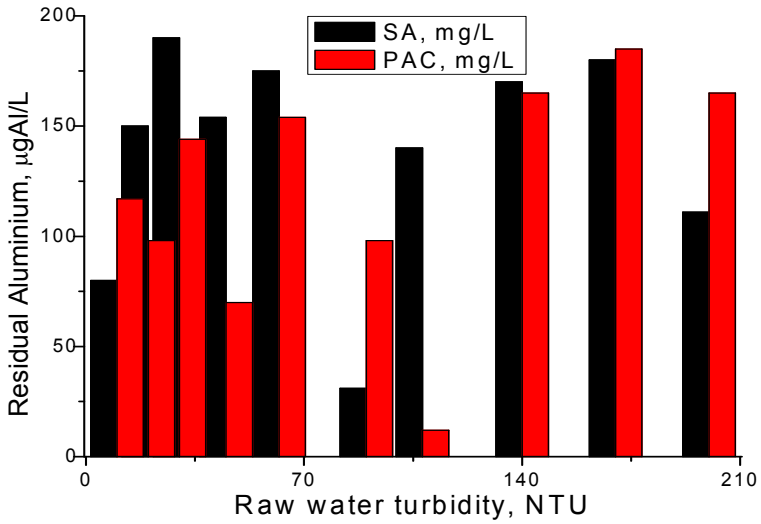

Figure 6. Residual aluminum content for treated water at optimal coagulant dose depending on the turbidity of the raw water for the two coagulation agents: SA-aluminum sulphate and PAC –polyaluminum chloride

Figure 6 shows the residual aluminum content of the treated water for different values of raw water turbidity when optimal doses of the two coagulants were used: PAC and SA. The Al residual content is lower in the case of PAC except for turbidity values higher than 170 NTU.

The turbidity of the treated water depending on the turbidity of the raw water was shown in figure 7.

It can be observed that, at the optimal doses, the remaining turbidity of the treated water has close values for the two studied coagulation reagents and these values are between 2.00 -5.00 NTU.

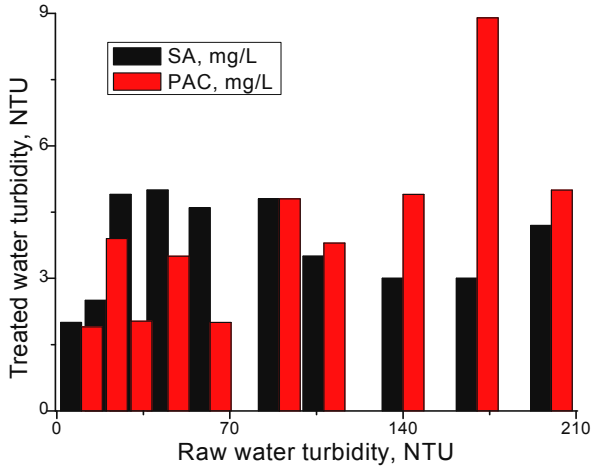

Figure 7. Influence of raw water turbidity on the treated water turbidity for the two tested coagulants

The efficiency of coagulation process is quantified by the relation Efficiency = $(T_{raw\ water} - T_{treated\ water}) * 100 * T_{raw\ water}^{-1}$ (T is the turbidity).

Raw water turbidities and potable water turbidities resulting during the study period (one month), using the corresponding doses of aluminum sulphate and polyaluminum chloride established in the laboratory for initial turbidities< 20 NTU are presented in figures 8 and 9.

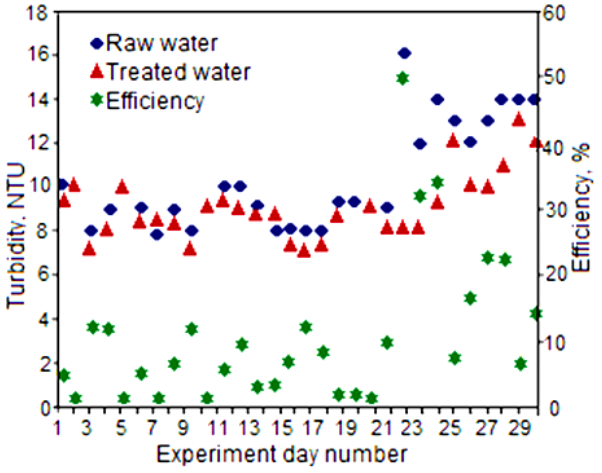

Figure 8. Raw water, potable water turbidity and the coagulation efficiency during the study period; coagulant: aluminum sulphate

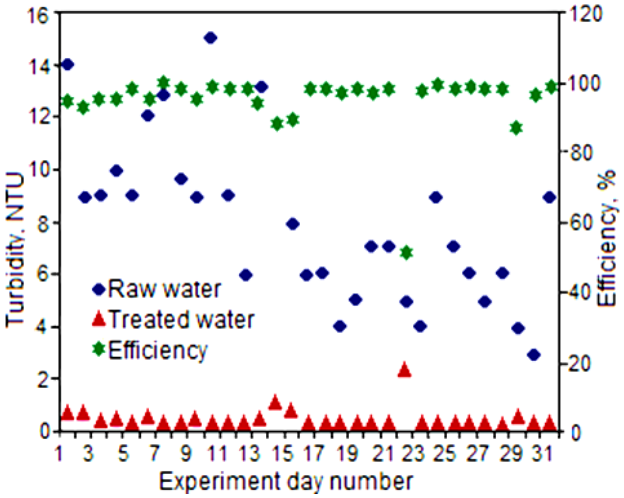

Figure 9. Raw water, potable water turbidity and the coagulation efficiency during the study period; coagulant: polyaluminum chloride (PAC)

Analyzing the data presented in Figures 8 and 9, one can observe that water treatment using basic polyaluminum chloride and calcium hydroxide presents high efficiency compared with the water treatment using aluminum sulphate and calcium hydroxide

Considering the aluminum sulphate, the low temperatures affect the rate of the hydrolysis reaction and of the flakes sedimentation due to a high water viscosity [24]. Increasing the coagulant dose (SA) and not providing the optimal conditions for the mixture process (fast for 2 minutes and slow for 15 minutes) that influences directly the flakes formation and their sedimentation, does not improve the efficiency of the coagulation-colloidal material separation process. On the other hand, the coagulation process with polyaluminum chloride and calcium hydroxide ensures high efficiency in the turbidity reduction even if the raw water shows turbidity values under 20 NTU, low alkalinity and a temperature below 10ºC because the basic aluminum polychloride is a partially hydrolyzed coagulation reagent [16].

CONCLUSIONS

The water treatment technique using aluminum sulphate and calcium hydroxide has a low efficiency, even the obtained water turbidities are in accordance with the law limit.

By using the basic polyaluminum chloride in the coagulation process the treatment efficiency was optimized and all the turbidities were below the law limit.

The originality and the importance of the study consist in the solving of an important problem: the establishment of the optimal doses of polyaluminum chloride for water treatment with different qualities and a high variability across the seasons.

The study brings new data about the seasonal variability of lake water and demonstrates that by using polyaluminum chloride as coagulant agent, drinking water with improved quality characteristics (high clearness and low residual aluminum content) can be obtain even for raw water with low alkalinity, low temperature and turbidity.

By using polyaluminum chloride as coagulant reagent high efficiencies in the turbidity reduction were obtained.

Future studies will focus on the treatment of the water with very high turbidity using polyaluminum chloride and polymeric organic flocculants.

EXPERIMENTAL SECTION

All the reagents used in chemical analysis were of analytical degree. Aluminum sulphate was a commercial product with 15.3 % of Al_2O_3. The polyaluminum chloride (PAC) used in the experiments was a commercially available product containing 18,9 % Al_2O_3, a basicity of 83% and density of 1.27 Kg/dm^3.

Sampling and analysis of raw water

The samples of raw water were taken at the entrance of the water treatment plant. Turbidity, oxidability and aluminum content of raw water were determined according to the Romanian standard methodology, adapted after the EU methodology.

Samples were taken daily and the month average values of the studied indicators were calculated and registered. Turbidity was measured using a turbidimeter (model 350 IR, WTW). The water oxidability was measured using the standard volumetric method.

To determine the aluminum content of water, a molecular absorption spectrophotometer Hach DR 2000 was used.

Coagulation tests

We assessed the efficiency of the coagulation process using as chemical reagents PAC and calcium hydroxide in comparison with the conventional aluminum sulphate and calcium hydroxide. Studies were carried out both in the laboratory of the water plant of SC Vital and in the microfactory (industrial pilot).

The experimental studies carried out in the laboratory took place during a 6 months period of time with the main objective of determining the doses and the optimal coagulation conditions for aluminum sulphate and for PAC. We used raw water with turbidity between 10.0 - 90.0 NTU. In order to obtain the optimum coagulation pH, the calcium hydroxide was used as a pH correction reagent. The determination of the optimal coagulation conditions was carried out using the „Jar-test" method.

The doses of the two coagulants used, were 1.51 – 4.00 mg Al/ L for aluminum sulphate and 1.10 - 2.20 mg Al/ L for PAC, correspondingly added to raw water samples of 1 liter. These samples were stirred rapidly (140 rotation/ min) for 2 minutes and slowly (40 rotation/ min) for 15 minutes. After 30 minutes of sedimentation, samples of the treated water were taken from the supernatant and the parameters of turbidity, oxidability and residual aluminum were determined. The optimum dose was established depending on the turbidity of the treated water. The studies carried out on the industrial pilot (microfactory) took place during the technological probation of the installation. The optimal coagulation doses experimentally obtained in the laboratory for the aluminum sulphate and for the basic polyaluminum chloride were applied in the technological flux depending on the raw water turbidity during the study period.

The water treatment technique using aluminum sulphate and calcium hydroxide was studied for one month and the water treatment technique using the basic polyaluminum chloride and calcium hydroxide was also studied for one month.

The technological flux applied on the industrial pilot consists of the following stages: collecting raw water, mixing water with the coagulation reagents in the water mixture room, coagulation process finishing in the reaction room combined with the lamellar decantation device, water filtration using under pressure filters, water disinfection using sodium hypochlorite and the potable water storage. Practically, the behavior of the two studied coagulants on the technological flux was followed and also their performances on obtaining turbidity values according to the Romanian legislation concerning drinking water quality [31] were registered and compared in the dynamic regime.

REFERENCES

1. M. Kyncl, *Carpathian Journal of Earth and Environmental Science*, **2014**, *9*, 179.
2. X. Xue, M.E. Schoen, X.(C) Ma, T.R. Hawkins, N.J Ashbolt, J. Cashdollar, J. Garland, *Water Research*, **2015**, *77*, 155.
3. R.E.S Bain, J.A. Wright, E. Christenson, J.K. Bartram, *Science of the Total Environment*, **2014**, *490*, 509.
4. J.P. Ritson, M. Bell, N.J.D. Graham, M.R. Templeton, E. Richard, R.E. Brazier, A. Verhoef, C. Freeman, M. Joanna, J.M. Clark, *Water Research*, **2014**, *67*, 66.
5. G.C. Woods, R.A. Trenholma, B. Hale, Z. Campbell, E.R.V. Dickenson, *Science of the Total Environment*, **2015**, *520*, 120.
6. J.T. Alexander, F.I. Hai, T.M. Al-Aboud, *Journal of Environmental Management*, **2012**, *111*, 195.
7. A. Székács, M. Mörtl, G. Fekete, A. Fejes, B. Darvas, M. Dombos, O. Szécsy, A. Anton, *Carpathian Journal of Earth and Environmental Sciences*, **2014**, *9*, 47.
8. A.M. Kennedy, A.M. Reinert, R.U. Detlef, D.R.U. Knappe, I. Ferrer, R.S. Summers, Water Research, **2015**, *68*, 238.
9. D. Polomčić, B. Hajdin, M. Ćuk, P. Papić, Z. Stevanović, *Carpathian Journal of Earth and Environmental Sciences*, **2014**, *9*, 97.
10. E. Cical, M. Mecea, G. Vatca, C. Mihali, N. Duteanu, *Carpathian Journal of Food Science and Technology*, **2011**, *3*, 1.
11. S.D. Faust, M.A. Osman, "Chemistry of Water Treatment", 2nd edition CRC Press, Stonenham, **1998**, chapter 5.
12. X. Yuan, L. Zhang, J. Li, C. Wang, J. Ji, *Catena*, **2014**, *119*, 52.
13. F.E. Aboussabiq, I.K. Yettefti, J. Amine, M.M. Sicias-Viciana, O. Assobhei, *Carpathian Journal of Earth and Environmental Science*, **2014**, *9* (1), 33-34.
14. P. Jarvis, B. Jefferson, S.A. Parson, *Water Research*, **2006**, *40*, 2727.
15. T.K. Trinh, L.K. Kang, *Chemical engineering research and design*, **2011**, *89*, 1126.
16. M. Vaananen, L. Kupiainen, J. Ramo, A. Sarpola, J. Tunskanen, *Separation and Purification Tehnology*, **2012**, *86*, 242-247.
17. P. Niquette, F. Monette, A. Azzouz, R. Hausler, *Water Quality Research Journal of Canada*, **2004**, *39* (3), 303–310.
18. Z.M. Liu, Y.M. Sang, Z.G. Tong, Q.H. Wang, T.G. Sun, *Water Environ. J*., **2012**, *26* (1), 85-93.
19. E. Cical, G. Oprea, C. Mihali, L Ardelean, G. Burtică, L. Lupa, *Revista de chimie*, **2008**, *59*, 1030.
20. E. Vulpașu, E. Dineț, *Rom Aqua*, **2009**, *64*, 16.
21. A. Mihu-Pintilie, G.Romanescu, C. Stoleriu, *Carpathian Journal of Earth and Environmental Sciences*, **2014**, *9*, 113.
22. M. Guida, M. Mattei, C.D. Rocca, G. Melluso, S. Meriç, *Desalination*, **2007**, *211*, 113.
23. M. Kimura, Y. Matsui, K. Kondo, T.B. Ishikawa, T. Matsushita, N. Shirasaki, *Water Research*, **2013**, *47*, 2075.
24. F.R. Spellman, "Handbook of Water and Wastewater Treatment Plant Operations", Second Edition, CRC Press., **2008**, chapter 16, chapter 20.

25. World Health Organization, Guidelines for Drinking-Water Quality, fourth edition, **2011**, chapter 4.
26. O. Gibert, B. Lefèvre, A. Teulerc, X. Bernat, *Journal of Water Process Engineering*, **2015**, *6*, 64.
27. A. Scheili, M.J. Rodriguez, R. Sadiq, *Science of the Total Environment*, **2015**, *508*, 514.
28. W. Wang, W. Wang, Q. Fan, Y. Wang, Z. Qiao, X. Wang, *Chemical Engineering Journal*, **2014**, *256*, 137.
29. A. Matilainen, M. Vepsäläinen, M. Sillanpää, *Advances in Colloid and Interface Science*, **2010**, *159*, 189.
30. S. Meshitsuka, A. David, D.A. Aremu, T. Nose, *Psychogeriatrics*, **2002**, *2*, 263.
31. ***, The law 458/2002 regarding the quality of drinking water, *Official Monitor*, **2002**, *268*.

STUDIA UBB CHEMIA, LXI, 2, 2016 (p. 239-248)
(RECOMMENDED CITATION)

THE STUDY OF PIT AND FISSURE SEALANTS CONCERNING WATER SORPTION AND SOLUBILITY

DANIELA CORNEA[a*], LAURA SILAGHI-DUMITRESCU[b], ROBERT BALAZSI[c], RADU OPREAN[d], DIANA DUDEA[a], MĂRIOARA MOLDOVAN[b]

ABSTRACT. Improved dental materials are a requirement in these modern times, because of the highly percent of dental decay found at children. Four commercial pit and fissure sealants have been studied in respect of water sorption and solubility (1, 3, 7 and 14 days).These measurements prove the stability of a material, as well as the adhesion to enamel and the resistance to wear. The materials taking into account are two resin- based sealants - Fotoseal® (Babeş-Bolyai University, Raluca Ripan Chemistry Research Institute), Fissurit FX® (VoCo), one gass-ionomer - Fuji Triage® (GC Fuji) and one compomer - Dyract Seal® (Dentsply). The statistical analysis used a Mixt ANOVA design, with the significance level set at $p \leq 0.01$. Firstly, there were analised the differences between the days of measurement, without taking into account the material type. Secondly, there were examined the differences between materials and finally, the interaction between material type and day of measurement. We also calculated the magnitude of the clinical effect of material type, on each of the days of measurement. Differences in chemical composition determine a modified behavior of these materials. The results showed that Fissurit FX had the lowest values of water sorption and solubility, closely followed by Fotoseal. Dyract Seal had higher values. In the same time, Fuji Triage showed the highest rates for water sorption and a fluctuant behavior concerning solubility, with increased level in the first day of measurement, decreased values in the next days (3, 7) and another small enhancement in the last day of measurement (14).

Keywords: *dental materials, composite resin, glass-ionomers, compomer, water sorption, solubility*

[a] *University of Medicine and Pharmacy Iuliu Hatieganu, Faculty of Dental Medicine, 32 Clinicilor Str., RO-400006, Cluj-Napoca, Romania*
[*] *Corresponding author: danico_81@yahoo.com*
[b] *Babeş-Bolyai University, Raluca Ripan Chemistry Research Institute, 30 Fantanele Str., RO-400294, Cluj-Napoca, Romania*
[c] *Babeş-Bolyai University, Faculty of Psychology,7 Sindicatelor Str., RO-400029, Cluj-Napoca, Romania*
[d] *University of Medicine and Pharmacy Iuliu Haţieganu, Faculty of Pharmacy,4 Louis Pasteur Str., RO-400349, Cluj-Napoca, Romania*

INTRODUCTION

The chemical composition is closely correlated with the clinical behavior of a dental material. From 1962, since Bowen discovered the resin bis-GMA (2,2-bis(4-(2'-hydroxy-3'methacryloyloxy-propoxy)phenyl)propane), the development of dental composites dedicated to adhesive dentistry grew a lot.

Among the methods used in preventive dentistry, pit and fissure sealing is frequently indicated on both primary and permanent teeth, aiming to block the dental plaque retention in deep, narrow zones on the dental surface and to minimize dental decay initiation. Most pit and fissure sealants are composite resins, having an organic fraction based on bis-GMA, UDMA (urethane dimethacrylate) or TEGDMA (triethylene glycol dimethacrylate) or other dimethacrylates, small inorganic particles of fused silica, quartz, barium, strontium or zirconium silicates as fillers, and a separation interface, silane [1].

Before Bowen's achievement, Buonocore introduced in 1955 the enamel etching technique, with orthophosphoric acid 35-40% [2,3], that allows for mechanical and chemical retention of the composite resins to the dental enamel [4]. The setting is achieved through a polymerization reaction and the result is a polymeric matrix. The polymerization can be initiated by a radiation- UV or visible light, which acts on aromatic ketones, or a chemical reaction between benzoil peroxide (initiator) and tertiary amine (activator), resulting free radicals [1,5]. Dental resins used as pit and fissure sealants have less particles than composites used for fillings, because they need a low viscosity and the capacity to flow and penetrate the small spaces on the dental surfaces. Bis-GMA has a high viscosity, which explain for the addition of a diluent in the form of either methyl methacrylate (MMA), glycol dimethacrylate (GDMA) or triethylene glycol dimethacrylate (TEGDMA).

However, the decreased filler percentage is responsible for polymerization shrinkage and a low elasticity module [6,7].

Glass-ionomer cements, a different group of materials used in preventive dentistry, were introduced in 1972, by Wilson and Kent and they contain polyacrylic acid, itaconic, maleic, mesaconic or other unsaturated acids [8]. The advantages of these materials are physical and chemical bond with the enamel, biocompatibility, fluoride releasing and ease of handling; as disadvantages, their lower retention and resistance to wear in comparison with dental composites, are of clinical relevance [9].

In 1997 a hybrid material was introduced, a composite combined with a polyacid, which was named compomer, containing strontium-alumino-fluoro-phosphor- silicate glass, highly dispersed silicone dioxide, ammonium salt of phosphoric acid modified methacrylate resin, carboxylic acid modified methacrylate resin and diethylenglycol dimethacrylate.

Other hybrid materials are resin-modified glass-ionomer cements, with improved properties than the conventional glass-ionomer cements: photo-polymerization ability, better marginal sealing, better resistance and fluoride release, less material wear and fractures [10,11].

Sorption is the penetration capacity of a liquid within the mass of the composite resins. The results are hydrolytic degradation of the bonding agent, silane, at the interface between matrix and inorganic filler, resulting in particle detachment.

Solubility is the dilution of the unreactive monomer in a solvent, effecting the dimensional stability, mechanical properties and bonding strength [12]. Water sorption and solubility are related with the chemical and dimensional stability of the resin matrix [13]. Degradation induced by water influences the clinical performances of a material and is proportionally reverse with the filler content [14]. Also, the degradation of the organic matrix depends on the conversion degree of C-C double bonds into single bonds. For that, the initiation system of photo-polymerization and the composition of the monomers are important factors [15].

Solubility and water diffusion inside the matrix are lower with the increase of the polymerization rate and density of the matrix.

The aim of this study was to compare the sorption and solubility of a local material, Fotoseal, with a commercial composite (Fissurit FX), a compomer (Dyract Seal) and a glass-ionomer (Fuji Triage). The null hypothesis is that there were no difference among the 1. water sorption and 2. solubility rates of the tested materials.

RESULTS AND DISCUSSION

In order to analyze data, we used a Mixt ANOVA design with two independent variables, the ***material type*** (Fissurit FX, Fotoseal, Dyract Seal and Fuji Triage) and the ***day of measurement*** (Day 1, Day 3, Day 7 and Day 14); the significance level was set at $p \leq 0.01$.

Results for **water sorption** are presented in table 1.

The main effect for *day of measurement* was found to be statistically significant, $F(5.36)=49.047$ (SSE=105.75, $p=0.001$, $\eta^2=.803$, where $\eta^2>0.14$ showes a major clinical effect). Post-hoc Bonferroni comparison showed statistically significant differences between Day 1 compared with Day 7 ($p<0.001$) and Day 14 ($p<0.001$), Day 3 compared with Day 7 ($p<0.001$) and Day 14 ($p<0.001$) and Day 7 compared with Day 14 ($p<0.001$).

There was a significant main effect of *material type*, $F(3. 12)=86.178$ (SSE=360.128, $p=0.001$, $\eta^2=.956$, where $\eta^2>0.14$ showes a major clinical effect), nonsignificant differences were found only between Fotoseal and Fissurit, all other pairwise comparison was found to be significant ($p<0.001$).

Table 1. Water sorption (µg/mm³) as resulted from measurements in day 1, 3, 7 and 14 for the tested materials.

	Material	Mean	Std. Deviation
Day1	Dyractseal	16.515	1.549
	Fissurit	3.576	0.728
	Fotoseal	6.18	1.487
	GC-Fuji	24.84	7.383
Day3	Dyractseal	18.072	1.498
	Fissurit	2.4575	0.957
	Fotoseal	6.642	0.288
	GC-Fuji	25.017	1.645
Day7	Dyractseal	20.477	2.463
	Fissurit	3.075	0.988
	Fotoseal	9.075	1.054
	GC-Fuji	33.8	6.041
Day14	Dyractseal	20.815	0.881
	Fissurit	3.76	0.723
	Fotoseal	8.19	0.391
	GC-Fuji	43.342	6.600

We found a significant *material type x day of measurement interaction*, $F(9.36)=21.568$ (SSE=567.11, $p=0.001$, $\eta^2=.844$, major clinical effect), meaning that the main effect of one variable is not constant regarding the level of the other variable (figure 1).

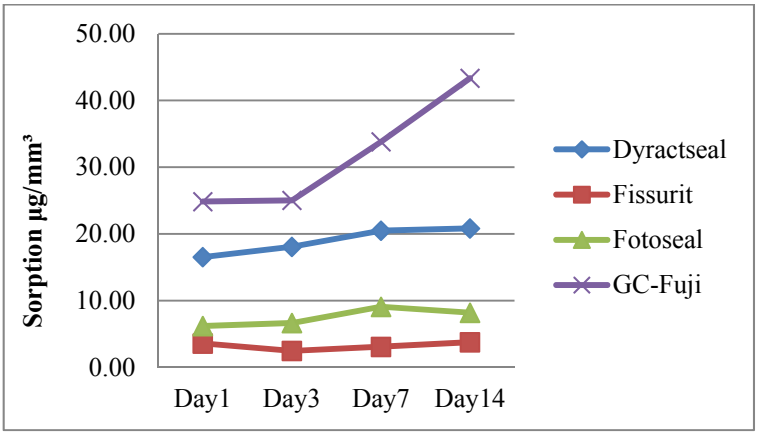

Figure 1. Water sorption for different types of material. Fissurit FX has the lowest water sorption, followed by Fotoseal, Dyract Seal and Fuji Triage.

Data collected on Day 1 showed a significant effect of *material type*, F(3.12)=25.713 (SSE=178.99, p=0.001, η^2=.865, a large clinical effect). At Day 1 we found significant differences between Fissurit and Dyract Seal (p<0.001), Fissurit and Fuji Triage (p<0.001), Fotoseal and Fuji Triage (p<0.001), Fotoseal and Dyract Seal (p<0.001).

Data collected on Day 3 illustrated a significant effect of *material type*, F(3.12)= 288.137 (SSE=17.86, p=0.001, η^2=.986, with a large clinical effect). We found significant differences between Fissurit and Fotoseal (p=0.002), Fissurit and Dyract Seal (p<0.001), Fissurit and Fuji Triage (p<0.001), Fotoseal and Dyract Seal (p<0.001), Fotoseal and Fuji Triage (p<0.001), Dyract Seal and Fuji Triage (p<0.001).

Data collected on Day 7 demonstrated a significant effect of *material type*, F(3.12)= 65.754 (SSE=133.95, p=0.001, η^2=.943, with a major clinical effect). At Day 7 the significant differences were between Fissurit and Dyract Seal (p<0.001), Fissurit and Fuji Triage (p<0.001), Fotoseal and Dyract Seal (p<0.001), Fotoseal and Fuji Triage (p<0.001), Dyract Seal and Fuji Triage (p<0.001). Only between Fissurit and Fotoseal, there were no significant differences.

Data collected on Day 14 showed a significant effect of *material type*, F(3.12)=11.939 (SSE=135.06, p=0.001, η^2=.965), with significant differences between Fissurit and Dyract Seal (p<0.001), Fissurit and Fuji Triage (p<0.001), Fotoseal and Dyract Seal (p<0.001), Fotoseal and Fuji Triage (p<0.001), Dyract Seal and Fuji Triage (p<0.001). As in Day 7, between Fissurit and Fotoseal, there were no significant differences.

Solubility measures were analyzed using the same design (table 2).

Table 2. Solubility for the tested materials (μg/mm³)

	Material	**Mean**	**Std. Deviation**
Day1	Dyractseal	-24.425	0.923
	Fissurit	-5.3875	1.465
	Fotoseal	-14.992	3.071
	GC-Fuji	-35.977	23.150
Day3	Dyractseal	-38.74	2.891
	Fissurit	-9.98	1.560
	Fotoseal	-21.372	1.086
	GC-Fuji	-18.947	11.347
Day7	Dyractseal	-41.8	5.444
	Fissurit	-14.105	0.605
	Fotoseal	-23.747	2.517
	GC-Fuji	-14.345	12.170
Day14	Dyractseal	-42.34	5.594
	Fissurit	-15.782	0.575
	Fotoseal	-27.077	1.061
	GC-Fuji	-16.51	11.861

Main effect for *day of measurement* was found to be statistically significant, F(5.36)=4.895 (SSE=567.11, p=0.006, η^2=.29, a major clinical effect). Post-hoc Bonferroni comparison, showed statistically significant differences between Day 3 compared with Day 14 (p<0.001), Day 7 compared with Day 14 (p<0.001).

There was also a significant main effect of *material type*, F(3.12)=8.242 (SSE=2574.03, p=0.003, η^2=.673, with a major clinical effect), significant differences were found only between Dyract Seal and Fissurit.

More important, we found a significant *material type x day of measurement interaction*, F(9.36)=16.639 (SSE=567.11, p=0.001, η^2=.806, a major clinical effect), meaning that main effect of one variable are not constant across the level of the other variable (figure 2).

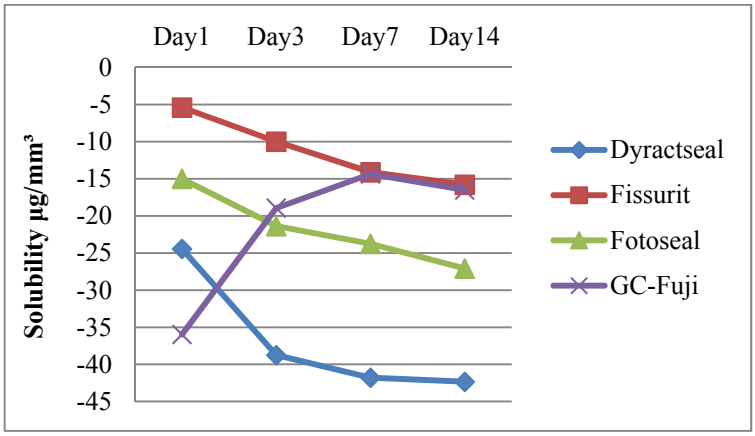

Figure 2. Solubility for different type of materials. Fissurit FX has the lowest value, followed by Fotoseal, Dyract Seal. Fuji Triage has the highest value in Day 1, then the values decrese in Day 3 and Dat 7 and increase slightly in Day 14.

Data collected on Day 1 didn't show a significant effect of *material type*, F(3.12)=4.992 (SSE=1645.17, p=0.018, η^2=.555).

Data collected on Day 3 showed a significant effect of *material type*, F(3.12)=16.452 (SSE=422.23, p=0.001, η^2=.804), with significant differences between Fissurit and Dyract Seal (p<0.001), Fotoseal and Dyract Seal (p=0.008), Dyract Seal and Fuji Triage (p=0.003).

Data collected on Day 7 illustrated a significant effect of *material type*, F(3.12)=14.659 (SSE=553.43, p=0.001, η^2=.786). There were significant differences between Fissurit and Dyract Seal (p=0.001), Fotoseal and Dyract Seal (p=0.001), Dyract Seal and Fuji Triage (p=0.001).

Data collected on Day 14 showed a significant effect of *material type,* $F(3.12)=14.185$ (SSE=520.31, $p=0.001$, $\eta^2=.780$), with significant differences between Fissurit and Dyract Seal ($p=0.001$), Fotoseal and Dyract Seal ($p=0.001$), Dyract Seal and Fuji Triage ($p=0.001$).

The first requisite for an efficient sealant is a viscosity that allows penetration into low-dimension spaces [16]. Chemically-cured sealants have usually no inorganic filler, so, the water sorption and solubility demonstrate very high levels. Photo-cured sealants are with or without inorganic filler added, but they have a low permeation rate and good physical properties, such as low levels of abrasion, heat expansion, water sorption and solubility [17]. In our study. Fissurit FX and Fotoseal, as bis-GMA based materials present lower water sorption and solubility, than Dyract Seal and Fuji Triage.

Also, because of the resin- matrix, Fissurit FX and Fotoseal have high retention rates, but in a clinical moist environment, a glass-ionomer is more suitable [18].

Other requirements for a good sealing material are: short setting time, same thermal conductivity as tooth, good bond strength with the enamel, fluoride-releasing or chemically inert, anti-cariogenic, reduced polymerization shrinkage.

Fluoride containing sealants are of two types. In the first instance, soluble fluoride is added to unpolymerized resin and after the polymerization, the salt dissolves and fluoride ions are released. In this case, the solubility and water sorption are increased. In the second case, an organic fluoride component, chemically bond to the resin, is added and enhances the fluoride release, while maintaining the physical properties of the material [9].

Fissurit FX contains fluoridel (2% NaF), wich is an inorganic component [19,20], as well as, the fluoro-silicate glass, included in Dyract Seal. This affects the physical properties, of water sorption and solubility. Fuji Triage has a high fluoride content, but a low rate of released fluoride [21,22]. For that, it has the highest water sorption and solubility, in the first day, but, also, a low cytotoxic effect.

Besides of the disadvantages, fluoride release is a very important property of glass-ionomers and resin-modified glass-ionomer cements, because fluoride ions reduce the amount of microorganisms and reinforces the structure of enamel. It also determines the clinical selection of the patients who need this type of material [10]. Two reactions occur in the curing of Dyract Seal: quick photo-initiated polymerization and slow acid-base reaction. The last one represents the basis of the continuous release of fluoride ions, an important property of Dyract Seal [23].

Water sorption has not only disadvantages. Because of the increased volume of the material, it contributes to closure of the microscopic gaps resulted from polymerization shrinkage [24].

CONCLUSIONS

It can be concluded that water sorption and solubility levels are depending on material type and time.

1. Resin-based sealants, Fissurit FX and Fotoseal, the local material, demonstrated low values of water sorption and solubility.

2. Fuji-Triage, glass-ionomer based material, showed the highest values of water sorption for each day of measurement and the highest value of solubility in the first day of measurement.

3. Dyract Seal, polyacid modified composite resin, showed intermediate values of water sorption for each day of measurement and just in the first day for solubility. Differences concerning solubility became statistically significant in day 3, 7 and 14.

EXPERIMENTAL SECTION

Materials

Table 3. Materials used in this study: Bis-GMA - 2,2-bis(4-(2'-hydroxy-3'methacryloyloxy-propoxy)phenyl)propane, UDMA- urethane dymethacrylate TEGDMA- triethyleneglycol- dimethacrylate

Material	Class of Material	Organic phase	Inorganic phase	Company
Fissurit FX	Composite resin	-Bis-GMA -UDMA	55%fiiling	VOCO
Fotoseal	Composite resin	-Bis-GMA -UDMA -TEGDMA	-hidroxylapatite with fluorine -alumino- silicate glass -colloidal silica	ICCRR,Cluj-Napoca
Dyract Seal	Compomer	-carboxylic acid modified methacrylate resin -ammonium salt of phos-phoric acid modified methacrylate resin -diethylenglycol dimethacrylate.	-strontium-alumino- fluoro-phosphor- silicate glass, -highly dispersed silicone dioxide	Dentsply
Fuji Triage	Glass-ionomer	-unsaturated polyacid	-high fluoride content	GC America

Bis-GMA and hydroxylapatite from Fotoseal were synthetized in ICCRR, Cluj-Napoca laboratory.

Method

A total of forty specimens were fabricated, ten for each material (n=10), following ISO specifications 4049/2000.

Materials were inserted in a teflon mold, disk-shaped, to obtain samples of 15±1 mm diameter and 1 mm thickness. The sealing material were photo-cured with a LED Woodpecker lamp (Guilin Woodpecker Medical Instrument Co., Ltd), for 30 seconds; after the disks removal, they were polished with sandpaper to gain a smooth and flat surface.

Specimens have been placed in a desiccator DURAN (DURAN Produktions GmbH&Co.KG, Mainz, Germania), at a temperature of 23ºC, until a constant weight was achieved (m1) (Partner 220mg, Partner Corporation, Bucharest). At this constant mass, the volume was calculated, as a result between diameter and thickness. Then, the disks were submerged in glass test tubes (SIMAX, 25ml, Czech Republic), that contained distilled water (10 ml) and they were maintained at 37ºC. In the day 1st, 3rd, 7th and 14th, specimens were removed from water and dried with absorbent paper, then weighed (m2). After which, the samples were reconditioned to constant mass in the desiccator (m3).

Water absorption and solubility were calculated according to the formulas:

$$W = \frac{m2 - m3}{V}$$

$$S = \frac{m1 - m3}{V}$$

$m1$- constant sample weight before immersion in water (μg)
$m2$- sample weight after immersion in water (μg)
$m3$- constant sample weight kept in a desiccator, after immersion in water (μg)
V- sample volume after a constant mass (m1) was obtained (mm3) [25, 26].

ACKNOWLEDGMENTS

This study was supported by Research Project PN-II-PT-PCCA-2011-3-2-1275.

REFERENCES

1. R. McDonald, D.R. Avery, J. Dean, “Dentistry for the Child and Adolescent”, 8th ed, Mosby, **2004**, 342.
2. M.G. Buonocore, *Journal of Dental Research*, **1955**, *34*(6), 849.
3. R. Curtis, T. Watson, “Dental Biomaterials: Imaging, Testing and Modelling”, Woodhead Publishing Ltd, **2008**.

4. A.M. de Andrade, S.K. Moura, A. Reis, A.D. Loguercio, E.J. Garcia, R.H.M. Grande, *Journal of Applied Oral Science*, **2010**, *18*(6), 591.
5. M. Mesaroș, A. Muntean, "Medicină dentară pediatrică", Cluj- Napoca, **2012**.
6. K. Bukovinszky, L. Molnár, J. Bakó, M. Szalóki, C. Hegedus, *Fogorvosi Szemle*, **2014**, *107*(1).
7. M. Irie, J. Tanaka, Y. Maruo, G. Nishigawa, *Dental Materials*, **2014**, *30*(7), 189.
8. S. Bhole, "Use of glass-ionomer cement as a pit and fissure sealant", Department of Preventive Dentistry, Faculty of Dentistry, University of Sidney, **1986**, 1.
9. R. Kaur, "Pit and fissure sealants", Department of Pedodontics SDC, Sri Ganga Nagar available at: www.slideshare.net/ramniqkaur/pit-and-fissure-sealants, 2012, cited Feb. 23. 2016.
10. A. Singla, S. Garg, S. Jindal, H. Suma Sogi, D. Sharm, *Indian Journal of Dental Research,* **2011**, *22*(2), 205.
11. M. Selimović-Dragaš, L. Hasić-Branković, F. Korać, N. Đapo, A. Huseinbegović, S. Kobašlija, M. Lekić, Š. Hatibović-Kofman, *Bosnian Journal of Basic Medical Sciences*, **2013**, *13*(3), 197.
12. G.M. Gusmão, T.V. De Queiroz, G.F. Pompeu, P.F. Menezes Filho, C.H. da Silva, *Indian Journal of Dental Research*, **2013**, *24*(1), 60.
13. Y. Song-Yi, P. Yin-Zhu, K. Sung-Min, L. Yong-Keun, K. Kyoung-Nam, K. Kwang-Mahn, *Dental Materials,* **2013**, *29*(12), 1228.
14. L.M. Cavalcante, L.F. Jochims Schneider, M. Hammadc, D.C. Watts, N. Silikas, *Journal of Dentistry*, **2012**, *40*(1), 86.
15. D. Prodan, L. Silaghi-Dumitrescu, C. Prejmerean, R. Silaghi-Dumitrescu, L. Bolojan, G. Damian, *Studia UBB Chemia*, **2011**, *56*(3), 201.
16. A.R. Prabhakar, S.A. Murthy, S. Sugandhan, *Contemporary Clinical Dentistry*, **2011**, *2*(4), 324.
17. H. Dong-Keun, A. Kwan-Duk, J. Jin-Hee, "Photo-cured dental pit and fissure sealant composition for caries prevention", Patent No. U.S.6573312B2, Date of Patent Jun. 3. **2003.**
18. S. Bayrak, E. Sen Tunc, A. Aksoy, E. Ertas, D. Guvenc, S. Ozere, *European Journal of Dentistry*, **2010**, *4*(3), 245.
19. W. Dukic, O. Lulic Dukic, S. Milardovic, Z. Vindakijevic, *Collegium Antropologicum,* **2007**, *31*(4), 1019.
20. C. Nuca, D.P. Balaban, A. Caraiane, V. Badea, *Ovidius Dentistry Journal*, **2014**, *1*(1), 4.
21. E. Haznedaroglu, S. Sozkes, A.R. Mentes, *European Journal of Paediatric Dentistry,* **2014**, *15*(4), 397.
22. T. Kanjevac, M. Milovanovic, V. Volarevic, M.L. Lukic, N. Arsenijevic, D. Markovic, N. Zdravkovic, Z. Tesic, A. Lukic, *Medicinal Chemistry*, **2012**, *8*(1), 40.
23. "Dyract Seal®", Dentsply, available at: www.dentsply.de/bausteine.net/f/7032/TM_SEALE.pdf?fd=2, **1998**, cited Feb. 25. 2016.
24. E. Jodkowska, "Contemporary Approach to Dental Caries", Dr. Ming-Yu Li (Ed), InTech, **2012**, cap.13.
25. S. Sava, C. Sarosi, S. Boboia, A. Tonea, C. Alb, D. Dudea, *Studia UBB Chemia,* **2015**, *60*(*2*), 71.
26. M.Q. Al Qahtany, S.S. Binsufayyan, H.A.A. Al Shaibani, H.G.L. Amri, *Pakistan Oral & Dental Journal*, **2012**, *32*(2), 304.

STUDIA UBB CHEMIA, LXI, 2, 2016 (p. 249-260)
(RECOMMENDED CITATION)

EVALUATION OF THE MORPHOLOGY AND STRUCTURE OF E GLASS FIBER-REINFORCED COMPOSITES FOR CRANIO-FACIAL BONE RECONSTRUCTION

MĂDĂLINA-ANCA LAZAR[a], HORAŢIU ROTARU[a*], DOINA PRODAN[b], GABRIEL ARMENCEA[a], PAUL BERE[c], CĂLIN RAREŞ ROMAN[a], RADU SEPTIMIU CÂMPIAN[a]

ABSTRACT. New E-glass fiber reinforced composites developed to serve cranio-facial bone reconstruction were investigated using scanning electron microscopy, atomic force microscopy and X ray diffraction to evaluate their morphology and structure. The morphological analysis of the external surface of experimental composite materials has shown that the reinforcing material was well incorporated in the polymer matrix and no monofilaments of fiber glass could be observed on the material surface. Structure analysis of the experimental composites revealed the optimal interfacial adhesion obtained using A 174 silane. Woven E glass fibers were more favourable than unidirectional fibers for manufacturing cranio-facial implants. The flexural strength of the experimental composite materials was directly influenced by the degree of reinforcement. Taking into account the obtained results, the perspective of continuing the studies appears for improving the mechanical properties so as to be as close as possible to the ones of the human bone.

Keywords: *biocomposites, reconstructive surgery, surface, interface, bending test, scanning electron microscopy, atomic force microscopy, elemental distribution*

INTRODUCTION

In spite of the huge progress made in reconstructive surgery in recent decades, restoring cranio-facial bone structures, pathologically affected, keeps being an endless challenge. The consecutive morphological and functional deficits, significantly impairs life quality because they involve a highly exposed anatomic segment.

[a] *"Iuliu Haţieganu" University of Medicine and Pharmacy, Faculty of Dental Medicine, 8 V. Babes Str., 400012 Cluj-Napoca, Romania*
[b] *"Babeş Bolyai" University, "Raluca Ripan" Institute for Research in Chemistry, 30 Fantanele Str, 400294 Cluj-Napoca, Romania*
[c] *Technical University, Department of Manufacturing Engineering, 103-105 Muncii Avenue, 3400 Cluj-Napoca, Romania*
[*] *Corresponding author: hrotaru@yahoo.com*

Reconstruction of craniofacial bone defects, especially dysfunctions and dysmorphysm that they induce, is a burning issue in the medical field. Materials used to serve this purpose are of great diversity, but they still have some shortcomings that limit their application and sometimes cause clinical problems [1, 2].

Recently, the biomaterial research is focused also on biodegradable and biocompatible composites. The main concerns related to clinical application of composite implants are the negative biological reactions that these materials may produce. The local reactions that composites may induce are due not only to the elution of leachable components from composites, but also to the mechanical irritation they cause [3, 4]. Also, mechanical properties of composites meant for bone reconstruction should be tailored in order to avoid stress-shielding and bone over-loading, which have negative effects on surrounding bone and ultimately lead to bone resorption, loosening and failure of the implant [5, 6, 7].

This study aims to analyse the morphology and the structure of experimental E-glass fiber reinforced composites that will serve the fabrication of custom-made implants for craniofacial bone reconstruction.

The surface morphological analysis had as an objective to determine the implants quality in terms of surface roughness and the influence of the gentamicin coating on this aspect through atomic force microscopy and scanning electronic microscopy examinations.

Likewise, the structural analysis of the experimental composite materials has pursued to investigate the following aspects: if the structure of the composite materials is uniform or if any material defect is found; if the suitable compatibility is made between the organic phase and the inorganic phase of the composite materials; which is the influence of the degree of reinforcement and of the glass fibers geometry on the mechanical properties of the composite materials. In order to investigate these aspects, the analysis of the experimental composite materials was made through scanning electronic microscopy, both before and after subjecting the specimen tubes to the bending test. Taking into account that cranial implants are fixed rigidly marginally, out of all mechanical trials the bending test was chosen because it best stimulates the conditions in which such an implant might be subjected to an accidental force.

RESULTS AND DISCUSSION

Morphological analysis of the surface

The morphological analysis of the external surface of experimental composite materials (MCE) using SEM (fig. 1) has shown that the reinforcing material was well incorporated in the matrix. Monofilaments of fiber glass could not be observed on the material surface. The quality of the obtained surface was

good, the roughness being acceptable for the surface of an implant. In fact, this roughness copies the quality of the matrix surface which was used to prepare the respective samples. This aspect is critical for composites meant for medical implant fabrication, since the inflammatory reaction of the surrounding tissues may be caused not only by the leachable compounds, but also by the surface of the implant itself. The presence of the gentamicin coating (fig. 1 D) did not notably influence the roughness of the obtained material. Moreover, the presence of gentamicin on the surface of the implant impaired bacterial adhesion and growth [8].

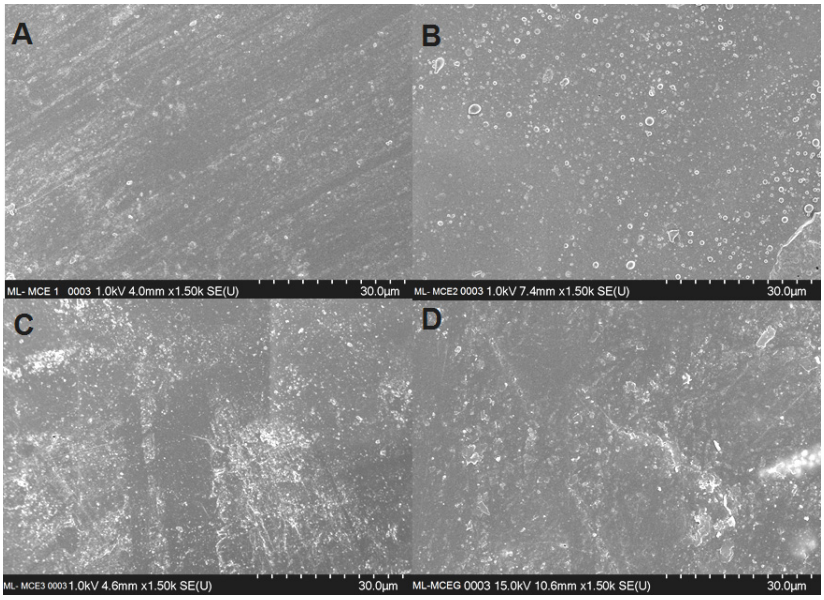

Figure 1. Morphological analysis of the external surface of the experimental composite materials MCE 1 (A), MCE 2 (B), MCE 3 (C), MCE 1-G (D).

The 3D topography of the surface of the four materials analysed using atomic force microscopy emphasized their minimal roughness, with level differences of maximum 30 nm for MCE 1- MCE 3. In the situation where the gentamicin layer was added, the level differences were smaller, to a maximum of 8 nm. This can be explained by the fact that the gentamicin molecules have smaller sizes thus creating a higher uniformity degree. In the figure 2 are exemplified the AFM images obtained for MCE 1 and MCE 1G.

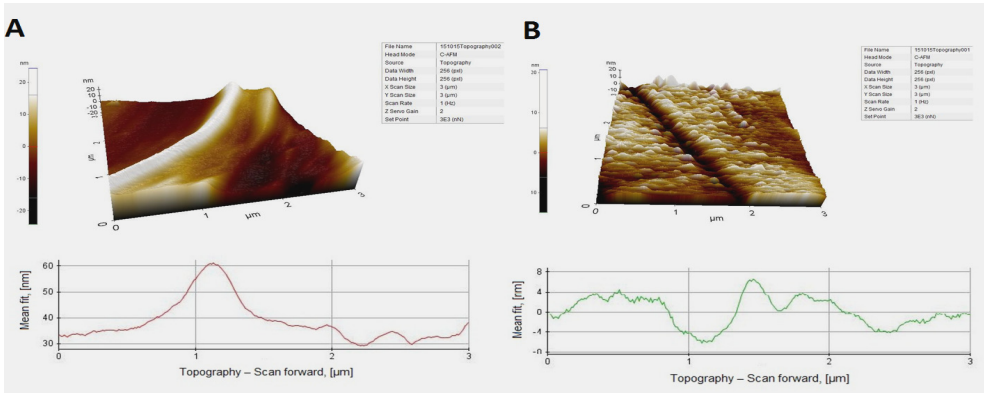

Figure 2. 3D Topography and the variation of topographic heights of MCE 1 (A) and MCE1- G (B) on the analyzed surface

Structure analysis using X-Ray diffraction

The diffractogram of the resin sample (fig. 3 A) was specific to amorphous carbon based materials meaning disordered polymer chains. Also the diffractogram of glass fibers was rendered (fig. 3B), which was specific to amorphous vitreous materials. No matter the fiber glass used in the composition of composites, the degree of reinforcement or the geometry of reinforcement, their diffractograms present a totally amorphous character (fig. 3 C).

In the diffractogram of the composite coated with gentamicin MCE 1-G one can identify the peaks characteristic to the crystalline phase of the gentamicin (18 peaks) (fig. 3D), besides the amorphous halo given by the composite made of resin and glass fibers.

The structural analysis of the experimental composite materials before and after subjecting them to the bending test.

The structural analysis of the MCE1- MCE3 experimental composite materials has revealed that the organic matrix integrates the reinforcing material, with no material defects detected.

In figure 4 was exemplified MCE 1 for which the bidirectional fibers could be observed, before the composite was subjected to mechanical stress for its characterization. The singular points represent the warp of the fabric and the fibers which appear to be continuous represent the weft of the fabric. There were no material defects highlighted, the matrix integrating the enforcing material throughout the entire structure of the material.

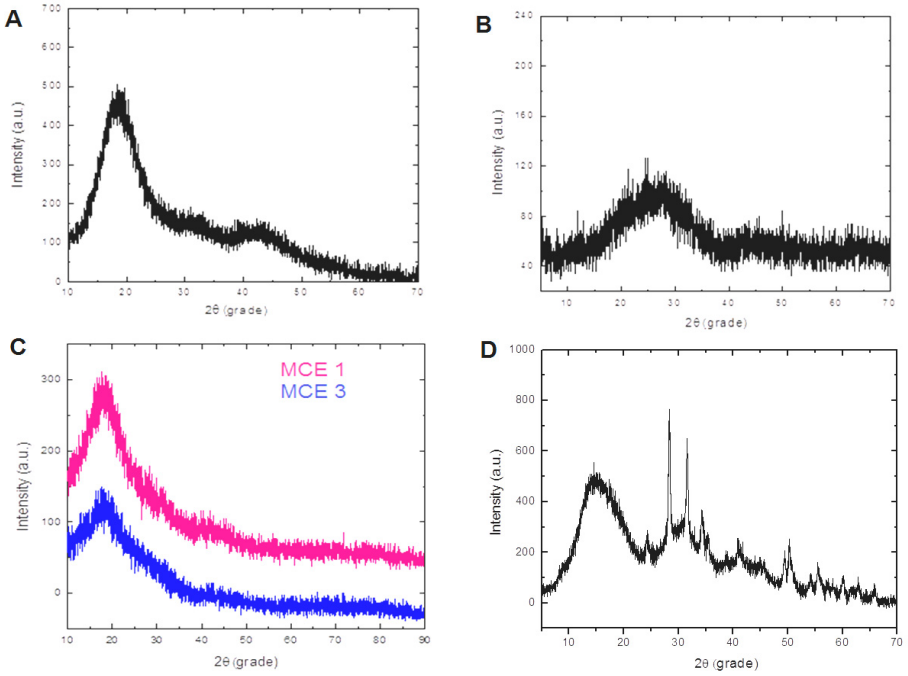

Figure 3. Diffractograms of resin (A), E-glass fibers (B), MCE1 AND MCE 3 (C), MCE 1-G (D)

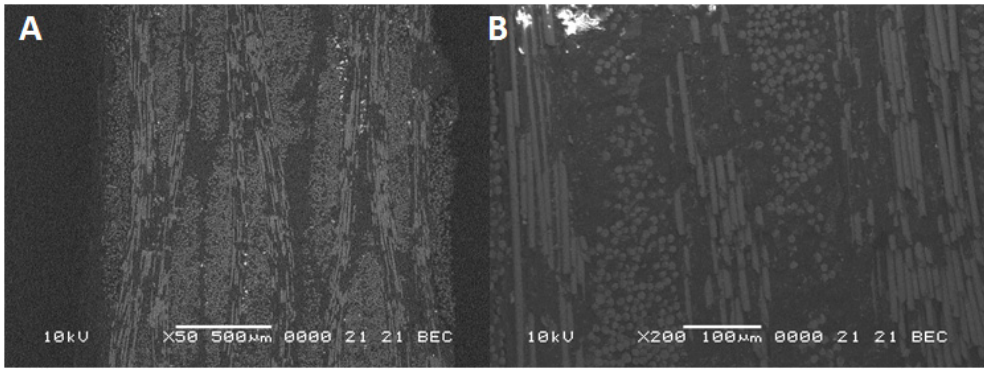

Figure 4. SEM Images for sample MCE 1 before the bending test
A- Image recorded lengthwise (x50)
B- Image recorded transversally (x200)

The bending test to which the samples made of experimental composite materials were subjected to has indicated the values for flexural strength and respectively for Young's modulus comprised in table 1.

Table 1. Mechanical properties of the experimental composite materials

Codes of experimental composite materials	Glass fibers	Reinforcement /degree of reinforcement %	Flexural strength (Mpa)	Young's modulus (Gpa)
MCE 1	Woven	65	394.45	16.295
MCE 2	Woven	60	319.35	14.849
MCE 3	Unidirectional	65	717.50	21.706

After subjecting the samples from composite materials to the bending test, other important structural aspects have been identified by analyzing the obtained values and through further examination with scanning electronic microscopy. Therefore, during the bending process, the first to cede was the polymer matrix while the reinforcement fought against fissure propagation, thus taking place a stress transfer from the matrix towards the fibers.

It was also observed that for the samples MCE 1 the reinforcing fibers had broken gradually. Also, according to the diagram presented in figure 5, MCE 1 has flexural strength lowering thresholds near the maximum breaking values. While crossing the thresholds, the sample continues to stretch and then it breaks completely. From a value point of view, the flexural strength for MCE 1 and MCE 2 was measured at approximately 350 MPa and of over 700 MPa for the MCE 3 samples.

For the samples type MCE 2 one can observe a specific longer stretch, because the quantity of resin is larger, thus assuring a greater elongation (4% as opposed to 3%).

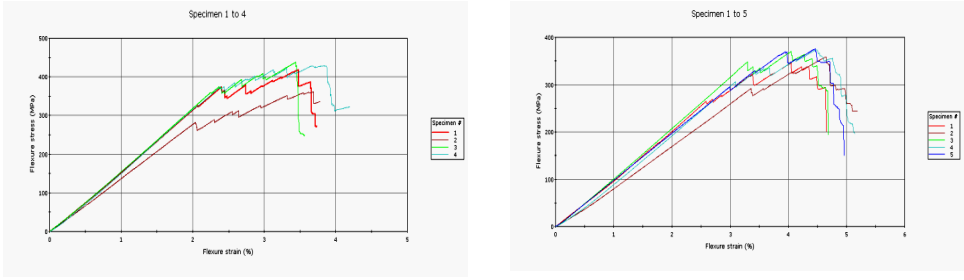

MCE 1 MCE 2

Figure 5. The flexural strength diagrams for MCE 1 as compared to MCE 2

The phenomena taking place in the MCE 1 structure during the bending test are exemplified in figure 6. The blackened zone which appears after the bending stress represents the delamination of the layers of the reinforcing material. After the start of this phenomenon, the actual breaking of the monofilaments may occur.

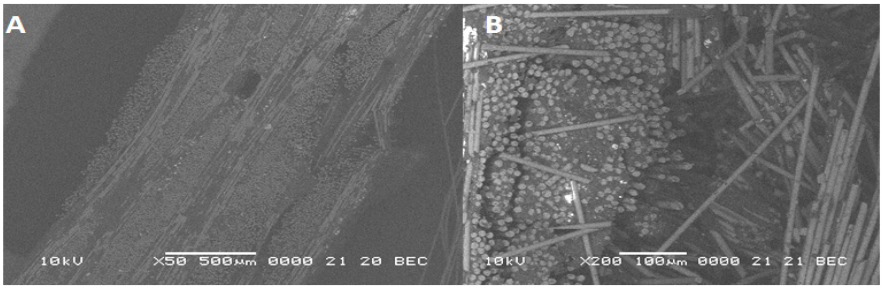

Figure 6. SEM Images for MCE 1 after the bending test
A - Imagine recorded lengthwise (x50),
B - Imagine recorded transversally (x200)

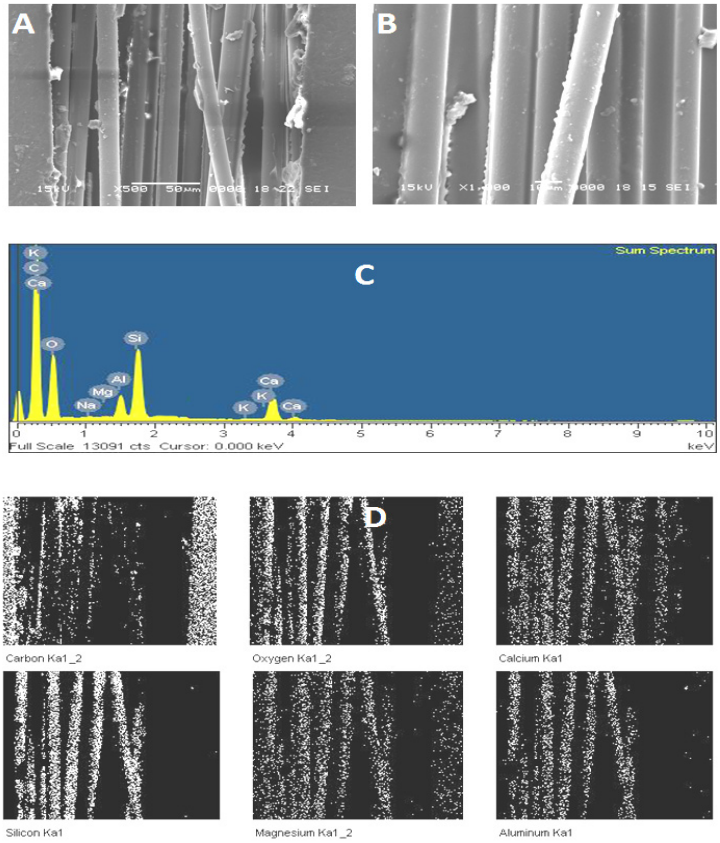

Figure 7. SEM and EDX images for MCE 3 after the bending test
A - SEM Image for MCE 3 after the bending test (x1000)
B - SEM Image for MCE 3 after the bending test (x 5000)
C - EDX spectrum corresponding to the area from point A
D - The distribution of elements on the surface of the sample from point A

For a much better visualization of the polymer matrix which remains attached to the glass fibers superior enhancements were used and the samples were covered in Au, thus avoiding electrostatic charge. Figure 7 presents electronic microscopy aspects for sample MCE 3, after the bending test. The glass fibers had polymer portions on their external surface. This indicated a very good compatibility between the fibers and the matrix, the treatment used being adequate for obtaining the suitable interface. The monofilaments are grouped, having a uniform allocation in the structure of the composite material. They are arranged longitudinally in regard to the direction of the mechanical stress. During mechanical stress, they have acted together and remained grouped even after breaking.

With the help of the X-ray microanalysis a quantification was made of the chemical elements detected on the surface from figure 7A, thus creating a compositional analysis of the sample after the mechanical testing. The elemental chemical compositions on the analyzed microarea are presented in figure 7C.

The distribution of the main chemical elements (carbon, calcium, oxygen, aluminum, magnesium and silicon) on the surface of the sample from figure 7B is characterized by a relative uniformity. Although the calcium, oxygen, aluminum, magnesium and silicon are elements of the glass fibers, the presence of the carbon is given by the existence of polymer resin traces on the surface of the reinforcement. The relatively uniform distribution of the carbon atoms strengthens the affirmation stating that the compatibility organic phase – inorganic phase was made accordingly.

The flexural strength of the experimental composite materials was directly influenced by the degree of reinforcement, as it is also shown by other literature studies [9]. However, it must be taken into account that in the case of high degrees of charge the glass fibers can remains “too poor”, which leads to structural defects. Moreover, considering the field of application for the manufactured materials there is no need for the mechanical resistances / Young’s modulus to have great values. For a degree of reinforcement of 60%, the flexural strength still exceeds the one of human bone structures [10].

The mechanical properties of composite materials were also influenced by the geometry of the reinforcement [11]. The fabrics used in this study for the samples MCE 1 and MCE 2 have had the weft and warp in equal proportions, arranged perpendicularly to each other. Such a fabric is favorable for manufacturing the landmarks with a complex geometry, to which the stresses are not only unidirectional or only bidirectional, but the stresses may also be complex. In the case of the material with unidirectional fibers, MCE 3, all the monofilaments are arranged on the direction of the stress if it is a unidirectional stress (traction, bend or compression). This makes the values of

the specific resistance of the material to be double compared to a similar material but reinforced with fabric, in which case only half the quantity of integrated fibers takes the respective stress.

CONCLUSIONS

The morphological analysis of the external surface of experimental composite materials has shown that the reinforcing material was well incorporated in the polymer matrix and no monofilaments of fiber glass could be observed on the material surface. The usage of the A 174 silane has allowed the chemical binding of the two phases of the experimental composite materials. Thus was created a stable interface, which notably increases the mechanical resistance. Taking into account the obtained results, the perspective of continuing the studies appears for tailoring the mechanical properties so as to be as close as possible to the ones of the human bone, starting from the already proven aspects: the reinforcement shoud use woven fibers and the degree of reinforcement must not exceed 60%.

EXPERIMENTAL SECTION

In order to produce the experimental composite materials (MCE) included in the study, following materials were used: bisphenol A glycidylmethacrylate (Bis-GMA), urethane dimethacylate (UDMA), triethylene glycol dimethacrylate (TEGDMA), benzoyl peroxide (POB), 2,2-dihydroxyethyl-p-toluidine (DHEPT), butylatedhydroxy toluene (BHT), 3-methacryloyloxypropyl-1-trimethoxy-silane (A-174 silane, Sigma Aldrich Chemical Co., Taufkirchen, Germany), bi-woven E-glass fibers (Owens Corning, Brussels, Belgium), Gentamycin sulphate (BioChemica, Activity 641 I.U./mg; Lot:3Q008363).

Two resins (base resin and catalyst resin) were prepared to produce each MCE. The composition of resins is UDMA 60 wt%, Bis-GMA 10 wt%, TEGDMA 30 wt%. POB (1 wt%) was used as the initiator in the catalyst resins and DHEPT (1 wt%) was used as the accelerator in the base resin. BHT was used as an antioxidant and dissolved in each resin in an amount of 0.65 wt%. To ensure good interfacial adhesion and stress transfer across the interface, E glass fibers were treated with a coupling agent [12, 13]. 1 wt % A-174 (γ-methacryloxypropyl-1-trimethoxysilane) was added to the amount of E-glass fibers. The silane solution was prepared by dissolving A-174 silane in ethanol–water 90/10 vol.% acidified to pH 3.8. PH level was maintained using glacial acetic acid. The glass fibers were immersed in this solution for 1 h. After that, the silane layer was dried at 110 °C for 2 h [14].

Each MCE was obtained using the laminate lay-up process. The bottom layer in the mold was the base resin, over which the E- glass fibers were applied. On the top surface of this last material a layer of catalyst resin was added. Then the glass fibers and the resins were applied alternatively using the following pattern: base resin, woven glass fibers, catalyst resin, woven glass fibers, base resin, etc.

For MCE 1 the degree of reinforcement was of 65% and it was made with woven fiber glass; for MCE 2 the degree of reinforcement was of 60% and it was made with woven glass fibers; for MCE 3 the degree of reinforcement was of 65% and it was made with unidirectional glass fibers extracted from the same fabric used for manufacturing MCE 1 and MCE 2. A part of the specimens manufactured from MCE 1 were covered with a gentamicin layer following the previously published protocol [8], and were coded MCE 1-G.

The MCE hardened through the chemically initiated polymerization of the resins at room temperature, followed by a thermic treatment (post-polymerization) for 2 hours at 100 ^{0}C in a specialized oven. The polymerization started the moment a base resin is mixed with a catalyst resin and continued during the application of the successive layers of resins and woven E-glass fibers.

Scanning electronic microscopy and atomic force microscopy techniques were used for the morphological analysis of the surface. The amorphous character of the composite materials was highlighted through X-ray diffractometry. For the structural analysis of the experimental composite materials, scanning electronic microscopy techniques were used both before and after the mechanical tests.

Hereinafter are presented the details regarding the devices and techniques used, and also the protocol followed for the bending test.

The examination through electronic microscopy was made with a SEM scanning microscope JEOL – JSM 5600 LV, equipped with an EDX spectrometer (Energy dispersive X-ray spectrometer) (Oxford Instruments Soft Inca 200). The EDX spectrometer was used to quantify the chemical elements detected on the specimens' surfaces. In order to avoid electrostatic charge, the test tubes of experimental biocomposite materials which are not electrically conductive have been metallized with gold using a Denton Vacuum apparatus (Desk V) (They have a thickness of layer of the order of 25 Å).

The *XE 70* ***atomic force microscope*** was used to determine the roughness state of MCE. This type of microscope is used to determine different mechanical, structural and morphological characteristics, but also to obtain

the topography of some surfaces with a resolution of 2 nm. The tests have been at a 25°C temperature and a relative humidity of 56%. The testing strength was of 25 μN. Using the same microscope, 3D images were made of the tested samples. The resulted images were processed by using the XEI Image Processing Tool for SPM Data software.

For the analysis of specimens through ***X-ray diffraction*** a Shimadzu XRD-6000 diffractometer was used, with Cu Ka radiation (λ = 1.5418 Å) and a Ni filter. The specters have been registered between 10° and 70°, and 20° and 110° in the continuous scanning mode 2θ, with 2°/minute. The tension and current were of 40 kV, respectively 30 mA.

The analyses have been made within the laboratory of Micro- and Nano- Systems (MiNaS) from the Department of Mechanical Systems Engineering, the Technical University from Cluj-Napoca.

The bending test

The *flexural strength and modulus of elasticity* were determined using MCE specimens of rectangular form (length 25.0 mm, height 2.0 mm and width 2.0 mm), according to ISO 4049/2000 three-point bending test. The measurements of the flexural properties were made using a Lloyd LR5K Plus mechanical testing apparatus connected with a computer. The crosshead speed of the testing machine was 1.0 mm/min.

ACKNOWLEDGMENTS

The research was partially supported by Romanian Executive Unit for Financing Education Higher, Research Development and Innovation, code PN-II-PT-PCCA 2013-4-0917, grant no 115/2014.

REFERENCES

1. A. Seckin, K. Baris, A. Bashar, A. Sabri, Z.S. Galip, *Journal of neurosciences in rural practice*, **2011**, *2*, 162.
2. U. Spetzger, V. Vougioukas, J. Schipper, *Minimally Invasive Therapy & Allied Technologies,* **2010**, *19*, 110.
3. J.L. Ferracane, *Journal of oral rehabilitation,* **1994**, *21*, 441.
4. N. Ivković, D. Božović, S. Ristić, V. Mirjanić, O. Janković, *Contemporary Materials,* **2013**, *1*, 84.
5. R. Huiskes, R. Ruimerman, G.H. van Lenthe, J.D. Janssen, *Nature*, **2000**, 405, 704.
6. R. Suuronen, N. Ashammakhi, H. Peltoniemi, E. Waris, W. Serlo, M. Kellomaki, T. Waris, *Plast Reconstr Surg*, **2001**, *108*, 167.

7. J. Brandt, M. Pfennig, C. Bieroegel, W. Grellmann, A. Bernstein (April). *Key Engineering Materials,* **2009**, *396*, 331.
8. M.A. Lazar, D. Vodnar, D. Prodan, H. Rotaru, R.C. Roman, L.A. Sorcoi, G. Băciuț, R.S. Câmpian, *Clujul Medical*, **2016**, DOI: 10.15386/cjmed-599.
9. G. Furtos, L. Silaghi-Dumitrescu, M. Moldovan, B. Baldea, R. Trusca, C. Prejmerean, *Journal of Materials Science*, **2012**, *47*, 3305.
10. Kokubo T., Kim H.M., Kawashita M., *Biomaterials*, **2003**, *24*(13), 2161.
11. R.K. Alla, S. Sajjan, V.R. Alluri, K. Ginjupalli, N. Upadhya N., *Journal of Biomaterials and Nanobiotechnology*, **2013**, *4*, 91.
12. M. Sonmez, D. Ficai, A. Ficai, L. Alexandrescu, G. Voicu, E. Andronescu, *Revista Romana de Materiale-Romanian Journal of Materials,* **2014**, *44*, 88.
13. M. Sönmez, M. Georgescu, M. Vâlsan, M. Radulescu, D. Ficai, G. Voicu, L. Alexandrescu, *Journal of Applied Polymer Science*, **2015**, *132.*
14. G. Furtos, B. Baldea, L. Silaghi-Dumitrescu, *Materials science and engineering* **2016**, *59*, 855.

STUDIA UBB CHEMIA, LXI, 2, 2016 (p. 261-281)
(RECOMMENDED CITATION)

FIXING SYSTEMS FOR DENTAL CAD/CAM PROSTHETIC RESTORATIONS: A SYSTEMATIC REVIEW

DANIELA POPA[a], MARIANA CONSTANTINIUC[a*], RADU-SEPTIMIU CÂMPIAN[b]

ABSTRACT. This study was conducted to review the current scientific literature regarding the fixing systems for CAD-CAM prosthetic restoration. An electronic search was conducted for relevant articles using PubMed database followed by manual search, with the following association of terms: (CAD CAM, cements) then (CAD CAM, cements, bonding) and finally (CAD CAM, cements, bonding agents). The study included articles published between 01.01.1995 and 01.09.2015. A table was designed for this review with the following information: authors, CAD-CAM system used, fixing agent/agents used, restoration type and abutment type. The most studied dental CAD-CAM system was Cerec and the most used fixing agent was RelyX. In summary, the objective of any surface treatment method is to enhance the adhesive bond strength and durability.

Keywords: CAD CAM, crowns, dental cements, bonding agents

INTRODUCTION

The development of computer-aided design/computer aided manufacturing (CAD-CAM) technology in dentistry provide more accurate prosthetic frameworks by using new biocompatible materials, especially high performance ceramics, such as zirconia and lithium disilicate [1].

Patient, tooth and treatment cost guide the selection of one or another restorative material. The selection of an all-ceramic material for tooth restoration opens a floodgate of information about emerging materials and techniques, central among these techniques is CAD-CAM [2].

CAD-CAM system is popular because of high aesthetic and short fabrication time. But, there is limited information available about the micro-tensile bonding of luting cements to CAD-CAM inlays and to dentin [3]. Unfortunately these materials are brittle and tend to fracture under heavy occlusal load [4].

[a] *Department of Prosthetic Dentistry, "Iuliu Haţieganu" UMPh, 32 Clinicilor Street, Cluj-Napoca, RO-400006, Romania*
[*] *Corresponding author: mconstantiniuc@umfcluj.ro*
[b] *Department of Oral Rehabilitation,"Iuliu Haţieganu" UMPh, 15 Victor Babes Street, Cluj-Napoca, RO-400012, Romania*

Multiple factors affect the success of fixed prosthodontic restorations with preparation design, oral hygiene/microflora, mechanical forces, and restorative materials being some of them. However, key factor to success is the choice of a proper luting agent and cementation procedure [5].

Dental luting agents provide a link between the restoration and prepared tooth, bonding them together through some form of surface attachment, which may be mechanical, micro-mechanical, chemical or combination [6]. Due to the relatively recent entry of zirconia and alumina based ceramics in dental practice, there is a lack of information about adhesive cementation technique respectively, about the special preparation of zirconia and alumina surface in order to use adhesive cement [7].

Restorative dentistry constantly evolves and the clinicians cannot indicate the ideal cement for all situations [8].

Bonded indirect restorations constitute a substantial part of contemporary dentistry [9].

Prosthetic restorations have a weak part which is the resin luting agent layer exposed at the margin [10-14].

The scientific knowledge of the materials currently available as well as the acknowledgment of their limitations and indications are key factors for durable restorations [8].

The purpose of this review was to identify the proper technique and the proper selection of luting agent for fixing CAD-CAM restoration.

RESULTS AND DISCUSSION

Relevant articles were search using PubMed database. The search was made using the following combination of keywords: (1)(CAD CAM, cements); (2)(CAD CAM, cements, bonding); (3)(CAD CAM, cements, bonding agents). The last search was conducted on September 2, 2015. Studies considered for this review were English-language articles published between 01.01.1995 and 01.09.2015, focused on the luting cements and fixing technique for CAD-CAM restoration.

The review excluded studies regarding non CAD-CAM restorations.

From each article, the following information were extracted: the type of CAD-CAM system used, fixing agent/agents used, restoration-type (veneer, inlay, coverage crown etc.), abutment type (natural tooth, implant abutment etc.) and a table was made (Table 1).

For the first search (CAD CAM, cements), a total of 326 articles were identified. Searching after the second keywords combination (CAD CAM, cements, bonding) generated a number of 116 articles and for the third search (CAD CAM, cements, bonding agents) 35 articles were found.

Table 1. Dental CAD/CAM system, fixing agent/agents, prosthetic restoration and restoration support used in the studies

Nr. Crt	Material		CAD CAM	Restoration type	Abutment type	Authors
1.	Dual cure resin cement (RelyX ARC, 3M ESPE)	**Composition:** BisGMA and TEGDMA polymer Paste A: zirconia/silica filler (68 wt.%), pigments, amine and photo initiator system. Paste B: zirconia/silica filler (67 wt.%), BPO activator (Filler= 67.5 wt.%; avg. = 1.5 µm)	Secotom-50 cutting machine	Experimental model made of CAD/CAM resin	Experimental model made of CAD/CAM resin	Gilbert S., Keul C., Ross M., Edelhoff D., Stawarczyk B. [15]
	Dual cure resin cement (Clearfil SA, Kuraray)	**Composition:** Paste A: 10-MDP, Bis-GMA, TEGDMA, Hydrophobic aromatic dimethacrylate, dl-Camphorquinone, BPO Initiator, Silanated barium glass filler and Silanated colloidal silica. Paste B: Bis-GMA, Hydrophobic aromatic dimethacrylate, Hydrophobic aliphatic dimethacrylate, Accelerators, Pigments, and Surface treated sodium fluoride, Silanated barium glass filler and Silanated colloidal silica. (Filler= 45 % vol., 66 wt.%; avg. 2.5µm)				
	Dual cure resin cement (Variolink II, Ivoclar Vivadent)	**Composition:** The monomer matrix: Bis-GMA, urethane dimethacrylate, triethylene glycol dimethacrylate. The inorganic fillers: barium glass, ytterbium trifluoride, Ba-Al-fluorosilicate glass, spheroid mixed oxide. Additional contents: catalysts, stabilizers, pigments				

Nr. Crt	Material		CAD CAM	Restoration type	Abutment type	Authors
2.	Dual cure resin cement (NX3 Nexus, Kerr)	**Composition:** glass, oxide, chemicals ytterbium trifluoride Poly(oxy-1,2-ethanediyl), α,α'-[(1-methylethylidene)di-4,1-phenylene] bis[ω-[(2-methyl-1-oxo-2-propen-1-yl)oxy]-7,7,9(or 7,9,9)-trimethyl-4,13-dioxo-3,14-dioxa-5, 12-diazahexadecane-1,16-diyl bismethacrylate 2,2'-ethylenedioxydiethyl dimethacrylate, 2-Hydroxyethyl methacrylate Silanamine, 1,1,1-trimethyl-N-(trimethylsilyl)-, hydrolysis products with silica Cumene hydroperoxide 1,1,3,3-tetramethylbutyl hydroperoxide, 2-Pyridylthiourea Oils, peppermint	Lava	Experimental model made of CAD/CAM composite	Experimental model made of CAD/CAM composite	Lührs AK, Pongpruek sa P, De Munck J, Geurtsen W, Van Meerbeek B [16]
	Dual cure resin cement (RelyX Ultimate, 3M ESPE)	**Composition:** Base Paste Methacrylate monomers Radiopaque, silanated fillers Initiator components, Stabilizers, Rheological additives Catalyst Paste Methacrylate monomers, Radiopaque alkaline (basic) fillers, Initiator components, Stabilizers, Pigments, Rheological additives, Fluorescence dye, Dark cure activator				
3.	Dual cure resin cement (RelyX Ultimate, 3M ESPE)	**Composition:** Base Paste Methacrylate monomers Radiopaque, silanated fillers Initiator components, Stabilizers, Rheological additives Catalyst Paste Methacrylate monomers, Radiopaque alkaline (basic) fillers, Initiator components, Stabilizers, Pigments, Rheological additives, Fluorescence dye, Dark cure activator	Cerec	Inlay made of nano-ceramic resin	Natural tooth (intraoral)	Poticny DJ [17]

Nr. Crt	Material		CAD CAM	Restoration type	Abutment type	Authors
4.	Dual cure resin cement (RelyX Unicem Clicker, 3M ESPE)	**Composition:** Base paste (white) Methacrylate monomers containing phosphoric acid groups, Methacrylate monomers, Silanated fillers Initiator components, Stabilizers Catalyst paste (yellow) Methacrylate monomers, Alkaline (basic) fillers, Silanated fillers, Initiator components, Stabilizers, Pigments	Cerec Lava	Ceramic full crowns	Extracted human teeth (maxillary premolar)	Donnelly TJ, Burke FJ [18]
5.	Dual cure resin cement (Variolink, Ivoclar	**Composition:** See Nr. Crt. 1	Cerec	Ceramic veneers	Artificial tooth (Frasaco model)	Aboushelib MN, Elmahy WA, Ghazy MH [19]
6.	Light-curing luting composite (Variolink veneer, Ivoclar	**Composition:** Urethanedimethacrylate, inorganic fillers, ytterberiumtrifluoride, initiators, stabilizers, pigments	Cerec	Polimeric full crowns (Telio Cad)	Natural tooth (intraoral)	Edelhoff D, Beuer F, Schweiger J, Brix O, Stimmelmayr M, Guth JF [20]
7.	Self-curing non-eugenol temporary cement (Temp Bond	**Composition:** Base Mineral Oil, Zinc Oxide, Cornstarch Accelerator Ortho-Ethoxybenzoic acid, carnauba wax, octanoic acid	Cerec	Full crowns	Astra Tech abutments	Carnaggio TV, Conrad R, Engelmeier RL, Gerngross P, Paravina R, Perezous L, Powers JM [21]
	Self-curing non-eugenol temporary cement (ImProv,	**Composition:** eugenol-free acrylic urethane cement				
8.	Dual cure resin cement (RelyX Unicem, 3M ESPE)	**Composition:** See Nr. Crt. 4	Cerec	Inlays made of glass ceramic	Extracted human molars	Frankenberge R, Hehn J, Hajtó J, Krämer N, Naumann M, Koch A,

Nr. Crt	Material		CAD CAM	Restoration type	Abutment type	Authors
	Dual cure resin cement (G-Cem, GC)	**Composition:** G-CEM powder: fluoro-alumino-silicate glass G-CEM liquid: strong frame-forming resins, UDMA and Dimethacrylate, as well as acidic resins; 4-MET and phosphoric acid ester monomer, small amount of water				Roggendorf MJ [22]
	Dual cure resin cement (Maxcem Elite, Kerr)	**Composition:** glass, oxide, chemicals, ytterbium trifluoride 1,6-hexanediyl bismethacrylate 2-hydroxy-1,3-propanediyl bismethacrylate 7,7,9(or 7,9,9)-trimethyl-4,13-dioxo-3,14-dioxa-5, 12-diazahexadecane-1,16-diyl bismethacrylate, Silanamine, 1,1,1-trimethyl-N-(trimethylsilyl)-, hydrolysis products with silica, Oils, peppermint, 1,1,3,3-tetramethylbutyl hydroperoxide, Cumene hydroperoxide, 2-Pyridylthiourea				
	Light-curing composite resin (Clearfil Majesty Posterior, Kuraray)	**Composition:** Silanated barium glass filler, Pre-polymerized organic filler, Bisphenol A diglycidylmethacrylate (Bis-GMA), Hydrophobic aromatic dimethacrylate, dl-Camphorquinone				
	Dual cure resin cement (Variolink II, Ivoclar Vivadent)	**Composition:** See Nr. Crt. 1				
9.	Dual cure resin cement (RelyX Unicem, 3M ESPE)	**Composition:** See Nr. Crt. 4	Cerec	Polymer full crowns	Extracted human teeth	Stawarczyk B, Basler T, Ender A, Roos M, Ozcan M, Hämmerle C [23]
	Dual cure resin cement (G-Cem, GC)	**Composition:** See Nr. Crt. 8				

Nr. Crt	Material		CAD CAM	Restoration type	Abutment type	Authors
	Dual curing luting composite (artCem, Merz Dental)	**Composition:** polyacrylic acid, methacrylate, phosphoric acid ester, catalyst, stabilizers in ethanol				
	Dual cure resin cement (Variolink II, Ivoclar Vivadent)	**Composition:** See Nr. Crt. 1				
10..	Dual cure resin cement (Panavia F2.0, Kuraray)	**Composition:** **Paste A:** 10-Methacryloyloxydecyl dihydrogen phosphate (MDP), Hydrophobic aromatic dimethacrylate, Hydrophobic aliphatic dimethacrylate, Hydrophilic aliphatic dimethacrylate, Silanated silica filler, Silanated colloidal silica, dl-Camphorquinone, Catalysts, Initiators **Paste B:** Hydrophobic aromatic dimethacrylate, Hydrophobic aliphatic dimethacrylate, Hydrophilic aliphatic dimethacrylate, Silanated barium glass filler, Surface treated sodium fluoride, Catalysts, Accelerators, Pigments	Cerec	Feldspathic ceramic full crowns Composite resin full crowns	Extracted human molars	Kassem AS, Atta O, El-Mowafy O [24]
	Dual cure resin cement (RelyX Unicem, 3M ESPE)	**Composition:** See Nr. Crt. 4				
11.	Dual cure resin cement (RelyX Unicem, 3M ESPE)	**Composition:** See Nr. Crt. 4	Procera	Zirconia based 3 units bridge (replacing a molar or a premolar)	Human teeth (intraoral)	Sorrentino R, De Simone G, Tetè S, Russo S, Zarone F [25]

Nr. Crt	Material		CAD CAM	Restoration type	Abutment type	Authors
12.	Dual cure resin cement (RelyX Unicem, 3M ESPE)	**Composition:** See Nr. Crt. 4	Lava	Zirconia based 3 units bridge for maxillary anterior area	Human teeth (intraoral)	Madan N, Pannu K [26]
13.	Non-lutted		Cerec	Ceramic or composite inlay	Extracted human teeth (molars and premolars)	Magne P, Paranhos MP, Schlichting LH [27]
14.	Self-cure and dual cure resin cement (SpeedCEM,Ivoclar	**Composition:** Dimethacrylates, Ytterbium trifluoride, Co-polymer, Glass filler (base only), Silicon dioxide, Adhesive monomer, Initiators, Stabilizers and Pigments	Cerec	Ceramic inlays	Extracted human molars	Flury S, Lussi A, Peutzfeldt A, Zimmerli B [28]
	Dual cure resin cement (RelyX Unicem Aplicap, 3M	**Composition:** See Nr. Crt. 4				
	Dual cure resin cement (Smart Cem2, Dentsply)	**Composition:** UDMA Resin, EBPADMA Urethane Resin, Di- and tri-functional Diluents, PENTA, Proprietary Photoinitiating system, Proprietary self-cure initiating system, 69% fillers by wt., 46% by vol.				
	Dual cure luting composite (iCEM, Heraeus	**Composition:** Composition based on methacrylates 2-component material comprising base paste and matching catalyst paste				
	Dual cure resin cement (Variolink II, Ivoclar Vivadent)	**Composition:** See Nr. Crt. 1				

Nr. Crt	Material		CAD CAM	Restoration type	Abutment type	Authors
15.	Dual cure resin cement (Calibra, Dentsply)	**Composition:** Cement Base: Dimethacrylate Resins; Camphorquinone (CQ) Photoinitiator; Stabilizers; Glass Fillers; Fumed silica; Titanium Dioxide; Pigments Cement Catalyst: Dimethacrylate Resins; Peroxide Catalyst; Stabilizers; Glass Fillers; Fumed Silica Resin Cement Try-In Paste: Glycerine; Fumed Silica; Titanium Dioxide; Pigments Silane Coupling Agent: Acetone; Ethyl Alcohol; Organo Silane	Cerec	Ceramic inlays	Human molars (intraoral)	Rechenberg DK, Göhring TN, Attin T [29]
16.	Light curing composite resin (Filtek Z100 cement, 3M ESPE)	**Composition:** Bis-GMA, TEGDMA Silica/zirconia (84.5 wt%; 0.6 µm average particle size), photoinitiator	Cerec	Composite overlays	Extracted human premolars	Magne P, Knezevic A [30]
17.	Dual cure resin cement (RelyX Unicem, 3M ESPE)	**Composition:** See Nr. Crt. 4	Cerec	Ceramic full crowns	Extracted human molars	Mörmann W, Wolf D, Ender A, Bindl A, Göhring T, Attin T [31]
	Dual cure resin cement (Multilink Sprint, Ivocalr Vivadent)	**Composition:** Dimethacrylates; adhesive monomer; Fillers; initiators / stabilizers				
	Light cure resin cement (Variolink Ultra, Ivoclar Vivadent)	**Composition:** Base ytterbium trifluoride , Bis-GMA, urethane dimethacrylate, triethylene glycol dimethacrylate, titanium dioxide Catalyst ytterbium trifluoride, Bis-GMA, urethane dimethacrylate, triethylene glycol dimethacrylate, dibenzoyl peroxide				
	Glass ionomer cement (Ketac Cem, 3M ESPE)	**Composition:** Powder Glass powder, Polycarboxylic acid, Pigments Liquid Water, Tartaric acid, Conservation agents				

Nr. Crt	Material		CAD CAM	Restoration type	Abutment type	Authors
18.	Dual curing luting composite (Vita Cerec Duo Cement, VITA)	**Composition:** Base triethylene glycol dimethacrylate Catalyst triethylene glycol dimethacrylate, dibenzoyl peroxide	Cerec	Ceramic full crowns	Natural teeth	Zimmer S, Göhlich O, Rüttermann S, Lang H, Raab WH, Barthel CR [32]
19.	Dual cure resin cement (Variolink II, Ivoclar Vivadent)	**Composition:** See Nr. Crt. 1	Cerec	Feldspathic ceramic cylinders	Extracted human teeth	Graiff L, Piovan C, Vigolo P, Mason PN [33]
	Dual cure resin cement (RelyX ARC, 3M ESPE)	**Composition:** See Nr. Crt. 1				
20.	Dual cure composite resin (Link Max, GC)	**Composition:** 4-MET, HEMA, Ethanol, Water EP-B Ethanol Base paste UDMA, HEMA, Fluoroalminosilicate glass filler, Silica filler Catalyst paste UDMA, HEMA, Fluoroalminosilicate glass filler, Silica filler	MicroSpecimen Former	Ceramic block GN-I (GC)	Ceramic block GN-I (GC)	Peumans M, Hikita K, De Munck J, Van Landuyt K, Poitevin A, Lambrechts P, Van Meerbeek B [34]
	Dual cure resin cement (Panavia F2.0, Kuraray)	**Composition:** See Nr. Crt. 10				
	Dual cure resin cement (RelyX Unicem, 3M ESPE)	**Composition:** See Nr. Crt. 4				
	Dual cure resin cement (Variolink II, Ivoclar Vivadent)	**Composition:** See Nr. Crt. 1				
21.	Dual cure resin cement (Panavia F2.0, Kuraray)	**Composition:** See Nr. Crt. 10	Cerec	Ceramic inlays	Extracted human molars	Oztürk AN, Inan O, Inan E, Oztürk B [35]

Nr. Crt	Material		CAD CAM	Restoration type	Abutment type	Authors
	Dual cure resin cement (Variolink II, Ivoclar Vivadent)	**Composition:** See Nr. Crt. 1				
22.	Dual cure resin cement (Panavia F2.0, Kuraray)	**Composition:** See Nr. Crt. 10	Procera	Zirconia copyings	Extracted human molars	Palacios RP, Johnson GH, Phillips KM, Raigrodski AJ [36]
	Dual cure resin cement (RelyX Unicem, 3M ESPE)	**Composition:** See Nr. Crt. 4				
	Dual cure resin cement (RelyX Unicem, 3M ESPE)	**Composition:** See Nr. Crt. 4				
23.	Light curing microhybrid composite (Tetric, Ivoclar Vivadent)	**Composition:** Bis-GMA, Triethylenglycole Dimethacrylate, Urethane dimethacrylate Barium glassfiller, Ytterbiumtrifluoride, High dispersed silica, Mixed oxide Catalysts and Stabilizers Pigments	Cerec	Ceramic inlays	Extracted i maxillary premolars	Hannig C, Westphal C, Becker K, Attin [37]
24.	Light curing microhybrid composite (Tetric Flow, Ivoclar Vivadent)	**Composition:** Urethane dimethacrylate, Bis-GMA Ethoxylated Bis-EMA, Triethyleneglycol dimethacrylate, Barium glass, ytterbium trifluoride, mixed oxide, silicon dioxide, Prepolymers, Additives, tabilizers, catalysts, pigment	Cerec	Ceramic block	Ceramic surface	El Zohairy AA, De Gee AJ, Hassan FM, Feilzer AJ [38]
	Dual cure resin cement (NX2 Nexus, Kerr)	**Composition:** 2-hydroxyethyl methacrylate, Ytterbium trifluoride ,Methacrylated poly(acrylic acid) copolymer 2-hydroxy-1,3-propanediyl bismethacrylate				

Nr. Crt	Material		CAD CAM	Restoration type	Abutment type	Authors
25.	Dual curing luting composite (Vita Cerec Duo Cement, VITA)	**Composition:** See Nr. Crt. 18	Cerec	Conuri trunchiate din Dicor MGC sau blocuri Cerec Vita Mark II	Extracted anterior teeth	Chang JC, Hart DA, Estey AW, Chan JT [39]
	Dual cure resin cement (EnForce, Dentsply)	**Composition:** Bis-GMA: 2,2-bis[p-(2 -hydroxy-3 - methacryloxypropoxy)phenyl]propane. TEGDMA: triethylene glycol dimethacrylate				
	Self-cure resin cement (Panavia 21, Kuraray)	**Composition:** Catalyst Paste 10-Methacryloyloxydecyl dihydrogen phosphate, Hydrophobic aromatic dimethacrylate, Hydrophobic aliphatic dimethacrylate, Silanated silica filler, Colloidal silica, Catalysts Universal Paste Hydrophobic aromatic dimethacrylate, Hydrophobic aliphatic dimethacrylate, Hydrophilic aliphatic dimethacrylate, Silanated titanium oxide, Silanated barium glass filler, Catalysts, Accelerators, Pigments				
	Self-cure resin cement (C&B Metabond cement, Parkell)	**Composition:** Base Methyl Methacrylate Monomer Powders Polymethylmethacrylate (PMMA), Metal Oxide				
	Glass ionomer cement (Fuji Duet, GC)	**Composition:** Powder aluminosilicate glass Liquid aqueous solution of polyacrylic acid, 2-hydroxyethyl, methacrylate (2-HEMA), tartaric acid				
26.	Light curing microhybrid composite (Tetric, Ivoclar Vivadent)	**Composition:** See Nr. Crt. 23	Cerec	Ceramic partial crowns	Extracted human molars	Bindl A, Mörmann WH [40]

Nr. Crt	Material		CAD CAM	Restoration type	Abutment type	Authors
27.	Dual cure resin cement (Variolink II, Ivoclar Vivadent)	**Composition:** See Nr. Crt. 1	Celay milling machine	Ceramic onlays	Human molars (intraoral)	Sevük C, Gür H, Akkayan B [41]
28.	Dual curing luting compo site (Vita Cerec Duo Cement, VITA)	**Composition:** See Nr. Crt. 18	Cerec	Inlays	Human tooth (intraoral)	Molin MK, Karlsson SL [42]
	Dual cure composite resin (Mirage FLC, Chameleon Dental)	**Composition:** Bisphenol a diglycidyl methacrylate, 1,6-hexanediol dimethacrylate, dimethylaminoethyl methacrylate				
	Dual cure resin cement (IPS Empress dual cement, Ivoclar Vivadent)	**Composition:** urethane dimethacrylate, ytterbium trifluoride, tricyclodocane dimethanol dimethacrylate, Bis-GMA				
29.	Dual cure composite resin (Link Max, GC)	**Composition:** 4-MET, HEMA, Ethanol, Water EP-B Ethanol Base paste UDMA, HEMA, Fluoroalminosilicate glass filler, Silica filler Catalyst paste UDMA, HEMA, Fluoroalminosilicate glass filler, Silica filler	Isomet 11-1180-170 low-speed cutting saw	Experimental model made of CAD/ CAM composite	Experimental model made of CAD/CAM composite	Yoshida K, Kamada K, Atsuta M [43]
	Dual curing luting composite (Vita Cerec Duo Cement, VITA)	**Composition:** See Nr. Crt. 18				
30.	*N		Cerec	Ceramic inlays	Extracted human molars	LoPresti JT, David S, Calamia JR [44]

*N-unidentified fixing agent

Five studies were excluded because they were considered ineligible for this review, so a number of 30 studies were analyzed. Cerec dental CAD/CAM system was used in 73.3% of these studies.

Twenty-four fixing agents were tested and the most used were RelyX, Variolink and Panavia (Table 2).

Table 2. Fixing agents most used.

30 studies		
Fixing agent	**No. Articles**	**Percentage**
Rely X	14	58.33%
Variolink II	11	45.83%
Panavia	5	20.83%

Self-adhesive cements do not require any tooth surface pre-treatment, and their application is easy, similar to the more conventional zinc-phosphate and polycarboxylate cements [45].

Our results were compared with literature data and they are in good agreement with Monticelli et al. [46] "RelyX Unicem is the most investigated self-adhesive cement in the current literature published in Medline cited journals".

In order to choose the proper luting agent suitable for different clinical indications technical data sheet should be consulted (Table 3).

Table 3. Technical data summary for the most used fixing agents.

Fixing Agent	**Technical Data Summary**
RelyX Luting Cement (3M ESPE)	Compressive Strength (MPa) 111.7±26.0 Flexural Strength (MPa) 27.6±4.3 Film thickness (microns) 17.0±2.6 Radiopacity (mm) 1.53±0.02
Variolink II (Ivoclar Vivadent)	Compressive Strength (MPa)278.8±30.9 Flexural Strength (MPa) 148.5±22.4 Film thickness (microns) 9.4±2.4 Radiopacity (mm) 4.07±0.5
Panavia F 2.0 (Kuraray)	Compressive Strength (MPa) 290 Flexural Strength (MPa) 77 Film thickness (microns) 19.2±2.2 Radiopacity (mm) 1.44±0.7

The most studied type of prosthetic restorations were inlays (nine articles) and coverage crowns (eight articles), on the third place were experimental models (seven articles).

The evolution of materials and adhesive systems permits the clinician to choose a technique that is more aesthetic and less invasive and this explain why the inlays were the most studied.

Regarding prosthetic restoration support the most used were extracted human teeth (53.33%) and experimental models were used in a percentage of 16.66% (five studies of thirty).

Extracted teeth are routinely used in dentistry to learn technical and preclinical skills before entering clinics and treating patients. It is necessary to use freshly extracted teeth to simulate in vivo conditions [47].

A requirement for the successful function of a ceramic restoration is adequate adhesion between ceramic and tooth substance, however, the literature is unclear on which cement, ceramic, conditioning treatment and dentine bonding agent produce the highest bond strength [48].

The prosthetic restoration success depends of a number of steps and some of the factors involved in the process derive from the particularities of dental CAD-CAM systems, pretreatment of the surfaces that come into contact, cement type, material selection and, of course, the role of human intervention.

Dental CAD-CAM system

Donnelly et al [18] consider that ceramic crown constructed with the same characteristics but with different dental CAD-CAM systems show significant statistically differences. His study showed that the fracture resistance of teeth restored with Lava crown is significantly greater than a similar group of teeth restored with Cerec crowns.

Pretreatment of the surfaces

Gilbert et al [15] showed that for a clinical use of XHIPC-CAD/CAM-resin (Xplus 3, Echzell, Germany), the bond surface should be additionally pretreated with visio.link as bonding agent.

Lührs et al [16] revealed a significant influence of the factors “curing mode” and “composite cement” and a less significant effect of the factor “restoration-surface pre-treatment”. The curing mode is decisive for the bonding effectiveness of adhesively luted composite CAD-CAM restoration to dentin.

Stawarczyk et al [23] concluded that airborne particle abrasion before cementation of polymeric CAD-CAM crowns minimally improved the tensile strength. This study showed that although the tensile strength results were low, crowns cemented with RelyX Unicem showed, after aging, the highest tensile strength. Non-treated CAD-CAM resin crowns showed no bonding for all cements. Pre-treatment with alumina improved the results. The tensile strength of pre-treated resin crowns cemented with all tested cements

presented significantly lower values than those of the adhesively luted glass ceramic crowns [23].

The study of Graiff et al [33] demonstrated that the application of a silane-coupling agent to the ceramic surface after etching with hydrofluoric acid increased the adhesion strength with both adhesive materials used (Variolink II, Rely X ARC).

Some clinicians have suggested the use of surface abrasion with alumina and the subsequent placement of a tribochemical silica coating to allow the creation of chemical bonds between silane and a resin cement [49].

Another technique is the application of molecular vapor deposition of gas-phase chlorosilane ($SiCl_4$) pretreatment to place an ultra-thin silica seed layer. This is achieved by combining chlorosilane with water vapor to form a more reactive surface. This 2nm to 3nm layer allows the creation of bond strength statistically equivalent to traditional bonded porcelain materials [50].

It was developed a surface treatment called selective infiltration etching which use the heat-induced maturation concept and grain boundary diffusion to form a highly retentive surface on Y-TZP. Because selective infiltration etching is only a surface treatment, the mechanical properties of yttria stabilized zirconia (Y-TZP) are not affected [51-52].

Laser treatment has also been shown to create acid-etch type effects. Hydrophobicity of the substrate surface can be improved during laser texturing. Laser texturing of yttria stabilized zirconia is carried out at high pressure nitrogen assisting gas environment (Figure 1) [53].

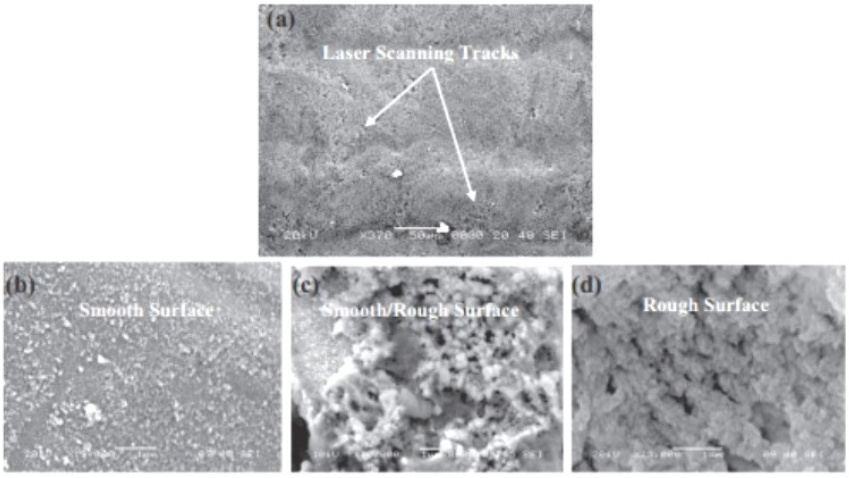

Figure 1. Surface texture of laser treated Y-TZP surface, SEM images [53].

Cement type and material selection

The study of Kassem et al [24] demonstrated that micro-leakage scores of ceramic crowns cemented with Panavia F 2.0 were significantly lower than those of ceramic crowns cemented with RelyX Unicem Clicker and those of composite crowns.

Magne et al [27] concluded that the material selection has a significant effect on the risk of CAD/CAM inlay fracture during pre-cementation functional occlusal tapping.

El Zohairy et al [38] showed in their study that strong and durable bonds to ceramics can be achieved with resin cements and in particular those of hydrophobic nature, when these are applied directly to hydrofluoric acid etched and silanized surfaces.

Study of Felizer et al [54] found that the stress relaxation by water sorption of the composites based on BisGMA/TEGDMA and urethane dimethacrylate resins differed from composite based on tricyclodecane diacrylate which allow to occure very little hygroscopic relaxation.

Monomer-based primers can also be used with zirconia that have not been treated or sandblasted [55].

According to El Zohairy AA application of an intermediate layer of Visio Bond showed a substantial increase in bond strength for both resin cements only to H3PO4 treated surfaces and not to HF-treated surfaces The results also showed that the 1 d bond strength values for Visio Bond as an intermediate resin was consistently lower than with Syntac Single Component or OptiBond Solo Plus regardless the surface treatment (HF or H3PO4) or resin cement used (Tetric Flow or Nexus 2). The most probable explanation for this interesting finding is a decreased possibility for the Visio Bond monomer Tricyclodecane diacrylate to react with the silane-C=C-bonds by severe steric hindrance. The reactive C=C-bonds are too closely positioned to this bulky monomer (Figure 2), that they cannot easily reach the silane-C=C-bonds to react with. Synthesis of a similar monomer with longer chains carrying the C=C-groups may significantly improve coupling to the silane layer [56].

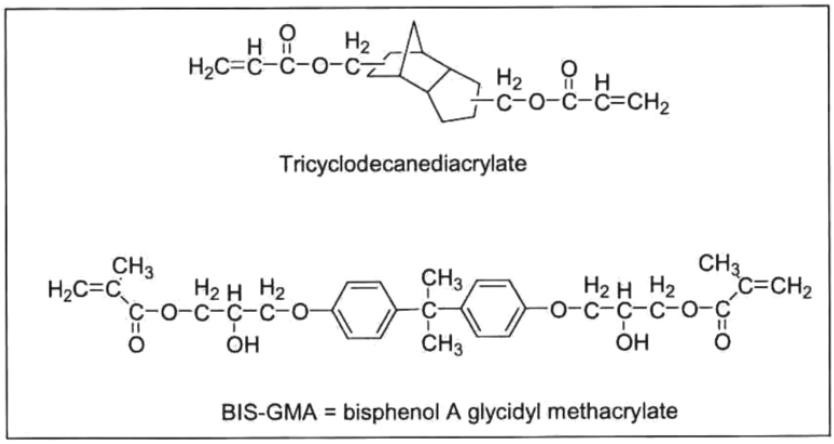

Figure 2. Chemical structure of Tricyclodecane diacrylate and BIS-GMA. The reactive C=C-bonds of Tricyclodecanee diacrylate are more closely positioned to the central core of the monomer molecule in comparison to BIS-GMA [56]

CONCLUSIONS

Adhesion has two aspects and for durable prosthetic restoration not only the conditioning of restoration material but also the dentin is crucial for good attachment of the resin cement to both substrates. Etching and rinse bonding systems are still considered the gold standard for conditioning of dentin. However due to their technique sensitivity, some of the conventional resin cement systems involve self-etch adhesives. On the other hand, self-adhesive cements do not require any conditioning of the dentin, which eliminates technique sensitivity [57]. Light curing after inlay insertion showed improved marginal adaptation. Using dual-curing adhesive and Luting Cements, advantages in marginal adaptation between Luting Cements and dentin were observed [58].

The authors of this paper tried to provide an overview of currently available luting agents, the chemical composition and properties intending to help the clinician to choose the suitable luting agent for a particular clinical situation.

In summary, the objective of any surface treatment method is to enhance the adhesive bond strength and durability. The basic requirements for a good adhesive bond are following: proper choice of adhesive, good joint design, cleanliness of surfaces, wetting of adherends (surfaces that are to be bonded together by the adhesive), proper adhesive bonding process (solidification and cure) [59-60].

CONFLICT OF INTERESTS

The authors declare that they have no conflict of interests.

ACKNOWLEDGMENTS

Dr. Popa Daniela is a fellow of POSDRU grant no. 159/1.5/S/138776 grant with title: "Model colaborativ instituţional pentru translarea cercetării ştiinţifice biomedicale în practica clinică- TRANSCENT"

REFERENCES

1. E. Yuzbasioglu, H. Kurt, R. Turunc, H. Bilir. *BMC Oral Health,* **2014**, *14*, 10
2. L. Cooper. *CAD/CAM the international C.E. magazine of digital dentistry,* **2011**, *1,* 6
3. A.N. Oztürk, O. Inan, E. Inan, B. Oztürk. *European Journal of Dentistry*, **2007**, *1*, 91-6
4. J.C. Chang, D.A. Hart, A.W. Estey, J.T.Chan. *Journal of Prosthetic Dentistry*, **2003**, *90*,18-23
5. K. Ladha, M. Verma. *The Journal of Indian Prosthodontic Society,* **2010**, *10*, 79-88
6. D. Bratu, L. Mikulik, D. Munteanu. Tehnici adezive în stomatologie. Ed. Facla. Timisoara **1982**
7. A. Petre, R. Sfeatcu. *Romanian Journal of Oral Rehabilitation*, **2011,** 3
8. A.P. Manso, N.R. Silva, A.E. Bonfante, T.A. Pegararo, R.A. Dias, R.M. Carvalho. *Dental Clinics of North America*, **2011**, *55*, 311–332
9. M. Peumans, B. Van Meerbeek, P. Lambrechts, G. Vanherle. *Journal of Dentistry*, **2000**, *28*, 163–167
10. I. Krejci, F. Lutz, M. Reimer, J.L. Heinzmann. *Journal of Prosthetic Dentistry*, **1993**, *69*, 425-430
11. S.J. O'Neal, R.L. Miracle,K.F. Leinfelder. *The Journal of the American Dental Association* ,**1993**, *124*, 48-54
12. K. Kawai, B.P. Isenberg, K.F. Leinfelder. Quintessence International, **1994**, *25*, 53-58
13. K. Shinkai, S. Suzuki, K.F. Leinfelder, Y. Katoh. *American Journal of Dentistry*, **1995**, *8*, 149-151
14. R. Zuellig-Singer, R.W. Bryant. *Quintessence International*, **1998**, *29*, 573-582
15. S. Gilbert, C. Keul, M. Roos, D. Edelhoff, B. Stawarczyk. *Clinical Oral Investigation*, **2016**, *20*, 227-236
16. A.K. Lührs, P. Pongprueksa, J. De Munck, W. Geurtsen, B. Van Meerbeek. *Dental Materials Journal*, **2014**, *30*, 281-291

17. D.J. Poticny. *Dentistry Today*, **2013**, *2*, 79-80, 82-83
18. T.J. Donnelly, F.J. Burke. *European Journal of Prosthodontics and Restorative Dentistry*, **2011**, *19*,111-116
19. M.N. Aboushelib, W.A. Elmahy, M.H. Ghazy. *Journal of Dentistry,* **2012,** *40*, 670-677
20. D. Edelhoff, F. Beuer, J. Schweiger, O. Brix, M. Stimmelmayr, J.F. Guth. *Quintessence International*, **2012**, *43*, 457-467
21. T.V. Carnaggio, R. Conrad, R.L. Engelmeier, P. Gerngross, R. Paravina, L. Perezous, J.M. Powers. *Journal of Prosthodontics*, **2012**, *21*, 523-528
22. R. Frankenberger, J. Hehn, J. Hajtó, N. Krämer, M. Naumann, A. Koch, M.J. Roggendorf. *Clinical Oral Investigation*, **2013**, *17*, 177-183
23. B. Stawarczyk, T. Basler, A. Ender, M. Roos, M. Ozcan, C. Hämmerle. *Journal of Prosthetic Dentistry*, **2012**, *107*, 94-101
24. A.S. Kassem, O. Atta, O. El-Mowafy. *Journal of Prosthodontics*, **2012**, *21*, 28-32
25. R. Sorrentino, G. De Simone, S. Tetè, S. Russo, F. Zarone. *Clinical Oral Investigation*, **2012**, *16*, 977-985
26. N. Madan, K. Pannu. *International Journal of Computerized Dentistry*, **2011**, *14*, 47-53
27. P. Magne, M.P. Paranhos, L.H. Schlichting. *Dental Materials Journal*, **2011**, *27*, 109-113
28. S. Flury, A. Lussi, A. Peutzfeldt, B. Zimmerli. *Dental Materials Journal*, **2010**, *26*, 855-863
29. D.K. Rechenberg, T.N. Göhring, T. Attin. *The Journal of Adhesive Dentistry*, **2010**, *12*, 189-196
30. P. Magne, A. Knezevic. *Dental Materials Journal*, **2009**, *25*, 1264-1268
31. W. Mörmann, D. Wolf, A. Ender, A. Bindl, T. Göhring, T. Attin. *Journal of Prosthodontics*, **2009**, *18*, 403-410
32. S. Zimmer, O. Göhlich, S. Rüttermann, H. Lang, W.H. Raab, C.R. Barthel. *Operative Dentistry*, **2008**, *33*, 484-487
33. L. Graiff, C. Piovan, P. Vigolo, P.N. Mason. *Journal of Prosthodontics*, **2008**, *17*, 294-299
34. M. Peumans, K. Hikita, J. De Munck, K. Van Landuyt, A. Poitevin, P. Lambrechts, B. Van Meerbeek. *Operative Dentistry*, **2007**, *32*, 372-379
35. A.N. Oztürk, O. Inan, E. Inan, B. Oztürk. *European Journal of Dentistry*, **2007**, *1*, 91-96
36. R.P. Palacios, G.H. Johnson, K.M. Phillips, A.J. Raigrodski. *Journal of Prosthetic Dentistry*, **2006**, *96*, 104-114
37. C. Hannig, C. Westphal, K. Becker, T. Attin. *Journal of Prosthetic Dentistry*, **2005**, *94*, 342-349
38. A.A. El Zohairy, A.J. De Gee, F.M. Hassan, A.J. Feilzer. *Dental Materials Journal*, **2004**, *20*, 778-787
39. J.C. Chang, D.A. Hart, A.W. Estey, J.T. Chan. *Journal of Prosthetetic Dentistry*, **2003**, *90*, 18-23
40. A. Bindl, W.H. Mörmann. *European Journal of Oral Science*, **2003**, *111*, 163
41. C. Sevük, H. Gür, B. Akkayan. *Quintessence International*, **2002**, *33*, 353-357

42. M.K. Molin, S.L. Karlsson. *International Journal of Prosthodontics*, **2000**, *13*, 194-200
43. K. Yoshida, K. Kamada, M. Atsuta. *Journal of Prosthetic Dentistry*, **2001**, *85*, 184-189
44. J.T. LoPresti, S. David, J.R. Calamia. *American Journal of Dentistry*, **1996**, *9*, 37-39
45. A.M. Diaz-Arnold, M.A. Vargas, D.R. Haselton. *Journal of Prosthetic Dentistry*, **1999**, *8*, 135-141
46. F. Monticelli, M. Ferrari, M. Toledano. *Medicina Oral Patologia Oral y Cirurgia Bucal*, **2008**, *13*, 214-221
47. N.V. Lolayekar, V.S. Bhat, S.S. Bhat. *Journal of Oral Health and Community Dentistry*, **2007**, *1*, 27–29
48. G.P. Stewart, P. Jain, J. Hodges. *Journal of Prosthetic Dentistry*, **2002**, *88*, 277-284
49. M. Ozcan, P.K. Vallittu. *Dental Materials Journal*, **2003**,*19*, 725-731
50. J.R. Piascik, E.J. Swift, J.Y. Thompson. *Dental Materials Journal*, **2009**, *25*, 1116-1121
51. M. Aboushelib, H. Mirmohamadi, J. Matinlinna. *Dental Materials Journal*. **2009**, *25*, 989-993
52. M.N. Aboushelib, J.P. Matinlinna, Z. Salameh. *Dental Material Journal*, **2008**, *24*, 1268-1272
53. B.S. Yilbas. *Journal of Alloys and Compounds*, **2015**, *625*, 208–215
54. A.J. Felizer, A.J. De Gee, C.L. Davidson. *Journal of Dental Research*, **1990**, *69*, 36-39
55. M. Kalogirou, R. Trushkowsky, J. Andrade, S. David. *Compendium of Continuing Education in Dentistry*, **2011,** *32*, 40-46
56. A.A. El Zohairy. Esthetic and bonding enhancements of tooth colored indirect restorations. Acta **2004**
57. M. Behr, M. Rosentritt, T. Regnet, R. Lang, G. Handel. *Dental Materials Journal*, **2004**, *20*, 191-197
58. D.K. Rechenberg, T.N. Göhring, T. Attin. *Journal of Adhesive Dentistry*, **2010**, *12*, 189-196
59. E.M. Petrie. Plastics and adhesives as adhesives. In: Harper CA, editor. Handbook of plastics and elastomers. New York: Mc Graw-Hill; **1975**
60. S. Ebnesajjad, C. Ebnesajjad. Surface Treatment of Materials for Adhesive Bonding. William Andrew is an imprint of Elsevier. The Boulevard, Langford Lane, Kidlington, Oxford, OX5 1GB, 225 Wyman Street, Waltham, MA 02451, USA, Second Edition **2014**